SAPIENZA
UNIVERSITÀ DI ROMA

PhD Course in Biochemistry
XXX Cycle (Academic Years 2014-2017)

Hydrogen sulfide metabolism in cancer and homocystinuria: towards the development of new pharmacological strategies

PhD student
Francesca Malagrinò

Tutor
Dr. Alessandro Giuffrè

PhD coordinator
Prof. Francesco Malatesta

December 2017

To Anna Giusi

ACKNOWLEDGMENTS

I would like to thank all people who supported and ispirated me during during these PhD years.

Firstly, I want to turn my thanks to my supervisor, Dr. Alessandro Giuffrè, for his rigourous scientific advices and for his precious academic guidance.

I would like to thank Prof. Paolo Sarti, who has always encouraged and motivated me with great enthusiasm.

My best gratitude goes, moreover, to Dr. Pierpaolo Ceci, Dr. Elisabetta Falvo and Dr. João B. Vicente, for the scientific support and affectionate help.

I want to thank Prof. Elena Forte, Dr. Marzia Arese and Dr. Daniela Mastronicola for their insightful comments and precious encouragement.

For the stimulating scientific discussions, the loving closeness and their sincere friendship, a special thank goes to Dr. Maria Chiara Magnifico and Dr. Karim Zuhra.

I would like to thank, furthermore, the coordinator of the PhD in Biochemistry, Prof. Francesco Malatesta, for his meticulous guidance.

Thanks to all of my colleagues and friends of these PhD years, in particular Giulia, Filippo, Alessia, Vincenzo, Serena, Ilaria, Matilde, Daniela, Ludovica and Giulia for their precious closeness.

Last but not least, thanks to my dear mother, my grandparents, my aunt Linda and my uncle Giovanni for the love and continous support.

This work was partly supported by Ministero dell'Istruzione, dell'Università e della Ricerca (MIUR) of Italy (PNR-CNR Aging Program 2012–2014 and PRIN 20158EB2CM_003 to Alessandro Giuffrè).

My PhD was funded by a Sapienza University of Rome fellowship for three years

SCIENTIFIC COMMUNICATIONS

Publications

- **F. Malagrinò**, K. Zuhra, L. Mascolo, D. Mastronicola, J.B. Vicente, E. Forte, A. Giuffrè. "Effect of hypoxia on mitochondrial hydrogen sulfide catabolism", **to be submitted**

- E. Falvo[*], **F. Malagrinò[*]**, A. Arcovito, F. Fazi, G. Colotti, E. Tremante, P. Di Micco, G. Fracasso, A. Giuffrè and P. Ceci. "A novel ferritin-based nanocarrier for efficient mitoxantrone encapsulation and selective delivery to cancer cells", **to be submitted**

- J.B. Vicente, H. G. Colaço, **F. Malagrinò**, P. E. Santo, A. Gutierres, T. Bandeiras, P. Leandro, J. A. Brito and A. Giuffrè. "A clinically relevant variant of the human hydrogen sulfide-synthesizing enzyme cystathionine ß-synthase: increased CO reactivity as a novel molecular mechanism of pathogenicity?", Oxidative Medicine and Cellular Longevity (2017), 2017, 8940321.

- J.B Vicente, **F. Malagrinò**, M. Arese, E. Forte, P. Sarti and A. Giuffrè. "Bioenergetic relevance of hydrogen sulfide and the interplay between gasotransmitters at human cystathionine beta-synthase", Biochim. Biophys. Acta – Bioenergetics (2016), 1857, 1127-38.

*** Equally contributing authors**

Selected communications by the candidate at scientific conferences

- **F. Malagrinò**. "H_2S metabolism in colon cancer cells: effect of hypoxia", *BeMM Symposium (2017)* – Rome, Italy. (poster presentation)

- **F. Malagrinò**, K. Zhura, D. Mastronicola, L. Mascolo, J.B. Vicente, E. Forte, A. Giuffrè. "Effect of hypoxia on H_2S metabolism in colon cancer cells", *59th Congress of the Italian Society for Biochemistry and Molecular Biology (2017)* – Caserta, Italy. (poster communication)

- **F. Malagrinò**, K. Zhura, D. Mastronicola, L. Mascolo, J.B. Vicente, E. Forte, A. Giuffrè. "Hypoxia and H_2S metabolism in colon cancer cells", *Mitochondrial Physiology, from organelle to organism (2017)* – Copenhagen, Denmark. (poster presentation)

- **F. Malagrinò**, H. G. Colaço, K Zuhra, P. E. Santo, E. Forte, A. Gutierres, M. Arese, T. M. Bandeiras, P. Sarti, P. Leandro, J. A. Brito, J. B. Vicente and A. Giuffrè. "Novel pathogenic mechanisms from investigation of human hydrogen sulfide metabolism", *First international meeting of the Italian Group of Bioenergetics and Biomembranes (2017)* – Catania, Italy. (oral presentation)

- J.B. Vicente, H.G. Colaço, **F. Malagrinò**, M. Arese, E. Forte, P. Sarti, P. Leandro, A. Giuffrè. "S-adenosyl-L-methionine and the cross-talk between the bioenergetically relevant gasotransmitters H_2S, NO and CO at human cystathionine β-synthase", *19th European Bioenergetics Conference* (2016) - Riva del Garda, Italy. (poster communication)

INDEX

OBJECTIVES

Objectives

Hydrogen sulfide (H_2S), similarly to the other two gasotransmitters carbon monoxide (CO) and nitric oxide (NO), plays a fundamental role in human (patho)physiology, acting as a signalling molecule at low concentrations or exerting toxic effects at higher levels (Wang, 2012). Interestingly, H_2S plays such a dual role also on mitochondrial function, inhibiting cytochrome *c* oxidase (complex IV) at higher concentrations or stimulating mitochondrial respiration at lower concentrations. Sulfide oxidation by mitochondria is indeed coupled to electron injection into the mitochondrial respirator chain and thus stimulates cellular respiration, while preventing toxic accumulation of sulfide (Szabo, 2014). Because H_2S is crucially involved in the regulation of cellular homeostasis, the bioavailability of this gaseous signalling molecule must be finely controlled through a correct balance between its synthesis and breakdown (Kabil & Banerjee, 2014). H_2S biologic effects are interestingly interconnected with O_2 and the action of the other two gasotransmitters CO and NO. Perhaps not surprisingly, abnormally increased or decreased H_2S levels are widely reported to be associated with various pathologies (Hellmich & Szabo, 2015; Wallace & Wang, 2015). Hence the relevance of investigating the molecular mechanisms that control the cell bioavailability of H_2S and its cross-talk with O_2, CO and NO, as well as the specific role of H_2S in human diseases.

Objectives

One of the goal of the present thesis work has been to gain insight into the molecular bases of classic homocystinuria. This is a rare metabolic disease caused by mutations in the gene of cystathionine β-synthase (CBS), one of the major H_2S-synthesizing enzymes in humans (Mendes, 2014). CBS activity regulates homocysteine levels in humans and was previously shown to be fine-tuned by both the allosteric stimulator S-adenosyl-L-methionine and the inhibitory action of CO and NO (Vicente, 2014; Vicente, 2016). Here, we aimed to investigate the structural and functional properties of a CBS variant (p.P49L) causing a mild form of classic homocystinuria. The goal was to test if the disease is associated to altered regulatory mechanisms, in particular regarding the cross-talk between H_2S and CO.

Endogenously produced H_2S has been recently shown to stimulate the energy metabolism and proliferation in cancer cells. In light of this information, we aimed to evaluate the effect of hypoxia, a common feature in the tumour microenvironment, on the ability of cells to dispose H_2S. Because hypoxic conditions are associated to enhanced H_2S synthesis and higher H_2S levels have been reported to have key protective effects against hypoxia and ischemia/reperfusion damage, it seems relevant to assess the effect of hypoxia on the H_2S breakdown, mostly occurring at a mitochondrial level. To this end, we performed high-resolution respirometric measurements on a cell model of colon cancer (SW480).

Finally, in order to identify new pharmacological interventions against colorectal cancer (CRC), we have focused our attention on the study of human ferritin (HFt)-based drug delivery systems. HFt can interact with and be internalized by the transferrin receptor 1 (TfR1) overexpressed in many cancer cells, including colon cancer cells. As HFt-based constructs can efficiently entrap chemotherapeutic molecules, these nanodevices represent innovative drug delivery systems (Falvo, 2016). In this thesis work we aimed to improve HFt as a drug-delivery system and test the efficacy of novel HFt-based nanocarriers on a suitable cell model of colon cancer progression (SW480 and SW620 cells). The long-term of this research is to exploit these nanocarriers as delivery systems for drugs with solubility issues or high toxicity.

BACKGROUND

1. Physico-chemical properties of H_2S

Hydrogen sulfide is a compound with chemical formula *H_2S* and a molecular weight of 34.08. H_2S is a colourless, flammable, corrosive and water-soluble (~100 mM at 1 atm and 25 °C) gas characterized by a typical smell of rotten eggs (Nagy, 2014). The sulfur is a chalcogen element, positioned in group 16 of the periodic table. The electron configuration 1s2 2s2 2p6 3s2 3p4 corresponds to 6 valence electrons and a vacant 3d orbital. Therefore, sulfur can have oxidation states from −2 to +6. The oxidation state of sulfide sulfur is −2 which makes H_2S a reducing species, with a strong nucleophilic character (Nagy, 2014). In biological systems, hydrogen sulfide reacts with oxidising species, like reactive oxygen species (ROS) and reactive nitrogen species (RNS) (Hancock & Whiteman, 2016), and can generate persulfides, recently discovered to have signalling biological effects. Further, H_2S directly or indirectly (*via* persulfide) promotes protein sulfhydration, which consists in the addition of a persulfide moiety on protein cysteine residues by reduction of protein-disulfides or oxidation of thiol groups by the $HS^{\bullet}$ radical species (Kimura, 2017; Nagy, 2013; Nagy, 2014). Persulfides and polysulfides are common contaminants of H_2S aqueous solutions. Aqueous solutions of H_2S are prepared by dissolving sulfide salts. The sodium salts NaHS and Na_2S are very soluble in water (s ≅ 19g/100g H_2O at 20°C) and, for this reason, are often used as H_2S donors in biological

studies. In aqueous solution, H_2S dissociates into hydrosulfide anion (HS–), sulfide (S^{2-}) and 2 protons (H^+), according to the following equilibria:

$$H_2S \leftrightharpoons HS^- + H^+ \quad \text{pKa} = 7.05$$

$$HS^- \leftrightharpoons S^{2-} + H^+ \quad \text{pKa} > 14$$

Consistently, at physiological pH 7.4 the $[H_2S]/[HS^-]$ ratio is 0.45 and, therefore, one third of H_2S is present in the undissociated form (H_2S) and two thirds as hydrosulfide anion HS^-, whereas the amount of the sulfide anion (S^{2-}) is negligible.

The chemical undissociated specie H_2S is highly liposoluble and highly volatile, in contrast to HS^- and S^{2-} that can form strong bonds with the solvent (Nagy, 2014; Ono, 2014; Wang, 2012).

2. H_2S, the new gasotransmitter

Along with carbon monoxide (CO) and nitric oxide (NO), hydrogen sulfide (H_2S) belongs to a small group of gaseous signalling molecules, termed *gasotransmitt*ers (Wang, 2002). H_2S is able to diffuse across biological membranes and dose-dependently regulates multiple physiological processes. While displaying toxic effects at high (μM) concentrations, it acts

as a direct biological mediator (Wang, 2012) and a bioenergetic 'fuel' at low (nM) concentrations. Additionally, H_2S plays a critical role in several pathological processes (Kimura, 2014; Wang, 2012). Therefore, the bioavailability of this gaseous molecule must be finely regulated through a correct balance between its synthesis and breakdown (Kabil & Banerjee, 2014). Notably, sulfide biosynthesis proved to be regulated by CO and NO (Taoka, 1999, Vicente, 2014; Vicente, 2016) suggesting a cross-talk between the three gasotransmitters which appears to be fundamental for the maintenance of cellular homeostasis (Wang, 2012).

2.1. Synthesis

2.1.1 Endogenous H_2S production - Enzymes and pathways

In mammals, H_2S is enzymatically produced by the pyridoxal 5'-phosphate (PLP)-dependent enzymes cystathionine β-synthase (CBS) and cystathionine γ-lyase (CSE or CGL), and the mitochondrial enzyme 3-mercaptopyruvate sulfurtransferase (MST) or by the peroxisome-localized D-amino acid oxidase (DAO) (Kabil & Banerjee, 2014; Shibuya & Kimura, 2013; Singh & Banerjee, 2012; Shibuya, 2013). CBS and CSE are involved **i**n the trans-sulfuration pathway of methionine, a cytosolic metabolic pathway leading to the synthesis of cysteine from homocysteine with

formation of cystathionine as intermediate. H_2S is a *secondary* product of these reactions**.**

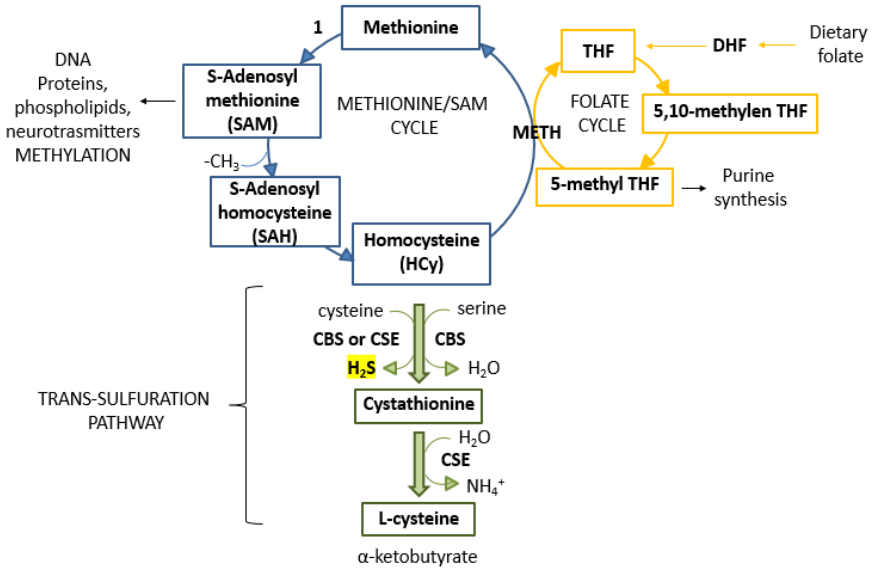

Figure 1. Methionine/SAM cycle (blu), folate cycle (yellow) and trans-sulfuration pathway (green).

CBS- and CSE- catalysed reactions

The first metabolite in the transulfuration pathway is homocysteine (HCy), which is also an intermediate of the SAM/methionine cycle. Dietary methionine provides cells with methyl groups through the generation of S-adenosylmethionine (SAM or AdoMet) which transfers a methyl group to different acceptors generating S-adenosyl homocysteine (SAH or AdoHcy).

AdoHcy is reversibly hydrolysed to adenosine and homocysteine. HCy has then two fates; it can be remethylated by methionine synthase (MS or METH) regenerating methionine and thus completing the cycle, or can enter the trans-sulfuration pathway (*fig.1*). In mammals, the trans-sulfuration pathway is irreversible; therefore, sulfur exits from methionine cycle and can be used to generate cysteine, H_2S and other sulfur-containing metabolites. In particular, cysteine becomes the limiting substrate for the synthesis of glutathione (GSH), coenzyme A (CoA), taurine and sulfate (SO_4^{2-}). GSH together with its oxidized form (GSSG) is an important antioxidant compound implicated in the control of cellular redox homeostasis. Coenzyme A can transfer acetyl groups and it is involved in energy metabolism (e.g., in the Krebs cycle and fatty acids oxidation), while taurine and sulfate are the final metabolites derived from the oxidative degradation of the cysteine in excess *via* cysteine dioxygenase (CDO) (Kabil, 2014). The reactions involved in the trans-sulfuration pathway and H_2S generation are reported below (*fig. 2*).

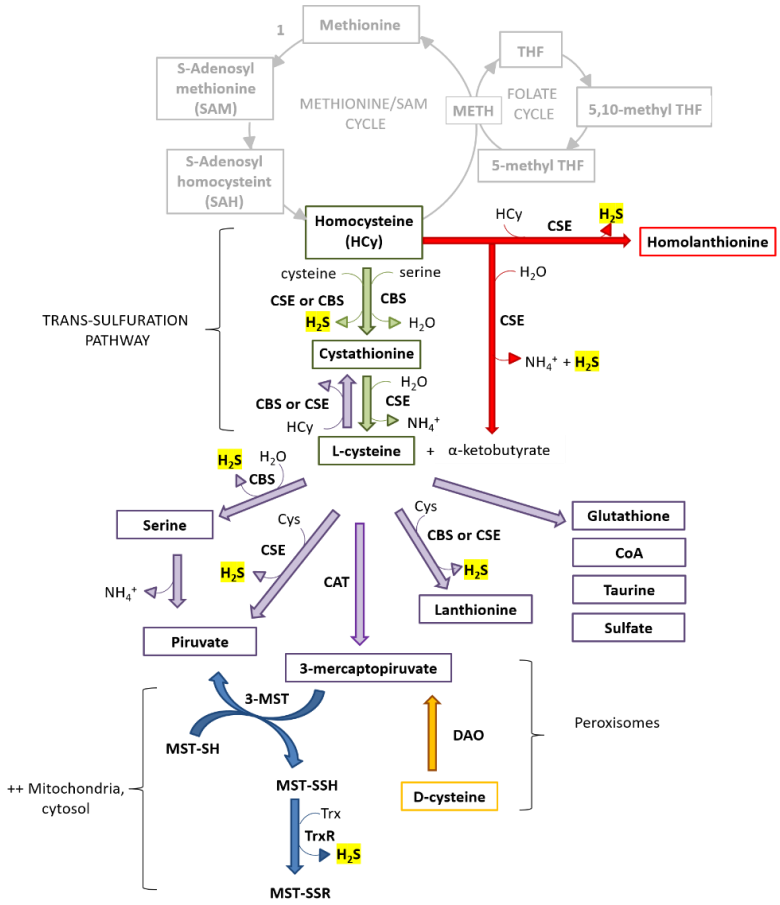

Figure 2. Reactions involved in the production of H_2S and other sulfur metabolites. Trans-sulfuration pathway (green arrows); CSE-catalysed synthesis of H_2S from homocysteine (red arrows); Generation of H_2S, 3-mercaptopyruvate and other sulfur metabolites from L-cysteine (violet arrows); MST-catalysed reaction of H_2S synthesis (blue arrows); Contribution of DAO to H_2S synthesis (yellow arrows).

The first reaction of transulfuration pathway is catalysed by CBS and leads to formation of cystathionine. The enzyme uses serine and homocysteine as substrates and produces one molecule of water as co-

product (*reaction 1*). CBS is a member of the β-family of PLP-containing enzymes which are typically able to catalyse β-replacement or β-elimination reactions.

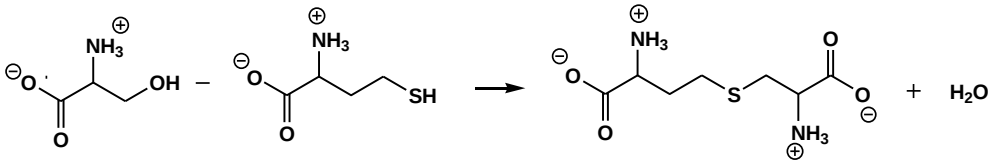

L-serine **L-homocysteine** **L-cystathionine**

Reaction 1. Canonical β-elimination reaction catalysed by CBS.

Du Vigneaud and co-workers were the first ones to note the production of H_2S in the presence of homocysteine during his studies on trans-sulfuration pathway (Binkley & Du Vigneaud, 1944). CBS can indeed catalyse the condensation of homocysteine and cysteine (derived from diet, *via* degradation of endogenous proteins or *via* trans-sulfuration pathway) producing cystathionine and one molecule of H_2S (Chen, 2004) (*reaction 2*).

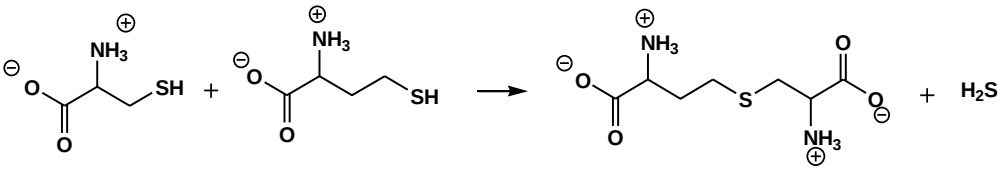

L-cysteine **L-homocysteine** **L-cystathionine**

Reaction 2. Alternative reaction catalysed by CBS, yielding H_2S from cysteine and homocysteine.

Homocysteine is a substrate of many "accessory" reactions involved in H_2S generation. In particular, CSE catalyses the synthesis of α-ketobutyrate, ammonia and H_2S from homocysteine and H_2O (*reaction 3*)

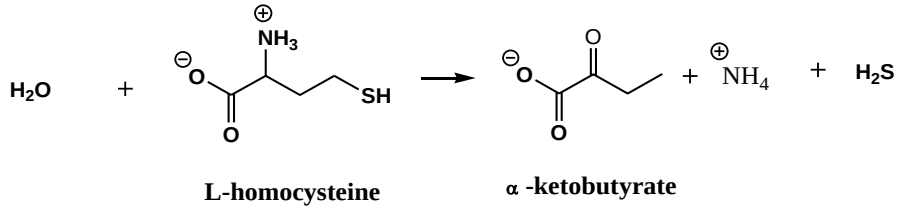

Reaction 3. α-γ elimination reaction catalysed by CSE yielding H_2S and α-ketobutyrate from homocysteine.

or the condensation of two molecules of homocysteine generating homolanthionine and H_2S (*reaction 4*) (Singh, 2009).

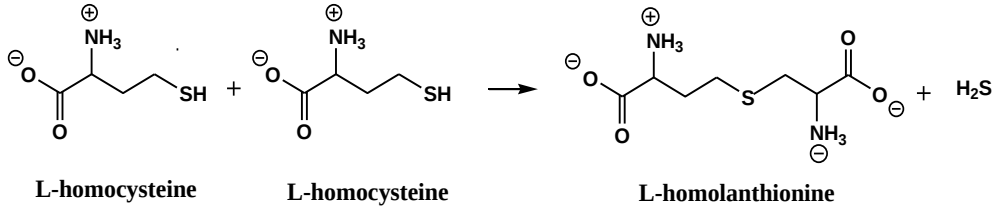

Reaction 4. γ-replacement reaction catalysed by CSE, yielding H_2S and homolanthionine from homocysteine. Homolanthionine is a biomarker of hyperhomocisteinemia/homocystinuria (Chiku, 2009).

The second and last step of the trans-sulfuration pathway is the generation of cysteine from cystathionine and H_2O catalysed by CSE (*react. 5*).

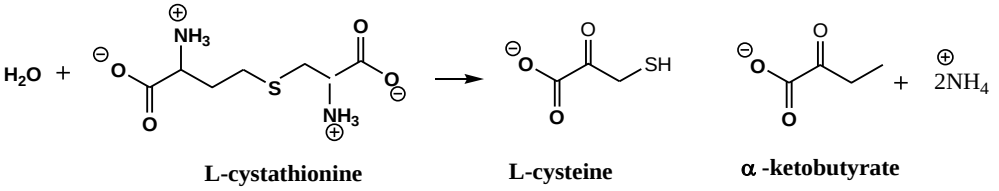

L-cystathionine **L-cysteine** **α -ketobutyrate**

Reaction 5. Canonical α–γ elimination reaction catalysed by CSE.

Cysteine in turn is a substrate of alternative reactions catalysed by CSE yielding H_2S and ultimately pyruvate (*reaction 6*) or L-lanthionine (*reaction 7*) (Singh, 2009).

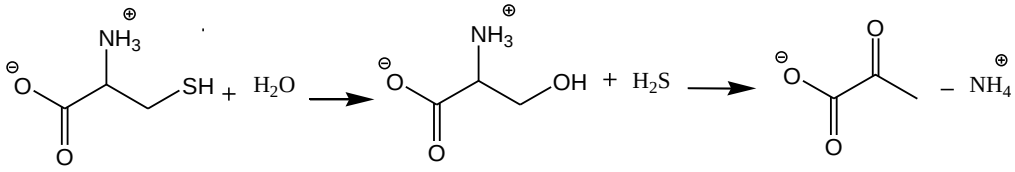

L-cysteine **L-serine** **Pyruvate**

Reaction 6. α–β elimination reaction catalysed by CSE.

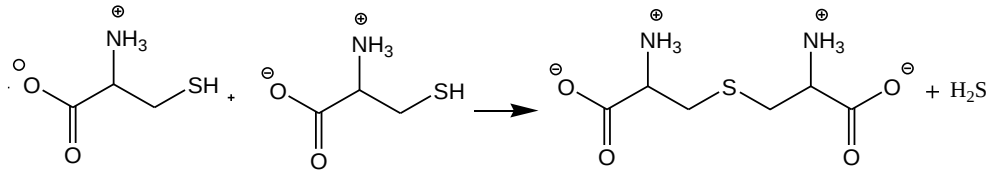

L-cysteine **L-cysteine** **L-lanthionine**

Reaction 7. β- replacement reaction catalysed by CSE. L-lanthionine is a biomarker of hyperhomocisteinemia/homocystinuria. (Chiku, 2009).

Furthermore, CBS proved to catalyse H_2S production through β-replacement of cysteine by several compounds (β-mercaptoethanol, dithiothreitol, cysteamine and methanethiol) with formation of the corresponding thioethers (Singh, 2009).

MST- and DAO- catalysed reactions

Cysteine can also be converted to 3-mercaptopyruvate *via* a transamination reaction catalysed by cysteine (or aspartate) aminotransferase (CAT). In the cytosol and in the mitochondria matrix, 3-mercaptopyruvate is desulfurated by 3-mercaptopyruvate sulfurtransferase (MST), which has a redox-active cysteine residue in the active site (MST-SH), to generate pyruvate and persulfidated enzyme (MST-SSH). Sulfur is then transferred by the NADPH-dependent enzyme thioredoxin reductase (TrxR) to the preferred reducing acceptor, thioredoxin (Trx) or glutathione (GSH), generating H_2S (Kabil & Banerjee, 2014). Alternatively 3-mercaptopyruvate can be generated through the oxidative deamination of D-cysteine catalysed by D-amino acid oxidase (DAO) in peroxisomes (Shibuya & Kimura, 2013), leading to H_2S generation (Shibuya, 2013).

Biological relevance

The catalytic promiscuity of the enzymes responsible for H_2S production may be viewed as a manner to ensure H_2S generation from different substrates and under several physiological conditions (Singh, 2009). The regulation of H_2S generation is expected to be a physiological mechanism for augmenting or diminishing sulfur metabolites levels on demand. Indeed, the physiological relevance of this pathway is both set on the production of important cysteine-derived metabolites, such as glutathione and H_2S, and on the prevention of toxic accumulation of homocysteine (Kabil, 2014).

Compound	**Human plasma levels** (Kabil, 2014)
Methionine	20-100 µM
AdoMet	Low micromolar or trace quantities
Homocysteine	Low micromolar or trace quantities
Cystathionine	Low micromolar or trace quantities
Cysteine	~100-200 µM
Taurine	~50-90 µM
GSH and GSSG	~100-200 µM
H_2S	Low nanomolar (*except aorta, 20- to 100-fold higher)

Table 1. Plasma levels of sulfur compounds derived from the CBS- and CSE-catalysed reactions.

Tissue and cellular localization of H_2S synthesis enzymes

The relative contribution of CBS, CSE and MST to H_2S synthesis varies among different tissues, depending on the expression levels of the enzymes and the concentration of their respective substrates. In terms of tissue localization, CSE is expressed in the cardiovascular system but also in the liver, kidney, uterus, placenta, pancreatic islet, lung and gastrointestinal tract. CBS is preferentially expressed in the brain and other tissues, such as liver, kidney, pancreas, lung and gastrointestinal tract; more recently, it was also detected in the cardiac tissue. MST is expressed in the central system, mostly in glial cells, but it is also detected in the vascular smooth muscle, cardiomyocytes, kidney and liver (reviewed in Wallace & Wang 2015). Finally, DAO is localized in brain and kidney (Shibuya & Kimura 2013; Shibuya, 2013). In terms of cellular localization, CBS and CSE are mostly cytosolic enzymes, whereas MST is present in mitochondria and has a role in H_2S-based energy production, as confirmed by Szabo and collaborators (Modis, 2013) (see *Bioenergetics*). However, under specific conditions both

CBS and CSE can be found in mitochondria or nuclei, and MST in the cytosol (Fu, 2012; Teng, 2013) (see *Hypoxia*).

2.1.1.1 Focus on cystathionine β synthase (CBS)

Structure

Human cystathionine β-synthase (*h*CBS) is a homotetrameric enzyme characterized by a complex domain structure and peculiar regulatory mechanism. Each 63 kDa subunit contains 551 amino acid residues organized in three functional domains (Meier, 2001). The *N*-terminal domain harbours a hexacoordinate heme with cysteine 52 (C52) and histidine 65 (H65) as endogenous Fe ligands; the central catalytic domain binds the pyridoxal-5'-phosphate (PLP) cofactor, whereas the *C*-terminal domain consists of a motif, named "Bateman module" (Bateman, 1997), that binds the positive regulator S-adenosyl-L-methionine (AdoMet) and is responsible for CBS tetramerization (Ereño-Orbea, 2013). Each CBS subunit binds three different substrates (homocysteine, serine and cysteine) and is further regulated allosterically by AdoMet, leading to an increase in catalytic activity by approximately two- to five-fold (Ereño-Orbea, 2014).

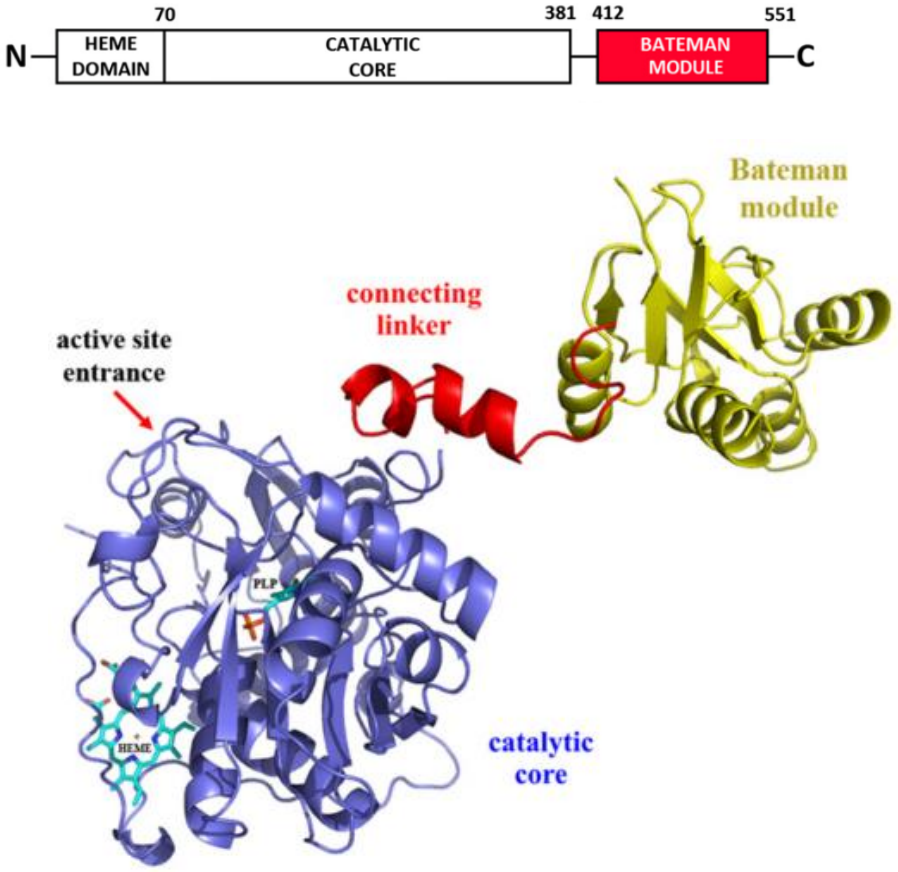

Figure 3. Protein domains and crystallographic structure of monomeric *h*CBS. Image from (Ereño-Orbea, 2013).

Limited proteolysis of the *full-length* enzyme yields the `catalytic core' of CBS (amino acid residues 40-413). The reduction in size is accompanied by a significant increase in the specific activity of the enzyme and a change in its oligomerization state. In particular, removal of the regulatory *C*-terminal regulatory domain leads to a dimer with increased activity (four-fold higher k_{cat}) unable to bind AdoMet. The *truncated* form of

CBS (45 kDa) lacking the *C*-terminal domain is a dimer which does not exhibit the aggregating properties which make physical studies on the wild-type *full-length* protein (63 kDa) difficult (Meier, 2001).

Regulation of enzymatic activity and cross-talk between gasotransmitters

The regulation of the enzymatic activity of *h*CBS is physiologically relevant (see *Metabolic disease* and *Cancer*) (Banerjee, 2003). The effectors and mechanisms involved in the activity modulation are reported below.

Pyridoxal-5'-phosphate (PLP)

The pyridoxal-5'-phosphate (PLP) is present under two tautomeric forms; enolimine and ketoimine (Garret, 1998). The pyridoxal-5'-phosphate (PLP)-dependent enzymes catalyse several metabolically critical transformations including trans-aminations and crucial reactions in the metabolism of amino acids and amino sugars. Members of this protein family share a common first reaction step: the formation of an aldimine intermediate (*via* Schiff base) between the PLP cofactor and the substrate (e.g., the α-amino group of amino acids) (Toney, 2012). Following this initial step, each enzyme catalyses specific reactions, such as α- and β-decarboxylation, racemization, transamination, aldolic reaction, β- and γ-elimination, etc.

(Toney, 2012). *h*CBS belongs to the β-family of the PLP-containing enzymes which are typically able to catalyze β-replacement or β-elimination reactions (Meier et al., 2001). In CBS, the PLP is deeply buried between the *N*- and *C*-terminal domains, and the active site is accessible only *via* a narrow channel. The cofactor is linked to the protein through the ε-amino group of Lys119 forming a Schiff base named `internal aldimine' (*fig. 4*). The nitrogen of the pyridine ring generates a hydrogen bond with the Oγ of serine 349 (Ser349). Another hydrogen bond is formed between the 3'-hydroxyl group of PLP and the $N_{\delta 2}$ of asparagine 149 (Asn149). The phosphate binding loop is located between β-strand 8 and α-helix 8 and forms an extended hydrogen bonding network with several amino acid residues, including threonine 257 (Thr257) and threonine 260 (Thr260) (Meier, 2001).

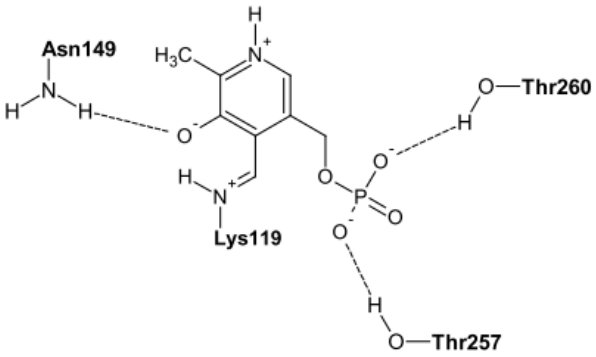

Figure 4. PLP in the CBS catalytic site.

In the presence of the substrate (serine or cysteine), the formation of a new aldimine intermediate (*via* Schiff base) between the PLP and the aminoacidic substrate (L-homocysteine) takes place. The protonation of the Schiff base, stabilized by a hydrogen bond with the oxygen of the ring, leads to increased acidity of the proton linked to Cα. The ketoenamine is key to PLP reactivity because, when its imine bond is protonated, it facilitates the nucleophilic attack by serine or cysteine. (1). The carbanion forming by the loss of hydrogen bond to Cα is stabilized by electronic delocalization on the pyridinic ring, where the positive charge on the nitrogen atom trapped the electrons (2). The β-elimination of the β -OH group of serine (or β-SH group of cysteine) leads to formation of the amino acrylate intermediate and elimination of one molecule of H_2O (or H_2S) (3). The carbon atom in β position of the amino acrylate intermediate undergoes nucleophilic attack by homocysteine generating cystathionine (4) that is eventually released (5) (*fig. 5*) (Weeks, 2009)

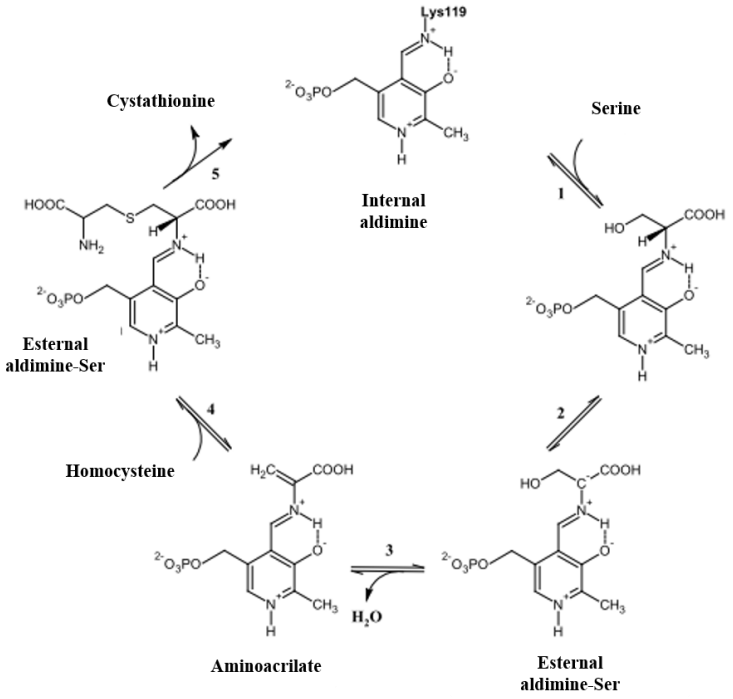

Figure 5. Reaction mechanism of CBS. Image adapted from (Weeks, 2009).

S-adenosyl-L-methionine (SAM or AdoMet)

Full-length CBS contains a *C*-terminal regulatory domain of ~140 residues, including the so-called `CBS domain' or 'Bateman domain' of 53 residues (Bateman, 1977). The *C*-terminal domain of CBS contains an autoinhibitory region harbouring the active site upon binding of the allosteric activator AdoMet (Ereño-Orbea et al., 2014). The *C*-terminal regulatory domain occludes the entrance to the catalytic site of the complementary monomer (*fig. 6*). Therefore, removal of the regulatory region in the truncated dimeric CBS leads to increased activity (Ereño-Orbea, 2014).

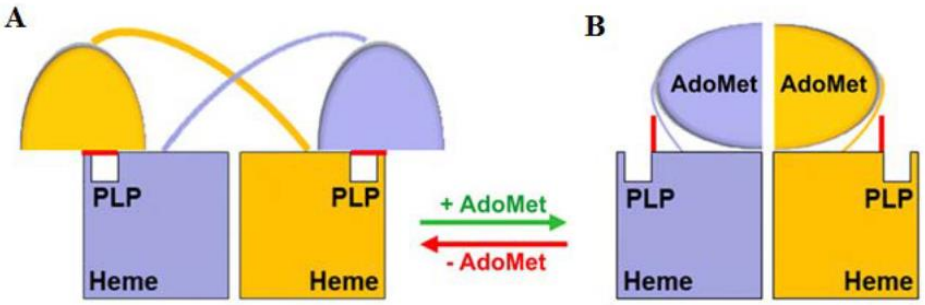

Figure 6. Mechanism of CBS allosteric regulation by AdoMet. Image from (Ereño-Orbea, 2014).

The presence of pathogenic missense mutations in this region often does not impair enzyme activity, but typically interferes with the binding of AdoMet and/or the enzyme activation by AdoMet (see *Metabolic diseases*) (Mendes, 2014).

Heme

In *h*CBS, the heme has been proposed to act not only as a redox sensor able to bind exogenous ligands (CO and NO) and modulate CBS activity (reviewed in Singh, 2010), but also to structurally stabilize CBS and improve its folding (Oliveriusova, 2002). The B-type heme of *h*CBS is in a

hydrophobic pocket located in the *N*-terminal domain between the α-helices 6 and 8. The heme iron, both in oxidized (FeIII) and reduced (FeII) state, coordinates the four pyrrolic rings of the protoporphyrin IX cofactor, whereas axially it binds the imidazolic nitrogen atom of histidine 65 (His65) and the thiolate moiety of cysteine 52 (Cys52), generating a low-spin hexacoordinate complex with octahedral geometry (Taoka, 2001). The enzyme is fully active when the heme is in the ferric state (FeIII), whereas heme reduction has been reported to promote a slow inactivation of the enzyme, that has been attributed to a ligand switch process (Cherney, 2007). Notably, the CBS heme in the reduced state is able to bind the gasotransmitters NO and CO resulting in a reversible inhibition of the enzyme (Vicente, 2014; Taoka, 2001). The communication between the heme and PLP active site has been attributed to molecular interactions with the α-helix 8 (Singh, 2010). As previously reported, the heme axially binds Hys65 and Cys52. The cysteine 52 establishes electrostatic interactions with arginine 266 (Arg266) at the end of this helix. Upon reduction, the heme increases its affinity for exogenous ligands, like CO and NO (Weeks, 2009). Moreover, AdoMet was found to further increase the CO affinity of the ferrous heme in human CBS (Vicente, 2016). Despite the low redox potential (-350mV) of the *full-length* CBS heme (Singh, 2010), in the presence of NADPH the human enzyme methionine synthase reductase (MSR) is able to catalyze the reduction of the CBS heme

in vitro. This finding shows that reduction of the CBS heme may occur under physiological conditions (Kabil, 2001), making the enzyme susceptible to inhibition by the other gasotransmitters *in vivo*.

CO inhibition

CO binding to ferrous CBS is characterized by two dissociation constants, K_{d1} =0.7–1.5 μM and K_{d2}= 45–68 μM (Taoka, 1999), attributed to differences in the heme microenvironment (Taoka, 1999) and/or an anti-cooperative effect between adjacent monomers within a functional CBS dimer (Puranik et al., 2009). The reaction follows a biphasic time course with a major slow phase, the rate constant of which is hyperbolically dependent on CO concentration yielding a limiting value k_{lim}= 0.012 – 0.017 s^{-1}. This rate constant has been attributed to the slow rate-limiting dissociation of the endogenous Cys52 thiolate ligand from the ferrous heme iron (Puranik, 2009).

NO inhibition

NO binds to ferrous CBS at rates orders of magnitude higher than CO, and it dissociates from the ferrous heme iron much more slowly than CO (Vicente, 2014). Altogether, these data show that CBS has a higher affinity for NO than for CO. The kinetics of NO binding is not limited by the off-rate

of the Cys52 ligand and NO was proposed to initially attack the Fe from the His65 side, rather than from the Cys52 side (Vicente et al., 2014).

O_2 binding

The ferrous heme [Fe(II)] of CBS can be rapidly oxidized by O_2. Under normoxic conditions, the protein with ferric heme [Fe(III)] is a target of Lon protease, one of the most expressed protease at the mitochondrial level involved in the regulation of the mitochondrial protein turnover. Under hypoxic condition, the Lon protease does not bind ferrous CBS [Fe(II)], determining an accumulation of the CBS inside mitochondria (see *Hypoxia* and *Synthesis*) (Teng, 2013).

Heme spectral properties

Upon reduction, the Soret band of the CBS heme shifts from 428 nm to 449 nm. On CO binding to the ferrous CBS heme, the band further shifts to 422 nm, resulting in a hexacoordinate ferrous-CO adduct with the endogenous Cys52 ligand displaced. NO binding to ferrous CBS results instead in a notable broadening of the Soret band, accompanied by an intensity decrease and a shift to ~395 nm, which have been attributed to formation of a high-spin pentacoordinate ferrous- NO adduct with both endogenous ligands displaced (Vicente, 2014; Taoka, 2001).

2.1.2 H_2S production by the gut microbiota

The gut microbiota is a major source of H_2S. In particular, anaerobic sulfate-reducing bacteria produce sulfide from the metabolism of dietary proteins in the lumen of the human large intestine (reviewed in Blachier, 2010; Carbonero, 2012). Approximately, one millimolar has been reported for the total sulfide content, but a much lower value (60 μM) has been reported for free H_2S. Due to the potentially toxic sulfide levels, colonocytes have been adapted in order to neutralize the sulfide content and, therefore, show an unusually high sulfide oxidizing activity (Goubern, 2007; Lagoutte, 2010; Leschelle, 2005) (see *Mitochondrial H_2S oxidation in colonocytes*). Alterations of H_2S metabolism in colonocytes are associated to pathological condition discussed in *H_2S and colorectal cancer* (Carbonero, 2012).

2.2. Catabolism

As H_2S is an important signalling molecule exerting dose- and time-dependent biological effects, the balance between hydrogen sulfide synthesis and consumption rates plays a critical role in the maintenance of cellular homeostasis (Módis, 2014; Szabo, 2014). H_2S, is the only gasotransmitter

that is enzymatically catabolised (Hildebrandt & Grieshaber, 2008) by two different pathways: it can be oxidized inside the mitochondria (Jackson, 2012) or it can enter the cytosolic methylation pathway (Weisiger 1980).

2.2.1. Mitochondrial H_2S oxidation - Enzymes and pathways

Oxidative phosphorylation: a brief overview

The oxidative phosphorylation takes place at the inner mitochondrial membrane where the four complexes (I-IV) of the electron transport chain (ETC), as well as the electron transporters coenzyme Q (CoQ) and cytochrome *c* (cyt *c*), and the ATP synthase, are located. The oxidative phosphorylation couples the electron flux derived from the oxidation of NADH and succinate, with the ADP phosphorylation, thus generating ATP. In a first step, electrons transported by NADH and succinate are transferred to Complex I (NADH:ubiquinone dehydrogenase) or Complex II (succinate dehydrogenate or SDH) and subsequently, through Complex III (cytochrome bc_1 or ubiquinol:cytochrome *c* reductase), cytochrome *c* and Complex IV (cytochrome *c* oxidase or CcOX), are then transferred to the final acceptor, molecular O_2. The process is overall accompanied by the vectorial translocation of 10 protons (for one molecule of NADH) or 6 protons (for

one molecule of succinate or $FADH_2$) from the mitochondrial matrix side to the intermembrane space. The electron transport chain contributes to the formation of an electro-chemical gradient across the inner membrane which generates the proton motive force (PMF) used by ATP synthase (ATPase or complex V) to generate ATP from ADP and P_i (2.5 molecules of ATP *per* NADH or 1.5 molecules of ATP *per* $FADH_2$) (Nicholls & Ferguson, 2013). More recent studies have shown that the oxidation of H_2S is associated with the concomitant injection of electrons into the mitochondrial electron chain, thus sustaining the electron flow and promoting the ATP synthesis at lower concentrations of sulfide (Goubern, 2007).

Hydrogen sulfide catabolic pathway

The mitochondrial sulfide oxidation pathway is involved in the breakdown of sulfide, with the concomitant stimulation of mitochondrial respiration (Goubern, 2007) (*see Bioenergetics*). The pathway has been initially identified in the lugworm *Arenicola marina* (Hildebrandt and Grieshaber, 2008). This enzymatic system responsible for H_2S metabolism at the mitochondrial level, also named *sulfide-oxidizing unit* (SOU), couples the oxidation of 2 sulfide molecules with the consumption of 1.5 molecule of oxygen (Goubern, 2007; Lagoutte, 2010). The system comprises the

mitochondrial inner membrane-associated enzyme sulfide:quinone oxidoreductase (SQR) and the mitochondrial matrix-localized enzymes persulfide dioxygenase or ethylmalonic encephalopathy 1 (ETHE1), thiosulfate sulfurtransferase or Rhodanese (TST or Rhod) and sulfite oxidase (SOx). Overall the pathway oxidizes H_2S leading to formation of a variety of species, including sulfite (SO_3^{2-}), thiosulfate ($S_2O_3^{2-}$), sulfate (SO_4^{2-}) and glutathione persulfide (GSSH) (Kabil & Banerjee, 2014; Libiad, 2014; Szabo, 2014).

The first step of sulfide metabolism is catalysed by sulfide:quinone oxidoreductase (SQR). In the catalytic site of SQR, a reactive cysteine disulphide transfers a sulfur atom derived from H_2S to glutathione (GSH) generating glutathione persulfide (GSSH). Concomitantly, the sulfide-derived electrons are transferred *via* a flavin adenin dinucleotide (FAD) moiety to coenzyme Q, thus leading to injection of two electrons into mitochondrial chain and reduction of 0.5 molecule of O_2 to H_2O by CcOX. The sulfur-acceptor has been a topic of discussion in the literature (Jackson, 2012; Libiad, 2014): it was proposed to be reduced glutathione (GSH), sulphite (SO_3^{2-}) or an unknown acceptor. Recently, GSH has been proposed as the preferred sulfur acceptor for SQR-mediated H_2S oxidation under physiological conditions (Libiad, 2014). Indeed, increased GSH synthesis by administration of the cysteine precursor *N*-acetylcysteine improves H_2S

clearance in patients with ethylmalonic encephalopathy caused by mutation in the ETHE1 gene, implicating GSH as the persulfide carrier in the sulfide oxidation pathway (Tiranti, 2009).

$$H_2S + GSH \xrightarrow{SQR} GSSH$$

Subsequently, the persulfide dioxygenase (ETHE1), a mononuclear non-heme iron enzyme structurally belonging to the family of metallo-β-lactamases, uses O_2 as co-substrate to convert the GSSH into sulfite and GSH. GSSH and sulfite are further converted into thiosulfate and GSH by thiosulfate sulfur transferase (Rhod). Rhodanese has a single redox-active cysteine in the active site and catalyses several reactions involving numerous substrates, but the generation of thiosulfate appears to be the most catalytically favourable reaction at physiologically relevant substrate concentrations (Kabil & Banerjee, 2014; Libiad, 2014).

$$GSSH + O_2 + H_2O \xrightarrow{ETHE1} SO_3^{2-} + GSH$$

$$SO_3^{2-} \xrightarrow{SOX} SO_4^{2-}$$

The last step in the sulfide oxidation pathway is catalysed by sulfite oxidase (SOx, Fig. 1B) (Johnson-Winters, 2010).

$$GSSH \xrightarrow{TST} S_2O_3^{2-}$$

Overall, the mitochondrial SOU couples the oxidation of two H_2S with the consumption of 1.5 molecules of O_2: the stoichiometry is thus 1.5/2 = 0.75, as reported by Laguette and co-workers (Lagoutte, 2010).

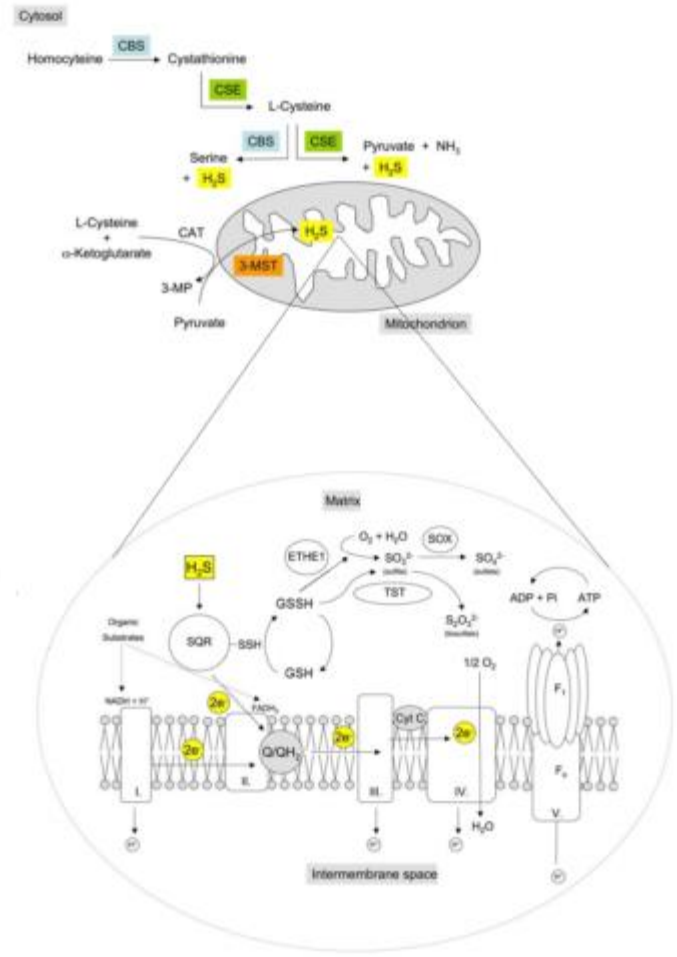

Figure 7. Hydrogen sulfide synthesizing-enzymes, Sulfide-oxidizing unit (SOU) and electron transport chain (ETC). Image from (Szabo, 2014).

A large variety of mammalian cell types (including colonocytes, macrophages, hepatocytes, neurons, etc.) have been assayed for their ability to consume H_2S at the mitochondrial level (Goubern, 2007; Lagoutte, 2010; Mimoun, 2012), revealing a large variability among cell types in terms of SOU activity. The activity is high in cells physiologically exposed to relatively high H_2S levels, such as colonocytes, but absent or hardly detectable in other cell types, such as neuroblastoma or other nervous system-derived cell lines (Lagoutte, 2010).

2.2.2. Mitochondrial H_2S oxidation in colonocytes

The gut microbiota produces sulfide in a concentrations ranging from high micromolar to low millimolar as reviewed in (Blachier, 2010) (see *H_2S production by the gut microbiota*). The effect of sulfide on the metabolism of colonocytes was studied in the HT29 cell line derived from human colon cancer (Leschelle, 2005). After 24 hours exposure to high levels of sulfide (1 mM), HT29 cells have shown a general suppression of mitochondrial bioenergetics (decreased CcOX activity and increased proton leak), enhanced anaerobic glycolysis (decreased cell proliferation and increased lactate release) and unchanged K_i of cytochrome *c* oxidase (0.3 μM). Therefore,

colonocytes appear well adapted to the sulfide-rich colon environment in that they are able to neutralize the exogenous sulfide (Leschelle, 2005; Szabo, 2014). When sulfide exposure is maximal, indeed, complex I, complex II and SQR compete for coenzyme Q. However, according to the redox conditions, Complex I can work in a reverse mode in the presence of sulfide (Leschelle, 2005). This process appears to be specific to colonocytes (Lagoutte, 2010). In a previous study, reversal of Complex II activity was also suggested (Goubern, 2007). When Complexes I or II operate in reverse mode, oxidation of sulfide is favoured as these repiratory complexes can accept electrons from coenzyme Q, even in the presence of severe CcOX inhibition by high sulfide concentrations. The impact of these reverse reactions on ATP production is null or negative; indeed, reversal of Complex I activity would cause uncoupling (Lagoutte, 2010). However, when complete inhibition of Complex IV takes place, the cell must use anaerobic glycolysis to produce energy (Szabo, 2014).

3. Physiological and pathological role of H_2S

Hydrogen sulfide (H_2S) has emerged as an important signalling molecule. The lipid-soluble nature of H_2S allows it to target a large variety of proteins in different cellular compartments. Due to its chemical versatility,

H_2S can interact with protein sulfhydryl groups and metals (reviewed in (Wallace & Wang, 2015). Hydrogen sulfide, therefore, has unique properties that make it a selective and powerful modulator of a large range of biological targets, with stimulatory or inhibitory effects.

3.1. H_2S, a Janus-faced molecule

At low (nM) concentration H_2S ensures anti-inflammatory, anti-oxidant and cytoprotective responses, whereas at higher (μM) concentrations it can lead to toxicity and eventually cell death. Indeed, high levels of H_2S promote pro-inflammatory pathways and inhibit CcOX, thus blocking the electron transfer through the respiratory chain with the induction of pro-oxidant and DNA-damaging effects eventually culminating in cell death (Kimura, 2015; Wallace & Wang, 2015). Furthermore, H_2S has a very interesting dual role on vascular remodelling. It was indeed reported to induce smooth muscle relaxation in the portal vein and the thoracic aorta, associated with opening of ATP-sensitive K^+ channels. However, H_2S pre-treatment was also found to induce vasoconstriction by scavenging endothelial NO. The response of blood vessels to H_2S depends on the vessel type, exposure time and concentration. Another variable that influences the effects of H_2S on the smooth muscle of blood vessels is O_2, with low and

high concentrations inducing vasodilation and vasoconstriction, respectively (see *Hypoxia*) (Kabil, 2014; Wallace & Wang, 2015). However, the major and perhaps most interesting dual role induced by sulfide is the one exerted on cell bioenergetics.

3.2. Bioenergetics

3.2.1. H_2S as mitochondrial substrate or inhibitor

In mitochondria, H_2S exerts a dual effect on cell bioenergetics. At high (high μM) concentration, it blocks mitochondrial respiration by inducing a potent, reversible and non-competitive inhibition of complex IV (C*c*OX) (Cooper & Brown, 2008); at the opposite, at lower concentrations (from high nM to low μM), H_2S is a substrate for most mitochondria (see *Mitochondrial H_2S oxidation*) (Goubern, 2007; Lagoutte, 2010), thus stimulating cell respiration. H_2S has therefore been recognized as the first inorganic substrate used by mitochondria to generate ATP (Yong and Searcy, 2001). This makes H_2S a very interesting molecule from a bioenergetic viewpoint, able to induce opposite effects on mitochondrial respiration depending on its bioavailability.

H_2S as a mitochondrial substrate

The first evidence for mitochondrial sulfide oxidation associated with oxygen consumption and ATP synthesis was obtained by investigating the invertebrate *Solemya reidi* (Powell and Somero, 1986). Following this observation, Bouillaud and co-workers have reported the first evidence of sulfide stimulation of energy metabolism in a human cell model (human colon adenocarcinoma cell lines) (Goubern, 2007). As described above (see *Mitochondrial H_2S oxidation*), H_2S oxidation by the sulfide-oxidizing unit (SOU) occurs with the injection of electrons in the ETC. The major contribution of this pathway to cellular bioenergetics arises from the SQR-catalysed reduction of coenzyme Q.

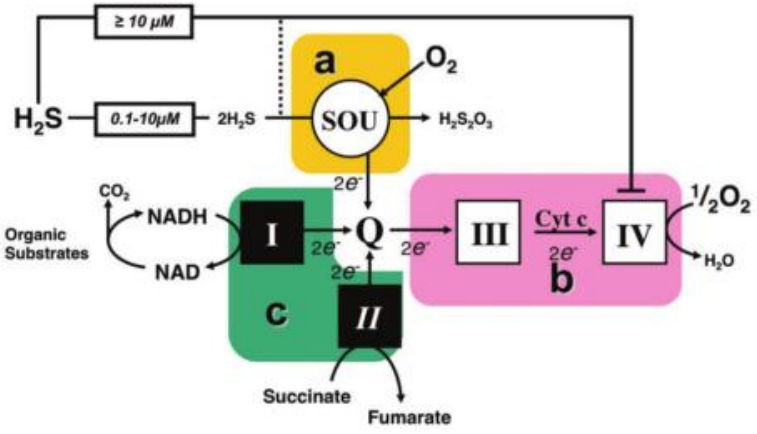

Figure 8. Scheme of sulfide oxidation. Complexes of the mitochondrial respiratory chain are numbered with roman numerals. H_2S can either induce a stimulation of electron flow *via*

SQR in the SOU or inhibit mitochondrial oxygen binding at Complex IV, thereby stopping electron flow. Image from (Szabo et al., 2014).

That sulfide-derived electrons enter the mitochondrial respiratory chain at the level of coenzyme Q is demonstrated by the finding that, whereas inhibition of Complex I with rotenone has not effect on sulfide catabolism, inhibition of Complex III or Complex IV by antimycin A or cyanide, respectively, blocks mitochondrial sulfide oxidation (Goubern, 2007). Complexes I and II therefore compete with SQR for the reduction of coenzyme Q, while complexes III and IV are required for sulfide oxidation. Interestingly, the maximal rate of sulfide oxidation was found to increase with cell differentiation (Mimoun, 2012) and a maximal rate of sulfide oxidation approaching the theoretical limit was observed, under which condition all the electrons travelling in the respiratory Complexes III–IV are expected to come from H_2S *via* SQR.

Biological relevance

Compared to other substrates of the mitochondrial respiratory chain, H_2S oxidation has a relative low energetic yield, due to the relatively high cost in terms of oxygen [injection of electrons into coenzyme Q is associated

with the consumption of additional O_2 by ETHE1 (Hildebrandt and Grieshaber, 2008)] and the low contribution in terms of electrons injected into respiratory chain. On the other hand, H_2S diffuses freely across cell membranes, it does not need any 'biochemical preparation' (which has an energy cost), the affinity of SQR for sulfide is high and, in addition, in the gut an abundant sulfide production occurs with no energy cost. All that guarantees that sulfide oxidation takes place with high efficiency at low concentrations of sulfide, thereby preventing its toxic accumulation (Szabo, 2014). Additionally, sulfide was suggested to serve as an 'emergency' substrate. Indeed, although in terms of quantitative bioenergetics it is clearly inferior to carbon metabolism, under physiological or stress conditions, H_2S production by endogenous enzymes can contribute to cellular bioenergetics (Fu, 2012; Goubern, 2007). A bioenergetic role has been clearly demonstrated for 3-MST, the enzyme that is responsible for the majority of mitochondrial H_2S production, which shows preferential mitochondrial localization as described above (see *Synthesis*). The role of 3-MST in the regulation of cellular bioenergetics is supported by a large body of evidences (Módis, 2013). SQR silencing suppresses both basal and 3-MP mediated stimulation of bioenergetic function (Módis, 2013). Interestingly, oxidative stress impairs the bioenergetic role of 3-MST (Módis, 2013). Also CSE and CBS contribute to the physiological regulation of bioenergetic function, since

the H_2S produced in cytosol by these enzymes can freely diffuse across the cell. Additionally, since the distribution of both CSE and CBS is cell type- and tissue-dependent, effects of CBS/CSE are also cell type- and organ-dependent. Under conditions of cell dysfunction (such as hypoxia), CSE sustains cellular bioenergetics by translocating to the mitochondria (Fu, 2012), while in colon cancer cells (HCT116 cell model) it is the endogenous H_2S production by CBS that supports cellular bioenergetics and cell proliferation (Szabo, 2013). Intriguingly, CBS was also found to accumulate in mitochondria under hypoxic/ischemic conditions (see *Cancer* and *Hypoxia*), although the physiological relevance of this process needs to be established.

H_2S as a mitochondrial inhibitor

Sulfide inhibition of isolated mitochondrial CcOX is reversible, potent (K_i = 0.2 μM at pH 7.4) and non-competitive in that H_2S affects the enzyme V_{max}, but not the K_M for O_2 (Petersen, 1977). Interestingly, sulfide inhibition of CcOX is pH dependent, the K_i dropping from 2.6 μM to 0.07 μM as the pH decreases from 8.05 to 6.28 (Nicholls, 1982). Consistently, CcOX inhibition by sulfide is more effective under acidosis conditions (Szabo, 2014), probably because under these conditions H_2S prevails over the

HS− form. The active site of CcOX, being located in an apolar environment, is expected to preferentially bind electroneutral species, such as H_2S, or proton-neutralized anionic species ($HS^- + H^+$) (Rich, 1996), both favoured at lower pH. (Nicholls, 2013). H_2S inhibits CcOX with a low K_i value. This notwithstanding, inhibition of respiration in isolated mitochondria or intact cells requires much higher H_2S concentrations (µM, see (Leschelle, 2005). The sulfide-mediated inhibition of CcOX leads to decreased electron flow through the ETC and thus to a decline in ATP production (Hill, 1984). This effect has been well documented both *in vivo* and in cell models (Leschelle, 2005). The inhibitory effect has been observed at 10-100 µM H_2S depending on the experimental approach. Indeed, quantitative information on sulfide oxidation and related bioenergetic effects was often obtained in these studies by supplying sulfide at selected injection rates rather than as a single bolus, an approach reviewed in (Abou-Hamdan, 2015). After tissue homogenates exposure to a single bolus of NaHS, the complex I activity has been shown to return to its original level within 10-30 min. Due to the opposite effects of sulfide on mitochondrial respiration, stimulation of oxygen consumption and mitochondrial energization is best appreciated at low sulfide concentrations, non-inhibitory towards CcOX (Abou-Hamdan, 2015).

3.3. Cancer

Recent studies revealed increased expression of various hydrogen H_2S-producing enzymes in colon, ovarian, prostate and breast cancer cells (reviewd in Szabo, 2013), and a new role of H_2S in cancer has emerged (Chao 2016; Hellmich & Szabo, 2015; Szabo, 2015). H_2S seems to have a dual role also in the cancer, promoting angiogenesis and proliferation and sustaining cellular bioenergetics or, at the opposite, displaying a cytotoxic effect and becoming deleterious for the tumour cell at higher concentration (Szabo, 2014a) (see *H_2S metabolism as drug target)*.

3.3.1. H_2S in colorectal cancer (CRC)

Colonocytes are exposed to high levels of H_2S produced by the gut microbiota (Blachier, 2010). These cells therefore show efficient systems to metabolize H_2S (Lagoutte, 2010). On the other hand, high levels of H_2S in the gut have been associated to ulcers, chronic inflammation, DNA damages and colon cancer (CRC- colorectal cancer) (Carbonero, 2012). In particular, tissues isolated by patients with CRC display a reduced expression of Rhod, one of the enzymes involved in sulfide catabolism, underlining the importance of the role of H_2S metabolism in CRC (Ramasamy, 2006). More recent studies have shown in cancer cells an over-expression of the H_2S-generating enzyme CBS and a functional role of CBS-derived H_2S, which

promotes proliferation through the stimulation of cellular bioenergetic at both mitochondrial and cytosolic level (Hellmich & Szabo, 2015; Szabo, 2013; Szabo & Hellmich, 2013). In the mitochondrion, H_2S acts as a metabolic 'fuel' injecting electrons into mitochondrial chain (Szabo, 2013; Szabo & Hellmich, 2013), whereas in the cytosol, hydrogen sulfide stimulates the glycolytic activity (Mustafa, 2010).

Additionally, inhibition (with aminooxiacetic acid, AOAA) or silencing of CBS in colon cancer cells HCT116 decreases bioenergetic functions *in vitro*. Implantation into the mice of CBS-silencing colon cancer cells, reduces tumour growth and inhibits peritumour angiogenesis (Szabo, 2013) *in vivo*. Furthermore, interestingly, inhibition (with AOAA) or silencing of CBS also sensitizes the cancer cells to chemotherapy (Chao & Zatarain, 2016; Chao, 2014). In colon cancer cell lines SW480, instead, high expression levels of CSE were observed. Inhibition (with propargylglycine, PAG) or silencing of CSE in SW480 cell lines reduces the proliferation *in vitro* and tumour growth *in vivo* (Fan, 2014).

Therefore, H_2S produced by CBS or CSE promotes bioenergetics, proliferation, migration, invasiveness, and neoangiogenesis, thus creating the ideal conditions for tumour cell survival (Cai, 2010; Hellmich & Szabo, 2015; Szabo & Hellmich, 2013). Following these studies, scientific interest in

H_2S metabolism has increased in the perspective of developing new pharmacological interventions in the therapy of cancer (Hellmich, 2015).

3.4. Hypoxia

Hypoxia is a common factor of the microenvironment of solid tumours that is associated to drug-resistance and malignancy (reviewed in Muz, 2015). Under hypoxic conditions a central role is played by the hypoxia inducible factor (HIF) which appears to be directly involved in the up- or down-regulation of key enzymes in pathways implicated in cancer metabolism and thus in cell survival (Semenza, 2013). The relationship between hypoxia and metabolic reprogramming in cancer has been widely reported and is reviewed in (Masson & Ratcliffe, 2014).

3.4.1. H_2S as an oxygen sensor

The interplay between the two gaseous molecules H_2S and O_2 has been thoroughly investigated (reviewed in Olson, 2015; Wu, 2015). H_2S mimics hypoxia-induced responses like vasodilation (Zhao, 2001), neo-angiogenesis (Papapetropoulos, 2009) and the expression of HIF-1a (Beaumont, 2016). Furthermore, the H_2S levels proved to be regulated by the O_2 concentration in tissues. Olson et al. proposed a model in which both cytosolic synthesis and mitochondrial oxidation of sulfide are regulated in an

O_2-dependent manner (Olson, 2015). The higher H_2S levels in hypoxic/ischemic conditions is primarily due to the over-expression and/or activity stimulation of the H_2S-synthesizing enzymes (Takano, 2014; Kolluru, 2015). Under hypoxic conditions both CBS and CSE were shown to display increased activity due to release of CO inhibition, following activity down-regulation of the isoform 2 of heme-oxygenase (enzyme involved in the heme degradation generating CO) (Morikawa, 2012; Yuan 2015). Hypoxia also leads to the translocation of CSE from the cytosol to mitochondria, where CSE uses approximately three-fold higher concentrations of L-cysteine to produce H_2S (Fu, 2012). In addition, whereas under normoxic conditions CBS is degraded inside mitochondria by Lon protease, upon hypoxic stress Lon protease cannot recognize the deoxygenated/ferric haem group in CBS, and therefore CBS is not degraded. This leads to accumulation of CBS in the mitochondrion and increased mitochondrial H_2S levels (Teng, 2013). The enhanced production of H_2S occurring under hypoxia may be interpreted as a mechanism to ensure H_2S-mediated protection against ischemia injuries and against the cytotoxic and inflammatory damages induced by hypoxic conditions (Takano, 2014; Kolluru, 2015; Morikawa, 2012; Hine, 2016). Enhanced H_2S levels proved to be a compensatory response to hypoxia promoting vasodilation (Yuan, 2015; Morikawa, 2012) in many O_2 sensitive tissues. On the other hand, hypoxia

makes complex IV more sensitive to H_2S inhibition (Matallo, 2014; Abou-Hamdan, 2016) and induces notable metabolic changes: it enhances anaerobic glycolysis and reduces mitochondrial mass and activity (as a result of enhanced mitophagy and reduced mitochondrial biogenesis) (Solaini, 2010; Zhang 2008, Wu 2015), thus shifting the action of H_2S from protective to detrimental.

3.5. Metabolic diseases

Alterations of H_2S metabolism are also involved in pathological metabolic dysfunctions (Wallace & Wang, 2015), like lipid metabolism disorders, liver diseases, diabetes and homocystinuria. The role of hydrogen sulfide metabolism in homocystinuria is reported below.

3.5.1. H_2S in hyperhomocysteinaemia and homocystinuria

Hyperhomocysteinemia is a clinical metabolic condition characterized by elevated homocysteine plasma levels which have been linked to a variety of human diseases, including heart attack, stroke and osteoporosis. The major causes of hyperhomocysteinaemia are deficiencies in vitamins B4, B9 and B12 and mutations in the genes encoding 5-methyltetrahydrofolase or CBS (Maron and Loscalzo, 2009). CBS is involved in the trans-sulfuration pathway of methionine and H_2S metabolism and regulates both homocysteine

and H_2S levels in the human body (see *Synthesis*). Banerjee and collaborators, have demonstrated that the H_2S generation catalysed by cystathionine γ-lyase (CSE) increases progressively with the grade of hyperomocysteinemia. Indeed, at severely elevated homocysteine (200 mM), both α–, γ-elimination (*reaction 5*) and the γ–replacement (*reaction 4*) reactions of homocysteine catalysed by CSE lead to the generation of H_2S with concomitant production of homolanthionine and lanthionine, respectively. The elevated H_2S production by CSE may contribute to the hyperhomocysteinemia-associated cardiovascular disturbances. Based on these data, the inhibition of CSE has been suggested as a pharmacological strategy to treat hyperhomocysteinemia, and homolanthionine and lanthionine were proposed as novel biomarkers of the disease (Chiku, 2009)

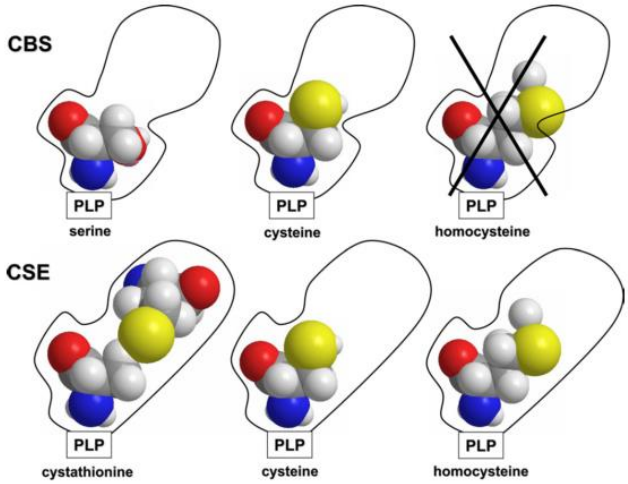

Figure 9. Proposal mechanism for the CSE selective affinity for homocysteine. Image from (Chiku, 2009).

Classical homocystinuria (OMIM#236200) is an inborn error of metabolism associated with mutations in the in CBS gene. It has a variable incidence of 1:1.800 to 1:900.000 and is biochemically detected by markedly high homocysteine and methionine levels in plasma and urine. The clinical presentation includes complications in the vascular, neurological and skeletal systems (Mudd, 1975) and an oxidative stress condition due to the high plasmatic levels of homocysteine. The major therapeutic approach for classical homocystinuria consists in dietary methionine restriction and administration of pyridoxine (vitamin B6), a precursor of the PLP cofactor essential for CBS activity (Mudd, 1975). However, a significant part of patients (approximately half) does not respond to this treatment (Schiff & Blom, 2012). The CBS mutations identified in patients with classical homocystinuria are often missense mutations resulting in single amino acid substitutions which often affect the enzyme folding and/or activity (Hnízda, 2012). Additionally, some of these mutations have been shown to affect the positive allosteric regulation of CBS by AdoMet, pointing to such dysregulation as a new pathogenic mechanism in classical homocystinuria (Mendes, 2014). A novel therapeutic approach is currently under development based on enzyme replacement therapy using PEGylated recombinant CBS (Bublil, 2016).

4. New pharmacological strategies in cancer

4.1. H_2S metabolism as drug target

CBS has recently emerged as a drug target in cancer (Druzhyna, 2016). CBS-derived H_2S was indeed shown to play a key role in the survival and proliferation of tumour cells. Different strategies have been proposed for the treatment of cancer, based on the dual effect of sulfide on cell bioenergetics. The dose-dependent effect of H_2S on cancer has been demonstrated in colon adenocarcinoma cell lines using increasing concentration of H_2S in the presence or absence of aminooxiacetic acid (AOAA), an inhibitor of CBS (*fig. 10*). These studies showed enhanced cell proliferation induced by H_2S, the effect being related to the balance between endogenous and exogenous H_2S.

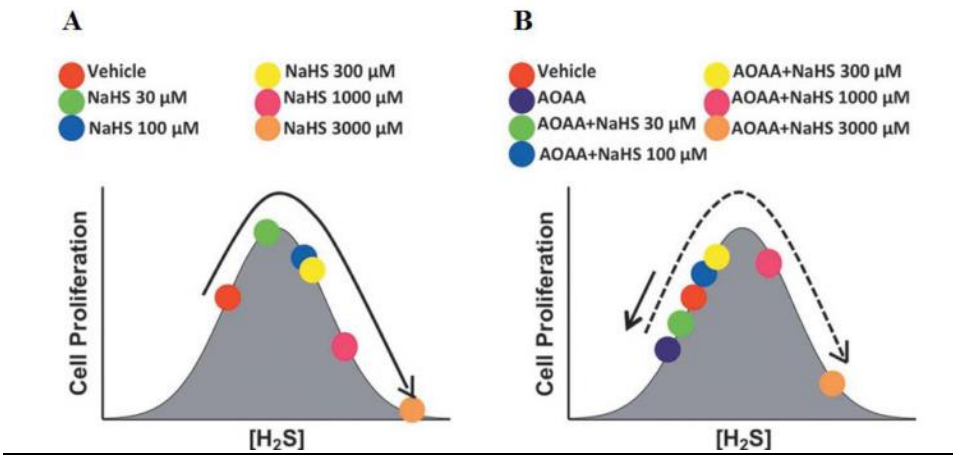

Figure 10. Biphasic (bell-shaped) dose-response of H_2S on tumour cell proliferation. Image from (Hellmich, 2015).

Based on these studies two possible pharmacological approaches, both aiming to reduce the cell proliferation, seem applicable: i) increasing the H_2S production using either H_2S-donors or inhibitors of the H_2S-consuming enzymes, or ii) reducing the H_2S generation using inhibitors of H_2S-synthesis enzymes (Chao, 2016, Chao, 2014; Asimakopoulou, 2013; Druzhyna, 2016; Hellmich, 2015).

4.2. Ferritin-based nanoparticles as a new drug delivery system

Ferritin

Ferritin (Ft) is a member of the iron storage protein family with ubiquitous distribution among all life forms, except in yeast (Crichton & Boelaert, 2009). Ft consists of 24 subunits forming a globular shell-like protein containing a cavity with external and internal diameters of 12 nm and 8 nm, respectively (Harrison & Arosio, 1996). Each subunit is folded in four-helical bundle, formed by four antiparallel helices (A-D, named in order from the amino terminus) and a shorter helix on the top (E).

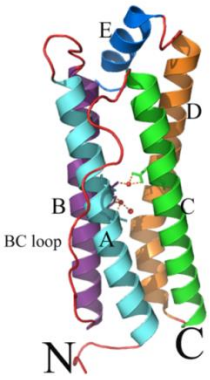

Figure 11. Monomeric subunit fold of human H ferritin.

The N-terminal ends of each subunit are located on the ferritin surface, with the C-termini pointing toward the inner cavity of the protein.

The protein coat is perforated by several small channels, formed by subunits with 3- or 4-fold symmetry, which traverse the protein cage and allow the passage of ions and small molecule.

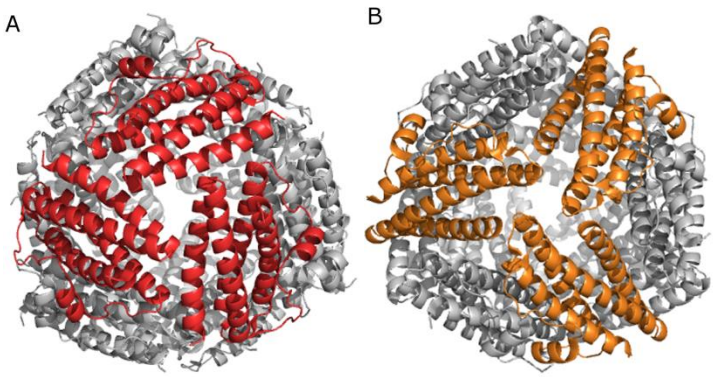

Figure 12. Quaternary structure of ferritin from *Pyrococcus furiosus* (PDB code: 2JD7).

A. View along the four-fold axis. **B.** View along the three-fold axis.

In particular, three-fold pores are involved in the uptake of ferrous iron [Fe (II)]. The pores expose negatively charged residues generating a negative electrostatic gradient thanks to which iron enters the channel and binds the catalytic sites, named ferroxidase sites, where it is oxidized by molecular oxygen (O_2) to ferric iron [Fe (II)]. Ferric iron then moves to the iron nucleation sites where Fe(III)-mineral formation takes place. When the Fe(III)-mineral reaches a sufficient size, Fe(II) atoms can also be oxidized directly on the surface of the growing mineral. The cavity may contain up to

4.000 iron atoms, often stored as ferric oxy-hydroxide mineral, while the ferritin without loaded iron is also referred as apoferritin (Ceci, 2012).

All animal ferritins are assembled from two subunit types, the heavy (H chain; 21 kDa) and light chains (L chain; 20 kDa); H chains contain the catalytic centres and are more abundant in tissues with an active iron metabolism. L chains contain many nucleation sites and are more abundant in iron storage tissues like spleen.

Drug delivery and Ferritin-based nanoparticles (NPs)

Heavy human protein ferritin (HFt) is an intriguing system for biotechnology applications for the outstanding features described below (Heger, 2014; Lee, 2016; Truffi, 2016).

HFt is an ideal nanocarrier for human applications *in vivo*, being a natural self-constituent present both inside the cells and in the bloodstream; therefore, it shows high solubility, biocompatibility, biodegradability and, additionally, a high stability in a large range of temperature (up 80°C) and pH (2-10) (Jain, 1999). Moreover, HFt dimensions (<20 nm) increase the chances of passing human body barriers and reaching specific targets since HFt is small enough to penetrate tumor capillary fenestrations and large

enough to avoid rapid clearance through the kidney. Of particular relevance, especially in view of potential applications in cancer therapy, is the ability of HFt to be easily internalized by many types of protein- and iron-avid cancer cells. (Li, 2010). Additionally, HFts are an ideal template for encapsulation of several compounds inside their internal cavity (Zhen, 2013; Falvo, 2013; Fan, 2012, Vannucci, 2012; Uchida, 2006; Fantechi, 2014). HFt can be produced at low cost and high yield through recombination techniques, the uniformity of the quaternary structure guarantees a high homogeneity in both size and shape and, furthermore, the interior of the cage provides an isolated environment, protected from bulk solution, where chemical reactions can take place. Generally, the method used for nanoparticles (NPs) formation is based simply on the addition of various ions or small molecules to apoferritin under specific oxidizing (O_2 or H_2O_2) or reducing ($NaBH_4$) conditions, allowing the diffusion inside the protein. An alternative approach was reported to incorporate metal particles and other compounds that cannot pass through the ferritin channels. According to this method, the protein cage is reversibly disassembled in acidic conditions (~ pH 2.0) and the compounds are passively encapsulated within the cavity by raising the pH to neutral values (Kim, 2011). Using this method, several diagnostic agents (Truffi, 2016; Fan, 2012) and drug molecules were encapsulated in ferritin, such as cisplatin,

doxorubicin, curcumin, methylene blue, etc (Xing, 2009; Blazkova, 2013; Ma-Ham, 2011; Simsek & Kilic, 2005; Cutrin, 2013).

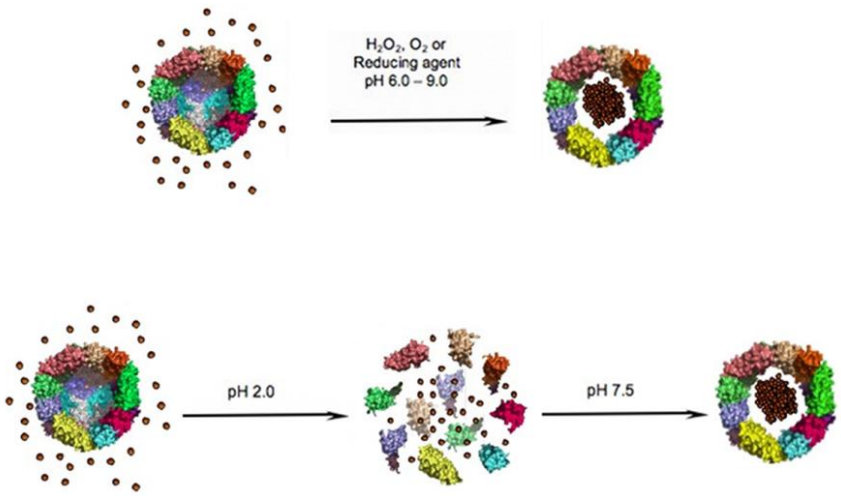

Figure 13. Schematic illustration of nanoparticles synthesis using ferritins as nano-reactors.

HFt possesses all features necessary to operate as an appropriate platform for specific cell targeting/delivery discriminating healthy from cancerous cells (Schoonen, 2014). HFt has indeed an exterior surface which can be easily functionalized through genetic engineering and/or chemical conjugation. For instance, short peptide and antibodies recognizing specific cell receptors, can be genetically conjugated with the N-terminal region of HFt (Vannucci, 2012). A breakthrough in the ferritin-based drug delivery field was recently reported by Li et al. (Li, 2010). They discovered that HFt

(but not LHFt) has the ability to effectively bind cancer cells and be internalized using the transferrin receptor 1 (TfR1) (Li, 2010). TfR1 is up-regulated on the surface of many cancer types (such as colon, liver, lung, pancreas, cervical, ovarian, prostate, breast, sarcoma and thymus cancer), reaching up to 100-fold higher levels than in normal cells. HFt was shown to be internalized by TfR1 in more than 474 clinical tissue specimens and specifically recognize several types of tumor over non-tumor tissues with 98% sensitivity and 95% specificity (Fan, 2012). The high expression of TfR1 in cancer could arise from the high demand of DNA synthesis in these rapidly dividing cells through the ribonucleotide reductase enzyme. This enzyme needs iron as a cofactor providing a plausible explanation for the high expression of TfR1 in tumor cells (Daniels, 2006). In addition, two papers by (Zhang, 2015) and (Bellini, 2014) underline the selective capability of HFt, but not LFt, to shuttle doxorubicin (DOXO) molecules to the cell nucleus. In this case, HFt nanocages loaded with DOXO could behave like a "Trojan horse": called back within the nucleus for the purpose of defense given its the well-known HFt antioxidant activity, HFt releases instead the cytotoxic anticancer drug directly into the most effective site of action (*fig.14*).

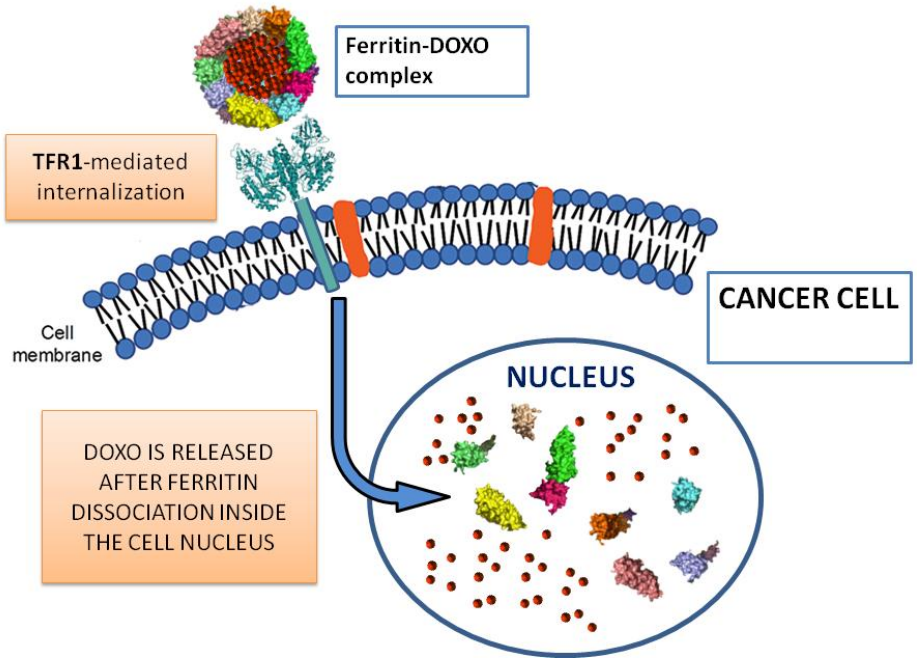

Figure 14. Schematic representation of the nuclear delivery of DOXO by HFt complexes.

Despite the several advantageous features, HFt half-life in plasma after systemic injection may be too short (i.e., ~ 2 hours; Worwood, 1982) to attain sufficient accumulation at the tumour level. Although HFt was reported to bind and encapsulate some types of drugs, both the yields and stability of the resulting ferritin-drug complexes were not satisfactory. During the last three years ferritin-doxorubicin complexes have been obtained by several groups, mostly by performing reversible, pH-dependent HFt dissociation (pH 2) and reassociation (pH 7.5) in the presence of the drug. Typically, this process resulted in the loss of more than 50% of the starting protein material and an average of 25-30 doxorubicin molecules encapsulated within each protein

cavity. Moreover, more than 30% of the drug leaked by the first week of storage, indicating that the stability of the ferritin-doxorubicin complexes is quite low for drug development purposes. (Zhen, 2013; Liang, 2014; Bellini, 2014; Gumulec, 2014; Zhang, 2015; Kilic, 2012). Recently, Falvo *et al*. have developed a novel HFt-based construct in order to increase the *in vivo* half-life and the stability of HFt-drug complexes, called HFt-MP-PAS, suitable for drug delivery. In this construct the *N*-terminus of each HFt subunit is genetically fused to: i) a PAS polypeptide sequence, *i.e.*, a sequence rich in proline (P), alanine (A) and serine (S) residues; (Fracasso, 2016; Falvo, 2016) and ii) a tumor-selective sequence (MP) responsive to proteolytic cleavage by tumour proteases (MMPs), inserted between each HFt subunit and the outer PAS polypeptide (Fracasso, 2016). The exposed unstructured polypeptide PAS was used to increase ferritin stability during the pH jump (2.0-7.5) step occurring in the drug-encapsulation reaction, and has also the advantage of extend the HFt plasma half-life, eliminating the disadvantages occurring in the case of protein-PEGylation for following biopharmaceutical development and production (Schlapschy, 2013; Harari, 2014). The PAS shield was aimed at hampering the interaction between drug-loaded HFt and TfR1 in healthy tissues and reducing internalization by normal cells, already limited by the low expression of the receptor. The MP sequence allows the PAS shield to be selectively removed by stimuli present in the tumour microenvironment, *i.e.*,

metalloproteinases (MMPs) specific for this sequence. In particular, MMP-2 and MMP-9 have been recognized as key MMPs over-expressed at the tumor microenvironment and involved in tumor angiogenesis, invasion, and metastasis (Rundhaug 2003) so that the resulting unmasked HFt can freely interact with and be internalized by TfR1 overexpressed in cancer cells. The HFt-MP-PAS constructs proved to i) encapsulate in the internal cavity three times more doxorubicin (DOXO) than wild-type HFt, ii) form more stable complexes (*i.e.*, drug leakage was negligible) and iii) possess higher *in vivo* circulation time. Importantly, DOXO-loaded HFt-MP-PAS (HFt-MP-PAS-DOXO) displayed excellent therapeutic efficacy in a human pancreatic cancer model *in vivo,* significantly increasing overall animal survival (Falvo 2016). The nanocarriers efficacy was even superior to the novel albumin-based DOXO delivery system (INNO-206), currently in phase III clinical trials, ascribing to the PAS shield the increase in DOXO encapsulation, protein-drug complex stability and circulation time with respect to HFt. The higher *in vivo* efficacy of HFt-MP-PAS-DOXO with respect to other DOXO delivery systems is likely due to both effective PAS removal by tumour specific MMPs and efficient DOXO delivery into the cell nucleus, as revealed by confocal microscopy studies (Falvo, 2016).

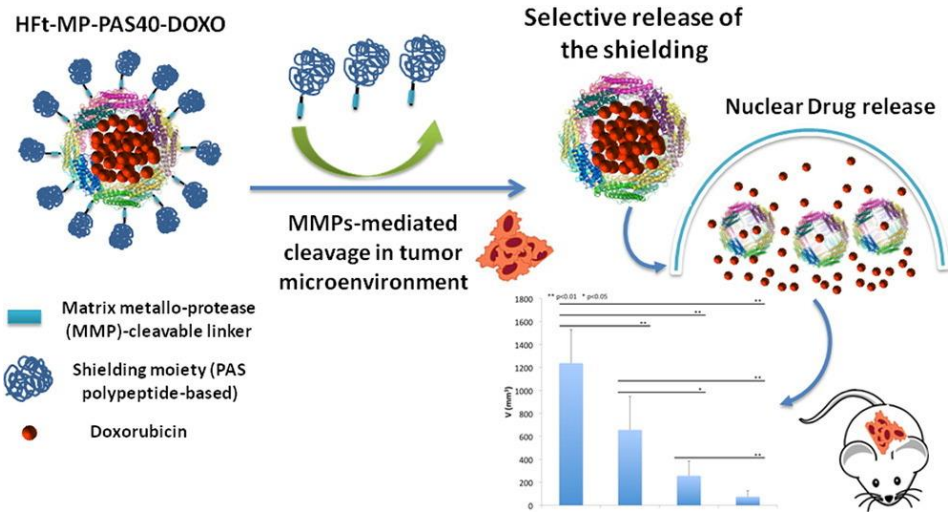

Figure 15. HFt-MP-PAS40-DOXO. Image from (Falvo 2016).

RESULTS AND DISCUSSION

Paper 1

Bioenergetic Relevance of Hydrogen Sulfide and the Interplay Between Gasotransmitters at Human Cystathionine β-synthase[1]

João B. Vicente[1,#], Francesca Malagrinò[2], Marzia Arese[2], Elena Forte[2], Paolo Sarti[2], Alessandro Giuffrè[3,#]

[1] *Instituto de Tecnologia Química e Biológica António Xavier, Universidade Nova de Lisboa, Av. da República (EAN), 2780-156 Oeiras, Portugal*
[2]*Department of Biochemical Sciences and Istituto Pasteur-Fondazione Cenci Bolognetti, Sapienza University of Rome, Piazzale Aldo Moro 5, I-00185 Italy*
[3]*CNR Institute of Molecular Biology and Pathology, Piazzale Aldo Moro 5, I-00185 Rome, Italy*

[#] **To whom correspondence should be addressed**:
- Dr. Alessandro Giuffrè, Institute of Molecular Biology and Pathology (IBPM), National Research Council of Italy (CNR), Piazzale Aldo Moro 5, I-00185 Rome, Italy. Phone: +39-06-49910944; Fax: +39-06-4440062; Email: alessandro.giuffre@uniroma1.it;
- Dr. João B. Vicente, Instituto de Tecnologia Química e Biológica, Universidade Nova de Lisboa, Av. da República (EAN), 2780-156 Oeiras, Portugal. Phone: +351-214469662; Fax: +351-214433644; Email: jvicente@itqb.unl.pt

Abstract

Merely considered as a toxic gas in the past, hydrogen sulfide (H_2S) is currently viewed as the third 'gasotransmitter' in addition to nitric oxide

[1] **Abbreviations:** H_2S, hydrogen sulfide; NO, nitric oxide; CO, carbon monoxide; CcOX, cytochrome *c* oxidase; CBS, cystathionine β-synthase; AdoMet, S-adenosyl-L-methionine; CGL, cystathionine γ-lyase; PLP, pyridoxal 5'-phosphate; MST, 3-mercaptopyruvate sulfurtransferase; CAT, cysteine aminotransferase; 3-MP, 3-mercaptopyruvate; SOU, sulfide oxidizing unit; SQR, sulfide:quinone oxidoreductase; GSH, reduced glutathione, GSSH, glutathione persulfide; ETHE1, persulfide dioxygenase; Rhod, rhodanese; SOx, sulfite oxidase; FCCP, *p*-trifluoromethoxyphenylhydrazone, MSR, methionine synthase reductase; AOAA, aminooxyacetic acid; AdoHcy, S-adenosyl-L-homocysteine.

(NO) and carbon monoxide (CO), playing a key signalling role in human (patho)physiology. H_2S can either act as a substrate or, similarly to CO and NO, an inhibitor of mitochondrial respiration, in the latter case by targeting cytochrome *c* oxidase (CcOX). The impact of H_2S on mitochondrial energy metabolism crucially depends on the bioavailability of this gaseous molecule and its interplay with the other two gasotransmitters. The H_2S-producing human enzyme cystathionine β-synthase (CBS), sustaining cellular bioenergetics in colorectal cancer cells, plays a role in the interplay between gasotransmitters. The enzyme was indeed recently shown to be negatively modulated by physiological concentrations of CO and NO, particularly in the presence of its allosteric activator S-adenosyl-L-methionine (AdoMet). These newly discovered regulatory mechanisms are herein reviewed.

Keywords

Sulfide metabolism, gasotransmitters, mitochondrial respiration, cytochrome *c* oxidase, cystathionine β-synthase, heme chemistry

1. Hydrogen sulfide synthesis and breakdown in human physiology

Hydrogen sulfide (H_2S) has emerged in the past decades as the third recognized 'gasotransmitter' in human physiology. Much like its 'predecessors' nitric oxide (NO) and carbon monoxide (CO), H_2S was historically considered a poisonous gas that was subsequently discovered to be endogenously synthesized to fulfil a myriad of signalling and regulatory functions [1-4]. This colourless gas with a strong characteristic odor (the smell of rotten eggs) is slightly polar, which allows it to freely diffuse across biological milieu, including membranes. In aqueous solution, H_2S equilibrates with hydrosulfide (HS^-) and sulfide (S^{2-}), according to the pK_{a1} ~7.0 (H_2S/HS^-) and pK_{a2} ~19 (HS^-/S^{2-}) measured at 25°C. At a 'physiological' pH of 7.4, HS^- is the predominant species (70-80%) and H_2S occurs at 20-30%, whereas S^{2-} is supposedly present in negligible amounts [3, 5, 6]. Unless otherwise stated, the terms 'H_2S' and 'sulfide' are herein employed interchangeably to collectively indicate the H_2S/HS^- pair.

H_2S has a dose-dependent effect on multiple physiological processes, acting as a signalling molecule (mostly resulting in persulfidation of cysteine residues in proteins [4, 5, 7]) and a bioenergetic 'fuel' at low concentrations, and displaying deleterious effects at high concentrations. Although the *in vivo* free H_2S levels in mammalian physiology are difficult to estimate and remain a matter of debate, it is presently accepted that high nanomolar to low micromolar concentrations may occur under non-pathological conditions [8]. Disturbances in H_2S metabolism either impairing or enhancing H_2S production and/or breakdown are currently and growingly associated with many pathological conditions, ranging from cardiovascular [9] and neurodegenerative diseases [10] to cancer [11].

H_2S is generated in humans via two major routes: ubiquitous endogenous enzymes (described below) and the gut microbiota, particularly

sulfate-reducing bacteria. The three major human enzymes recognized as endogenous H_2S sources are the methionine cycle transsulfuration pathway enzymes cystathionine β-synthase (CBS) and cystathionine γ-lyase (CGL), and the 3-mercaptopyruvate sulfurtransferase (MST) (Figure 1A) [1, 12]. Whereas CBS and CGL are both pyridoxal 5'-phosphate (PLP)-dependent enzymes, MST has a single redox-active cysteine residue in the active site. As mentioned above, both CBS and CGL participate in the transsulfuration pathway of methionine metabolism. Therefore, their physiological relevance is both set on homocysteine homeostasis and on H_2S generation [13]. Indeed, both enzymes produce H_2S via reactions that are 'alternative' to their historically-considered canonical activities. The CBS canonical activity concerns the condensation of serine and homocysteine into cystathionine and water, but the enzyme can also use cysteine alone or together with homocysteine to generate H_2S and different co-products [13] (Figure 1A). Similarly, CGL, whose canonical reaction is the conversion of cystathionine into cysteine with the production of α-ketobutyrate and ammonia, can generate H_2S from cysteine and/or homocysteine [13] (Figure 1A). This seemingly catalytic promiscuity may be viewed as a robust system to ensure H_2S generation from different substrate combinations and under several physiological conditions. MST functions together with another enzyme, cysteine aminotransferase (CAT), which converts cysteine and α-ketoglutarate into glutamate and 3-mercaptopyruvate (3-MP), the latter used as a substrate for the MST-catalyzed H_2S production [1]. An additional pathway has been recently demonstrated involving MST, where 3-MP alternatively derives from D-cysteine and a D-amino acid oxidase [14]. In terms of cellular localization, the classical view is that CBS and CGL are cytosolic enzymes, whereas MST is located in the mitochondria. However, there are numerous exceptions where both CBS and CGL can be found in

mitochondria and MST in the cytosol, which preclude taking a firm position in this regard. Examples of CBS localization in the mitochondria and its impact on cellular bioenergetics and mitochondrial function are detailed below.

As any other potentially toxic gaseous molecule endogenously synthesized with signalling purposes, H_2S levels must be kept under strict control. Indeed, as reviewed in [1, 15], human cells are equipped with an H_2S breakdown enzymatic system associated to the mitochondria (Figure 1B), initially identified in the lugworm *Arenicola marina* [16], and more recently denoted as 'sulfide oxidizing unit' (SOU) [17]. The enzymatic unit comprises a sulfide:quinone oxidreductase (SQR), a persulfide dioxygenase (also known as ETHE1 or sulfur dioxygenase), a thiosulfate sulfurtransferase (rhodanese) and a sulfite oxidase (SOx), that overall catalyze the breakdown of H_2S to thiosulfate and sulfate, the main sulfide catabolites (Figure 1B). A more detailed description of the mitochondrial SOU is given in section 2.3,

2. Hydrogen sulfide and mitochondrial respiration

As a common feature, the three gasotransmitters NO, CO and H_2S can all inhibit mitochondrial cytochrome *c* oxidase (CcOX), causing a decline in the electron flux of the respiratory chain and thus in ATP synthesis (reviewed in [18], Figure 2). NO can also inhibit Complex I *via* S-nitrosation [19-22], the inhibition being dependent on a reversible conformational change of the enzyme [23]. More recent studies, however, have shown that, unlike the other two gasotransmitters, at low concentrations (nanomolar to low micromolar) H_2S can also stimulate mitochondrial respiration by acting as a mitochondrial electron donor [17, 24-30] (Figure 2). This makes H_2S a very interesting molecule from a bioenergetic viewpoint, able to induce opposite effects on

mitochondrial respiration depending on its bioavailability (reviewed in [8, 15, 31, 32]).

2.1 H_2S as an inhibitor of mitochondrial respiration

Cytochrome c oxidase (CcOX), considered as the main target of gasotransmitter-mediated inhibition of mitochondrial respiration, is inhibited by the three gasotransmitters with different kinetics [18]. CO acts a simple competitive inhibitor, lowering the enzyme K_M for O_2 by binding at the O_2-reactive, fully-reduced heme a_3-Cu_B active site ([33], Figure 3). CcOX inhibition by NO is more complex (reviewed in [34-39]). It can proceed through two alternative reaction pathways [40-45], one competitive and the other uncompetitive towards O_2, i.e., leading to a decrease of both V_{max} and K_M for O_2 yet keeping their ratio unchanged [46, 47]. The O_2-competitive pathway, prevailing at higher electron flux and lower O_2 levels, leads to an adduct of CcOX with NO bound to ferrous heme a_3, whereas the O_2-uncompetitive one, favoured at lower electron flux and higher O_2 levels, results into the formation of an inhibited state of the enzyme with nitrite bound to ferric heme a_3 ([18, 44, 46, 48], Figure 3).

Differently from CO and NO, H_2S was reported to be a non-competitive inhibitor of isolated mitochondrial CcOX [49], i.e., affecting the enzyme V_{max}, but not the K_M for O_2. The inhibition is reversible, potent (K_i = 0.2 μM at pH 7.4) and independent of oxygen concentration [49]. Interestingly, sulfide inhibition of CcOX is pH dependent, the K_i dropping from 2.6 μM to 0.07 μM as the pH decreases from 8.05 to 6.28 [50]. Consistently, CcOX inhibition by sulfide is more effective under acidosis conditions (see [8, 31] and references therein). Although the effect of pH has not been investigated in mechanistic details, the enhanced inhibition is likely

related to the fact that H_2S, with its pK_a of ~ 7.0, prevails over HS^- in acidic conditions. The active site of CcOX, being located in an apolar environment, is indeed expected to preferentially bind electroneutral species, such as H_2S, or proton-neutralized anionic species ($HS^- + H^+$) [51], both favoured at lower pH. Sulfide inhibition of isolated mitochondrial CcOX is not only effective, but also relatively fast, proceeding with an initial rate constant of 2.2×10^4 M^{-1} s^{-1}, as measured at pH 7.4 with the enzyme in turnover with O_2 in the presence of ascorbate and cytochrome *c* [52]. Unlike NO and CO [53], H_2S does not bind ferrous heme a_3. The inhibited enzyme displays sulfide bound to ferric heme a_3 (Figure 3), preventing the reaction with O_2 and thus leading to electron accumulation at the Cu_A and heme *a* sites [54, 55]. Based on electron paramagnetic resonance (EPR) spectroscopy [56], Cu_B in sulfide-inhibited CcOX was suggested to be in the cuprous state, possibly bound to a second H_2S molecule (Figure 3), with a substantial increase of the reduction potential. The mechanism of inhibition is only partly understood. H_2S was suggested to bind the enzyme in turnover at cupric or cuprous Cu_B to be transferred intramolecularly to ferric heme a_3, leading to enzyme inhibition [52].

2.2 H_2S oxidation by mitochondrial cytochrome c oxidase

Somewhat similarly to the other two gasotransmitters, H_2S is not only an inhibitor, but it can also serve as a reducing substrate for CcOX [50, 52, 57]. Besides being able to slowly oxidize CO to CO_2 [58, 59] and much more quickly NO to nitrite [42, 60, 61], CcOX can also oxidize sulfide probably to a persulfide species [50, 52, 57]. Sulfide directly reacts with the oxidized heme a_3-Cu_B active site in the so-called 'pulsed' state of the enzyme [52]. This state is obtained by subjecting to a reduction/oxidation cycle the

'resting' enzyme, much less reactive with external ligands. This 'pulsing' procedure has been discovered in 1977 by Antonini and co-workers [62]. It remains to be demonstrated whether the enhanced reactivity of 'pulsed' CcOX towards H_2S arises from Cl^- dissociation from the active site, as previously shown for NO [63]. With pulsed CcOX, in the absence of reducing substrates, the heme a_3-Cu_B site is directly reduced by low sulfide levels and the produced ferrous heme iron under aerobic conditions is promptly converted into a ferryl state, optically resembling the 'P' catalytic intermediate [52]. This species eventually decays slowly (tens of seconds) into the 'F' ferryl form of the enzyme by reacting with residual sulfide or by auto-reduction [52]. The physiological relevance of this CcOX-mediated oxidative degradation of H_2S remains to be determined, because mitochondrial SQR seems to provide a very effective H_2S dissimilatory pathway, probably out-competing the H_2S-metabolizing activity of CcOX. Finally, it is worth mentioning that H_2S can also directly reduce cytochrome *c* [50]. The reaction, however, is probably too slow and with too low affinity to have a physiological relevance, although to our knowledge it has not been investigated yet with cardiolipin-bound cytochrome *c*, much more reactive towards external ligands [64].

2.3 H_2S as an effective substrate of the mitochondrial respiratory chain

Despite the low K_i value measured with isolated CcOX (K_i = 0.2 μM at pH 7.4 [49]), inhibition of respiration in isolated mitochondria or intact cells requires much higher H_2S concentrations (micromolar to tens of micromolar, see for instance [65, 66]). This finding is fully consistent with the observation that H_2S at relatively low concentrations (nanomolar to low micromolar) also acts as an effective substrate of the mitochondrial respiratory chain. Evidence for mitochondrial sulfide oxidation associated

with oxygen consumption and ATP synthesis was first obtained by investigating the invertebrate *Solemya reidi* [24]. This is the first study in which the dual effect of H_2S on mitochondrial respiration, inhibitory at higher concentration and stimulatory at lower levels, was demonstrated. These initial observations were expanded in more recent studies conducted on isolated mitochondria as well as on permeabilized or intact cells from higher organisms, including human cell lines [17, 25-30]. Quantitative information on sulfide oxidation and related bioenergetic effects was often obtained in these studies by supplying sulfide at selected infusion rates rather than as a single bolus, an approach reviewed in [32]. Due to the opposite effects of sulfide on mitochondrial respiration, stimulation of oxygen consumption and mitochondrial energization is best appreciated at low sulfide concentrations, non-inhibitory towards CcOX.

Electrons derived from sulfide oxidation are accepted by coenzyme Q (Figure 2). Sulfide-stimulated oxygen consumption is indeed blocked by inhibitors of the bc_1 complex (antimycin) or of CcOX (cyanide), being unaffected by rotenone inhibition of Complex I [26, 65, 67, 68], except in colonocytes where Complex I has been suggested to work in a reverse mode [17, 26] (see section 2.4). Based on this and other evidence [16], the existence of a mitochondrial sulfide oxidizing unit (SOU) was envisaged [17]. In such unit the primary sulfide oxidizing enzyme is the membrane-associated sulfide:quinone oxidoreductase (SQR), having a cysteine disulphide in its active site and harboring a non-covalent flavin adenine dinucleotide moiety from where sulfide-derived electrons are transferred to coenzyme Q [69] (Figure 1B). H_2S oxidation by human SQR involves the transfer of a sulfur atom to an acceptor which has been a topic of discussion in the literature [70, 71]: it was proposed to be i) reduced glutathione (GSH) yielding glutathione persulfide (GSSH), ii) sulphite (SO_3^{2-}) yielding

thiosulfate ($S_2O_3^{2-}$) or iii) an unknown acceptor. Recently, it has been proposed that at physiological GSH and sulfite concentrations, GSH is the preferred sulfur acceptor for SQR-mediated H_2S oxidation [71]. The next step in the sulfide oxidation pathway is catalyzed by the persulfide dioxygenase ETHE1 (Figure 1B), a mononuclear non-heme iron enzyme structurally belonging to the metallo-β-lactamase family, which uses oxygen as a co-substrate for generation of sulfite from GSSH [71-73]. GSSH and sulfite are further converted into thiosulfate and GSH by rhodanese (Rhod, Figure 1B), having a single redox-active cysteine in its active site [71, 74]. Rhodanese catalyzes a myriad of reactions involving numerous substrates, but the transfer of a sulfur atom from GSSH to sulfite to generate thiosulfate appears to be the most catalytically favourable reaction at physiologically relevant substrate concentrations [71]. The last step in the sulfide oxidation pathway is catalyzed by sulfite oxidase (SOx, Figure 1B), a multi-domain cytochrome b_5 containing a molybdenum cofactor [75]. Electrons derived from sulfite are intramolecularly transferred through the heme cofactor to cytochrome *c*, while the oxygen atom is supplied by water, with concomitant production of sulfate (SO_4^{2-}) [75]. Overall, the mitochondrial SOU couples the oxidation of H_2S to thiosulfate and sulfate with the injection of electrons into coenzyme Q, leading to consumption of 0.79 O_2 per H_2S molecule oxidized, as reported by Goubern and co-workers [26].

Despite the apparent simplicity of the sulfide oxidation pathway herein described, the intricate sulfur chemistry and the remarkable substrate promiscuity of this pathway's enzymes allows one to envisage a number of alternative reaction pathways occurring under different (patho)physiological conditions. Irrespectively of the fate of sulfide-derived species, the major contribution of this pathway to cellular bioenergetics arises from the SQR-catalyzed reduction of coenzyme Q.

2.4 H_2S and cellular bioenergetics

A large variety of mammalian cell types (including colonocytes, macrophages, hepatocytes, neurons etc.) have been assayed for their ability to consume H_2S at the mitochondrial level [17, 26-29], revealing a large variability of this sulfide oxidizing activity between cell types. The activity is high in cells physiologically exposed to relatively high H_2S levels, such as colonocytes, but absent or hardly detectable in other cell types, such as neuroblastoma or other nervous system-derived cell lines. Moreover, for yet unknown reasons, in mitochondria isolated from animal organs, the SOU activity relative to the basal respiratory oxygen consumption is typically much less than measured in intact cultured cells. As discussed in [8], this has been tentatively ascribed to an up-regulation of the SOU enzymes and/or to a down-regulation of the respiratory enzymes in cultured cells, typically relying on glycolytic metabolism .

Particularly interesting is the case of colonocytes. It has long been known that the intestinal microbiota, especially abundant in the colon, represents a major source of sulfide. Consistently, in this tract of our gut, sulfide reaches particularly high levels: up to 60 μM free H_2S was reported in equilibrium with up to one millimolar total sulfide-derived species [76-79]. It is therefore not surprising that colonocytes exhibit a high sulfide oxidizing activity, even at such high sulfide levels inhibitory for CcOX [17, 26]. In these cells, when sulfide is oxidized, Complex I has been reported to work in a reverse mode, thus making oxidized coenzyme Q available for reduction by SQR, even in the presence of a severe CcOX inhibition [17, 26]. Thus, colonocytes appear well adapted to the sulfide-rich colon environment: they are able to extract energy from a bacterial metabolic waste (H_2S) and are

suitably equipped with an efficient dissimilatory system to prevent sulfide toxicity [76].

From the bioenergetic point of view and particularly in comparison with NADH oxidation, sulfide oxidation doesn't seem to be very efficient in terms of energy yield. This is not surprising as the oxidation of H_2S, while injecting electrons into coenzyme Q, is associated with the consumption of additional (with respect to the respiratory chain) O_2 by ETHE1 [16] (Figure 1B). Despite this low energy yield, as discussed in [8], H_2S has several advantages, namely over NADH. It freely diffuses across the membranes, without the need to be synthesized or transported inside mitochondria to feed the respiratory chain with electrons. In addition, H_2S is used with high affinity by SQR which ensures H_2S to be an effective respiratory 'fuel' at low, non-toxic concentrations. Last but not least, H_2S bioavailability inside the cell can be rapidly and finely controlled through regulation of the H_2S-synthesizing and -consuming enzymes (see below). Based on these properties, sulfide was suggested to serve as an 'emergency' substrate, particularly in some body regions and under specific physiological or stress conditions [8]. In this regard, it is intriguing that CGL, preferentially located in the cytosol, under cell dysfunction conditions translocates into the mitochondrion [80] and that under hypoxic conditions CBS does the same, exerting mitochondrial protective effects, as shown in cultured hepatocytes and liver tissue [81].

Several lines of evidence show that endogenously produced H_2S can contribute to cellular bioenergetics [29, 80, 82], but more work is needed in this direction. A bioenergetic role has been clearly demonstrated for MST [29]. Using cultured hepatoma cells and isolated rat liver mitochondria, low concentrations of the MST substrate, 3-MP, proved to lead to H_2S production and bioenergetic enhancement, and these effects proved to be mediated by

MST and SQR by gene silencing [29]. In contrast, under normal conditions, at least in vascular smooth-muscle cells, CGL does not seem to support cellular bioenergetics. It is worth noticing, however, that upon intracellular calcium loading, the enzyme translocates to the mitochondrion where it exerts positive bioenergetic effects under hypoxic conditions [80]. Regarding CBS, an *in vivo* bioenergetic role was envisaged in *Caenorhabditis elegans*, whose basal and maximal carbonyl cyanide *p*-trifluoromethoxyphenylhydrazone (FCCP)-stimulated oxygen consumption was shown to be attenuated by silencing a CBS homologue, the main H_2S-producing enzyme in this model organism [83, 84].

More recently, endogenous H_2S production by CBS was found to support cellular bioenergetics and cell proliferation in HCT116 colorectal cancer cells [82]. In these cells, CBS is selectively up-regulated (like in human colon adenocarcinoma specimens) and a significant fraction of the enzyme is associated to mitochondria. Moreover, as shown by CBS silencing or inhibition with aminooxyacetic acid (AOAA), the CBS-generated H_2S enhances cell proliferation and energy metabolism. Both oxidative phosphorylation and glycolysis proved to be stimulated by CBS-produced H_2S, the glycolytic pathway being presumably enhanced in response to sulfhydration and consequent activation of glyceraldehyde 3-phosphate dehydrogenase [85, 86]. Interestingly, AOAA, which has been reported to inhibit both CBS and CGL [87], decreased the migration and invasion of cancer cells, reduced the migration of endothelial cells co-cultured with colon cancer cells and, notably, affected the growth rate of both HCT116 and patient-derived tumour xenografts [82]. None of the effects described above was observed upon CGL silencing or pharmacological inhibition with the CGL-selective inhibitor propargylglycine, pointing to a specific role for CBS in colorectal cancer cell bioenergetics.

In summary, there is growing evidence that H_2S, depending on its bioavailability, can impact cellular bioenergetics by stimulating or inhibiting the mitochondrial respiratory chain and, under certain conditions, enhancing glycolysis. These functions of H_2S are interestingly intertwined with the action of the other two gasotransmitters CO and NO. Hence the relevance of shedding light into the molecular mechanisms controlling the cell bioavailability of H_2S and its cross-talk with the other gasotransmitters.

3. Gasotransmitters interplay at human cystathionine β-synthase

3.1. Cellular localization and structure of human CBS

CBS is a key enzyme of the transsulfuration branch of methionine metabolism, that plays a key role in mammalian physiology both contributing to homocysteine homeostasis and acting as a source of H_2S [13, 88, 89]. Whereas CBS is typically considered a cytosolic enzyme, its localization has been shown to vary in different (patho)physiological contexts. Microvascular endothelial cells and hepatocytes have been reported to secrete CBS and CGL, which circulate as part of the plasma proteome, generating H_2S from homocysteine, particularly when its concentration rises in human blood [90]. In endothelial cell models, exogenous H_2S afforded higher cell viability and decreased DNA oxidative damage upon serum starvation and hypoxia/reoxygenation. Moreover, immunoprecipitation of CBS and CGL from serum prior to its supplementation with homocysteine makes the serum more stressful for endothelial cells. These observations led to the proposal that secreted CBS and CGL ensure both the clearance of elevated homocysteine and the production of H_2S to exert a protective role in the endothelium [90]. CBS has also been shown to be a target for sumoylation, leading to accumulation of the protein in the nucleus, as associated with the nuclear scaffold [91]. Of greater relevance for the effect of H_2S on cell

bioenergetics and respiration, CBS can translocate to mitochondria in different (patho)physiological conditions. Teng and co-workers [81] reported partial localization of CBS to liver mitochondria, transiently enhanced under hypoxia/ischemia to protect mitochondria from oxidative stress through H_2S generation. CBS levels are restored upon return to normoxia, the protein degradation being mediated by the mitochondrial Lon protease, targeting specifically the CBS heme-binding domain in the oxidized (ferric) form [81]. Moreover, in the HCT116 colorectal cancer cell line, a significant fraction of the total cellular CBS is localized to the mitochondria, particularly associated with the outer mitochondrial membrane, where it was proposed to stimulate mitochondrial functions [82], as described above. Increased accumulation of CBS concurrent with elevated H_2S has been recently reported in mitochondria isolated from the spinal cord of a mouse model of amyotrophic lateral sclerosis, where the increased H_2S production was proposed to be associated with impaired cytochrome *c* oxidase-dependent respiration [92].

Each CBS monomer comprises a PLP-binding core catalytic domain and two flanking regulatory domains: an N-terminal heme-binding domain and a C-terminal domain which binds the allosteric activator S-adenosyl-L-methionine (AdoMet) (Figure 4) [93]. The PLP-binding catalytic core is characteristic of type II PLP-dependent enzymes [93, 94]. The C-terminal domain, structurally also known as "Bateman" module, comprises a pair of so-called CBS motifs able to accommodate AdoMet [94-96]. This domain has been suggested to be also responsible for enzyme tetramerization, its removal resulting in stabilization of a dimeric form of CBS unresponsive to AdoMet and displaying increased basal activity [97].

3.2. Properties of the heme moiety of human CBS

The heme in CBS constitutes an evolutionary milestone, since its harbouring domain is absent in protein homologues from unicellular eukaryotes. This low-spin hexacoordinate B-type heme, axially bound to His65 imidazole and Cys52 thiolate moieties (human CBS numbering), has been proposed to act not only as a redox sensor able to bind exogenous ligands (CO and NO), but also to structurally stabilize CBS and improve its folding [97]. Whereas the enzyme is fully active when the heme is in the ferric state, heme reduction by excess sodium dithionite (a strong reductant) has been reported to promote a slow enzyme inactivation (>20 minutes at 37°C), attributed to a ligand switch process [98]. Notably, the CBS heme in the reduced state is able to bind the 'gasotransmitters' NO and CO, resulting in a reversible enzyme inhibition (detailed below) [99-101]. The CBS heme has thus been considered a redox and ligand sensor able to modulate CBS activity (reviewed in [102]). The communication between the heme and PLP active site has been attributed to molecular interactions at either end of the α-helix 8 [103-105]. While at the heme end of this helix Arg266 establishes electrostatic interactions with the Cys52 thiolate, on the opposite end Thr257 and Thr260 are involved in a hydrogen-bond network with the PLP phosphate moiety (Figure 4). The role of these residues in communicating the heme redox and ligand state to the PLP site has been confirmed by functional and spectroscopic studies on clinically relevant site-directed variants of Arg266, Thr257 and Thr260 [103-105]. Although the CBS heme has a low reduction potential (ca. -350 mV, [103]), in the presence of NADPH the human enzyme methionine synthase reductase (MSR) has been shown to be able to catalyze its reduction *in vitro* and generate both the ferrous-CO and the ferrous-NO adducts [106, 107].

The UV-visible spectral changes associated with heme reduction and CO or NO binding to the reduced heme are depicted in Figure 5A. Upon

reduction, the Soret band of the oxidized heme centered at 428 nm is shifted to 449 nm (Figure 5A), similarly to the heme thiolate-containing cytochromes P450. Upon CO binding to the ferrous CBS heme, the band shifts to 422 nm (Figure 5A), resulting in a hexacoordinate ferrous-CO adduct with the endogenous Cys52 ligand displaced, as confirmed by Raman spectroscopy [108]. NO binding to ferrous CBS results instead in a notable broadening of the Soret band, accompanied by an intensity decrease and a blue shift to ~395 nm (Figure 5A), which have been attributed to formation of a high-spin pentacoordinate ferrous-NO adduct with both endogenous ligands displaced, as confirmed by EPR spectroscopy [101]. Despite the inhibitory effect of CO and NO on CBS, the enzyme activity is restored upon reoxidation by O_2 or potassium ferricyanide, both converting the CO or NO ferrous adducts to the ferric state [99, 101].

The kinetics of this interplay between the three 'gasotransmitters' has been investigated by a combination of static and stopped-flow absorption spectroscopy [100, 101, 106, 107, 109-111] .

3.3 Physiological relevance of CBS inhibition by NO and CO

The physiological relevance of CBS regulation by NO and CO has been attested by different lines of *in vivo* evidence. In mice experiencing renal ischemia-reperfusion, elevated NO levels have been shown to inhibit CBS, yielding an increase in homocysteine deleterious for the kidney [112]. Increased NO production by endothelial cells and macrophages during endotoxemia has been shown to result in mitochondrial dysfunction and elevated oxidative stress in adrenocortical cells, leading to adrenal insufficiency, whereas the adverse effects of increased NO were suppressed upon supply of an exogenous H_2S donor [113]. It was proposed that NO-mediated inhibition of CBS contributes to mitochondrial dysfunction and

impaired steroidogenesis in adrenal cortex during endotoxemia [113]. Cerebral vasodilation in a mouse model of hypoxia was reported to be associated with CO-mediated CBS regulation [114]. Under hypoxic conditions, the CO-producing oxygen sensor heme oxygenase HO-2 is down-regulated. The resulting decreased CO levels alleviate the CO inhibitory effect on CBS-catalyzed H_2S production, contributing to mediate vasodilation of precapillary arterioles [114]. Increased CO in the liver has been shown to cause a decrease in H_2S levels and a concomitant increase of bile output. These effects were observed in wild-type but not in heterozygous CBS knockout mice, leading to the proposal that CO inhibition of CBS-mediated H_2S production affords a control mechanism of bile excretion, at least in stressful and/or pathological conditions [115]. The relevance of CO inhibition of CBS activity has been attributed not only to its H_2S-generating ability, but also to its 'hinge' role between the remethylation and the transsulfuration pathways (reviewed in [116]). CBS inhibition by CO diverts homocysteine to the remethylation pathway (Figure 1A), making AdoMet more available for protein and nucleic acid methylation. On the other hand, an opposing effect produced by CBS inhibition arises from the accumulation of S-adenosyl-L-homocysteine (AdoHcy), an inhibitor of specific methyltransferases. This imbalance caused by CO inhibition of CBS has been shown to affect the global protein methylation status (e.g. causing hyper-methylation of histone H3), leading to the hypothesis that CBS inhibition by CO plays a role in the regulation of cancer cell survival [116, 117].

3.3.1 CO binding to human CBS

In the past few years, several groups (including ours) have thoroughly investigated *in vitro* CO and NO binding to the heme moiety of human CBS, to bring together the data acquired on the isolated enzyme with the *in vivo*

data supporting the physiological relevance of this regulatory mechanism. CO binding to ferrous CBS is characterized by two dissociation constants, K_{d1} = 0.7-1.5 μM and K_{d2} = 45-68 μM [100, 110, 111], attributed to differences in the heme microenvironment [100] and/or an anti-cooperative effect between adjacent monomers within a functional CBS dimer [108]. Overall CO binding has been reported to proceed with a C_{50} value of 29 ± 4 μM [111] and >30 μM (estimated from Figure 2 in [100]). The kinetics of CO binding to ferrous CBS was investigated by time-resolved spectroscopy [108, 110, 111]. Upon mixing ferrous CBS with CO solutions, formation of the ferrous-CO adduct occurs without optical evidence for reaction intermediates, as judged by global fit analysis. The reaction time course is at least biphasic (Figure 5B), with a major slow phase the rate constant of which is hyperbolically dependent on CO concentration, yielding a limiting value k_{lim} = 0.012-0.017 s^{-1} [108, 110]. As confirmed by laser flash photolysis time-resolved Raman spectroscopy, this rate constant has been attributed to the slow rate-limting dissociation of the endogenous Cys52 thiolate ligand from the ferrous heme iron [108]. The k_{off} of CO was found to be 0.5 ± 0.1 s^{-1} in stopped-flow displacement experiments carried out mixing the ferrous-CO adduct with an excess (0.1-1.9 mM, before mixing) of authentic NO [110].

3.3.2 NO is a quick and tight ligand of human CBS

NO binding to the reduced heme of human CBS has been initially reported to be characterized by a very low affinity (K_d value of 281 ± 50 μM), incompatible with a physiological relevance of this reaction [101]. In that study, however, the K_d for NO was likely overestimated because measurements were carried out using a slow NO releaser (diethylamine NONOate) in the presence of large excess of dithionite, which is known to promptly react with free NO. Using a different reduction system, involving

NADPH and human MSR, a ~10-fold lower K_d value was reported (30 ± 5 μM), still considered an upper limit for this dissociation constant, as it was measured in the presence of multiple equilibria (NADPH ↔ MSR ↔ CBS ↔ CBS-NO) [107]. More recently, employing authentic NO stock solutions and low dithionite concentrations to reduce CBS, a $K_d \leq 0.23$ μM was measured [110], fully compatible with a physiological role of this molecular interaction. Reduced human CBS, therefore, displays a much (>100-fold) higher affinity for NO than for CO.

Interestingly, NO binds ferrous CBS much more quickly than CO (Figure 5B). The kinetics of NO binding to ferrous heme in human CBS was analyzed by stopped-flow absorption spectroscopy [110]. No reaction intermediates were detected during the conversion of hexacoordinate ferrous CBS into the pentacoordinate ferrous-NO species. Overall, the reaction of reduced CBS with NO was significantly faster than with CO. As shown in Figure 5B, 500 μM CO requires ~10 minutes for conversion of ferrous CBS into the ferrous-CO adduct, whereas formation of the ferrous-NO adduct is complete within ~3 seconds after mixing ferrous CBS with 400 μM NO. Also differently from CO, the observed association rate constant for NO is linearly dependent on [NO] up to ~800 μM, yielding $k_{bim} = 8 \times 10^3$ M^{-1} s^{-1} [110]. NO dissociation kinetics was analyzed by the Moore and Gibson method [118], by mixing ferrous-NO CBS with a CO-saturated 200 mM dithionite solution. In accordance with the high affinity for NO, dissociation of this ligand occurred slowly, with a $k_{obs} = 0.003$ s^{-1} more than 100-fold slower than the CO off rate constant (0.5 ± 0.1 s^{-1}) [110].

Thus, NO binds to ferrous CBS at rates orders of magnitude higher than those observed for CO binding and it dissociates from the ferrous heme iron much more slowly than CO. Altogether, these data neatly fit with the much higher affinity for NO with respect to CO. From a mechanistic

viewpoint, the fact that kinetics of NO binding is not limited by the off-rate of the Cys52 ligand was taken as the evidence that NO initially attacks the Fe from the His65 side, rather than from the Cys52 side [110] (Figure 6). Moreover, since that reaction yields a pentacoordinate ferrous-NO adduct as the final product [101] with no evidence for a transiently generated hexacoordinate Cys-Fe-NO adduct, NO binding to the His side was suggested to cause a concomitant displacement of Cys52, at rates much higher than its intrinsic off rate (that instead limits CO binding). It remains to be established whether the NO bound in the final pentacoordinate adduct lays on the His or the Cys side. For NO to end up on the Cys side, an obligate hexacoordinate ferrous-dinitrosyl (NO-Fe-NO) species should form transiently during the reaction, as observed with other hexacoordinate heme proteins (e.g. bacterial cytochrome *c*' and heme NO/O_2 sensor, and soluble guanylate cyclase) where high affinity for NO is attained by sequential NO binding steps preceding formation of the final pentacoordinate NO-bound species [119-123]. However, direct spectroscopic evidence for the formation of such a hexacoordinate ferrous-dinitrosyl intermediate during the reaction of CBS with NO is lacking. For this reason, these yet hypothetical reactions are depicted inside a dashed box in Figure 6. Irrespectively of the NO binding mechanism, it remains to be understood why in human CBS NO initially binds to the His side, whereas CO to the Cys side. In bacterial cytochrome *c*', binding of NO and CO on opposite sides of the heme has also been reported [121, 124-126]. The affinity for either gas in heme proteins has been assigned to the chemical nature of the endogenous iron axial ligands and to the properties of the heme pocket environment, as a cumulative effect of steric hindrance, electrostatic interactions and H-bonds [119, 120, 123].

3.3.3 Effect of S-adenosyl-L-methionine on CO and NO inhibition of human CBS

As a follow-up of the investigations described above, a thorough analysis of the effect of the allosteric activator AdoMet on the heme chemistry of human CBS has been recently undertaken, focusing on the CO and NO binding properties of the enzyme [111]. Structural studies have elucidated the molecular basis of AdoMet stimulation of CBS activity [94, 96]. In the AdoMet-free state, the C-terminal domain from one monomer hinders substrate accessibility to the active site of the adjacent monomer. Upon AdoMet binding, a large conformational change takes place and the C-terminal domains from the two monomers associate in a disk-like shape, thereby unblocking the entry to the substrate pocket and facilitating its access to the PLP active site.

Despite the significant distance between the C-terminal AdoMet-binding and the N-terminal heme-binding domains (>30 Å between adjacent monomers and >50 Å within one monomer in AdoMet-free CBS), the question was raised as to whether AdoMet binding at the C-terminus promotes a distal communication with the heme site [111]. Indeed, by analyzing H_2S production by reduced CBS as a function of CO concentration in the absence or presence of AdoMet, we estimated a K_i = 9.5 ± 1.0 μM for AdoMet-free CBS and a K_i = 0.7 ± 0.1 μM for the AdoMet-bound enzyme (Figure 7A) [111]. These data not only provided the first report of a K_i for CO regarding CBS-catalyzed H_2S production, but also revealed a marked functional effect of AdoMet on the heme-mediated CO inhibition of the enzyme.

Prompted by these observations, a thorough characterization of the CO and NO binding properties of human CBS in the presence or absence of AdoMet has been undertaken [111]. As shown in Figure 7B and in line with

the effect of AdoMet on CO inhibition, by performing anaerobic CO titrations of reduced CBS monitored by UV-visible absorption spectroscopy, AdoMet proved to significantly increase the affinity of the enzyme for CO. Particularly, AdoMet binding resulted in an overall ~5-fold decrease of the C_{50} value, from 29 ± 4 μM to 6 ± 1 μM. Carrying out control titrations with a truncated CBS form lacking the C-terminal AdoMet-binding domain, a C_{50} of 12 ± 1 μM was estimated both in the absence and presence of AdoMet, ruling out an unspecific direct effect of AdoMet on the heme [111].

The effect of AdoMet on CO binding kinetics was then evaluated by stopped-flow mixing AdoMet-free or AdoMet-bound ferrous CBS with CO solutions. In accordance with the increased affinity measured in the presence of AdoMet, CO association to the AdoMet-bound was markedly faster than to the AdoMet-free enzyme (Figure 7C) [111]. Indeed, incubation with AdoMet resulted in an overall ~10-fold faster association ($t_{1/2}$ = 5.5 s and $t_{1/2}$ = 55 s for AdoMet-bound and AdoMet-free CBS, respectively). The effect of AdoMet on CO binding was then analyzed at saturating CO concentrations and varying the AdoMet concentration [111]. The reaction followed a characteristic biphasic timecourse and both CO binding rate constants showed a hyperbolic dependence on AdoMet concentration, characterized by a C_{50} values of 12 ± 4 μM and 18 ± 3 μM for the fast and slow kinetic phase, respectively, showing a nearly saturating effect at physiological AdoMet concentrations (50-80 μM, [127]). Altogether, the acquired data show a significant functional impact of AdoMet on CO binding to ferrous human CBS resulting in an increased propensity towards CO inhibition of H_2S synthesis.

The effect of AdoMet was further evaluated on the binding affinity and association kinetics of NO [111]. As compared to CO, AdoMet exhibited a less pronounced effect on NO binding. Affinity for NO increased by ~2-

fold in the presence of AdoMet, consistent with a ~1.5-fold increase in the association bimolecular rate constant and ~1.3-fold decrease in the dissociation observed rate constant [111]. Notably, the association observed rate constants at a fixed NO concentration displayed a hyperbolic dependence on AdoMet concentration, yielding a C_{50} of 16 ± 2 μM for AdoMet, fully consistent with those determined for CO and with a modulation of NO binding to CBS at physiological AdoMet concentrations. As with CO, a truncated version of CBS lacking the C-terminal AdoMet-binding domain proved to be insensitive to AdoMet both in terms of NO binding affinity and kinetics [111].

The fact that AdoMet affects differently CO and NO binding is fully consistent with the proposal that NO and CO attack initially the CBS heme iron from different sides (Figure 6). Since AdoMet affects more pronouncedly CO binding, it is likely that AdoMet binding at the C-terminal regulatory domain results into a selective weakening of Fe-Cys52 bond. It remains to be determined whether this functional communication between distant regulatory sites within CBS also involves the catalytic core domain. Irrespectively of the mechanistic details entailing this functional and structural communication between the CBS domains, it is remarkable that an allosteric effector that increases the enzyme activity, at the same time makes the enzyme more prone to inactivation by the exogenous ligands CO and NO. Despite this seemingly paradoxical regulatory conundrum, it is not surprising that CBS, being a major source of H_2S, exhibits such intricate switching mechanisms to quickly, effectively and reversibly modulate H_2S production, although the reflection on bioenergetics of the gasotransmitters interplay at the level of CBS remains to be elucidated.

In conclusion, growing evidence suggests that endogenous H_2S can impact cellular bioenergetics by modulating (either positively or negatively) mitochondrial respiration and, under certain conditions, enhancing glycolysis. Depending on its concentration, H_2S can either act as an effective substrate or, similarly to CO and NO, as an inhibitor of the mitochondrial respiratory chain, targeting CcOX. This dual function of H_2S, while crucially depending on the bioavailability of this gaseous signalling molecule, is interestingly intertwined with the action of the other two gasotransmitters CO and NO. It is therefore important to increase our knowledge on the molecular mechanisms underlying H_2S metabolism, its regulation and the intricate cross-talk between the three gasotransmitters, all contributing to a correct balance between H_2S synthesis and breakdown. In this light, a key role could be played by human CBS, an enzyme sitting at the crossroad between the signalling pathways of the three gasotransmitters. The field is in its infancy and clearly deserves in the future more efforts to answer the many as yet open questions.

ACKNOWLEDGMENTS

This work was partly supported by: Ministero dell'Istruzione, dell'Università e della Ricerca of Italy (PNR-CNR Aging Program 2012–2014 to A.G. and PRIN 20107Z8XBW_005 to P.S.); Regione Lazio of Italy (FILAS-RU-2014-1020); Fundação para a Ciência e Tecnologia (FCT) of Portugal (Grant PTDC/SAU-MIC/111447/2009 to J.B.V); a bilateral grant award by Consiglio Nazionale delle Ricerche of Italy (CNR) of Italy and FCT of Portugal (to A.G. and J.B.V.). iNOVA4Health - UID/Multi/04462/2013, a program financially supported by FCT/Ministério da Educação e Ciência, through national funds and co-funded by FEDER under the PT2020 Partnership Agreement is acknowledged.

FIGURES AND LEGENDS

Figure 1

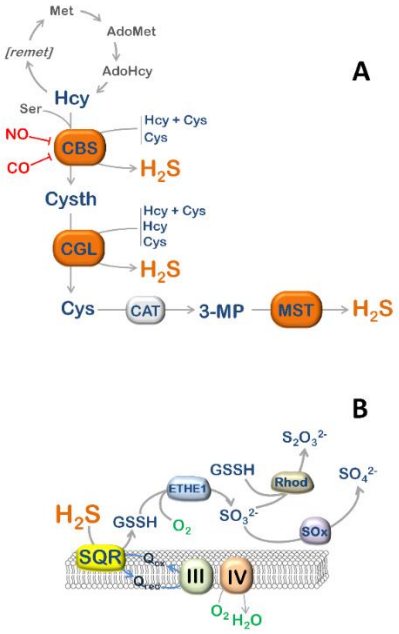

Figure 1. H_2S metabolism in human physiology. *Panel A*, H_2S biosynthetic pathway. Homocysteine (Hcy) is generated through the methionine cycle, involving the sequential conversion of methionine (Met) into S-adenosyl-L-methionine (AdoMet), followed by AdoMet demethylation into S-adenosyl-L-homocysteine (AdoHcy) and production of Hcy by hydrolysis. Cystathionine β-synthase (CBS) catalyzes the condensation of serine (Ser) and Hcy into cystathionine (Cysth) and water. Alternative reactions catalyzed by CBS, using cysteine (Cys) alone or Cys and Hcy, result in H_2S production. The next step in the transsulfuration pathways is catalyzed by cystathionine γ-lyase (CGL), which converts Cysth into Cys. Alternative reactions catalyzed by CGL, using Hcy and/or Cys as substrates, yield H_2S. Cys is converted by cysteine aminotransferase (CAT) into mercaptopyruvate (3-MP), which is used as a substrate by mercaptopyruvate sulfurtransferase

(MST) for H_2S production. *Panel B*, sulfide oxidizing unit: H_2S is oxidized by sulfide:quinone oxidoreductase (SQR), with reduced glutathione (GSH) as the preferred sulfur acceptor, yielding glutathione persulfide (GSSH) and reduced quinone (Q). GSSH is catabolized by persulfide dioxygenase (ETHE1) into sulfite, using O_2 as co-substrate. GSSH and sulfite are converted by rhodanese (Rhod) into thiosulfate. Finally, sulfite is oxidized to sulfate by sulfite oxidase (SOx). Reduced quinone (Q_{red}) supplies electron equivalents via Complex III to accomplish Complex IV-mediated oxygen respiration.

Figure 2

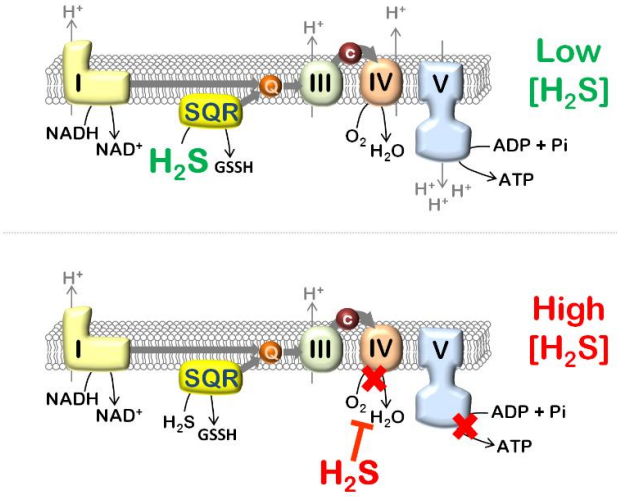

Figure 2. H_2S and mitochondrial respiration. Dual effect of H_2S on mitochondrial respiration depending on its bioavailability. At low concentrations, H_2S supplies the mitochondrial electron transfer chain, being oxidized by sulfide:quinone oxidoreductase (SQR) with concomitant

reduction of coenzyme Q. Reduced quinone (also derived from NADH oxidation by Complex I) is then oxidized by Complex III to generate reduced cytochrome *c*, finally used by Complex IV as the electron source for O_2 reduction to water. Proton translocation by complexes I, III and IV contribute to Complex V-mediated ATP production. At high H_2S concentrations, cytochrome *c* oxidase (Complex IV) is directly inhibited by H_2S, blocking respiration and concomitant ATP synthesis.

Figure 3

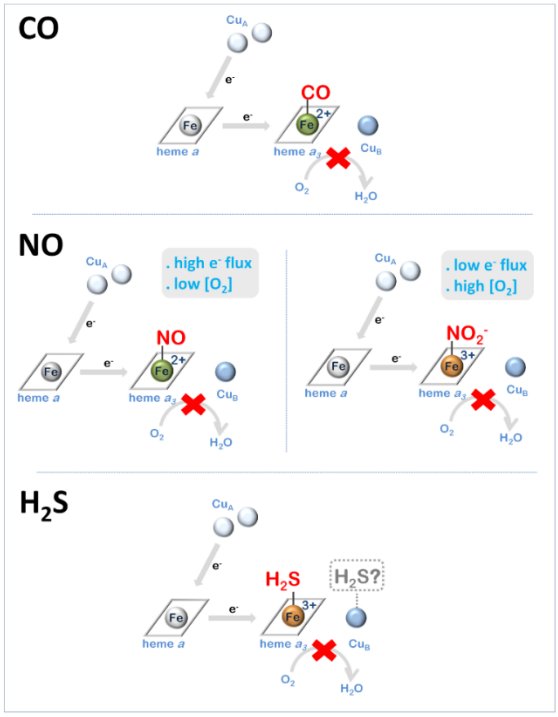

Figure 3. Inhibition of cytochrome oxidase by the three 'gasotransmitters' CO, NO and H_2S. Redox active metal centres of cytochrome oxidase (CcOX): the binuclear Cu_A centre is the electron entry point, heme *a* mediates electron transfer to the O_2-reducing binuclear active

site, composed by heme a_3 and Cu_B. CO inhibits CcOX by tight reversible binding to ferrous heme a_3. The CcOX inhibition pathway by NO varies depending on the electron flux and O_2 level. At high electron flux and low [O_2], NO binds to ferrous heme a_3. At low electron flux and high [O_2], the inhibited adduct has nitrite bound to ferric heme a_3. Sulfide-inhibited CcOX has H_2S bound to ferric heme a_3 and possibly another H_2S molecule bound to cuprous Cu_B.

Figure 4

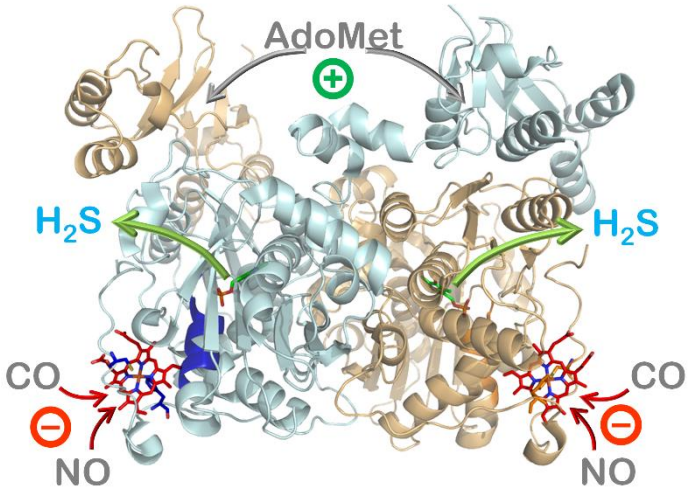

Figure 4. Structure of human cystathionine β-synthase. Cartoon representation of the 'full-length' human CBS homodimer (PDB ID: 4COO; Δ516-525; 2.0 Å resolution), where the C-terminal domain of each monomer (coloured cyan or light orange) hinders the substrate entrance to the active site of the opposite monomer. AdoMet binding causes the C-terminal domains to associate in a disk-like form, de-repressing the enzymatic activity. Red sticks, regulatory heme *b* with its Cys_{52} and His_{65} ligands, where NO or CO bind, resulting in enzyme inhibition. Green sticks, active site PLP

moiety, where H_2S production occurs. Bright blue and bright orange helices (residues T_{257}-G_{258}-G_{259}-T_{260}-I_{261}-T_{262}-G_{263}-I_{264}-A_{265}-R_{266}) communicate the heme redox and ligand binding state to the PLP active site. Figure generated with Pymol.

Figure 5

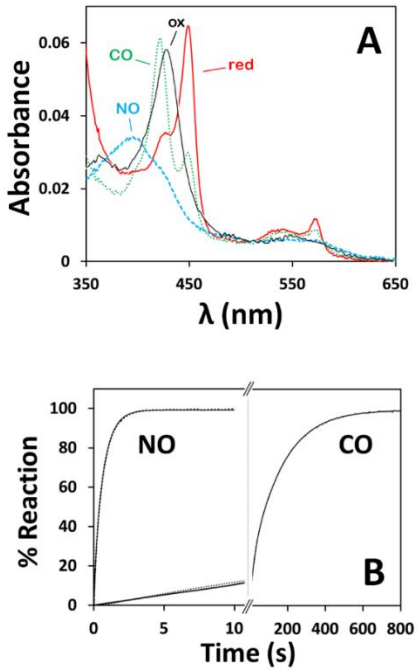

Figure 5. Spectroscopic and kinetic analysis of NO and CO binding to human CBS. *Panel A*, UV-visible absorption spectra of human CBS (in 50 mM phosphate buffer, 300 mM KCl, 10% glycerol, pH 7.0) in the oxidized (black line), dithionite-reduced (red line), ferrous-CO bound (dotted green line) and ferrous-NO bound (dashed blue line) states. *Panel B*, kinetic traces acquired after stopped-flow mixing ferrous human CBS with NO (400 μM after mixing) or CO (500 μM after mixing) at 25 °C. Adapted from [110].

Figure 6

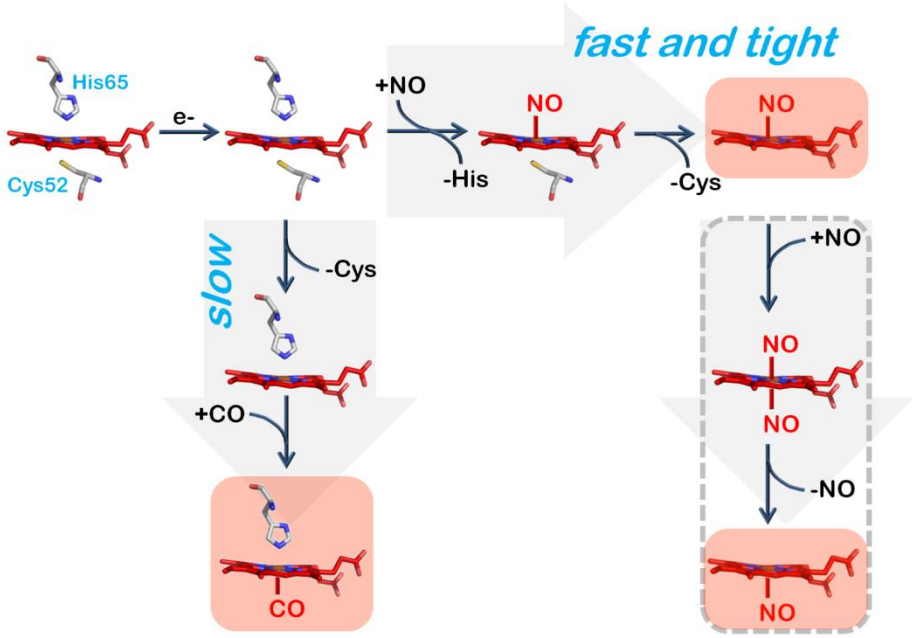

Figure 6. Proposed mechanisms for NO and CO binding to human CBS. Whereas CO binding to ferrous CBS appears to be rate-limited by the displacement of Cys52, NO is proposed to displace first the His65 ligand and end-up as a pentacoordinate ferrous-NO adduct with both endogenous axial ligands displaced and NO laying on either the His or the Cys side. In the latter case, an obligate hexacoordinate ferrous-dinitrosyl (NO-Fe-NO) species should form transiently. As there is no direct evidence for the occurrence of such a dinitrosyl intermediate in the reaction of CBS with NO, these yet hypothetical reactions are depicted inside a dashed box.

Figure 7.

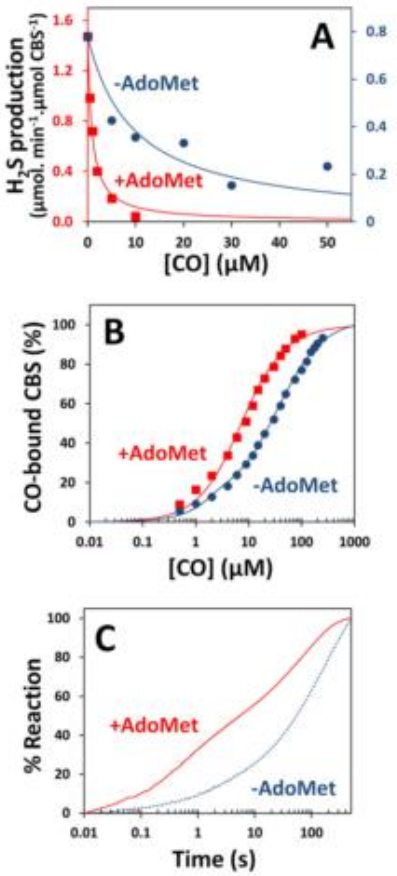

Figure 7. AdoMet enhances CO binding to human CBS and inhibition of H_2S **production.** *Panel A*, CO inhibition of H_2S production by human CBS in the absence or presence of S-adenosyl-L-methionine (AdoMet), assayed at 37 °C. Data fitting yielded K_i = 9.5 ± 1.0 μM and K_i = 0.7 ± 0.1 μM in the absence and presence of AdoMet, respectively. *Panel B*, CO titration profiles obtained by global fit of the UV-visible spectral data acquired in the absence (blue circles) or presence (red squares) of 500 μM AdoMet. Data fitting yielded C_{50} = 6 ± 1 μM and C_{50} = 29 ± 4 μM for AdoMet-bound and AdoMet-free CBS, respectively. *Panel C*, Reaction time courses obtained by stopped-flow mixing ferrous human CBS with 1 mM CO in the absence (blue

line) or presence (red line) of AdoMet (500 μM before mixing). Data fitting yielded $t_{1/2}$ = 5.5 s and $t_{1/2}$ = 55 s for AdoMet-bound and AdoMet-free CBS, respectively. Reaction conditions and data analysis detailed in [111].

REFERENCES

[1] O. Kabil, R. Banerjee, Enzymology of H_2S biogenesis, decay and signaling, Antioxid. Redox Signal. 20 (2014) 770-782.

[2] H. Kimura, Signaling molecules: hydrogen sulfide and polysulfide, Antioxid. Redox Signal. 22 (2015) 362-376.

[3] K.R. Olson, K.D. Straub, The role of hydrogen sulfide in evolution and the evolution of hydrogen sulfide in metabolism and signaling, Physiology (Bethesda) 31 (2016) 60-72.

[4] B.D. Paul, S.H. Snyder, H_2S: a novel gasotransmitter that signals by sulfhydration, Trends Biochem. Sci. 40 (2015) 687-700.

[5] P. Nagy, Mechanistic chemical perspective of hydrogen sulfide signaling, Methods Enzymol. 554 (2015) 3-29.

[6] K. Ono, T. Akaike, T. Sawa, Y. Kumagai, D.A. Wink, D.J. Tantillo, A.J. Hobbs, P. Nagy, M. Xian, J. Lin, J.M. Fukuto, Redox chemistry and chemical biology of H_2S, hydropersulfides, and derived species: implications of their possible biological activity and utility, Free Radic. Biol. Med. 77 (2014) 82-94.

[7] H. Kimura, Signaling of hydrogen sulfide and polysulfides, Antioxid Redox Signal 22 (2015) 347-349.

[8] C. Szabo, C. Ransy, K. Modis, M. Andriamihaja, B. Murghes, C. Coletta, G. Olah, K. Yanagi, F. Bouillaud, Regulation of mitochondrial bioenergetic function by hydrogen sulfide. Part I.

Biochemical and physiological mechanisms, Br. J. Pharmacol. 171 (2014) 2099-2122.

[9] R. Wang, C. Szabo, F. Ichinose, A. Ahmed, M. Whiteman, A. Papapetropoulos, The role of H_2S bioavailability in endothelial dysfunction, Trends Pharmacol. Sci. 36 (2015) 568-578.

[10] B.D. Paul, J.I. Sbodio, R. Xu, M.S. Vandiver, J.Y. Cha, A.M. Snowman, S.H. Snyder, Cystathionine gamma-lyase deficiency mediates neurodegeneration in Huntington's disease, Nature 509 (2014) 96-100.

[11] M.R. Hellmich, C. Coletta, C. Chao, C. Szabo, The therapeutic potential of cystathionine beta-synthetase/hydrogen sulfide inhibition in cancer, Antioxid. Redox Signal. 22 (2015) 424-448.

[12] S. Singh, R. Banerjee, PLP-dependent H(2)S biogenesis, Biochim. Biophys. Acta 1814 (2011) 1518-1527.

[13] S. Singh, D. Padovani, R.A. Leslie, T. Chiku, R. Banerjee, Relative contributions of cystathionine beta-synthase and gamma-cystathionase to H_2S biogenesis via alternative trans-sulfuration reactions, J. Biol. Chem. 284 (2009) 22457-22466.

[14] N. Shibuya, S. Koike, M. Tanaka, M. Ishigami-Yuasa, Y. Kimura, Y. Ogasawara, K. Fukui, N. Nagahara, H. Kimura, A novel pathway for the production of hydrogen sulfide from D-cysteine in mammalian cells, Nat. Commun. 4 (2013) 1366.

[15] F. Bouillaud, F. Blachier, Mitochondria and sulfide: a very old story of poisoning, feeding, and signaling?, Antioxid. Redox Signal. 15 (2011) 379-391.

[16] T.M. Hildebrandt, M.K. Grieshaber, Three enzymatic activities catalyze the oxidation of sulfide to thiosulfate in mammalian and invertebrate mitochondria, FEBS J. 275 (2008) 3352-3361.

[17] E. Lagoutte, S. Mimoun, M. Andriamihaja, C. Chaumontet, F. Blachier, F. Bouillaud, Oxidation of hydrogen sulfide remains a priority in mammalian cells and causes reverse electron transfer in colonocytes, Biochim. Biophys. Acta 1797 (2010) 1500-1511.

[18] C.E. Cooper, G.C. Brown, The inhibition of mitochondrial cytochrome oxidase by the gases carbon monoxide, nitric oxide, hydrogen cyanide and hydrogen sulfide: chemical mechanism and physiological significance, J. Bioenerg. Biomembr. 40 (2008) 533-539.

[19] V. Borutaite, A. Budriunaite, G.C. Brown, Reversal of nitric oxide-, peroxynitrite- and S-nitrosothiol-induced inhibition of mitochondrial respiration or complex I activity by light and thiols, Biochim. Biophys. Acta 1459 (2000) 405-412.

[20] L.S. Burwell, S.M. Nadtochiy, A.J. Tompkins, S. Young, P.S. Brookes, Direct evidence for S-nitrosation of mitochondrial complex I, Biochem. J. 394 (2006) 627-634.

[21] E. Clementi, G.C. Brown, M. Feelisch, S. Moncada, Persistent inhibition of cell respiration by nitric oxide: crucial role of S-nitrosylation of mitochondrial complex I and protective action of glutathione, Proc. Natl. Acad. Sci. USA 95 (1998) 7631-7636.

[22] C.C. Dahm, K. Moore, M.P. Murphy, Persistent S-nitrosation of complex I and other mitochondrial membrane proteins by S-nitrosothiols but not nitric oxide or peroxynitrite: implications for the interaction of nitric oxide with mitochondria, J. Biol. Chem. 281 (2006) 10056-10065.

[23] A. Galkin, S. Moncada, S-nitrosation of mitochondrial complex I depends on its structural conformation, J. Biol. Chem. 282 (2007) 37448-37453.

[24] M.A. Powell, G.N. Somero, Hydrogen sulfide oxidation is coupled to oxidative phosphorylation in mitochondria of *Solemya reidi*, Science 233 (1986) 563-566.

[25] D.G. Searcy, Metabolic integration during the evolutionary origin of mitochondria, Cell Res. 13 (2003) 229-238.

[26] M. Goubern, M. Andriamihaja, T. Nubel, F. Blachier, F. Bouillaud, Sulfide, the first inorganic substrate for human cells, FASEB J. 21 (2007) 1699-1706.

[27] S. Mimoun, M. Andriamihaja, C. Chaumontet, C. Atanasiu, R. Benamouzig, J.M. Blouin, D. Tome, F. Bouillaud, F. Blachier, Detoxification of H(2)S by differentiated colonic epithelial cells: implication of the sulfide oxidizing unit and of the cell respiratory capacity, Antioxid. Redox Signal. 17 (2012) 1-10.

[28] M. Groeger, J. Matallo, O. McCook, F. Wagner, U. Wachter, O. Bastian, S. Gierer, V. Reich, B. Stahl, M. Huber-Lang, C. Szabo, M. Georgieff, P. Radermacher, E. Calzia, K. Wagner, Temperature and cell-type dependency of sulfide effects on mitochondrial respiration, Shock 38 (2012) 367-374.

[29] K. Modis, C. Coletta, K. Erdelyi, A. Papapetropoulos, C. Szabo, Intramitochondrial hydrogen sulfide production by 3-mercaptopyruvate sulfurtransferase maintains mitochondrial electron flow and supports cellular bioenergetics, FASEB J. 27 (2013) 601-611.

[30] N. Helmy, C. Prip-Buus, C. Vons, V. Lenoir, A. Abou-Hamdan, H. Guedouari-Bounihi, A. Lombes, F. Bouillaud, Oxidation of hydrogen sulfide by human liver mitochondria, Nitric Oxide 41 (2014) 105-112.

[31] K. Modis, E.M. Bos, E. Calzia, H. van Goor, C. Coletta, A. Papapetropoulos, M.R. Hellmich, P. Radermacher, F. Bouillaud, C.

Szabo, Regulation of mitochondrial bioenergetic function by hydrogen sulfide. Part II. Pathophysiological and therapeutic aspects, Br. J. Pharmacol. 171 (2014) 2123-2146.

[32] A. Abou-Hamdan, H. Guedouari-Bounihi, V. Lenoir, M. Andriamihaja, F. Blachier, F. Bouillaud, Oxidation of H_2S in mammalian cells and mitochondria, Methods Enzymol. 554 (2015) 201-228.

[33] B. Chance, M. Erecinska, M. Wagner, Mitochondrial responses to carbon monoxide toxicity, Ann. NY Acad. Sci. 174 (1970) 193-204.

[34] C.E. Cooper, Nitric oxide and cytochrome oxidase: substrate, inhibitor or effector?, Trends Biochem. Sci. 27 (2002) 33-39.

[35] P. Sarti, M. Arese, A. Bacchi, M.C. Barone, E. Forte, D. Mastronicola, M. Brunori, A. Giuffrè, Nitric oxide and mitochondrial complex IV, IUBMB Life 55 (2003) 605-611.

[36] P. Sarti, A. Giuffrè, M.C. Barone, E. Forte, D. Mastronicola, M. Brunori, Nitric oxide and cytochrome oxidase: reaction mechanisms from the enzyme to the cell, Free Radic. Biol. Med. 34 (2003) 509-520.

[37] M. Brunori, A. Giuffrè, E. Forte, D. Mastronicola, M.C. Barone, P. Sarti, Control of cytochrome *c* oxidase activity by nitric oxide, Biochim. Biophys. Acta 1655 (2004) 365-371.

[38] C.E. Cooper, C. Giulivi, Nitric oxide regulation of mitochondrial oxygen consumption II: Molecular mechanism and tissue physiology, Am. J. Physiol. Cell. Physiol. 292 (2007) C1993-2003.

[39] P. Sarti, E. Forte, D. Mastronicola, A. Giuffrè, M. Arese, Cytochrome *c* oxidase and nitric oxide in action: molecular mechanisms and pathophysiological implications, Biochim. Biophys. Acta 1817 (2012) 610-619.

[40] J. Torres, V. Darley-Usmar, M.T. Wilson, Inhibition of cytochrome *c* oxidase in turnover by nitric oxide: mechanism and implications for control of respiration, Biochem. J. 312 (Pt 1) (1995) 169-173.

[41] A. Giuffrè, P. Sarti, E. D'Itri, G. Buse, T. Soulimane, M. Brunori, On the mechanism of inhibition of cytochrome *c* oxidase by nitric oxide, J. Biol. Chem. 271 (1996) 33404-33408.

[42] J. Torres, C.E. Cooper, M. Sharpe, M.T. Wilson, Reactivity of nitric oxide with cytochrome *c* oxidase: interactions with the binuclear centre and mechanism of inhibition, J. Bioenerg. Biomembr. 30 (1998) 63-69.

[43] A. Giuffrè, M.C. Barone, D. Mastronicola, E. D'Itri, P. Sarti, M. Brunori, Reaction of nitric oxide with the turnover intermediates of cytochrome *c* oxidase: reaction pathway and functional effects, Biochemistry 39 (2000) 15446-15453.

[44] P. Sarti, A. Giuffrè, E. Forte, D. Mastronicola, M.C. Barone, M. Brunori, Nitric oxide and cytochrome *c* oxidase: mechanisms of inhibition and NO degradation, Biochem. Biophys. Res. Commun. 274 (2000) 183-187.

[45] A. Giuffrè, M.C. Barone, M. Brunori, E. D'Itri, B. Ludwig, F. Malatesta, H.W. Muller, P. Sarti, Nitric oxide reacts with the single-electron reduced active site of cytochrome *c* oxidase, J. Biol. Chem. 277 (2002) 22402-22406.

[46] M.G. Mason, P. Nicholls, M.T. Wilson, C.E. Cooper, Nitric oxide inhibition of respiration involves both competitive (heme) and noncompetitive (copper) binding to cytochrome *c* oxidase, Proc. Natl. Acad. Sci. USA 103 (2006) 708-713.

[47] C.E. Cooper, M.G. Mason, P. Nicholls, A dynamic model of nitric oxide inhibition of mitochondrial cytochrome *c* oxidase, Biochim. Biophys. Acta 1777 (2008) 867-876.

[48] D. Mastronicola, M.L. Genova, M. Arese, M.C. Barone, A. Giuffrè, C. Bianchi, M. Brunori, G. Lenaz, P. Sarti, Control of respiration by nitric oxide in Keilin-Hartree particles, mitochondria and SH-SY5Y neuroblastoma cells, Cell. Mol. Life Sci. 60 (2003) 1752-1759.

[49] L.C. Petersen, The effect of inhibitors on the oxygen kinetics of cytochrome *c* oxidase, Biochim. Biophys. Acta 460 (1977) 299-307.

[50] P. Nicholls, J.K. Kim, Sulphide as an inhibitor and electron donor for the cytochrome *c* oxidase system, Can. J. Biochem. 60 (1982) 613-623.

[51] P.R. Rich, B. Meunier, R. Mitchell, J. Moody, Coupling of charge and proton movement in cytochrome *c* oxidase, Biochim. Biophys. Acta 1275 (1996) 91-95.

[52] P. Nicholls, D.C. Marshall, C.E. Cooper, M.T. Wilson, Sulfide inhibition of and metabolism by cytochrome *c* oxidase, Biochem. Soc. Trans. 41 (2013) 1312-1316.

[53] M. Brunori, A. Giuffrè, E. D'Itri, P. Sarti, Internal electron transfer in Cu-heme oxidases. Thermodynamic or kinetic control?, J. Biol. Chem. 272 (1997) 19870-19874.

[54] P. Nicholls, The effect of sulphide on cytochrome aa_3. Isosteric and allosteric shifts of the reduced alpha-peak, Biochim. Biophys. Acta 396 (1975) 24-35.

[55] P. Nicholls, L.C. Petersen, M. Miller, F.B. Hansen, Ligand-induced spectral changes in cytochrome *c* oxidase and their possible significance, Biochim. Biophys. Acta 449 (1976) 188-196.

[56] B.C. Hill, T.C. Woon, P. Nicholls, J. Peterson, C. Greenwood, A.J. Thomson, Interactions of sulphide and other ligands with cytochrome *c* oxidase. An electron-paramagnetic-resonance study, Biochem. J. 224 (1984) 591-600.

[57] P. Nicholls, J.K. Kim, Oxidation of sulphide by cytochrome aa_3, Biochim. Biophys. Acta 637 (1981) 312-320.

[58] C. Greenwood, M.T. Wilson, M. Brunori, Studies on partially reduced mammalian cytochrome oxidase. Reactions with carbon monoxide and oxygen, Biochem. J. 137 (1974) 205-215.

[59] P. Brzezinski, B.G. Malmstrom, The reduction of cytochrome *c* oxidase by carbon monoxide, FEBS Lett. 187 (1985) 111-114.

[60] M.T. Wilson, J. Torres, C.E. Cooper, M.A. Sharpe, Interactions of cytochrome *c* oxidase with nitric oxide: reactions of the 'turnover' intermediates, Biochem. Soc. Trans. 25 (1997) 905-909.

[61] C.E. Cooper, J. Torres, M.A. Sharpe, M.T. Wilson, Nitric oxide ejects electrons from the binuclear centre of cytochrome *c* oxidase by reacting with oxidised copper: a general mechanism for the interaction of copper proteins with nitric oxide?, FEBS Lett. 414 (1997) 281-284.

[62] E. Antonini, M. Brunori, A. Colosimo, C. Greenwood, M.T. Wilson, Oxygen "pulsed" cytochrome *c* oxidase: functional properties and catalytic relevance, Proc. Natl. Acad. Sci. USA 74 (1977) 3128-3132.

[63] A. Giuffrè, G. Stubauer, M. Brunori, P. Sarti, J. Torres, M.T. Wilson, Chloride bound to oxidized cytochrome *c* oxidase controls the reaction with nitric oxide, J Biol Chem 273 (1998) 32475-32478.

[64] L. Hannibal, F. Tomasina, D.A. Capdevila, V. Demicheli, V. Tortora, D. Alvarez-Paggi, R. Jemmerson, D.H. Murgida, R. Radi, Alternative

conformations of cytochrome *c*: structure, function and detection, Biochemistry (2016).

[65] R. Yong, D.G. Searcy, Sulfide oxidation coupled to ATP synthesis in chicken liver mitochondria, Comp. Biochem. Physiol. B Biochem. Mol. Biol. 129 (2001) 129-137.

[66] X. Leschelle, M. Goubern, M. Andriamihaja, H.M. Blottiere, E. Couplan, M.D. Gonzalez-Barroso, C. Petit, A. Pagniez, C. Chaumontet, B. Mignotte, F. Bouillaud, F. Blachier, Adaptative metabolic response of human colonic epithelial cells to the adverse effects of the luminal compound sulfide, Biochim. Biophys. Acta 1725 (2005) 201-212.

[67] S. Volkel, M.K. Grieshaber, Mitochondrial sulfide oxidation in *Arenicola marina*. Evidence for alternative electron pathways, Eur. J. Biochem. 235 (1996) 231-237.

[68] Ouml, S. Lkel, M. Grieshaber, Sulphide oxidation and oxidative phosphorylation in the mitochondria of the lugworm, J. Exp. Biol. 200 (1997) 83-92.

[69] T.V. Mishanina, P.K. Yadav, D.P. Ballou, R. Banerjee, Transient kinetic analysis of hydrogen sulfide oxidation catalyzed by human sulfide quinone oxidoreductase, J. Biol. Chem. 290 (2015) 25072-25080.

[70] M.R. Jackson, S.L. Melideo, M.S. Jorns, Human sulfide:quinone oxidoreductase catalyzes the first step in hydrogen sulfide metabolism and produces a sulfane sulfur metabolite, Biochemistry 51 (2012) 6804-6815.

[71] M. Libiad, P.K. Yadav, V. Vitvitsky, M. Martinov, R. Banerjee, Organization of the human mitochondrial hydrogen sulfide oxidation pathway, J. Biol. Chem. 289 (2014) 30901-30910.

[72] B.J. Henriques, T.G. Lucas, J.V. Rodrigues, J.H. Frederiksen, M.S. Teixeira, V. Tiranti, P. Bross, C.M. Gomes, Ethylmalonic encephalopathy ETHE1 R163W/R163Q mutations alter protein stability and redox properties of the iron centre, PLoS One 9 (2014) e107157.

[73] I. Pettinati, J. Brem, M.A. McDonough, C.J. Schofield, Crystal structure of human persulfide dioxygenase: structural basis of ethylmalonic encephalopathy, Hum. Mol. Genet. 24 (2015) 2458-2469.

[74] P.K. Yadav, K. Yamada, T. Chiku, M. Koutmos, R. Banerjee, Structure and kinetic analysis of H_2S production by human mercaptopyruvate sulfurtransferase, J. Biol. Chem. 288 (2013) 20002-20013.

[75] K. Johnson-Winters, G. Tollin, J.H. Enemark, Elucidating the catalytic mechanism of sulfite oxidizing enzymes using structural, spectroscopic, and kinetic analyses, Biochemistry 49 (2010) 7242-7254.

[76] F. Blachier, A.M. Davila, S. Mimoun, P.H. Benetti, C. Atanasiu, M. Andriamihaja, R. Benamouzig, F. Bouillaud, D. Tome, Luminal sulfide and large intestine mucosa: friend or foe?, Amino Acids 39 (2010) 335-347.

[77] F. Carbonero, A.C. Benefiel, A.H. Alizadeh-Ghamsari, H.R. Gaskins, Microbial pathways in colonic sulfur metabolism and links with health and disease, Front. Physiol. 3 (2012) 448.

[78] F. Carbonero, A.C. Benefiel, H.R. Gaskins, Contributions of the microbial hydrogen economy to colonic homeostasis, Nat. Re.v Gastroenterol. Hepatol. 9 (2012) 504-518.

[79] M. Medani, D. Collins, N.G. Docherty, A.W. Baird, P.R. O'Connell, D.C. Winter, Emerging role of hydrogen sulfide in colonic physiology and pathophysiology, Inflamm. Bowel Dis. 17 (2011) 1620-1625.

[80] M. Fu, W. Zhang, G. Yang, R. Wang, Is cystathionine gamma-lyase protein expressed in the heart?, Biochem. Biophys. Res. Commun. 428 (2012) 469-474.

[81] H. Teng, B. Wu, K. Zhao, G. Yang, L. Wu, R. Wang, Oxygen-sensitive mitochondrial accumulation of cystathionine beta-synthase mediated by Lon protease, Proc. Natl. Acad. Sci. USA 110 (2013) 12679-12684.

[82] C. Szabo, C. Coletta, C. Chao, K. Modis, B. Szczesny, A. Papapetropoulos, M.R. Hellmich, Tumor-derived hydrogen sulfide, produced by cystathionine-beta-synthase, stimulates bioenergetics, cell proliferation, and angiogenesis in colon cancer, Proc. Natl. Acad. Sci. USA 110 (2013) 12474-12479.

[83] R. Vozdek, A. Hnizda, J. Krijt, M. Kostrouchova, V. Kozich, Novel structural arrangement of nematode cystathionine beta-synthases: characterization of *Caenorhabditis elegans* CBS-1, Biochem. J. 443 (2012) 535-547.

[84] K. Modis, K. Wolanska, R. Vozdek, Hydrogen sulfide in cell signaling, signal transduction, cellular bioenergetics and physiology in *C. elegans*, Gen. Physiol. Biophys. 32 (2013) 1-22.

[85] A.K. Mustafa, M.M. Gadalla, N. Sen, S. Kim, W. Mu, S.K. Gazi, R.K. Barrow, G. Yang, R. Wang, S.H. Snyder, H_2S signals through protein S-sulfhydration, Sci. Signal. 2 (2009) ra72.

[86] B.D. Paul, S.H. Snyder, H(2)S signalling through protein sulfhydration and beyond, Nat. Rev. Mol. Cell. Biol. 13 (2012) 499-507.

[87] A. Asimakopoulou, P. Panopoulos, C.T. Chasapis, C. Coletta, Z. Zhou, G. Cirino, A. Giannis, C. Szabo, G.A. Spyroulias, A. Papapetropoulos, Selectivity of commonly used pharmacological inhibitors for cystathionine beta synthase (CBS) and cystathionine gamma lyase (CSE), Br. J. Pharmacol. 169 (2013) 922-932.

[88] X. Chen, K.H. Jhee, W.D. Kruger, Production of the neuromodulator H_2S by cystathionine beta-synthase via the condensation of cysteine and homocysteine, J. Bio.l Chem. 279 (2004) 52082-52086.

[89] O. Kabil, V. Vitvitsky, P. Xie, R. Banerjee, The quantitative significance of the transsulfuration enzymes for H_2S production in murine tissues, Antioxid. Redox Signal. 15 (2011) 363-372.

[90] S.E. Bearden, R.S. Beard, Jr., J.C. Pfau, Extracellular transsulfuration generates hydrogen sulfide from homocysteine and protects endothelium from redox stress, Am. J. Physiol. Heart Circ. Physiol. 299 (2010) H1568-1576.

[91] O. Kabil, Y. Zhou, R. Banerjee, Human cystathionine beta-synthase is a target for sumoylation, Biochemistry 45 (2006) 13528-13536.

[92] A. Davoli, V. Greco, A. Spalloni, E. Guatteo, C. Neri, G.R. Rizzo, A. Cordella, A. Romigi, C. Cortese, S. Bernardini, P. Sarchielli, G. Cardaioli, P. Calabresi, N.B. Mercuri, A. Urbani, P. Longone, Evidence of hydrogen sulfide involvement in amyotrophic lateral sclerosis, Ann. Neurol. 77 (2015) 697-709.

[93] J. Ereno-Orbea, T. Majtan, I. Oyenarte, J.P. Kraus, L.A. Martinez-Cruz, Structural basis of regulation and oligomerization of human cystathionine beta-synthase, the central enzyme of transsulfuration, Proc. Natl. Acad. Sci. USA 110 (2013) E3790-3799.

[94] J. Ereno-Orbea, T. Majtan, I. Oyenarte, J.P. Kraus, L.A. Martinez-Cruz, Structural insight into the molecular mechanism of allosteric

activation of human cystathionine beta-synthase by S-adenosylmethionine, Proc. Natl. Acad. Sci. USA 111 (2014) E3845-3852.

[95] A.L. Pey, T. Majtan, J.M. Sanchez-Ruiz, J.P. Kraus, Human cystathionine beta-synthase (CBS) contains two classes of binding sites for S-adenosylmethionine (SAM): complex regulation of CBS activity and stability by SAM, Biochem. J. 449 (2013) 109-121.

[96] T.J. McCorvie, J. Kopec, S.J. Hyung, F. Fitzpatrick, X. Feng, D. Termine, C. Strain-Damerell, M. Vollmar, J. Fleming, J.M. Janz, C. Bulawa, W.W. Yue, Inter-domain communication of human cystathionine beta-synthase: structural basis of S-adenosyl-L-methionine activation, J. Biol. Chem. 289 (2014) 36018-36030.

[97] J. Oliveriusova, V. Kery, K.N. Maclean, J.P. Kraus, Deletion mutagenesis of human cystathionine beta-synthase. Impact on activity, oligomeric status, and S-adenosylmethionine regulation, J. Biol. Chem. 277 (2002) 48386-48394.

[98] M.M. Cherney, S. Pazicni, N. Frank, K.A. Marvin, J.P. Kraus, J.N. Burstyn, Ferrous human cystathionine beta-synthase loses activity during enzyme assay due to a ligand switch process, Biochemistry 46 (2007) 13199-13210.

[99] O. Kabil, C.L. Weeks, S. Carballal, C. Gherasim, B. Alvarez, T.G. Spiro, R. Banerjee, Reversible heme-dependent regulation of human cystathionine beta-synthase by a flavoprotein oxidoreductase, Biochemistry 50 (2011) 8261-8263.

[100] S. Taoka, M. West, R. Banerjee, Characterization of the heme and pyridoxal phosphate cofactors of human cystathionine beta-synthase reveals nonequivalent active sites, Biochemistry 38 (1999) 2738-2744.

[101] S. Taoka, R. Banerjee, Characterization of NO binding to human cystathionine beta-synthase: possible implications of the effects of CO and NO binding to the human enzyme, J. Inorg. Biochem. 87 (2001) 245-251.

[102] R. Banerjee, C.G. Zou, Redox regulation and reaction mechanism of human cystathionine-beta-synthase: a PLP-dependent hemesensor protein, Arch. Biochem. Biophys. 433 (2005) 144-156.

[103] S. Singh, P. Madzelan, J. Stasser, C.L. Weeks, D. Becker, T.G. Spiro, J. Penner-Hahn, R. Banerjee, Modulation of the heme electronic structure and cystathionine beta-synthase activity by second coordination sphere ligands: The role of heme ligand switching in redox regulation, J. Inorg. Biochem. 103 (2009) 689-697.

[104] P.K. Yadav, P. Xie, R. Banerjee, Allosteric communication between the pyridoxal 5'-phosphate (PLP) and heme sites in the H_2S generator human cystathionine beta-synthase, J. Biol. Chem. 287 (2012) 37611-37620.

[105] A.T. Smith, Y. Su, D.J. Stevens, T. Majtan, J.P. Kraus, J.N. Burstyn, Effect of the disease-causing R266K mutation on the heme and PLP environments of human cystathionine beta-synthase, Biochemistry 51 (2012) 6360-6370.

[106] S. Carballal, E. Cuevasanta, I. Marmisolle, O. Kabil, C. Gherasim, D.P. Ballou, R. Banerjee, B. Alvarez, Kinetics of reversible reductive carbonylation of heme in human cystathionine beta-synthase, Biochemistry 52 (2013) 4553-4562.

[107] C. Gherasim, P.K. Yadav, O. Kabil, W.N. Niu, R. Banerjee, Nitrite reductase activity and inhibition of H(2)S biogenesis by human cystathionine beta-synthase, PLoS One 9 (2014) e85544.

[108] M. Puranik, C.L. Weeks, D. Lahaye, O. Kabil, S. Taoka, S.B. Nielsen, J.T. Groves, R. Banerjee, T.G. Spiro, Dynamics of carbon monoxide binding to cystathionine beta-synthase, J. Biol. Chem. 281 (2006) 13433-13438.

[109] S. Carballal, P. Madzelan, C.F. Zinola, M. Grana, R. Radi, R. Banerjee, B. Alvarez, Dioxygen reactivity and heme redox potential of truncated human cystathionine beta-synthase, Biochemistry 47 (2008) 3194-3201.

[110] J.B. Vicente, H.G. Colaco, M.I. Mendes, P. Sarti, P. Leandro, A. Giuffre, NO* binds human cystathionine beta-synthase quickly and tightly, J. Biol. Chem. 289 (2014) 8579-8587.

[111] J.B. Vicente, H.G. Colaco, P. Sarti, P. Leandro, A. Giuffrè, S-Adenosyl-L-methionine modulates CO and NO* binding to the human H_2S-generating enzyme cystathionine beta-synthase, J. Biol. Chem. 291 (2016) 572-581.

[112] G.A. Prathapasinghe, Y.L. Siow, Z. Xu, K. O, Inhibition of cystathionine-beta-synthase activity during renal ischemia-reperfusion: role of pH and nitric oxide, Am. J. Physiol. Renal Physiol. 295 (2008) F912-922.

[113] C.N. Wang, G.L. Duan, Y.J. Liu, Q. Yu, X.L. Tang, W. Zhao, X.H. Li, X.Y. Zhu, X. Ni, Overproduction of nitric oxide by endothelial cells and macrophages contributes to mitochondrial oxidative stress in adrenocortical cells and adrenal insufficiency during endotoxemia, Free Radic. Biol. Med. 83 (2015) 31-40.

[114] T. Morikawa, M. Kajimura, T. Nakamura, T. Hishiki, T. Nakanishi, Y. Yukutake, Y. Nagahata, M. Ishikawa, K. Hattori, T. Takenouchi, T. Takahashi, I. Ishii, K. Matsubara, Y. Kabe, S. Uchiyama, E. Nagata, M.M. Gadalla, S.H. Snyder, M. Suematsu, Hypoxic

regulation of the cerebral microcirculation is mediated by a carbon monoxide-sensitive hydrogen sulfide pathway, Proc. Natl. Acad. Sci. USA 109 (2012) 1293-1298.

[115] T. Shintani, T. Iwabuchi, T. Soga, Y. Kato, T. Yamamoto, N. Takano, T. Hishiki, Y. Ueno, S. Ikeda, T. Sakuragawa, K. Ishikawa, N. Goda, Y. Kitagawa, M. Kajimura, K. Matsumoto, M. Suematsu, Cystathionine beta-synthase as a carbon monoxide-sensitive regulator of bile excretion, Hepatology 49 (2009) 141-150.

[116] M. Suematsu, T. Nakamura, Y. Tokumoto, T. Yamamoto, M. Kajimura, Y. Kabe, CO-CBS-H_2S axis: From vascular mediator to cancer regulator, Microcirculation (2015) doi: 10.1111/micc.12253

[117] T. Yamamoto, N. Takano, K. Ishiwata, M. Suematsu, Carbon monoxide stimulates global protein methylation via its inhibitory action on cystathionine beta-synthase, J. Clin. Biochem. Nutr. 48 (2011) 96-100.

[118] E.G. Moore, Q.H. Gibson, Cooperativity in the dissociation of nitric oxide from hemoglobin, J. Biol. Chem. 251 (1976) 2788-2794.

[119] E. Martin, V. Berka, I. Sharina, A.L. Tsai, Mechanism of binding of NO to soluble guanylyl cyclase: implication for the second NO binding to the heme proximal site, Biochemistry 51 (2012) 2737-2746.

[120] A.L. Tsai, E. Martin, V. Berka, J.S. Olson, How do heme-protein sensors exclude oxygen? Lessons learned from cytochrome *c*', Nostoc puntiforme heme nitric oxide/oxygen-binding domain, and soluble guanylyl cyclase, Antioxid. Redox Signal. 17 (2012) 1246-1263.

[121] M.A. Hough, C.R. Andrew, Cytochromes *c*': structure, reactivity and relevance to haem-based gas sensing, Adv. Microb. Physiol. 67 (2015) 1-84.

[122] T. Shimizu, D. Huang, F. Yan, M. Stranava, M. Bartosova, V. Fojtikova, M. Martinkova, Gaseous O_2, NO, and CO in signal transduction: structure and function relationships of heme-based gas sensors and heme-redox sensors, Chem. Rev. 115 (2015) 6491-6533.

[123] A.L. Tsai, V. Berka, E. Martin, J.S. Olson, A "sliding scale rule" for selectivity among NO, CO, and O(2) by heme protein sensors, Biochemistry 51 (2012) 172-186.

[124] D.M. Lawson, C.E. Stevenson, C.R. Andrew, R.R. Eady, Unprecedented proximal binding of nitric oxide to heme: implications for guanylate cyclase, EMBO J. 19 (2000) 5661-5671.

[125] S.V. Antonyuk, N. Rustage, C.A. Petersen, J.L. Arnst, D.J. Heyes, R. Sharma, N.G. Berry, N.S. Scrutton, R.R. Eady, C.R. Andrew, S.S. Hasnain, Carbon monoxide poisoning is prevented by the energy costs of conformational changes in gas-binding haemproteins, Proc. Natl. Acad. Sci. USA 108 (2011) 15780-15785.

[126] C.R. Andrew, E.L. Green, D.M. Lawson, R.R. Eady, Resonance Raman studies of cytochrome *c*' support the binding of NO and CO to opposite sides of the heme: implications for ligand discrimination in heme-based sensors, Biochemistry 40 (2001) 4115-4122.

[127] J.D. Finkelstein, W.E. Kyle, B.J. Harris, J.J. Martin, Methionine metabolism in mammals: concentration of metabolites in rat tissues, J. Nutr. 112 (1982) 1011-1018.

Paper 2

A clinically relevant variant of the human hydrogen sulfide-synthesizing enzyme cystathionine β-synthase: increased CO reactivity as a novel molecular mechanism of pathogenicity?

João B. Vicente[1,*], Henrique G. Colaço[2], Francesca Malagrinò[3,4], Paulo E. Santo[1,5], André Gutierres[1], Tiago M. Bandeiras[1,5], Paula Leandro[6], José A. Brito[1], and Alessandro Giuffrè[3,*]

1 - Instituto de Tecnologia Química e Biológica António Xavier, Universidade Nova de Lisboa, Oeiras, Portugal
2 - Instituto Gulbenkian da Ciência, Oeiras, Portugal
3 - CNR Institute of Molecular Biology and Pathology, Rome, Italy
4 - Department of Biochemical Sciences, Sapienza University of Rome, Italy.
5 - Instituto de Biologia Experimental e Tecnológica, Oeiras, Portugal
6 - Research Institute for Medicines and Department of Biochemistry and Human Biology, Faculty of Pharmacy, University of Lisbon, Portugal

*To whom correspondence should be addressed:
Dr. Alessandro Giuffrè,
Institute of Molecular Biology and Pathology (IBPM)
National Research Council of Italy (CNR)
Piazzale Aldo Moro 5, I-00185 Rome, Italy
Phone: +39-06-49910944;
Email: alessandro.giuffre@uniroma1.it

Dr. João B. Vicente,
Instituto de Tecnologia Química e Biológica,
Universidade Nova de Lisboa,
Av. da República (EAN), 2780-156 Oeiras, Portugal.
Phone: +351-214469662
Email: jvicente@itqb.unl.pt

Conflict of Interest:
The authors declare that there is no conflict of interest regarding the publication of this paper.

ABSTRACT

The human disease classical homocystinuria results from mutations in the gene encoding the pyridoxal 5'-phosphate (PLP)-dependent cystathionine β-synthase (CBS), a key enzyme in the transsulfuration pathway that controls homocysteine levels and is a major source of the signaling molecule hydrogen sulfide (H_2S). CBS activity, contributing to cellular redox homeostasis, is positively regulated by S-adenosyl-L-methionine (AdoMet), but fully inhibited upon CO or NO• binding to a non-catalytic heme moiety. Despite extensive studies, the molecular basis of several pathogenic *CBS* mutations is not yet fully understood. Here we found that the ferrous heme of the reportedly mild p.P49L CBS variant has altered spectral properties and markedly increased affinity for CO, making the protein much more prone than wild type (WT) CBS to inactivation at physiological CO levels. The higher CO affinity could result from the slightly higher flexibility in the heme surroundings revealed by solving the crystallographic structure of a truncated p.P49L at 2.80-Å resolution. Additionally, we report that p.P49L displays impaired H_2S-generating activity, fully rescued by PLP supplementation along the purification, despite a minor responsiveness to AdoMet. Altogether, the results highlight how increased propensity to CO inactivation of an otherwise WT-like variant may represent a novel pathogenic mechanism in classical homocystinuria.

ABBREVIATIONS

AdoMet, S-adenosyl-L-methionine; CBS, cystathionine β-synthase; $CBS\Delta_{409-551}$, truncated cystathionine β-synthase lacking the C-terminal 143 residues; CBS p.P49L, cystathionine β-synthase variant harboring a proline-to-leucine substitution at residue 49; CO, carbon monoxide; CSE, cystathionine γ-lyase;

EDTA, ethylenediaminetetraacetic acid; H_2S, hydrogen sulfide; KPi, potassium phosphate; MME, monomethyl ether; MST, mercaptopyruvate sulfurtransferase; NO•, nitric oxide; PEG, polyethylene glycol; PLP, pyridoxal 5'-phosphate; r.m.s.d., root mean square deviation; SDS-PAGE, sodium dodecyl sulfate polyacrylamide gel electrophoresis; WT, wild-type

INTRODUCTION

Hydrogen sulfide (H_2S) has emerged as a key signaling molecule in human physiology and pathophysiology, being implicated in the regulation of several processes such as neuromodulation, angiogenesis, vasorelaxation, bioenergetics/respiration, cell survival and proliferation, among others [1-4]. The gas has a pivotal role in the control of cellular redox homeostasis and prevention of oxidative stress, modulating the expression of key antioxidant enzymes [2]. Similarly to other relevant gaseous signaling molecules like CO and NO•, at low concentrations H_2S can exert cytoprotective effects or become cytotoxic at higher concentrations.

At least three human enzymes have been identified as key endogenous sources of H_2S: cystathionine β-synthase (CBS) and cystathionine γ-lyase (CSE), both occurring in the transsulfuration pathway of methionine metabolism, and mercaptopyruvate sulfurtransferase (MST) [1]. Beyond enabling conversion of homocysteine to cysteine through their historically recognized canonical activities, CBS and CSE catalyze a number of 'alternative' reactions leading to H_2S synthesis, which has brought these enzymes into the limelight [1,5,6]. Indeed, a growing number of human pathologies, from cardiovascular and neurodegenerative diseases to different cancer types, are reportedly associated with disturbances of H_2S metabolism related to CBS, CSE and/or MST [7]. CBS, in particular, has been shown to be overexpressed in colorectal, ovarian and breast cancer, among other

cancer types (reviewed in [8,9]), as well as in neurodegenerative diseases, such as amyotrophic lateral sclerosis [10]. The enzyme is therefore currently recognized as a drug target [8].

CBS catalyzes the condensation of homocysteine and serine (or cysteine) leading to formation of cystathionine and H_2O (or H_2S). The human enzyme is a 551-amino acid protein with a central catalytic domain, harboring a pyridoxal 5'-phosphate (PLP) cofactor, flanked by a C-terminal domain with a binding site for the allosteric positive regulator S-adenosyl-L-methionine (AdoMet) and an N-terminal domain, harboring a hexacoordinate heme with C52 and H65 as endogenous Fe ligands [11]. Structural studies have shown that, whereas the AdoMet-binding domain occludes the substrate entry site in the catalytic core, AdoMet binding induces a conformational change clearing the path for substrates access to the active site [11-13]. In the presence of AdoMet enzymatic activity thus increases 2-5 fold, as measured with isolated proteins and bacterial or human cell lysates. Another interesting regulatory mechanism concerns the B-type heme moiety in the N-terminal domain. While the enzyme is fully active when the heme is in the oxidized state, reduction to the ferrous state negatively impacts enzyme activity, possibly through a ligand exchange mechanism involving the replacement of C52 by a yet unknown neutral ligand [14,15]. Such change in the Fe coordination is accompanied by a notable shift in the CBS heme Soret band from 449 to 424 nm, leading to an inactive protein species commonly referred to as 'C-424' [15]. Even more striking is that binding of NO• or CO to the ferrous heme results in enzyme inhibition [16-20], with different lines of evidence pointing to a physiological role of this regulatory mechanism *in vivo* [21-27]. According to structural and mutagenesis studies, changes in the heme redox and ligation state are communicated to the PLP active site through α-helix 8 [15,28,29]. This regulatory mechanism places CBS at the

crossroad between the signaling pathways of the three gasotransmitters (H_2S, CO and NO•) in human physiology [30]. More recently, it has been shown that AdoMet enhances CBS sensitivity to CO and NO•, further highlighting an intricate interplay between the three domains in the protein [20].

Classical homocystinuria (OMIM #236200) is an inborn error of metabolism associated with mutations in the *CBS* gene. With a variable incidence of 1:1,800 to 1:900,000, classical homocystinuria is biochemically detected by markedly high homocysteine and methionine levels in plasma and urine, with clinical presentation involving mental impairment, vascular complications, dislocated lenses and skeletal abnormalities [31]. Notably, elevated homocysteine levels are associated with oxidative stress conditions, well known to contribute to the onset and progress of a broad spectrum of diseases. Thus far, besides dietary methionine restriction, the major therapeutic approach for classical homocystinuria consists of administration of pyridoxine (vitamin B6), a precursor of the PLP cofactor [31], although a significant part of patients (approximately half) do not respond to this treatment [32]. The vast majority of the mutations identified in patients with classical homocystinuria are missense mutations resulting in single amino acid substitutions. Whereas most mutations affect the enzyme folding and/or activity [15,28,33-39], some of them have been shown to affect enzyme regulation by AdoMet, pointing to such dysregulation as a new pathogenic mechanism in classical homocystinuria [40]. The fact that several variants have impaired activity due to protein misfolding is underlined by the demonstration that some of them are amenable to be functionally rescued by chemical chaperones [34,36,38,39,41,42]. A novel therapeutic approach is currently under development based on enzyme replacement therapy using PEGylated recombinant CBS, which has been shown to afford a marked decrease in circulating homocysteine in a mouse model of homocystinuria

[43]. This therapeutic approach might be particularly relevant for PLP-unresponsive patients.

The 146 C>T transition in exon 1 of the *CBS* gene generates the clinically relevant p.P49L variant, identified in patients with classical homocystinuria [44-46]. The mutation results in mild to moderate symptoms and sporadic responsiveness to vitamin B6 treatment. When assayed in cell extracts or after purification, the protein variant shows impaired or wild type (WT)-like canonical activity in the absence or presence of PLP in the assays, respectively, and milder to normal responsiveness to AdoMet [36,37,39,40]. These findings point to defects in PLP incorporation, although the protein variant as purified after recombinant expression in *Escherichia coli* in the presence of suitable chemical chaperones at optimal concentrations exhibits unaffected PLP and heme incorporation, and unperturbed circular dicroism (CD) or UV-visible absorption spectra in the oxidized state [39].

Herein we demonstrate that the p.P49L variant of human CBS displays H_2S-synthesizing activity largely sensitive to PLP supplementation along the protein purification. The crystallographic structure of a truncated version of CBS p.P49L, devoid of the C-terminal Ado-Met binding domain, reveals no major differences at the level of the PLP catalytic site with respect to the WT, but slightly increased protein flexibility in the heme surroundings. As a novel finding we report a markedly increased CO affinity of p.P49L as compared to the wild-type enzyme, *en route* to enzyme inactivation. The obtained functional and structural data are discussed in light of the proposal that in pathogenic variants of human CBS increased reactivity towards exogenous ligands, such CO, represents a further molecular mechanism at the basis of classical homocystinuria.

MATERIALS AND METHODS

Protein expression and purification

Recombinant full-length human CBS p.P49L was expressed and purified as previously described for WT CBS [19] either in the absence or presence of 20 μM PLP, using the herein named pET28b-CBS-p.P49L vector generated in [40]. With this vector as template, site-directed mutagenesis was employed to obtain also a truncated form of the protein (denoted CBS$\Delta_{409\text{-}551}$ p.P49L) devoid of the C-terminal 143 residues corresponding to the AdoMet-binding domain. The 1227G>A mutant (cDNA numbering) carrying a premature stop codon at position 409 was generated from pET28b-CBS-p.P49L using the XL Quick Change Kit (Agilent) and the primers 5'-GAAGAAGCCCTGGTGATGGCACCTCCGTG (forward) and 5'-CACGGAGGTGCCATCACCAGGGCTTCTTC (reverse). All vectors were checked for the correct mutation by DNA sequencing. Expression and purification of CBS$\Delta_{409\text{-}551}$ p.P49L were carried out as described in [20].

Purity of the isolated proteins was assessed by SDS-PAGE and their concentration was determined by the Bradford method [47], whereas the heme concentration in the isolated oxidized proteins was determined using ε_{428nm} = 92,700 M^{-1} cm^{-1} [48].

Unless otherwise stated, the experiments were carried out in 50 mM KPi buffer, 300 mM KCl, 10% glycerol, 100 μM EDTA, pH 7.0 (Buffer A).

H_2S synthesis assays

H_2S production by recombinant human CBS variants was measured at 37 °C, either by amperometry using a H_2S-selective electrode (World Precision Instruments) or by the lead acetate method [5]. Purified CBS (0.5-1 μM) was incubated for 10 minutes with 50 μM PLP, 260 U/ml catalase and 0.4-2.0 mM homocysteine in the absence or presence of 0.5 mM AdoMet, after

which 10 mM cysteine was added to trigger the reaction. Amperometric assays were performed using an ISO-H2S-2 hydrogen sulfide sensor coupled to an Apollo 4000 Free Radical Analyzer (World Precision Instruments). After recording H_2S production for 3 minutes, the electrode was internally calibrated by adding 4 μM NaHS (corresponding to 2 μM H_2S at pH 7.0). Finally, 50 μM *O*-acetylserine and 200 nM *Entamoeba histolytica O*-acetylserine sulfhydrylase were added to the reaction mixture to remove H_2S from solution and bring the signal back to baseline [49]. Activity assays by the lead acetate method were carried out in a thermostated cuvette under stirring, according to [5]. Lead acetate (400 μM) was added to the reaction mix prior to cysteine addition, and H_2S production monitored at 390 nm in an Agilent Cary-60 spectrophotometer.

CO titrations

UV-visible absorption spectra of oxidized and reduced CBS p.P49L and WT were recorded in an Agilent Cary-60 spectrophotometer. Anaerobic titrations of reduced CBS p.P49L with CO were performed at 20 °C in an Agilent Cary-60 or a Shimadzu UVPC-1800 spectrophotometer. Gas exchange was prevented either by filling the quartz cuvette and sealing it with a rubber-cap or by adding mineral oil on top of the aqueous medium. Anaerobic conditions were ensured by nitrogen flushing and addition of glucose oxidase (4 units·ml^{-1}), catalase (13 μg·ml^{-1}), superoxide dismutase (12 units·ml^{-1}) and glucose (3 mM) to scavenge contaminant oxygen, hydrogen peroxide and superoxide anion. CBS p.P49L and WT (1.4-1.6 μM in heme) were reduced with 90 μM sodium dithionite, diluted from a 45 mM stock solution (quantitated using ε_{314nm} = 8,043 M^{-1}·cm^{-1} [50]). CO stock solutions were prepared by equilibrating thoroughly degassed buffer A with the pure gas at 1 atm, yielding 1 mM CO at 20 °C. After each CO addition with gas-tight

Hamilton syringes, the spectral changes were visually inspected in real time and a new addition was immediately made when no more changes were observed.

According to [16,19,20,51], two apparent K_d ($K_{d,1}$ and $K_{d,2}$) were used to satisfactorily fit the CO affinity data. The $K_{d,1}$ and $K_{d,2}$ values were obtained by fitting the data to Equation 1, where P_L is the concentration of CO-bound CBS p.P49L, P_T and L_T are, respectively, the total CBS p.P49L and CO concentrations, and α_1 and α_2 are, respectively, the protein fractions binding CO at higher (K_{d1}) and lower (K_{d2}) affinity.

$$PL = \frac{\alpha_1\left[(P_T + L_T + K_{d1}) - \sqrt{(P_T + L_T + K_{d1})^2 - 4P_T L_T}\right] + \alpha_2\left[(P_T + L_T + K_{d2}) - \sqrt{(P_T + L_T + K_{d2})^2 - 4P_T L_T}\right]}{2}$$

Equation 1.

Stopped-flow measurements

Time-resolved absorption spectroscopy experiments were carried out in a thermostated stopped-flow instrument (DX.17MV, Applied Photophysics), equipped with a photodiode-array (light path, 1 cm). To avoid light-induced artifacts, the intensity of the white-light incident beam was decreased and a filter cutting UV light at $\lambda < 360$ nm was employed. Absorption spectra were recorded with an acquisition time of 10 ms per spectrum according to a logarithmic time scale. All reactions were carried out at 25 °C in buffer A. CBS p.P49L was thoroughly flushed with nitrogen, after which glucose oxidase (4 units·ml^{-1}), catalase (13 µg·ml^{-1}), superoxide dismutase (12 units·ml^{-1}) and glucose (3 mM) were added to scavenge oxygen, hydrogen peroxide and superoxide anion. The protein was then placed on ice, protected from light to prevent possible damaging photoreactions. When indicated, CBS p.P49L was incubated with AdoMet for ≥10 minutes, prior to reduction with 90 µM sodium dithionite. CO association kinetics were studied by

mixing in the stopped-flow apparatus reduced CBS p.P49L, in the absence or presence of AdoMet, with CO solutions and the spectra recorded over time. CO dissociation kinetics were evaluated by mixing the Fe(II)-CO adduct of CBS p.P49L with NO• stock solutions, prepared by equilibrating degassed ultra-pure water with NO• gas at 1 atm, further kept on ice protected from light.

Spectral data analysis

CO affinity titrations and CO binding and dissociation kinetic data were analyzed with the software MATLAB (Mathworks). Global fit analysis of spectral data was performed by singular value decomposition analysis combined with curve fitting [52].

Protein crystallization

Initial crystallization screenings for CBS$\Delta_{409\text{-}551}$ p.P49L were performed in 96-well plates at 293 K using a Cartesian mini-Bee nanoliter-drop dispensing robot (Genomic Solutions). These screenings allowed for the identification of one hit for CBS$\Delta_{409\text{-}551}$ p.P49L from the JCSGplus^{TM} screen (Molecular Dimensions): G10 (0.15 M KBr, 30% w/v PEG 2000 MME). Crystals were optimized at the microliter scale using sitting-drop vapor diffusion with a drop composition of 0.5 µl protein solution (27.4 mg·ml^{-1} in Buffer A with 20 µM PLP) and 0.5 µl reservoir solution (0.15 M NaBr, 35% PEG 2000 MME) equilibrated against 500 µl precipitant solution in the well. Dark orange colored small needles as well as big rod-shaped crystals appeared after 12 h at 20 °C.

Data processing and refinement

Cryoprotection conditions for diffraction experiments were achieved by transferring the crystals to a 5 µl drop of 35% (w/v) PEG 2000 MME, 5% (v/v) glycerol, 0.15M NaBr. The crystals were flash-cooled by quick plunging into liquid nitrogen. A single crystal was used for data collection under a nitrogen-gas stream (Oxford Cryosystems 700) on beamline ID30A-3 at the ESRF synchrotron (Grenoble, France) using a PILATUS 6M detector (Dectris) at a wavelength of 0.9677 Å. After indexing and calculation of a data collection strategy using *EDNA* [53], a wedge of 360° of data was collected using a fine-slicing strategy (0.1° rotation per image). The data set was indexed and integrated with *XDS* [54] space-group assignment was performed with *POINTLESS* [55] and scaling was performed with *AIMLESS* [56] all within the *autoPROC* data-processing pipeline [57]. At this stage an R_{free}-flag set was created corresponding to 5% of the measured reflections of the data-set. Crystals belonged to the monoclinic space group *P*1 with unit cell parameters a = 86.2 Å, b = 86.8 Å, c = 97.8 Å, α = 102.6°, β = 103.1°, γ = 111.2°. Data were truncated at 2.80 Å. Data reduction and refinement statistics are depicted in Table 1. The structure of the CBSΔ$_{409\text{-}551}$ p.P49L variant was solved by molecular replacement using PDB entry 1JBQ devoid of any solvent and cofactors as search model using *phaser* [58] within the *PHENIX* software suite of programs [59]. Based on the Matthews coefficient, the search was performed for six molecules. Automated model building was performed using the *AutoBuild* wizard [60], also within *PHENIX*. Initial refinement rounds were carried out with *BUSTER-TNT* [61] using the macro that accounts for missing parts of the model ("-L"). At this point, electron density features attributed to the heme moieties were easily identified. Iterative cycles of manual model building and refinement were carried out with *COOT* [62] and *BUSTER-TNT* until convergence. Validation was

performed with *RAMPAGE* [63] and *MolProbity* [64] as implemented in *PHENIX*.

RESULTS

Hydrogen sulfide synthesis by CBS p.P49L

H_2S synthesis by the CBS p.P49L variant using homocysteine and cysteine as substrates was analyzed in comparison with the WT enzyme by amperometric and colorimetric (lead acetate) methods. Two sets of enzyme preparations, purified either in the absence or presence of the PLP cofactor, were evaluated in assays run in the presence of PLP. As shown in Figure 1, the p.P49L CBS variant isolated in the absence of PLP (PLP-'untreated') displays a basal activity more than 3-fold lower than that of the WT enzyme. Despite the markedly impaired enzymatic activity of 'untreated' CBS p.P49L, activity stimulation by AdoMet is similar between WT and p.P49L (respectively 1.5- and 1.4-fold). Conversely, the p.P49L CBS variant purified in the presence of PLP (PLP-'treated') displays a basal activity similar to the WT enzyme, despite presenting impaired activity stimulation by AdoMet (1.9-fold for WT to be compared with 1.1-fold for p.P49L). The AdoMet activation factor ($\leq$ 2 fold) observed for the WT enzyme was slightly lower than usually reported (2-5 fold). This could be related with a fraction of the enzyme lacking the C-terminal domain, which was also observed for the CBS p.P49L variant (Supplementary Figure S1).

Structure of CBS p.P49L variant

In an attempt to understand the structural impact of the proline-to-leucine substitution at position 49 of human CBS, we have determined the X-ray structure of a truncated form of the p.P49L variant (PDB entry 5MMS), lacking the C-terminal 143 residues (henceforth designated as $CBS\Delta_{409\text{-}551}$

p.P49L), similarly to the reported structure of truncated WT CBS (PDB entry 1JBQ) [65]. Crystals belong to the triclinic space group *P*1 with cell dimensions a = 86.2, b = 86.8 and c = 97.8 Å, α = 102.6°, β = 103.1° and γ = 111.2°. *XDS* as implemented in *autoPROC* clearly identifies two different lattices in the diffraction pattern rotated by 121.4° relative to each other. This diminishes the quality of the overall statistics since in some directions an almost perfect superposition of reflections makes the integration difficult (data collection and refinement statistics are depicted in Table 1).

There are six molecules in the asymmetric unit corresponding to a Matthews coefficient [66] of 2.31 $Å^3 \cdot Da^{-1}$ and a solvent content of approximately 47%. The structure was refined to 2.80 Å resolution with R_{cryst} of 18.2% and R_{free} of 22.1%. The final model comprises the residues from R45 to E400 (in chain D), 6 hemes, 6 PLP molecules, 3 sodium ions and 185 water molecules. The hemes are axially bridged by C52 and H65 and the PLP moieties covalently linked to the polypeptide chain through K119. The maps are generally of good quality except for two disordered loops (T193 to S199 and Q295 to T300), for which only in chain D there were complete electron densities. This contrasts with the published structure of the truncated human CBS WT (PDB entry 1JBQ), where the T193-S199 loop could not be modeled. The variant dimeric structure, shown in Figure 2A, displays an essentially identical overall fold with respect to the WT enzyme (r.m.s.d. of 0.4 Å for 344 aligned C_α carbon atoms between chain D of $CBS\Delta_{409\text{-}551}$ p.P49L and chain A of 1JBQ) and highly conserved features in the PLP active site and the N-terminally located heme moiety (Figure 2B).

Spectral properties of ferrous p.P49L CBS

In the absence of clear structural clues for pathogenicity of the p.P49L mutation, we sought to evaluate by UV-visible absorption spectroscopy the

impact of this residue substitution on the protein redox spectra, largely dominated by the heme absorption. In WT CBS, heme reduction leads to notable changes in the protein absorption spectrum, with a shift of the Soret band from 428 nm to 449 nm (Figure 3A). Upon incubation of the enzyme with AdoMet prior to reduction, the spectrum of the reduced enzyme is affected by a decrease in the 449-nm band intensity and the appearance of a feature centered at ~424 nm (Figure 3A, red solid line). Regardless of AdoMet, in the oxidized state, p.P49L CBS exhibits no differences in the absorption spectrum as compared to the WT protein (Figure 3, dashed lines). In contrast, major differences can be noted by comparing the spectra of the two proteins in the reduced state, with the mutant displaying markedly more pronounced appearance of the 424-nm spectral feature and decrease of the 449-nm band (Figure 3B, blue solid line), both further elicited in the AdoMet bound protein (Figure 3B, red solid line).

Enhanced affinity of p.P49L CBS for CO

Prompted by the observed spectral differences between reduced p.P49L and WT CBS, we analyzed the affinity of the mutated protein for the physiologically relevant CO ligand by performing anaerobic CO titrations. Similarly to the WT protein, conversion of ferrous CBS p.P49L to the CO adduct proved to result in the appearance of a band centered at 422 nm (Figures 4A and 4B). Global fit analysis of the spectral data set acquired along the titration revealed a much higher CO affinity (>50 fold) of p.P49L CBS (Figure 4C, full circles) as compared to the WT enzyme (Figure 4C, dotted line). Notably, as previously reported by Vicente et al. [20] for WT CBS (Figure 4C, dashed line) and consistent with the effect of AdoMet on the spectrum of reduced p.P49L CBS (Figure 3B), pre-incubation of the protein variant with AdoMet further enhances the CO affinity (Figure 4C,

hollow squares). CO titrations allowed to estimate the following K_d values: $K_{dCO,1}$ = 0.06 ± 0.03 μM and $K_{dCO,2}$ = 21 ± 5 μM (with 60%, and 40% relative amplitude, respectively) for AdoMet-free p.P49L CBS, and $K_{dCO,1} \leq$ 0.03 μM and $K_{dCO,2}$ = 1.5 ± 0.6 μM (with 70%, and 30% relative amplitude, respectively) for the AdoMet-bound enzyme. It should be noted that the CO affinity of the AdoMet-bound p.P49L variant is so high that the $K_{dCO,1}$ value actually represents an upper limit. A possible direct interference of CO with AdoMet was ruled out by performing a control experiment where an AdoMet solution was equilibrated with CO gas (or N_2 as control), yielding no spectral changes (*not shown*).

Kinetics of CO binding and dissociation from p.P49L CBS

The markedly higher CO affinity of p.P49L CBS as compared to the WT enzyme led us to investigate by time-resolved absorption spectroscopy the kinetics of CO binding to and dissociation from ferrous p.P49L CBS (Figure 5). Upon stopped-flow mixing reduced CBS p.P49L with 1 mM CO, the observed spectral changes were identical in shape to those shown for the CO titrations in Figure 4, i.e., the predominant 449-nm Soret band and the 424-nm spectral feature both shifted to 422 nm, with similar optical transitions for the AdoMet-free and -bound CBS p.P49L (inset to Figure 5A). Global fit analysis of the kinetic data revealed that both AdoMet-free and -bound p.P49L react with CO according to multiphasic time courses (Fig. 5A), as previously shown for WT CBS [19,20,51,67]. Interestingly, despite the markedly increased CO affinity of p.P49L with respect to the WT protein, under identical experimental conditions CO binding to the either of the two proteins in the absence of AdoMet proceeds at comparable rates ($t_{1/2}$ = 26.2 ± 9.6 s for CBS p.P49L, Figure 5A, to be compared with $t_{1/2}$ = 34.5 ± 10.5 s of WT, not shown). In the presence of AdoMet, where the spectral changes

(Figure 3) and the enhanced CO affinity (Figure 4) of CBS p.P49L point to significant effects on the heme properties, a marked increase in CO association rates is observed, with the $t_{1/2}$ decreasing to 5.4 ± 3.1 s (Figure 5A), to be compared with $t_{1/2}$ = 17.0 ± 2.7 s for WT CBS (not shown).

The kinetics of CO dissociation from CBS p.P49L was evaluated by anaerobically mixing in the stopped-flow apparatus the CO-bound ferrous protein with authentic NO• (900 μM after mixing) and monitoring the conversion of the 422-nm hexacoordinate CO-bound adduct spectrum into that of the pentacoordinate NO•-bound adduct with a broad absorption band centered at 395 nm (Inset to Figure 5B). Global fit analysis of the kinetic data revealed that under identical experimental conditions CO is displaced by NO• in CBS p.P49L at comparable rates (k_1 = 2.0 ± 0.1 s^{-1} and k_2 = 0.37 ± 0.05 s^{-1}, with 75%, and 25% relative amplitude, respectively) to the WT enzyme (k_1 = 2.0 ± 0.1 s^{-1} and k_2 = 0.33 ± 0.03 s^{-1}, with 75%, and 25% relative amplitude, respectively; *data not shown*), and showing no effect of AdoMet (Figure 5B).

DISCUSSION

Classical homocystinuria is an inborn error of metabolism associated with deficiency in cystathionine β-synthase (CBS), a key enzyme in the transsulfuration pathway of methionine metabolism. By catalyzing the conversion of homocysteine and serine into cystathionine, the enzyme prevents an excessive increase in homocysteine levels, a pathological condition associated with oxidative stress and clinical complications in the vascular, neurological and skeletal systems. CBS also has a relevant role in human physiology by being a major source of H_2S, a key endogenous signaling molecule whose dysregulation is at the basis of several human

pathologies, from cardiovascular and neurodegenerative diseases to cancer. Thus far, despite decades of research on classical homocystinuria, a full understanding of the molecular events at the basis of the pathogenicity of several CBS mutations remains elusive, although protein misfolding, dysfunctional regulation by AdoMet and impaired enzymatic activity have been put forward for some mutations [15,28,33-39].

This prompted us to investigate in the present study a reportedly mild pathogenic mutation associated with classical homocystinuria, a proline-to-leucine substitution at residue 49 in human CBS [44-46]. The recombinant CBS p.P49L variant was expressed in *E. coli*, purified and characterized both structurally and functionally. In line with previous reports focused on the canonical cystathionine synthase activity, this variant displayed a H_2S synthesizing activity remarkably sensitive to PLP supplementation along the purification procedure [36,37,39,40]. The functional rescue of p.P49L H_2S synthesis by PLP is indicative of a decreased affinity of this variant for the cofactor, a frequently observed consequence of missense mutations potentially associated with protein misfolding. The functional recovery of p.P49L observed upon PLP supplementation during protein purification was however not fully matched in terms of activity stimulation by AdoMet, as the H_2S-synthesizing activity of p.P49L showed poor responsiveness to AdoMet (Figure 1) as compared to its cystathionine synthase activity [36,37,39,40]. This is not surprising since for other CBS variants it has been shown that the extent of the stimulatory effect of AdoMet can differ between the canonical cystathionine synthase and the H_2S-synthesizing activities [28].

Further attempting to understand the molecular basis of pathogenicity of this mutation, the crystallographic structure of a truncated form of the CBS p.P49L variant ($CBS\Delta_{409-551}$ p.P49L) was obtained at 2.8 Å resolution and compared with that of the truncated WT enzyme (PDB 1JBQ) [65]. Within

the obtained resolutions, the structures display highly conserved features (Figure 2), particularly inspecting the PLP binding pocket with the cofactor covalently bound to K119, the heme ligands C52 and H65, α-helix 8 (responsible for the heme-PLP communication), the R266 residue forming a salt-bridge with C52, and the flexible loop where the mutated P49 residue is located. Therefore, at first glance, the structural data do not seem to provide a clue for the pathogenicity of the mutation.

The effect of the mutation on the spectroscopic and ligand-binding properties of the heme moiety was also investigated. The first hint for a perturbation in the CBS p.P49L heme microenvironment arose from inspection of the dithionite-reduced spectrum of this protein variant (Figure 3). Indeed, in the spectrum of reduced CBS p.P49L, the dominating 449-nm band assigned to the hexacoordinate ferrous heme with C52 and H65 as axial ligands, shows a significant intensity decrease as compared to the WT enzyme, and the appearance of a band at 424 nm (Figure 3B). The latter spectral feature has been assigned to a ligand exchange process in CBS leading to formation of an enzymatic species (called C-424), in which the cysteine thiolate ligand is replaced by a neutral species [14,15], negatively impacting the enzymatic activity. In WT CBS, this ligand exchange process occurs very slowly (> 48 h at 37 °C, [14]) in the presence of excess reductant. Similarly to p.P49L, other CBS variants have been previously reported to display an increased propensity to form the C-424 species, particularly CBS variants with mutated residues in α-helix 8 [28]. Furthermore, as observed for the WT CBS (Figure 3A), incubating the p.P49L variant with AdoMet prior to reduction further enhances the conversion of the ‘normal’ 449-nm into the ligand-exchanged C-424 species in the reduced protein (Figure 3B). Interestingly, among the several CBS variants studied by Yadav and co-workers [28], p.T257V shows the most similar spectra to CBS p.P49L and,

like this variant, it displays WT-like (and PLP-dependent) H_2S-generating activity and impaired activation by AdoMet [28]. Altogether, the spectral data herein reported point to changes at the heme moiety of CBS p.P49L that were further explored by evaluating the CO binding properties of the protein variant. CBS has been shown to be inhibited *in vitro* by exogenous ligands like CO and NO• [16-20], with different lines of evidence pointing to a physiological relevance of this regulatory mechanism *in vivo* [21-27] (see below).

By performing CO titrations under anaerobic conditions, we observed spectral changes (Figure 4) consistent with the formation of the hexacoordinate ferrous-CO adduct, with the C52 thiolate or the yet unknown 'X' ligand of the C-424 species being replaced by CO, and the heme retaining the H65 endogenous ligand. Notably, the CO affinity, herein measured for the first time in a CBS variant, is markedly increased (≥50 fold) in CBS p.P49L with respect to the WT enzyme (Figure 4C, [16,20,51]). As previously described for WT CBS, the CO titrations followed a biphasic profile, which has been previously attributed to heterogeneity in the heme micro-environment [16] or anti-cooperativity between hemes within a CBS dimer [51]. The remarkably higher CO affinity of CBS p.P49L is essentially due to the extremely low $K_{dCO,1}$ (0.06 ± 0.03 μM), close to the detection limit of the experimental setup. Notably, and as previously observed for the WT enzyme [20], incubation of CBS p.P49L with AdoMet induced a further increase in CO affinity (Figure 4C) and, therefore, only an upper limit value for $K_{dCO,1}$ (≤ 0.03 μM) could be estimated. In the WT enzyme, the increased CO affinity observed in the presence of AdoMet is fully matched with an enhanced propensity for CO inhibition of the protein H_2S producing activity [20]. Based on the remarkable increase in CO affinity herein documented for CBS p.P49L, this protein variant is expected to be more prone to inhibition at

low physiological CO levels. This may represent a more general mechanism of pathogenesis in classical homocystinuria, if other pathogenic CBS mutations will be demonstrated to lead to enhanced CO affinity, as shown for CBS p.P49L in the present study.

Although direct evidence for ferrous CBS formation *in vivo* is still missing in the literature, several reports have attested the physiological role of CBS inhibition by CO (reviewed in [26,27]), which requires the heme to be in the ferrous state. Regarding regulation of cerebral microcirculation by hypoxia, decreased oxygen levels impair CO production by heme oxygenase HO-2 and the release of CBS inhibition by CO promotes H_2S synthesis, that in turn mediates vasodilation of precapillary arterioles [23]. Stress-inducible levels of CO in mice liver cause metabolomic changes consistent with CBS inhibition, decrease in hepatic H_2S and concomitant stimulation of HCO_3^--dependent bile output in wild-type, but not in heterozygous CBS knockout mice [22]. Another proposed mechanism concerns the CO-mediated regulation of glucose utilization, where CBS inhibition by CO drives the demethylation of phosphofructokinase/fructose bisphosphatase type-3 (PFKFB3), diverting glucose from the glycolytic towards the NADPH-generating pentose phosphate pathway, with implications in chemoresistance and oxidative stress resistance in cancer cells [24]. Moreover, Banerjee and co-workers [25] have recently shown that, under endoplasmic reticulum stress conditions, CBS inhibition by CO, combined with CSE induction, flips the CSE substrate preference from cystathionine to cysteine, transiently stimulating H_2S production. These multiple lines of evidence provide compelling, though still indirect evidence for the formation of ferrous CBS *in vivo*. In line with these observations, an NADPH-dependent diflavin enzyme, methionine synthase reductase, has been shown to reduce the CBS heme *in vitro* in the presence of CO or nitrite, generating respectively the ferrous-CO

or ferrous-NO CBS adducts [18,67,68]. In light of this evidence, the high affinity of CBS p.P49L for CO is fully compatible with the formation of the ferrous-CO adduct at physiological CO concentrations.

To gain mechanistic insight into this high CO affinity, we studied by stopped-flow absorption spectroscopy the kinetics of CO association/dissociation to/from the reduced heme of this protein variant (Figure 5). Similarly to the WT [19,20,51], CO binding to reduced CBS p.P49L followed a multiphasic timecourse (Figure 5A). Taking into account the markedly increased CO affinity of this protein variant, surprisingly the reaction proceeded only slightly faster ($t_{1/2}$ = 26.2 ± 9.6 s) than for the WT enzyme ($t_{1/2}$ = 34.5 ± 10.5) under identical experimental conditions. Despite this minor difference, in the presence of AdoMet the fold increase in the CO association rate was overall higher in the p.P49L variant (~4.5 fold) than in the WT enzyme (~2 fold) under identical experimental conditions. Furthermore, by analyzing the kinetics of CO replacement by NO• in this protein variant, we observed essentially identical kinetic traces for the AdoMet-free and -bound CBS p.P49L (Figure 5B) and for the WT enzyme under the same experimental conditions (*not shown*).

The kinetics of CO association and dissociation therefore do not provide a clear cut explanation for the markedly higher CO affinity of CBS p.P49L, which requires further inspection. In Scheme 1 are represented the reaction steps for conversion of the hexacoordinate ferrous CBS, with the heme Fe ligated to H65 and either C52 or the unknown 'X' ligand in the C-424 species, into the ferrous-CO adduct. It has been previously postulated for the WT enzyme that CO association to the ferrous CBS heme is rate-limited by dissociation of C52 [19,20,51]. Since we observed similar CO association kinetics for WT and p.P49L, where a fraction of the mutant enzyme is likely to be in the ligand-exchanged C-424 state, the CO association appears to be

limited by the off-rate of the endogenous ligand regardless of its nature, C52 or 'X' ($k_{off,Cys/X\ (p.P49L)} \approx k_{off,Cys/X\ (WT)}$ in Scheme 1). Taking into account that the kinetics of CO dissociation were almost identical for WT and p.P49L CBS, regardless of AdoMet being present ($k_{off,CO\ (p.P49L)} \approx k_{off,CO\ (WT)}$ in Scheme 1), the dramatic increase in CO affinity of the p.P49L variant compared to the WT should be related to a slower rebinding of the endogenous ligand, C52 or 'X' ($k_{on,Cys/X\ (p.P49L)} << k_{on,Cys/X\ (WT)}$ in Scheme 1), and/or a faster combination of CO with the transiently generated pentacoordinate species ($k_{onCO\ (p.P49L)} >> k_{on,CO\ (WT)}$ in Scheme 1).

Regardless of these mechanistic details, the perturbed spectrum of the reduced protein and its remarkably higher affinity for CO point to possibly subtle structural changes in the CBS p.P49L variant affecting heme reactivity. To this end, we further compared the structures of the variant and WT enzymes in terms of local flexibility evaluated based on the B factor (Figure 6). This analysis interestingly reveals that the differences in flexibility are mostly located in specific regions of the protein. The α-helix 8, where some mutations have shown to affect the heme spectral properties and the H_2S-generating activity similarly to p.P49L, displays comparable rigidity between CBS p.P49L and the WT enzyme. We thus looked in greater detail at the heme binding region (Figure 6) and found in CBS p.P49L an increased flexibility of the loop surrounding the C52 ligand, which expands to the regions between the C52 and the H65 ligands and even after the latter residue. The p.P49L structure therefore displays a higher flexibility in the region harboring both heme ligands, which provides a possible structural basis for the proposed slower rebinding of the endogenous C52/X ligands upon CO dissociation, thereby accounting for the increased affinity of CBS p.P49L for CO.

CONCLUSIONS

Cystathionine β-synthase (CBS) is a key enzyme in the transsulfuration pathway that prevents oxidative stress conditions, both controlling homocysteine levels and promoting the expression of antioxidant enzymes through the synthesis of H_2S. Being implicated in metabolic, oncologic and neurodegenerative diseases, CBS is currently recognized as a promising drug target. Mutations in the *CBS* gene can lead to classical homocystinuria, a human disease associated with oxidative stress that affects the vascular, neurological and skeletal systems. Protein misfolding, enhanced propensity to aggregation, decreased cofactor affinity and dysfunctional regulation by the allosteric activator AdoMet, together with impaired enzymatic activity, have been proposed to account for the pathogenicity of several CBS mutations. As a novel finding, herein we reported that a clinically relevant variant of CBS (p.P49L) has markedly increased affinity for CO, a known inhibitor of CBS. On this basis, this variant is expected be much more prone than WT CBS to be inactivated by CO at the physiological levels occurring *in vivo*, thereby contributing to pathogenicity. The enhanced affinity for inhibitory gaseous ligands documented here may represent a new pathogenic mechanism at the basis of CBS-related diseases, like classical homocystinuria.

ACKNOWLEDGMENTS

This work was partially supported by Fundação para a Ciência e Tecnologia (FCT) PTDC/SAU-MIC/111447/2009 project grant to JBV, SFRH/BPD/79224/2011 fellowship to JAB, and PD/BD/113990/2015 fellowship to PES, by Ministero dell'Istruzione, dell'Università e della Ricerca of Italy (PNR-CNR Aging Program 2012–2014 and PRIN

20158EB2CM_003 to AG) and by a bilateral grant awarded by Consiglio Nazionale delle Ricerche of Italy and FCT to AG and JBV. JBV was the recipient of a short term fellowship from the Federation of European Biochemical Societies. iNOVA4Health Research Unit (LISBOA-01-0145-FEDER-007344), which is cofunded by Fundação para a Ciência e Tecnologia / Ministério da Ciência e do Ensino Superior, through national funds, and by FEDER under the PT2020 Partnership Agreement, is acknowledged. ESRF support for the ID30A-3 data collection is also acknowledged.

FIGURES AND LEGENDS

Figure 1

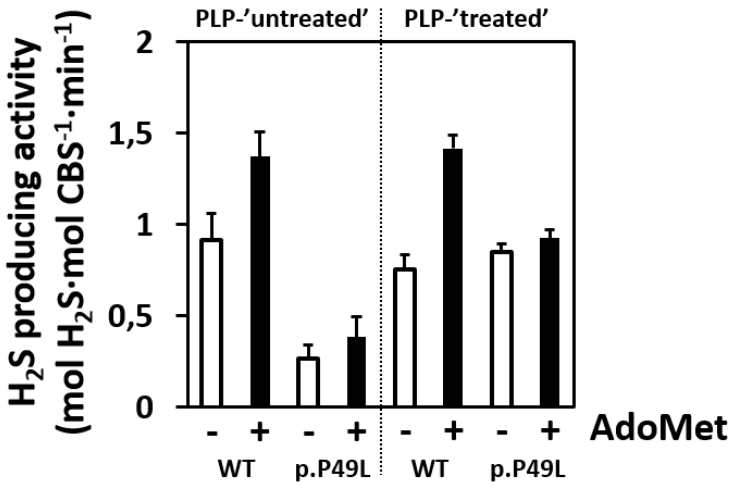

Figure 1. Hydrogen sulfide production by WT and p.P49L CBS. H_2S producing activity of CBS purified in the absence (PLP-'untreated') or presence (PLP-'treated') of PLP (20 μM). T = 37 °C. Buffer: 50 mM KPi,

300 mM KCl, 10% glycerol, 100 μM EDTA, pH 7.0. Reaction mixture contained 50 μM PLP, 0.4-2.0 mM homocysteine, 260 U/ml catalase and 10 mM cysteine. Assays were carried out in the absence (-) or presence (+) of 500 μM AdoMet.

Supplementary Figure 1.

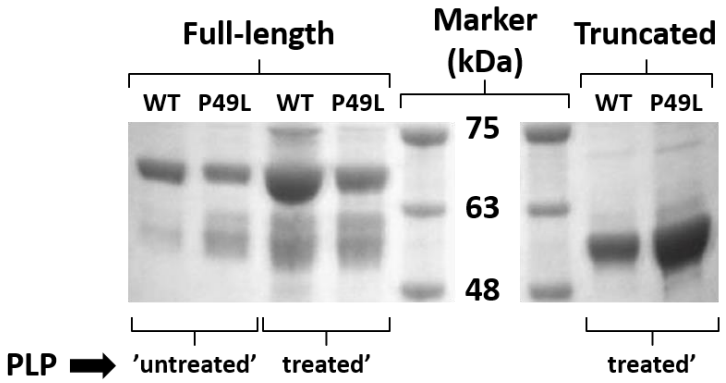

Supplementary Figure 1. SDS-PAGE analysis of CBS preparations. Analysis of CBS samples employed in this study, corresponding to full-length CBS WT and p.P49L purified in the absence ('untreated') or presence ('treated') of PLP (20 μM). Truncated WT and p.P49L CBS lacking the C-terminal AdoMet-binding domain were analyzed for comparison with the full-length protein. Denatured protein samples were loaded onto a pre-cast NuPAGE TM 10% Bis-Tris gel (Invitrogen) and ran at 200 V. Protein bands were stained with InstantBlue TM (Expedeon) according to the manufacturer's instructions. Protein marker: NZYColour Protein Marker II (Nzytech).

Figure 2

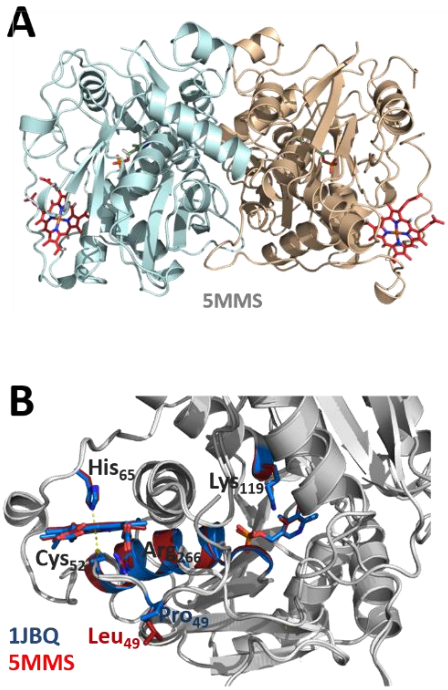

Figure 2. Structure of CBS p.P49L. X-ray crystallographic structure of CBSΔ$_{409-551}$ p.P49L solved at 2.80 Å resolution (PDB entry 5MMS). *Panel A*, cartoon representation of the protein dimer, each monomer being represented in a different color. Pyridoxal 5'-phosphate (PLP) and heme moieties shown in stick representation. *Panel B*, structure superposition of CBSΔ$_{409-551}$ p.P49L (PDB entry 5MMS) and truncated WT CBS (PDB entry 1JBQ), both colored in grey except for most relevant regions and residues, where CBSΔ$_{409-551}$ p.P49L is colored in red and CBSΔ$_{409-551}$ WT in blue; zoom in on the PLP and heme moieties, highlighting the proline to leucine substitution, as well as the R266 residue and α-helix 8 proposed to mediate communication between the heme and the PLP active site. Figure generated with Pymol 1.8.2 (The PyMOL Molecular Graphics System, Version 1.8 Schrödinger, LLC).

Figure 3

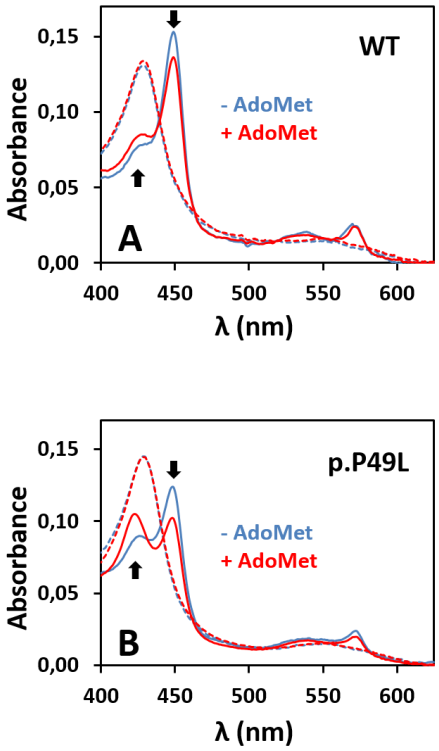

Figure 3. Absorption spectra of WT and p.P49L CBS. Absorption spectra of WT (*Panel A*) and p.P49L (*Panel B*) CBS (1.4-1.6 µM in heme) recorded at 20 °C, in degassed buffer A (50 mM KPi, 300 mM KCl, 10% glycerol, 100 µM EDTA, pH 7.0), containing glucose oxidase (4 units·ml^{-1}), catalase (13 µg·ml^{-1}), superoxide dismutase (SOD, 12 units·ml^{-1}) and glucose (3 mM). Spectra were collected in the oxidized state (dashed lines) and upon protein reduction (solid lines) by addition of 90 µM sodium dithionite, in the absence (blue lines) and presence (red lines) of AdoMet (500 µM). Arrows highlight direction of the spectral changes caused by AdoMet in the reduced proteins.

Figure 4

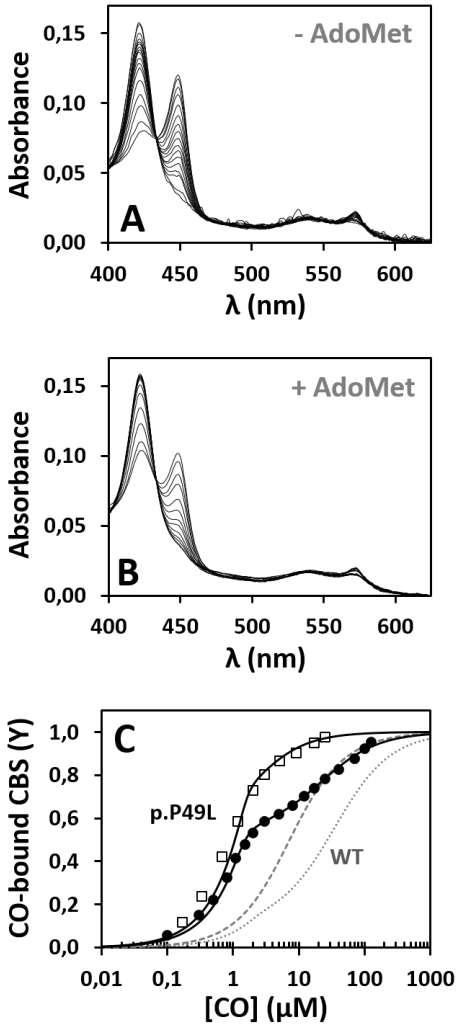

Figure 4. Enhanced CO affinity of p.P49L CBS. Absorption spectra collected upon anaerobic titration of reduced CBS p.P49L (1.4-1.6 μM in heme) with CO, in the absence (*Panel A*) or presence (*Panel B*) of AdoMet. T = 20 °C. *Panel C*, titration profiles obtained by global fit of the spectral data acquired in the absence (full circles) or presence (hollow squares) of 500 μM AdoMet. Data were best fitted according to Equation 1, yielding*:* $K_{dCO,1}$ =

0.05 μM (60%) and $K_{dCO,2}$ = 22.0 μM (40%) for AdoMet-free CBS p.P49L and $K_{dCO,1} \leq 0.03$ μM (70%) and $K_{dCO,2}$ = 2.1 (30%) for the AdoMet-bound enzyme. Gray lines represent titration curves for WT CBS in the absence (dotted line) and presence (dashed line) of 500 μM AdoMet.

Figure 5

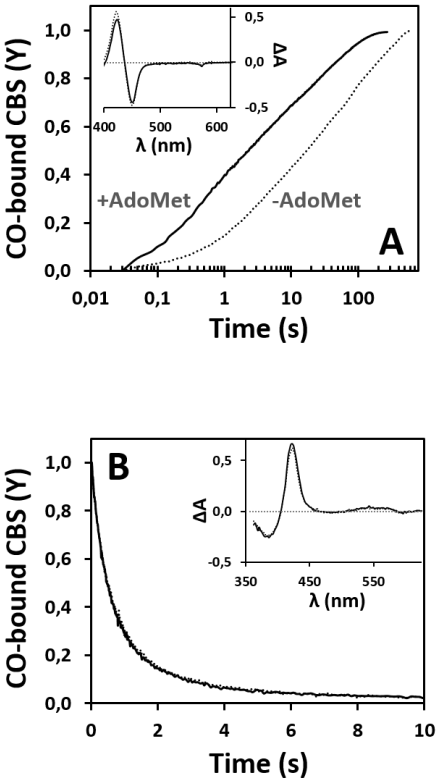

Figure 5. Kinetics of CO binding to ferrous CBS p.P49L. *Panel A*, Reaction time courses measured in the absence (dotted line) or presence of AdoMet (500 μM before mixing; solid line). Spectral data collected over 1000 s after stopped-flow mixing 1 mM CO with reduced CBS p.P49L (1.5 μM in heme) at 25 °C, in 50 mM potassium phosphate, 300 mM KCl, 10% glycerol, pH 7.0, containing 2 mM glucose, 4 units·ml^{-1} glucose oxidase, 13 μg·ml^{-1} catalase and 6 units·ml^{-1} SOD. Fitted rate constants (% reaction

amplitude): k_1 = 0.48 s^{-1} (25%), k_2 = 0.05 s^{-1} (30%) and k_3 = 0.006 s^{-1} (45%) for AdoMet-free CBS p.P49L ($t_{1/2}$ = 19.5 s) and k_1 = 2.55 s^{-1} (35%), k_2 = 0.26 s^{-1} (30%) and k_3 = 0.022 s^{-1} (35%) for the AdoMet-bound enzyme ($t_{1/2}$ = 2.3 s). Inset, optical transitions obtained by global fit analysis of the spectral data acquired in the absence (dotted line) or presence of AdoMet (solid line). *Panel B*, time courses of CO displacement from ferrous CBS p.P49L by 900 μM NO•, acquired in the absence (dotted line) or presence of AdoMet (solid line; 500 μM before mixing). Traces were best fitted with the following rate constants (% reaction amplitude): k_1 = 1.93 s^{-1} (75%) and k_2 = 0.035 s^{-1} (25%) for AdoMet-free CBS p.P49L; k_1 = 1.96 s^{-1} (75%) and k_2 = 0.038 s^{-1} (25%) for the AdoMet-bound enzyme. *Inset*, optical transitions obtained by global fit analysis of the spectral data acquired in the absence (dotted line) or presence of AdoMet (solid line).

Figure 6

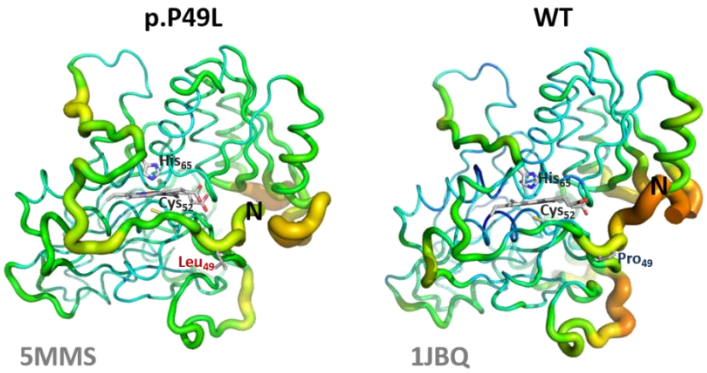

Figure 6. Increased flexibility of heme binding loop in p.P49L CBS. Representation of B factor variation along the structure of CBS p.P49L (PDB entry 5MMS) and WT (PDB entry 1JBQ) monomer, displaying in first plane the regions encompassing the proline to leucine mutation (sticks) and the heme ligands C52 and H65. Flexibility can be visualized both by the

thickness of the structural element and the respective color: highest flexibility represented in red (hot) thick elements; lowest flexibility in thin blue (cold) elements (color scale: red>orange>yellow>green>blue). Figure generated with Pymol 1.8.2 (The PyMOL Molecular Graphics System, Version 1.8 Schrödinger, LLC).

Scheme 1

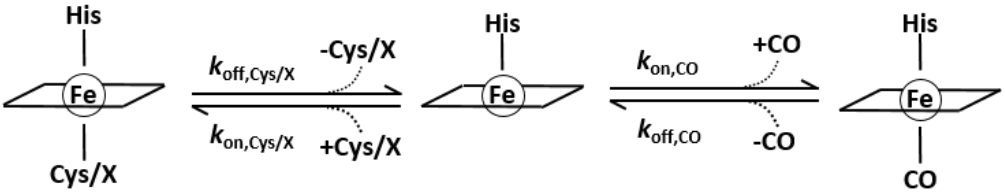

Table 1. Data reduction and refinement statistics of CBS p.P49L structure

	p.P49L CBS variant
PDB entry	5MMS
Data collection	
Synchrotron	ESRF (Grenoble – France)
Beamline	ID30A-3
Wavelength (Å)	0.968
Space group	*P*1
Unit cell	
a, *b*, *c* (Å)	86.2, 86.8, 97.8
α, *β*, *γ* (°)	102.7, 103.1, 111.2
Resolution range[a] (Å)	76.35 - 2.80 (2.90 - 2.80)
Total no. of reflections	121227 (1141)
No. of unique reflections	58862 (571)

Completeness (%)	98.5 (95.6)
Multiplicity	2.1 (2.0)
$\langle I/\sigma(I)\rangle$	4.8 (1.5)
R_{meas}[b] (%)	17.4 (68.7)
R_{pim}[c] (%)	11.2 (45.1)
$CC_{1/2}$[d] (%)	97.6 (62.1)
Wilson B-factor (Å^2)	41.8
Refinement	
R_{cryst}[e] (%)	18.2 (27.2)
R_{free}[f] (%)	22.1 (33.1)
No. of non-H atoms	16452
Protein	15916
Ligands	351
Waters	185
r.m.s.d bonds (Å)	0.010
r.m.s.d. angles (^{o})	1.12
Protein residues	2077
Ramachandran plot	
Most favoured (%)	96.6
Allowed (%)	3.2
Outliers (%)	0.3
Rotamer outliers (%)	0.3
Clashscore	0.46
MolProbity Score[g]	0.88
B-factors (Å^2)	45.4
Protein	41.3

Ligands	29.7

[a] Information in parenthesis refers to the last resolution shell.

[b] $R_{meas} = \Sigma_h (n_h/n_h - 1)^{1/2} \Sigma_i|<I_h> - I_{h,i}|/\Sigma_h \Sigma_i I_{h,I}$, where n_h denotes multiplicity

[c] $R_{pim} = \Sigma_h [1/(/n_h - 1)]^{1/2} \Sigma_i|<I_h> - I_{h,i}|/\Sigma_h \Sigma_i I_{h,i}$

[d] CC1/2 is as described previously [69]

[e] $R_{cryst}=\sum_{hkl}||F_{obs(hkl)}|-|F_{calc(hkl)}||/\sum_{hkl}|F_{obs(hkl)}|$, where $F_{obs(hkl)}|-|F_{calc(hkl)}$ are the observed and calculated structure factors for reflection (*hkl*), respectively.

[f] R_{free} was calculated as R_{cryst} but using only 5% of reflections randomly selected and omitted from refinement.

[g] MolProbity score provides a single number that represents the central MolProbity protein quality statistics; it is a log-weighted combination of Clashscore, Ramachandran not favored and bad side-chain rotamers, giving one number that reflects the crystallographic resolution at which those values would be expected.

REFERENCES

1. Kabil, O., and Banerjee, R. (2014) Enzymology of H_2S biogenesis, decay and signaling. *Antioxid. Redox Signal.* **20**, 770-782
2. Kimura, H. (2015) Signaling molecules: hydrogen sulfide and polysulfide. *Antioxid. Redox Signal.* **22**, 362-376
3. Paul, B. D., and Snyder, S. H. (2015) H_2S: a novel gasotransmitter that signals by sulfhydration. *Trends Biochem. Sci.* **40**, 687-700
4. Olson, K. R., and Straub, K. D. (2016) The role of hydrogen sulfide in evolution and the evolution of hydrogen sulfide in metabolism and signaling. *Physiology (Bethesda)* **31**, 60-72
5. Chiku, T., Padovani, D., Zhu, W., Singh, S., Vitvitsky, V., and Banerjee, R. (2009) H_2S biogenesis by human cystathionine gamma-lyase leads to the novel sulfur metabolites lanthionine and homolanthionine and is responsive to the grade of hyperhomocysteinemia. *J. Biol. Chem.* **284**, 11601-11612

6. Singh, S., Padovani, D., Leslie, R. A., Chiku, T., and Banerjee, R. (2009) Relative contributions of cystathionine beta-synthase and gamma-cystathionase to H_2S biogenesis via alternative trans-sulfuration reactions. *J. Biol. Chem.* **284**, 22457-22466
7. Wallace, J. L., and Wang, R. (2015) Hydrogen sulfide-based therapeutics: exploiting a unique but ubiquitous gasotransmitter. *Nat. Rev. Drug Discov.* **14**, 329-345
8. Hellmich, M. R., Coletta, C., Chao, C., and Szabo, C. (2015) The therapeutic potential of cystathionine beta-synthetase/hydrogen sulfide inhibition in cancer. *Antioxid. Redox Signal.* **22**, 424-448
9. Hellmich, M. R., and Szabo, C. (2015) Hydrogen sulfide and cancer. *Handb. Exp. Pharmacol.* **230**, 233-241
10. Davoli, A., Greco, V., Spalloni, A., Guatteo, E., Neri, C., Rizzo, G. R., Cordella, A., Romigi, A., Cortese, C., Bernardini, S., Sarchielli, P., Cardaioli, G., Calabresi, P., Mercuri, N. B., Urbani, A., and Longone, P. (2015) Evidence of hydrogen sulfide involvement in amyotrophic lateral sclerosis. *Ann. Neurol.* **77**, 697-709
11. Ereno-Orbea, J., Majtan, T., Oyenarte, I., Kraus, J. P., and Martinez-Cruz, L. A. (2013) Structural basis of regulation and oligomerization of human cystathionine beta-synthase, the central enzyme of transsulfuration. *Proc. Natl. Acad. Sci. U S A* **110**, E3790-3799
12. Ereno-Orbea, J., Majtan, T., Oyenarte, I., Kraus, J. P., and Martinez-Cruz, L. A. (2014) Structural insight into the molecular mechanism of allosteric activation of human cystathionine beta-synthase by S-adenosylmethionine. *Proc. Natl. Acad. Sci. U S A* **111**, E3845-3852
13. McCorvie, T. J., Kopec, J., Hyung, S. J., Fitzpatrick, F., Feng, X., Termine, D., Strain-Damerell, C., Vollmar, M., Fleming, J., Janz, J. M., Bulawa, C., and Yue, W. W. (2014) Inter-domain communication

of human cystathionine beta-synthase: structural basis of S-adenosyl-L-methionine activation. *J. Biol. Chem.* **289**, 36018-36030

14. Cherney, M. M., Pazicni, S., Frank, N., Marvin, K. A., Kraus, J. P., and Burstyn, J. N. (2007) Ferrous human cystathionine beta-synthase loses activity during enzyme assay due to a ligand switch process. *Biochemistry* **46**, 13199-13210
15. Singh, S., Madzelan, P., Stasser, J., Weeks, C. L., Becker, D., Spiro, T. G., Penner-Hahn, J., and Banerjee, R. (2009) Modulation of the heme electronic structure and cystathionine beta-synthase activity by second coordination sphere ligands: The role of heme ligand switching in redox regulation. *J. Inorg. Biochem.* **103**, 689-697
16. Taoka, S., West, M., and Banerjee, R. (1999) Characterization of the heme and pyridoxal phosphate cofactors of human cystathionine beta-synthase reveals nonequivalent active sites. *Biochemistry* **38**, 2738-2744
17. Taoka, S., and Banerjee, R. (2001) Characterization of NO binding to human cystathionine beta-synthase: possible implications of the effects of CO and NO binding to the human enzyme. *J. Inorg. Biochem.* **87**, 245-251
18. Gherasim, C., Yadav, P. K., Kabil, O., Niu, W. N., and Banerjee, R. (2014) Nitrite reductase activity and inhibition of H(2)S biogenesis by human cystathionine ss-synthase. *PLoS One* **9**, e85544
19. Vicente, J. B., Colaço, H. G., Mendes, M. I., Sarti, P., Leandro, P., and Giuffrè, A. (2014) NO* binds human cystathionine beta-synthase quickly and tightly. *J. Biol. Chem.* **289**, 8579-8587
20. Vicente, J. B., Colaço, H. G., Sarti, P., Leandro, P., and Giuffrè, A. (2016) S-Adenosyl-L-methionine modulates CO and NO* binding to

the human H_2S-generating enzyme cystathionine beta-synthase. *J. Biol. Chem.* **291**, 572-581

21. Prathapasinghe, G. A., Siow, Y. L., Xu, Z., and O, K. (2008) Inhibition of cystathionine-beta-synthase activity during renal ischemia-reperfusion: role of pH and nitric oxide. *Am. J. Physiol. Renal Physiol.* **295**, F912-922
22. Shintani, T., Iwabuchi, T., Soga, T., Kato, Y., Yamamoto, T., Takano, N., Hishiki, T., Ueno, Y., Ikeda, S., Sakuragawa, T., Ishikawa, K., Goda, N., Kitagawa, Y., Kajimura, M., Matsumoto, K., and Suematsu, M. (2009) Cystathionine beta-synthase as a carbon monoxide-sensitive regulator of bile excretion. *Hepatology* **49**, 141-150
23. Morikawa, T., Kajimura, M., Nakamura, T., Hishiki, T., Nakanishi, T., Yukutake, Y., Nagahata, Y., Ishikawa, M., Hattori, K., Takenouchi, T., Takahashi, T., Ishii, I., Matsubara, K., Kabe, Y., Uchiyama, S., Nagata, E., Gadalla, M. M., Snyder, S. H., and Suematsu, M. (2012) Hypoxic regulation of the cerebral microcirculation is mediated by a carbon monoxide-sensitive hydrogen sulfide pathway. *Proc. Natl. Acad. Sci. U S A* **109**, 1293-1298
24. Yamamoto, T., Takano, N., Ishiwata, K., Ohmura, M., Nagahata, Y., Matsuura, T., Kamata, A., Sakamoto, K., Nakanishi, T., Kubo, A., Hishiki, T., and Suematsu, M. (2014) Reduced methylation of PFKFB3 in cancer cells shunts glucose towards the pentose phosphate pathway. *Nat. Commun.* **5**, 3480
25. Kabil, O., Yadav, V., and Banerjee, R. (2016) Heme-dependent metabolite switching regulates H_2S synthesis in response to endoplasmic reticulum (ER) stress. *J. Biol. Chem.* **291**, 16418-16423

26. Kabe, Y., Yamamoto, T., Kajimura, M., Sugiura, Y., Koike, I., Ohmura, M., Nakamura, T., Tokumoto, Y., Tsugawa, H., Handa, H., Kobayashi, T., and Suematsu, M. (2016) Cystathionine beta-synthase and PGRMC1 as CO sensors. *Free Radic. Biol. Med.* **99**, 333-344
27. Suematsu, M., Nakamura, T., Tokumoto, Y., Yamamoto, T., Kajimura, M., and Kabe, Y. (2016) CO-CBS-H_2S axis: from vascular mediator to cancer regulator. *Microcirculation* **23**, 183-190
28. Yadav, P. K., Xie, P., and Banerjee, R. (2012) Allosteric communication between the pyridoxal 5'-phosphate (PLP) and heme sites in the H_2S generator human cystathionine beta-synthase. *J. Biol. Chem.* **287**, 37611-37620
29. Smith, A. T., Su, Y., Stevens, D. J., Majtan, T., Kraus, J. P., and Burstyn, J. N. (2012) Effect of the disease-causing R266K mutation on the heme and PLP environments of human cystathionine beta-synthase. *Biochemistry* **51**, 6360-6370
30. Vicente, J. B., Malagrinò, F., Arese, M., Forte, E., Sarti, P., and Giuffrè, A. (2016) Bioenergetic relevance of hydrogen sulfide and the interplay between gasotransmitters at human cystathionine beta-synthase. *Biochim. Biophys. Acta* **1857**, 1127-1138
31. Mudd, S. H., Skovby, F., Levy, H. L., Pettigrew, K. D., Wilcken, B., Pyeritz, R. E., Andria, G., Boers, G. H., Bromberg, I. L., Cerone, R., and et al. (1985) The natural history of homocystinuria due to cystathionine beta-synthase deficiency. *Am. J. Hum. Genet.* **37**, 1-31
32. Schiff, M., and Blom, H. J. (1985) Treatment of inherited homocystinurias. *Neuropediatrics* **43**, 295-304
33. Janosik, M., Oliveriusova, J., Janosikova, B., Sokolova, J., Kraus, E., Kraus, J. P., and Kozich, V. (2001) Impaired heme binding and

aggregation of mutant cystathionine beta-synthase subunits in homocystinuria. *Am. J. Hum. Genet.* **68**, 1506-1513

34. Singh, L. R., Chen, X., Kozich, V., and Kruger, W. D. (2007) Chemical chaperone rescue of mutant human cystathionine beta-synthase. *Mol. Genet. Metab.* **91**, 335-342
35. Kozich, V., Sokolova, J., Klatovska, V., Krijt, J., Janosik, M., Jelinek, K., and Kraus, J. P. (2010) Cystathionine beta-synthase mutations: effect of mutation topology on folding and activity. *Hum. Mutat.* **31**, 809-819
36. Majtan, T., Liu, L., Carpenter, J. F., and Kraus, J. P. (2010) Rescue of cystathionine beta-synthase (CBS) mutants with chemical chaperones: purification and characterization of eight CBS mutant enzymes. *J. Biol. Chem.* **285**, 15866-15873
37. Cozar, M., Urreizti, R., Vilarinho, L., Grosso, C., Dodelson de Kremer, R., Asteggiano, C. G., Dalmau, J., Garcia, A. M., Vilaseca, M. A., Grinberg, D., and Balcells, S. (2011) Identification and functional analyses of CBS alleles in Spanish and Argentinian homocystinuric patients. *Hum. Mutat.* **32**, 835-842
38. Kopecka, J., Krijt, J., Rakova, K., and Kozich, V. (2011) Restoring assembly and activity of cystathionine beta-synthase mutants by ligands and chemical chaperones. *J. Inherit. Metab. Dis.* **34**, 39-48
39. Hnizda, A., Jurga, V., Rakova, K., and Kozich, V. (2012) Cystathionine beta-synthase mutants exhibit changes in protein unfolding: conformational analysis of misfolded variants in crude cell extracts. *J. Inherit. Metab. Dis.* **35**, 469-477
40. Mendes, M. I., Colaço, H. G., Smith, D. E., Ramos, R. J., Pop, A., van Dooren, S. J., Tavares de Almeida, I., Kluijtmans, L. A., Janssen, M. C., Rivera, I., Salomons, G. S., Leandro, P., and Blom, H. J.

(2014) Reduced response of Cystathionine Beta-Synthase (CBS) to S-Adenosylmethionine (SAM): Identification and functional analysis of CBS gene mutations in Homocystinuria patients. *J. Inherit. Metab. Dis.* **37**, 245-254

41. Mendes, M. I., Smith, D. E., Vicente, J. B., Tavares De Almeida, I., Ben-Omran, T., Salomons, G. S., Rivera, I. A., Leandro, P., and Blom, H. J. (2015) Small aminothiol compounds improve the function of Arg to Cys variant proteins: effect on the human cystathionine beta-synthase p.R336C. *Hum. Mol. Genet.* **24**, 7339-7348
42. Melenovska, P., Kopecka, J., Krijt, J., Hnizda, A., Rakova, K., Janosik, M., Wilcken, B., and Kozich, V. (2015) Chaperone therapy for homocystinuria: the rescue of CBS mutations by heme arginate. *J. Inherit. Metab. Dis.* **38**, 287-294
43. Bublil, E. M., Majtan, T., Park, I., Carrillo, R. S., Hulkova, H., Krijt, J., Kozich, V., and Kraus, J. P. (2016) Enzyme replacement with PEGylated cystathionine beta-synthase ameliorates homocystinuria in murine model. *J. Clin. Invest.* **126**, 2372-2384
44. De Franchis, R., Sperandeo, M. P., Sebastio, G., and Andria, G. (1998) Clinical aspects of cystathionine beta-synthase deficiency: how wide is the spectrum? The Italian Collaborative Study Group on Homocystinuria. *Eur. J. Pediatr.* **157** Suppl 2, S67-70
45. Gaustadnes, M., Wilcken, B., Oliveriusova, J., McGill, J., Fletcher, J., Kraus, J. P., and Wilcken, D. E. (2002) The molecular basis of cystathionine beta-synthase deficiency in Australian patients: genotype-phenotype correlations and response to treatment. *Hum. Mutat.* **20**, 117-126
46. Evangelisti, L., Lucarini, L., Attanasio, M., Porciani, M. C., Romano, E., Prisco, D., Gensini, G. F., Abbate, R., and Pepe, G. (2009)

Vascular and connective tissue features in 5 Italian patients with homocystinuria. *Int. J. Cardiol.* **134**, 251-254

47. Bradford, M. M. (1976) A rapid and sensitive method for the quantitation of microgram quantities of protein utilizing the principle of protein-dye binding. *Anal. Biochem.* **72**, 248-254
48. Carballal, S., Madzelan, P., Zinola, C. F., Grana, M., Radi, R., Banerjee, R., and Alvarez, B. (2008) Dioxygen reactivity and heme redox potential of truncated human cystathionine beta-synthase. *Biochemistry* **47**, 3194-3201
49. Forte, E., Borisov, V. B., Falabella, M., Colaço, H. G., Tinajero-Trejo, M., Poole, R. K., Vicente, J. B., Sarti, P., and Giuffrè, A. (2016) The terminal oxidase cytochrome *bd* promotes sulfide-resistant bacterial respiration and growth. *Sci. Rep.* **6**, 23788
50. Dixon, M. (1971) The acceptor specificity of flavins and flavoproteins. I. Techniques for anaerobic spectrophotometry. *Biochim. Biophys. Acta* **226**, 241-258
51. Puranik, M., Weeks, C. L., Lahaye, D., Kabil, O., Taoka, S., Nielsen, S. B., Groves, J. T., Banerjee, R., and Spiro, T. G. (2006) Dynamics of carbon monoxide binding to cystathionine beta-synthase. *J. Biol. Chem.* **281**, 13433-13438
52. Henry, E. R., and Hofrichter, J. (1992) Singular value decomposition - Application to analysis of experimental-data. *Methods Enzymol.* **210**, 129-192
53. Incardona, M. F., Bourenkov, G. P., Levik, K., Pieritz, R. A., Popov, A. N., and Svensson, O. (2009) EDNA: a framework for plugin-based applications applied to X-ray experiment online data analysis. *J. Synchrotron Radiat.* **16**, 872-879

54. Kabsch, W. (2010) Xds. *Acta Crystallogr. D Biol. Crystallogr.* **66**, 125-132

55. Evans, P. R. (2011) An introduction to data reduction: space-group determination, scaling and intensity statistics. *Acta Crystallogr. D Biol. Crystallogr.* **67**, 282-292

56. Evans, P. R., and Murshudov, G. N. (2013) How good are my data and what is the resolution? *Acta Crystallogr. D Biol. Crystallogr.* **69**, 1204-1214

57. Vonrhein, C., Flensburg, C., Keller, P., Sharff, A., Smart, O., Paciorek, W., Womack, T., and Bricogne, G. (2011) Data processing and analysis with the autoPROC toolbox. *Acta Crystallogr. D Biol. Crystallogr.* **67**, 293-302

58. McCoy, A. J., Grosse-Kunstleve, R. W., Adams, P. D., Winn, M. D., Storoni, L. C., and Read, R. J. (2007) Phaser crystallographic software. *J. Appl. Crystallogr.* **40**, 658-674

59. Adams, P. D., Afonine, P. V., Bunkoczi, G., Chen, V. B., Davis, I. W., Echols, N., Headd, J. J., Hung, L. W., Kapral, G. J., Grosse-Kunstleve, R. W., McCoy, A. J., Moriarty, N. W., Oeffner, R., Read, R. J., Richardson, D. C., Richardson, J. S., Terwilliger, T. C., and Zwart, P. H. (2010) PHENIX: a comprehensive Python-based system for macromolecular structure solution. *Acta Crystallogr. D Biol. Crystallogr.* **66**, 213-221

60. Terwilliger, T. C., Grosse-Kunstleve, R. W., Afonine, P. V., Moriarty, N. W., Zwart, P. H., Hung, L. W., Read, R. J., and Adams, P. D. (2008) Iterative model building, structure refinement and density modification with the PHENIX AutoBuild wizard. *Acta Crystallogr. D Biol. Crystallogr.* **64**, 61-69

61. Blanc, E., Roversi, P., Vonrhein, C., Flensburg, C., Lea, S. M., and Bricogne, G. (2004) Refinement of severely incomplete structures with maximum likelihood in BUSTER-TNT. *Acta Crystallogr. D Biol. Crystallogr.* **60**, 2210-2221

62. Emsley, P., Lohkamp, B., Scott, W. G., and Cowtan, K. (2010) Features and development of Coot. *Acta Crystallogr. D Biol. Crystallogr.* **66**, 486-501

63. Lovell, S. C., Davis, I. W., Arendall, W. B., 3rd, de Bakker, P. I., Word, J. M., Prisant, M. G., Richardson, J. S., and Richardson, D. C. (2003) Structure validation by Calpha geometry: phi,psi and Cbeta deviation. *Proteins* **50**, 437-450

64. Davis, I. W., Leaver-Fay, A., Chen, V. B., Block, J. N., Kapral, G. J., Wang, X., Murray, L. W., Arendall, W. B., 3rd, Snoeyink, J., Richardson, J. S., and Richardson, D. C. (2007) MolProbity: all-atom contacts and structure validation for proteins and nucleic acids. *Nucleic Acids Res.* **35**, W375-383

65. Meier, M., Janosik, M., Kery, V., Kraus, J. P., and Burkhard, P. (2001) Structure of human cystathionine beta-synthase: a unique pyridoxal 5'-phosphate-dependent heme protein. *EMBO J.* **20**, 3910-3916

66. Matthews, B. W. (1968) Solvent content of protein crystals. *J. Mol. Biol.* **33**, 491-497

67. Carballal, S., Cuevasanta, E., Marmisolle, I., Kabil, O., Gherasim, C., Ballou, D. P., Banerjee, R., and Alvarez, B. (2013) Kinetics of reversible reductive carbonylation of heme in human cystathionine beta-synthase. *Biochemistry* **52**, 4553-4562

68. Kabil, O., Weeks, C. L., Carballal, S., Gherasim, C., Alvarez, B., Spiro, T. G., and Banerjee, R. (2011) Reversible heme-dependent

regulation of human cystathionine beta-synthase by a flavoprotein oxidoreductase. *Biochemistry* **50**, 8261-8263

69. Karplus, P. A., and Diederichs, K. (2012) Linking crystallographic model and data quality. *Science* **336**, 1030-1033

Paper 3

Effect of hypoxia on mitochondrial hydrogen sulfide catabolism

Francesca Malagrinò[1,2], Karim Zuhra[1,2], Ludovica Mascolo[1], Daniela Mastronicola[1], João B. Vicente[3], Elena Forte[1], Alessandro Giuffrè[2]

[1]*Department of Biochemical Sciences, Sapienza University of Rome, Rome, Italy*

[2]*CNR Institute of Molecular Biology and Pathology, Rome, Italy.*

[3]*Instituto de Tecnologia Química e Biológica António Xavier, Universidade Nova de Lisboa, Oeiras, Portugal.*

***To whom correspondence should be addressed:**

Dr. Alessandro Giuffrè, Institute of Molecular Biology and Pathology (IBPM), National Research Council of Italy (CNR), Piazzale Aldo Moro 5, I-00185 Rome, Italy.

Email: alessandro.giuffre@uniroma1.it

ABBREVIATIONS

CcOX, cytochrome *c* oxidase; CBS, cystathionine β-synthase; SQR, sulfide:quinone oxidoreductase; DTNB, 5,5'-dithiobis-(2-nitrobenzoic acid); PBS-T, phosphate buffered saline with 0.1% Tween 20 (v/v),

ABSTRACT

Hydrogen sulfide (H_2S) has emerged as a key molecule in human (patho)physiology, able to play crucial regulatory functions at physiological low concentrations or exert toxicity at higher levels. H_2S is synthesized through known enzymatic pathways and mainly metabolized by a mitochondrial sulfide-oxidizing pathway, comprising sulfide:quinone oxidoreductase (SQR) and a few other enzymes. Under hypoxic conditions, H_2S has expectedly higher stability and was reported to be synthesized at higher level with protective effects for the cell. Here, working on SW480 colon cancer cells, we evaluated the effect of hypoxia on the ability of cells to dispose H_2S at the mitochondrial level. The mitochondrial sulfide-oxidizing activity was assessed by quantitatively evaluating by high-resolution respirometry the stimulatory effect of sulfide on rotenone-inhibited cell respiration in the presence or absence of antimycin A. We report that, as compared to cells grown under normoxic conditions (air O_2), cells exposed for 24 h to hypoxia (1% O_2) display a significant reduction in their basal respiration (~65%) and maximal mitochondrial sulfide-oxidizing activity (~25%), consistent with the reduced mitochondrial content (~55%) assessed by citrate synthase activity assays. This notwithstanding, hypoxia-treated cells display a slightly (~40%) higher expression of SQR, as evaluated by immunoblotting. Based on these observations, we posit that the lower sulfide-detoxifying ability induced by hypoxia may contribute to ensure higher protective H_2S levels, but also increase the risk of sulfide toxicity.

INTRODUCTION

Hydrogen sulfide (H_2S), along with nitric oxide (NO) and carbon monoxide (CO), belongs to a small group of gaseous signalling molecules

known as 'gasotransmitters'. H_2S is involved in many important physiological and patho-physiological processes (Paul, 2015; Kimura, 2015; Olson, 2015). While playing key regulatory functions at low (nM) concentrations, at higher (μM) levels it exerts toxic effects via inhibition of complex IV (cytochrome *c* oxidase, CcOX) in the mitochondrial electron transport chain (Cooper & Brown, 2008) and derivatization of haemoglobin to a form named 'sulhemoglobin' with a covalent modification of the heme porphyrin ring, resulting in reduced O_2 affinity (reviewed in Pietri, 2011). It is therefore crucial that cells actively keep H_2S at low physiological levels to prevent toxicity.

In humans, several enzymes implicated in H_2S metabolism are currently known (reviewed in Kabil, 2014 and Szabo 2014**)**. At least three are directly involved in H_2S synthesis: the two pyridoxal 5'-phosphate (PLP)-dependent enzymes cystathionine β-synthase (CBS) and cystathionine γ-lyase (CSE), belonging to the transulfuration pathway, and the mitochondrial enzyme 3-mercaptopyruvate sulfurtransferase (MST) (Kabil, 2014; Singh 2011,). H_2S breakdown is afforded by a mitochondrial enzymatic pathway that couples the oxidation of H_2S (to sulfate, SO_4^{2-}, and thiosulfate, $S_2O_3^{2-}$) to ATP synthesis (Hildebrandt & Grieshaber 2008). The first step of sulfide breakdown is catalyzed by the membrane-associated enzyme sulfide:quinone oxidoreductase (SQR). This flavoprotein couples the oxidation of H_2S to the reduction of coenzyme Q, thus injecting sulfide-derived electrons to the mitochondrial electron transfer chain, making H_2S the first inorganic substrate to sustain mitochondrial respiration (Goubern, 2007). Concomitantly, SQR transfers the H_2S sulfur atom to a sulfur acceptor, leading to formation of glutathione persulfide (GSSH) (Mishanina 2015, Landry 2017) or, less likely, $S_2O_3^{2-}$ (Jackson, 2012). Three additional enzymes, persulfide dioxygenase (ETHE1), thiosulfate sulfur transferase

(TST) and sulfite oxidase (SOX), cooperate with SQR in the mitochondrial sulfide oxidation pathway, leading to formation of SO_4^{2-} and $S_2O_3^{2-}$. To oxidize 1 H_2S molecule, the mitochondrial sulfide-oxidizing pathway overall consumes ~0.75 O_2 molecules (0.25 by CcOX plus 0.5 by ETHE1, (Lagoutte 2010).

In vivo, H_2S can therefore exert a dual effect on cell bioenergetics, at lower concentrations stimulating *via* SQR mitochondrial respiration and thus ATP synthesis (Goubern, 2007), or causing a reversible inhibition of CcOX at higher concentrations (Cooper & Brown 2008). Notably, the sulfide oxidizing activity varies between different cell types and tissues, spanning from undetectable, as e.g., in neuroblastoma cells, to high, as observed in colonocytes (Goubern, 2007; Lagoutte, 2010; Mimoun, 2012). This is perhaps not surprising because colonocytes are physiologically exposed to the fairly high levels of H_2S produced by the gut microbiota and, particularly, by sulfate-reducing bacteria (reviewed in Blachier, 2010).

Several diseases, including cancer (Hellmich & Szabo 2015 and Hellmich, 2015), were found to be associated with alterations of H_2S metabolism. In particular, CBS has been shown to be overexpressed in colorectal cancer (CRC) (Szabo, 2013) and other cancer types (Panza, 2014; Zhang, 2005; Bhattacharyya, 2013). In CRC cell lines, CBS-derived H_2S was demonstrated to promote cell proliferation and angiogenesis, and to sustain cellular bioenergetics by stimulating both oxidative phosphorylation and glycolytic ATP synthesis. The enzyme is therefore currently recognized as a drug target (Druzhyna, 2016; Chao, 2016, Hellmich, 2015).

Hypoxia is a common factor in the microenvironment of solid tumours that has been recognized to be associated to drug-resistance (reviewed in Muz 2015) and malignance phenotype. The effect hypoxia has on cellular metabolism has been extensively investigated (reviewed in

Masson & Ratcliffe 2014). Among other changes, hypoxic cells undergo a reduction in mitochondrial mass, resulting from reduced biogenesis of this organelle and enhanced mitophagy (Zhang, 2008; Wu, 2015) and reviewed in (Solaini, 2010). Because mitochondria are the main site of sulfide oxidation, in the absence of compensatory mechanisms, a reduced ability to detoxify sulfide is expected for hypoxic cells. The intricate interplay between H_2S and O_2 has been extensively investigated (reviewed in Olson, 2015). In particular, as O_2 facilitates both the chemical and enzymatic oxidative decomposition of H_2S into persulfides and polysulfides, at low O_2 tension a higher stability of H_2S is expected. Furthermore, hypoxic/ischemic conditions have been reported to enhance H_2S synthesis, primarily through up-regulation of the sulfide-synthesizing enzymes (Takano, 2014; Kolluru, 2015). Moreover, under hypoxia the H_2S-generating enzymes CBS and CSE were shown to accumulate in the mitochondria, likely enhancing the H_2S mitochondrial levels (Teng, 2013; Fu, 2012). Hypoxia is thus expected to increase H_2S bioavailability, a condition that can have opposite physiological consequences. Indeed, while H_2S has been shown to be protective against ischemia injuries (Kolluru, 2015; Morikawa, 2012; Takano, 2014, Hine, 2016) the enhanced biosynthesis and chemical stability of H_2S, combined with the reduced content in mitochondria (the main sites of sulfide disposal), may increase the risk of H_2S toxicity in hypoxic cells.

This information prompted us to investigate in the present study the effect of hypoxia/reoxygenation on the mitochondrial sulfide-oxidizing activity in colorectal cancer cells. Here, we provide evidence that, after exposure to hypoxia, these model cells show reduced mitochondrial sulfide-oxidizing activity consistent with their lower content in mitochondria.

MATERIALS AND METHODS

Materials

The human colon cancer cell line SW480 was purchased from the American type Culture Collection (ATCC *no. CCL228*™). Sodium sulfide nonahydrate ($Na_2S·9H_2O$, 431648), 5,5'-dithiobis-(2-nitrobenzoic acid) (DTNB), acetyl coenzyme A, oxaloacetate, CelLytic^{TM}MT cell lysis reagent, protease inhibitor cocktail (P8340), anti-SQR antibody (HPA017079) and the bicinchoninic acid assay (BCA) kit were purchased from Sigma. Cell culture media and antibiotics were from Sigma, Euroclone or Gibco. Mini-PROTEAN TGX Stain-Free Precast Gels, the Clarity Western ECL substrate and the *Laemmli* protein sample buffer were purchased from Bio-Rad. Bovine serum albumin was from AppliChem.

Preparation of sulfide stock solutions

Stock solutions of Na_2S were prepared by quickly washing with degassed Milli-Q water the surface of a Na_2S crystal, and then dissolving it in degassed Milli-Q water under a N_2 atmosphere. The concentration of Na_2S in solution was measured spectrophotometrically using 5,5'-dithiobis-(2-nitrobenzoic acid) (DTNB) according to (Nashef, 1977) in a Cary 60 UV-VIS spectrophotometer. The concentration of Na_2S was then adjusted to 3-5 mM by dilution with degassed Milli-Q water in a gas-tight glass syringe.

Cell culture

The human colon cancer cell line SW480 was maintained in Dulbecco's Modified Eagle Medium (DMEM) containing 4.5 $g·L^{-1}$ glucose, supplemented with 2 mM L-glutamine, 10% (v/v) heat-inactivated fetal bovine serum (FBS), 100 $U·mL^{-1}$ penicillin and 100 $\mu g·mL^{-1}$ streptomycin. Cells at 37 °C and 5% CO_2 in 25 cm^2 or 75 cm^2 flasks were grown under

normoxic conditions (air O_2) or incubated for 24 h under hypoxic conditions (1% O_2) in a Galaxy 14 S incubator (Eppendorf). After trypsinization, the cells were washed in the culture medium, counted using the trypan blue dye exclusion test, centrifuged at 1.000 X g for 5 min and resuspended in fresh medium at a final density of 8 x 10^6 cells·mL^{-1}. Trypan blue-positive cells were always less than 5%. Henceforth, cells grown under normoxic conditions or exposed to hypoxia will be respectively referred to as 'normoxic' and 'hypoxia-treated' cells.

Measurements of the mitochondrial sulfide-oxidizing activity

The mitochondrial sulfide-oxidizing activity of tested cells was evaluated as described in [(Abou-Hamdan et al., 2015)], by measuring the stimulatory effect of sulfide on cellular O_2 consumption. Measurements were carried out at 37 °C, using a highresolution respirometer (Oxygraph-2k, Oroboros Instruments, Innsbruck, Austria), equipped with two 1.5-mL chambers and a micropump (TIP-2k) for sulfide injection. According to [Abou-Hamdan 2015], in these assays sulfide was injected into a cell suspension at increasing flux (determined by the pump rate) and sulfide-mediated stimulation of cellular O_2 consumption was measured until the concentration of injected sulfide became inhibitory for CcOX. To prevent reverse electron transfer through Complex I in SW480 cells [Lagoutte 2010], measurements were carried out in the presence of 10 µM rotenone. The assays were typically conducted in FBS-supplemented cell medium under stirring as it follows. After addition of cells (4.0 x 10^6), basal respiration was measured for ~10 min. Afterwards, following the addition of rotenone resulting in O_2 consumption inhibition, a solution of 3 - 5 mM sulfide was injected for time intervals (180 s) at increasing rates (10 nL·s^{-1}, 20 nL·s^{-1}, 40 nL·s^{-1}, 80 nL·s^{-1} and 160 nL·s^{-1}) and the effect on O_2 consumption was measured. Some

control experiments were carried out not only in the presence of rotenone, but also of antimycin A (5 µM), an inhibitor of quinol:cytochrome *c* reductase (Complex III). The latter assays allowed us to evaluate the effect of sulfide on extra-mitochondrial and non-enzymatic O_2 consumption and thus obtain by subtraction (from the experiments performed in the absence of antimycin A) the genuine mitochondrial sulfide-oxidizing activity.

Citrate synthase assay

Cells were harvested and lysed using the CelLytic™MT cell lysis reagent and protease inhibitor cocktail from Sigma according to the manufacturer instructions. Cell extracts were assayed spectrophotometrically for citrate synthase in 100 mM Tris-HCl, 0.3 mM acetyl-CoA, 0.1 mM DTNB and 0.1 mM oxaloacetate, as described in (Srere, 1969).

Immunoblotting assays

Cells were harvested, lysed as described in the previous section and, after total protein content determination by BCA assay, proteins (20 µg per lane) were separated by SDS-PAGE using Mini-PROTEAN TGX Stain-Free Precast Gels (from Bio-Rad). The formulation of these gels includes trihalo compounds which lead to UV fluorescence emission on reaction with proteins (Rivero-Gutiérrez, 2014; Short & Posch, 2011), allowing to estimate and normalize the total loaded protein, using a ChemiDoc MP imaging system (Bio-Rad) without resorting to any staining procedure. The proteins were transferred onto polyvinylidene difluoride (PVDF) membranes using a Trans-Blot SD Semi-Dry Electrophoretic Transfer Cell (from Bio-Rad) at 10V, 180 mA for 30 min. The membranes were blocked with PBS-T (phosphate buffered saline with 0.1% Tween 20 [v/v]) containing 3% bovine serum albumin (BSA, w/v) and then incubated overnight at 4 °C with rabbit

polyclonal antibody against human SQR (1:150, in PBS-T with 3% BSA (w/v)). After three washing steps of the membrane with PBS-T (15 min), the membranes were incubated with horseradish peroxidase-conjugated secondary antibody (1:5000, in PBS-T with 3% BSA [w/v]), followed by three washing steps with PBS-T (15 min) and detection by enhanced chemiluminescence (Clarity Western ECL Substrate, Biorad). Finally, the blotted membranes were subjected to densitometric analysis using Image Lab software (Biorad), followed by normalization of the target protein band intensity to total protein.

Data analysis

Oxygen consumption rates were calculated using the software DatLab4 (Oroboros Instruments, Austria). Data are reported as mean ± standard error of the mean (SEM). Statistical significance (P) was estimated using the Student's *t*-test in Microsoft Excel. *P ≤ 0.05, **P ≤ 0.01, ***P ≤ 0.001 and ****P ≤ 0.0001 were considered significant.

RESULTS

Colorectal cancer cells (SW480) were either grown under normoxic (air O_2) conditions or exposed for 24 h to hypoxia (1% O_2), and their sulfide-oxidizing activity was assayed by high resolution respirometry according to (Abou-Hamdan 2015) as described in the Material and Methods section. A representative oxygraphic trace acquired with untreated ('normoxic') cells is shown in Fig.1A. The trace clearly shows that most (~80%) of cell respiration was blocked by addition of the Complex I inhibitor rotenone, added to prevent reversal of Complex I activity upon sulfide injection, as

described in (Lagoutte, 2010; Helmy, 2014). Following respiration inhibition by rotenone, sulfide was injected into the oxygraphic chamber via a micropump following the protocol described in (Abou-Hamdan, 2015). Overall, five injections of 3 minutes were carried out at increasing injection rates (increasing by a factor of 2 from 10 nL·s^{-1} to 160·nL s^{-1}). The first four injections led to stimulation of O_2 consumption, pointing to a fully operative mitochondrial sulfide-oxidizing pathway in the tested cells. The stimulation persisted for the entire duration (3 minutes) of sulfide injection, after which the O_2 consumption rate declined back to the value measured in the absence of sulfide. The decline took a few minutes, as if some sulfide persisted in solution enhancing cell respiration even after the injection was stopped. In line with (Abou-Hamdan, 2015), the extent of O_2 consumption stimulation by sulfide increased with the rate of sulfide injection (up to 80 nL s^{-1}, Fig.1A). However, by further increasing the injection rate (to 160 nL s^{-1}) a decline in the O_2 consumption rate was observed during sulfide injection, likely due to CcOX inhibition by sulfide, as previously suggested (Abou-Hamdan, 2015).

For comparison, the experiments described above were carried out on the same cells after 24 h-exposure to hypoxic conditions. As shown in Fig.1B, the hypoxia-treated cells displayed a lower basal respiratory activity compared to untreated cells (25.1 ± 2.0 nM O_2 s^{-1} vs 68.3 ± 4.5 nM O_2 s^{-1}). Yet, similarly to normoxic cells, after rotenone addition a progressive stimulation of cell respiration was observed by injecting sulfide at increasing rate, until the amount of injected sulfide exceeded the detoxifying activity of the cells, and C*c*OX inhibition occurred, impairing cell respiration (see last sulfide injection in Fig.1B). By comparing normoxic and hypoxia-treated cells, it can be appreciated that in the latter cells, at any sulfide injection rate, stimulation of O_2 consumption by sulfide was lower than in normoxic cells, possibly in line with their lower basal respiration (Fig.1C). Consistently, at

the highest non-inhibitory sulfide injection rate, in hypoxia-treated cells sulfide sustained an O_2 consumption approximately 30% lower than observed in untreated cells even (see sulfide injection #4 in Fig.1C).

In order to evaluate the contribution of mitochondria to the observed sulfide-oxidizing activity, we used antimycin A. This well-known inhibitor of Complex III indeed blocks quinol oxidation in the respiratory chain and thus prevents sulfide oxidation by mitochondria (Abou-Hamdan, 2015). As shown in Fig.2, in the presence of rotenone, antimycin A largely prevented O_2 consumption stimulation by sulfide in both normoxic and hypoxia-treated cells, proving that under the tested conditions sulfide oxidation occurs mostly at the mitochondrial level. The effect of sulfide on the mitochondrial (not the total) O_2 consumption was quantitatively evaluated by subtracting the O_2 consumption rates measured during sulfide injection in the presence of both rotenone and antimycin A (Fig.2C) from those measured at identical sulfide injection rates in the presence of rotenone only (Fig.1C). According to this analysis, in line with the lower basal respiratory activity of hypoxia-treated cells, stimulation of mitochondrial O_2 consumption by sulfide was lower in hypoxia-treated than in untreated cells: at the highest non-inhibitory (for C*c*OX) injection rate, after subtracting the O_2 consumption rate measured in the presence of rotenone only, sulfide sustained a mitochondrial O_2 consumption of 38.6 ± 3.5 nM O_2 s^{-1} and 29.2 ± 3.0 nM O_2 s^{-1}, in normoxic and hypoxia-treated cells, respectively. Taking into account that measurements were carried out with 4 million cells and that the mitochondrial sulfide-oxidizing pathway overall consumes ~ 1.33 molecules of H_2S per O_2 molecule (Lagoutte, 2010), a mitochondrial sulfide-oxidizing activity of 12.8 ± 1.5 and 9.7± 1.1 nM H_2S s^{-1} per million cells can be calculated for normoxic and hypoxia-treated cells, respectively (Fig.3A). In an attempt to evaluate the effect of hypoxia on the cell mitochondrial content,

we carried out citrate synthase activity assays, commonly used as a marker of mitochondrial mass (Pereira, 2011). Interestingly, based on these assays, hypoxia-treated cells were found to display an ~ 1.8-fold lower citrate synthase activity, indicating a lower mitochondrial content compared to normoxic cells (Fig.3B). The reduced mitochondrial mass observed in hypoxia-treated cells is in agreement with the literature (Solaini, 2010) and likely accounts for the lower basal respiratory activity shown by these cells compared to normoxic cells (Fig.1C). The measured citrate synthase activity was used to normalize the calculated mitochondrial sulfide-oxidizing activity. After normalization, this activity proved to be in hypoxia-treated cells ~ 1.4-fold higher than in normoxic cells (Fig.3C). Finally, we have assayed in cell extracts the SQR expression levels by immunoblotting combined with '*stain-free'* imaging technology for total protein quantitation (Rivero-Gutiérrez, 2014; Short & Posch, 2011). We resorted to this technology because proteins commonly used as housekeepers, such as GAPDH and β-actin, are known to change their expression levels under hypoxia (Heerlein, 2005; Zhong, 2009). By performing immunoblotting assays, we found that hypoxia-treated cells display a ~40% higher SQR protein level as compared to normoxic cells.

DISCUSSION

Oxygen (O_2) and hydrogen sulfide (H_2S) and are key molecules in living systems, being able to control each other's availability and being involved in numerous processes in human physiology and patho-physiology. As reviewed in (Olson, 2015), the interplay between H_2S and O_2 is very intricate and relies on different mechanisms that include: i) direct reaction between the two species; ii) O_2-dependent breakdown of H_2S at the mitochondrial level; iii) H_2S-dependent stimulation or inhibition of mitochondrial O_2 consumption; iv) O_2-dependent expression and cellular re-

localization of sulfide-synthesizing enzymes, as CBS and CSE, and v) O_2-dependent control of CO-mediated inhibition of H_2S production by CBS. Indeed, this close relationship is such that H_2S has been recognized as an O_2 sensor (Olson, 2006). Numerous studies have been successfully carried out thus far to shed light on the interplay between H_2S and O_2 and their highly intertwined biologic effects (Olson, 2008 a-c; Olson, 2013). Despite these efforts, however, to our knowledge no studies have been conducted yet to explore the effect of prolonged exposure to hypoxia on the cell ability to dispose H_2S, that was the main objective of the present study.

Under hypoxic conditions, the H_2S levels are increased with beneficial effects for the cell. H_2S plays indeed a key protective role against ischemia/reperfusion damages as demonstrated in different model systems (Morikawa, 2012; Takano, 2014; Kolluru, 2015). The molecular mechanisms underlying H_2S protection are only partly understood and include induction of antioxidant and vasorelaxation effects on microcirculation. In neuronal ischemia/reperfusion models, the protective effect of H_2S was interestingly found to be mediated by thiosulfate, a product of sulfide oxidation (Muratani, 2015). In this context it is interesting to note that H_2S is also able to mimic hypoxia-induced responses such as vasodilation (Zhao, 2011), neo-angiogenesis (Papapetropoulos, 2009) and expression of the hypoxia inducible factor (HIF-1α; Beaumony, 2016), a master gene regulator promoting cell survival under hypoxic conditions. The increased H_2S levels occurring under hypoxic conditions are therefore part of a more general adaptive response adopted by the cells to ensure survival and protection from damages at low O_2 tensions (and possible reoxygenation).

In hypoxic cells, H_2S bioavailability therefore needs to be finely regulated through a correct balance between biosynthetic and catabolic pathways so that this gaseous signalling molecule can occur at higher

(physiologically protective) levels with no risk for the cell to be poisoned. In this regard, it seems relevant to gain insight into the regulation of H_2S production and breakdown at low O_2 tensions. Previous studies addressing this issue have shown that under hypoxic conditions the sulfide-synthesizing enzymes are up-regulated (Takano, 2014; Kolluru, 2015) and CBS accumulates in the mitochondria, due to reduced proteolytic activity of the mitochondrial LON protease (Teng, 2013). As a result, H_2S synthesis is enhanced (Olson, 2015). On the contrary, H_2S breakdown via both chemical and mitochondrial enzymatic reaction pathways is negatively affected by low O_2 tensions. Evidence for a lower mitochondrial sulfide-oxidizing activity at lower O_2 concentrations was initially provided in (Matallo, 2014) working on immortalised cells derived from alveolar macrophages and, then, corroborated by Abou-Hamdan *et al*. in a more recent investigation on CHO cells (Abou-Hamdan, 2016).

In the present study, using SW480 colorectal cancer cells as a model, we tested the effect of prolonged (24 h) exposure to 1% O_2 on the cellular ability to consume sulfide at mitochondrial level. The sulfide-oxidizing activity of normoxic and hypoxia-treated cells was assayed by high-resolution respirometry, following the approach described in (Abou-Hamdan, 2015). The method allows to indirectly assess the mitochondrial sulfide-oxidizing activity from the stimulation of cell O_2 consumption by sulfide administered with a micropump at increasing injection rates. In these assays we made use of rotenone to prevent reversal of Complex I activity upon sulfide injection, according to (Helmy, 2014), and antimycin A to subtract the effect of sulfide autoxidation and extra-mitochondrial O_2 consumption. Also, we comparatively evaluated in normoxic and hypoxia-treated cells both the mitochondrial content, with citrate synthase assays, and the expression level of SQR, by immunoblotting using ‘stain-free’ imaging technology for protein

normalization. As a major finding, we found that exposure to hypoxia leads to a significant reduction in the basal respiration (~65%) and maximal mitochondrial sulfide-oxidizing activity (~25%) of treated cells, consistent with their reduced mitochondrial content (~55% less than in untreated cells). The observed reduction in mitochondrial mass in hypoxic cells has been previously documented and suggested to result from enhanced mitophagic activity and reduced organelle biogenesis (Zhang 2008). Finally, we made the somewhat puzzling observation that hypoxia-treated cells, though displaying slightly reduced mitochondrial sulfide-oxidizing activity, have modestly (~40%) increased SQR levels. This result is intriguing in that it suggests that mitochondria in hypoxic cells are less numerous, but probably enriched in SQR. In light of this observation, it is tempting to speculate that the increased SQR levels in mitochondria could have a protective role in hypoxic cells preventing the organelle to be poisoned by enhanced *in situ* production of sulfide.

Summing up, this is to our knowledge the first study in which the effect of hypoxia on the mitochondrial sulfide-oxidizing activity has been evaluated. The collected evidence shows that, following prolonged exposure to hypoxia, the cells retain their ability to metabolize sulfide but with reduced efficacy, in line with their lower mitochondrial content. Whereas physiologically this may represent a regulatory mechanism to ensure higher protective H_2S levels, under pathological conditions resulting in chronic hypoxia the lower ability to detoxify sulfide may lead to higher risk of sulfide toxicity.

ACKNOWLEDGMENTS

Work partially supported by Ministero dell'Istruzione, dell'Università della Ricerca of Italy (PNR-CNR Aging Program 2012–2014 and PRIN

20158EB2CM 003 to AG). iNOVA4Health Research Unit (LISBOA-01-0145-FEDER-007344), which is cofunded by Fundação para a Ciência e Tecnologia / Ministério da Ciência e do Ensino Superior, through national funds, and by FEDER under the PT2020 Partnership Agreement, is acknowledged by JBV.

FIGURE LEGENDS

Figure 1

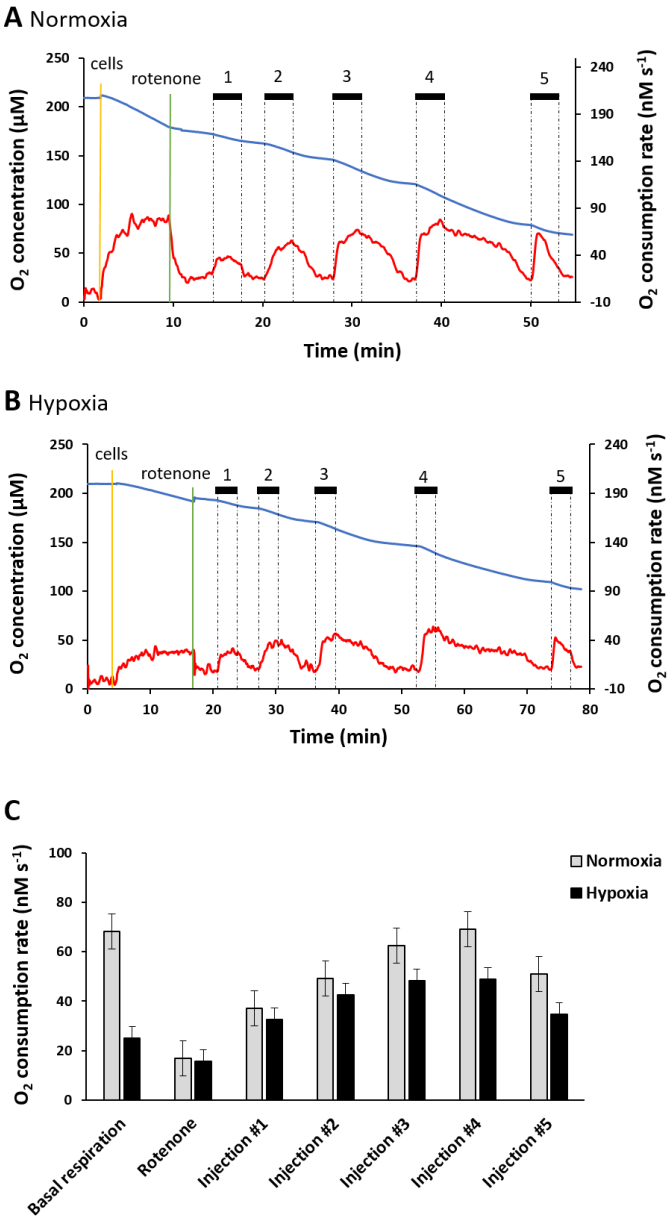

Figure 1. *Effect of sulfide on cell O_2 consumption. Panels A and B*: Representative oxygraphic traces (blue) acquired with normoxic (A) or

hypoxia-treated SW480 cells (B), following the addition of 4 x 10^6 cells (yellow line), 10 µM rotenone (green line) and subsequent injection of a 3-5 mM sulfide stock solution at increasing infusion rates (10 nL·s^{-1}, 20 nL·s^{-1}, 40 nL·s^{-1}, 80 nL·s^{-1}, 160 nL·s^{-1}). Red traces: O_2 consumption rate. *Panel C*: O_2 consumption rate measured with normoxic (n = 9; white bar) or hypoxia-treated cells (n = 8; black bar) under basal conditions and after addition of rotenone at increasing sulfide injection rate.

Figure 2

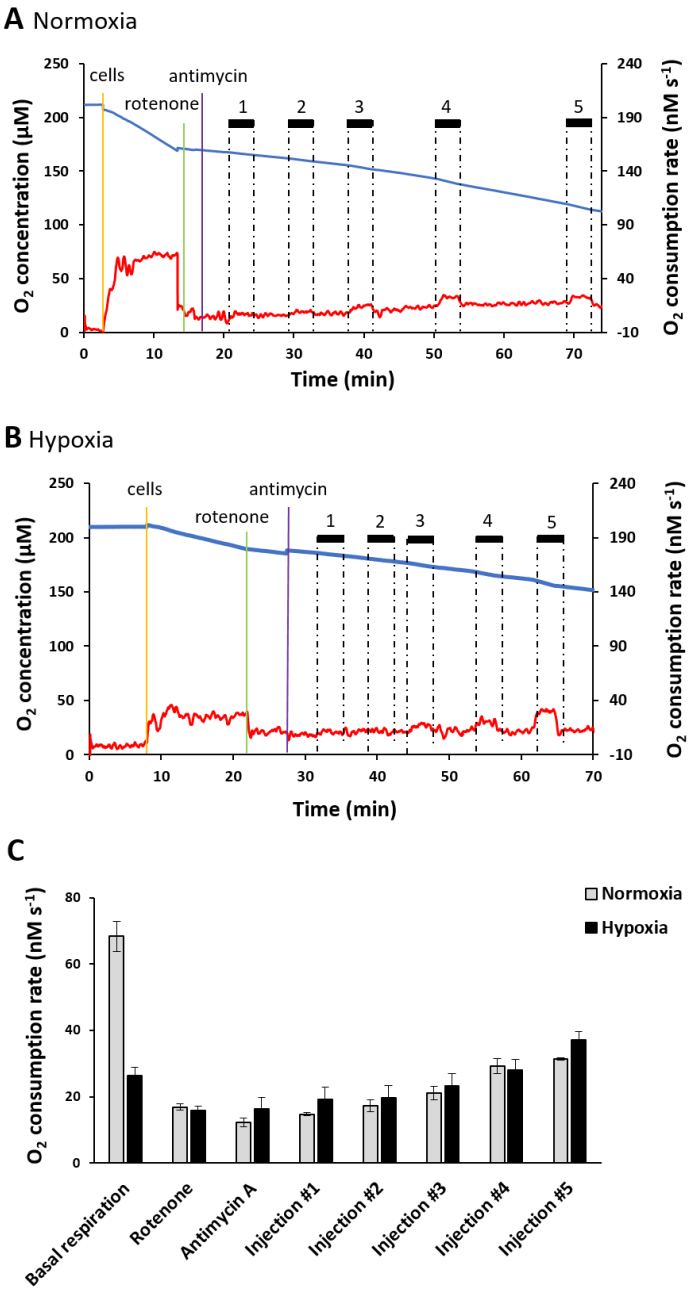
A Normoxia
cells
antimycin
rotenone
1
2
3
4
5
O2 concentration (µM)
O2 consumption rate (nM s-1)
Time (min)
B Hypoxia
cells
antimycin
rotenone
1
2
3
4
5
O2 concentration (µM)
O2 consumption rate (nM s-1)
Time (min)
C
Normoxia
Hypoxia
O2 consumption rate (nM s-1)
Basal respiration
Rotenone
Antimycin A
Injection #1
Injection #2
Injection #3
Injection #4
Injection #5

Figure 2. *Effect of sulfide on antimycin A-insensitive O_2 consumption*. *Panels A and B*: Representative oxygraphic traces (blue) acquired with normoxic (A) or hypoxia-treated SW480 cells (B), following the addition of 4 x 10^6 cells (yellow line), 10 µM rotenone (green line), 5 µM antimycin A (purple line) and subsequent injection of a 3-5 mM sulfide stock solution at increasing infusion rates (10 nL s^{-1}, 20 nL s^{-1}, 40 nL s^{-1}, 80 nL s^{-1}, 160 nL s^{-1}). Red traces: O_2 consumption rate. *Panel C*: O_2 consumption rate measured with normoxic (*n* = 3; white bar) or hypoxia-treated cells (*n* = 3; black bar) after addition of both rotenone and antimycin A at increasing sulfide injection rate.

Figure 3

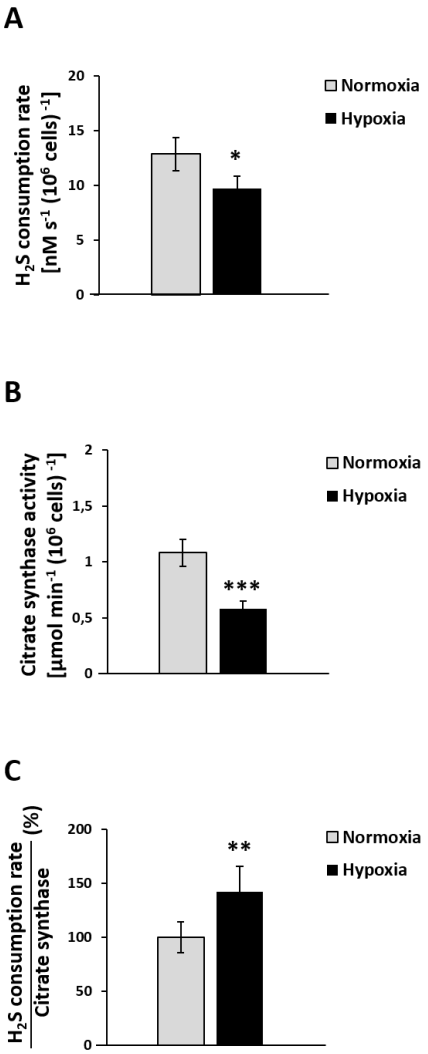

Figure 3 *Effect of hypoxia on mitochondrial sulfide consumption. Panel A*: maximal mitochondrial sulfide consumption activity calculated for normoxic (n = 9, white bar) and hypoxia-treated (n = 8, black bar) cells. *Panel B*: citrate synthase activity in normoxic (n = 13, white bar) and hypoxia-treated (n = 10, black bar) cells. *Panel C*: maximal mitochondrial sulfide consumption

activity detected in normoxic (white bar) and hypoxia-treated (black bar) cells, normalized to the citrate synthase activity (*P ≤ 0.05, **P ≤ 0.01 and ***P ≤ 0.001).

Figure 4.

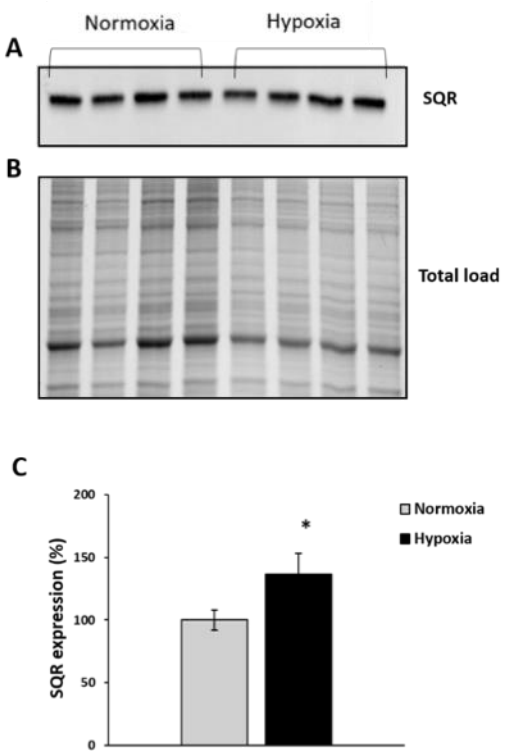

Figure 4. *Effect of hypoxia on SQR expression*. *Panel A*: representative immunoblot of SQR. *Panel B*: corresponding cell lysates analyzed by 'stain-free' SDS-PAGE technology for total protein determination (see Materials and Methods for details). *Panel C*: SQR levels normalized to total protein in normoxic (n = 4 in triplicate, white bar) and hypoxia-treated cells (n = 4 in triplicate, black bar). *P ≤ 0.05.

REFERENCES

1. Abou-Hamdan A. R., Guedouari-Bounihi H., Lenoir V., Blachier F., Bouillaud F., *Oxidation of H_2S in mammalian cells and mitochondria*, Methods in Enzymology (2015), 554, 201-228.
2. Abou-Hamdan A. R., Roger C.T., Guedouari-Bounihi H., Galardon E., Bouillaud, F., *Positive feedback during sulfide oxidation fine-tunes cellular affinity for oxygen,* Biochim Biophys Acta. (2016), 1857,1464-1472.
3. Beaumont M, Andriamihaja M., Lan A., Khodorova N., Audebert M., Blouin J.-M., Grauso M., Lancha L., Benetti P.-H, Benamouzig R., Tomé D., F. Bouillaud, Davila A.-M., Blachier F., *Detrimental effects for colonocytes of an increased exposure to luminal hydrogen sulfide: The adaptive response*, Free Radical Biology and Medicine (2016), 93, 155-164.
4. Bhattacharya S., Saha S., Giri K., Lanza I. R., Nair KS, Jennings N. B., Rodriguez-Aguayo C., Lopez-Berestein G., Basal E., Weaver A. L., Visscher D. W., Cliby W., Sood A. K., Bhattacharya R., and Mukherjee P., *Cystathionine beta- synthase (CBS) contributes to advanced ovarian cancer progression and drug resistance*, PLoS One 8 (2013), e79167.
5. Blachier F., Davila A. M., Mimoun S., Benetti P. H., Atanasiu C., Andriamihaja M., Benamouzig R., Bouillaud F., Tome D., *Luminal sulfide and large intestine mucosa: friend or foe?, Amino Acids* (2010), 39, 335–347.

6. Chao C. and Zatarain J. R., *Cystathionine-β-Synthase Inhibition for Colon Cancer: Enhancement of the Efficacy of Aminooxyacetic Acid via the Prodrug Approach*, Molecular Medicine (2016), 1.
7. Cooper C.E. and Brown G.C., *The inhibition of mitochondrial cytochrome oxidase by the gases carbonmonoxide, nitric oxide, hydrogen cyanide and hydrogen sulfide: chemical mechanism and physiological significance*, J. Bioenerg. Biomembr. (2008), 40, 533–539.
8. Druzhyna N., Szczesny B., Olah G., Módis K., Asimakopoulou A., Pavlidou A., Szoleczky P., Domokos G., Yanagi K., Törö G., López-García I., Myrianthopoulos V., Vikros E., Zatarain J. R., Chao C., Papapetropoulos A., Hellmich M. R., Szabo C., *Screening of a composite library of clinically used drugs and well-characterized pharmacological compounds for cystathionine β-synthase inhibition identifies benserazide as a drug potentially suitable for repurposing for the experimental therapy of colon*, Pharmacological Research (2016) 113, 18-37.
9. Fu M., Zhang W., Wu L., Yang G., Li H., Wang R., *Hydrogen sulfide (H_2S) metabolism in mitochondria and its regulatory role in energy production*, Proc Natl Acad Sci U S A (2012), 109, 2943-2948.
10. Goubern M., Andriamihaja M., Nubel T., Blachier F., Bouillaud F., *Sulfide, the first inorganic substrate for human cells*, FASEB J. (2007), 21, 1699–1706.
11. Hellmich M. R. and Szabo C., *Hydrogen Sulfide and Cancer, Handb Exp Pharmacol.* (2015), 233-241.
12. Hellmich M. R., Coletta C., Chao C., Szabo C., *The therapeutic potential of cystathionine β-synthetase/hydrogen sulfide inhibition in cancer*, Antioxid Redox Signal. (2015), 22, 424-448.

13. Helmy N., Prip-Buus C., Vons C., Lenoir V., Abou-Hamdan A., Guedouari-Bounihi, H., et al., *Oxidation of hydrogen sulfide by human liver mitochondria*, NitricOxide (2014), 41, 105–112.
14. Hildebrandt T.M. and Grieshaber M.K., *Three enzymatic activities catalyze the oxida- tion of sulfide to thiosulfate in mammalian and invertebrate mitochondria*, FEBS J. (2008) 275, 3352–3361.
15. Hine, C., Harputlugil, E., Zhang, Y., Ruckenstuhl, C., Cheon, B., Brace, L., Longchamp A., Treviño-Villarreal J. H., Mejia P., Ozaki C. K., Wang R., Gladyshev V. N., Madeo F., Mair W. B., Mitchell J. R., *Endogenous Hydrogen Sulfide Production Is Essential for Dietary Restriction Benefits.* Cell (2016), *160*(0), 132–144.
16. Jackson M. R., Melideo S. L., Jorns M. S., *Human Sulfide:Quinone Oxidoreductase Catalyzes the First Step in Hydrogen Sulfide Metabolism and Produces a Sulfane Sulfur Metabolite, Biochemistry* (2012), 51 6804–6815.
17. Kabil O. and Banerjee R., *Enzymology of H_2S biogenesis, decay and signalling*, Antioxid. Redox Signal. (2014), 20, 770–782.
18. Kimura H., *Signaling of hydrogen sulfide and polysulfides*, Antioxid. Redox Signal. (2015), 22, 347–349.
19. Kolluru, G. K., Bir, S. C., Yuan, S., Shen, X., Pardue, S., Wang, R., & Kevil, C. G., *Cystathionine γ-lyase regulates arteriogenesis through NO-dependent monocyte recruitment.* Cardiovascular Research, (2015), *107*(4), 590–600.

20. Lagoutte E., Mimoun S., Andriamihaja M., Chaumontet C., Blachier F., Bouillaud F., *Oxidation of hydrogen sulfide remains a priority in mammalian cells and causes reverse electron transfer in colonocytes*, Biochimica et Biophysica Acta (2010), 1797, 1500-1511.
21. Landry A. P., Ballou D. P., Banerjee R., *H_2S oxidation by nanodisc-embedded human sulfide quinone oxidoreductase*, J. Biol. Chem. (2017).
22. Leigh J., Saha M. N., Mok A., Champsi O., Wang R., Lobb I., Sener A., *Hydrogen Sulfide Induced Erythropoietin Synthesis is Regulated by HIF Proteins*, J Urol. (2016), 196, 251-60.
23. Liu X., Pan L., Zhuo Y., Gong Q., Rose P., Zhu Y., *Hypoxia-inducible factor-1alpha is involved in the pro-angiogenic effect of hydrogen sulfide under hypoxic stress*, Biol Pharm Bull (2010), 33, 1550-1554.
24. Masson N. and Ratcliffe P. J., *Hypoxia signaling pathways in cancer metabolism: the importance of co-selecting interconnected physiological pathways*, Cancer Metab. (2014), 2.
25. Matallo J., Vogt J., McCook O., Wachter U., Tillmans F., Groeger M., Szabo C., Georgieff M., Radermacher P., Calzia E., *Sulfide-inhibition o fmitochondrial respiration at very low oxygen concentrations*, Nitric Oxide (2014), 41, 79–84.
26. Mimoun S., Andriamihaja M., Chaumontet C., Atanasiu C., Benamouzig R., Blouin J. M., Tome D., Bouillaud F., Blachier F., *Detoxification of H_2S by differentiated colonic epithelial cells: implication of the sulfide oxidizing unit and of the cell respiratory capacity*, Antioxid. Redox Signal. (2012), 17, 1–10.
27. Mishanina T. V., Yadav P. K., Ballou D. P., and Banerjee R., *Transient kinetic analysis of hydrogen sulfide oxidation catalyzed by*

human sulfide quinone oxidoreductase, J. Biol. Chem. (2015), 290, 25072–25080.

28. Morikawa T., Kajimura M., Nakamura T., Hishiki T., Nakanishi T., Yukutake Y., Nagahata Y., Ishikawa M., Hattori K., Takenouchi T., Takahashi T., Ishii I., Matsubara K., Kabe Y., Uchiyama S., Nagata E., Gadalla M.M., Snyder S.H., Suematsu M., *Hypoxic regulation of the cerebral microcirculation is mediated by a carbon monoxide-sensitive hydrogen sulfide pathway*. Proceedings of the National Academy of Sciences (2012), 109, 1293–1298
29. Muratani E., Yamada M., Ida T., Tokuda K., Ikeda K., Kai S., Shiruzo K., Hayashida K., Kosugi S., Hanaoka K., Kaneki M., Akaike T., Ichinose F., *Thiosulfate Mediates Cytoprotective Effects of Hydrogen Sulfide Against Neuronal Ischemia*, J Am Heart Assoc. (2015).
30. Muz, B., De La, P., Feda, P., Abdel, A., Azab, K., & Azab, A. K., *The role of hypoxia in cancer progression, angiogenesis, metastasis, and resistance to therapy*. Hypoxia, (2015), 83—92.
31. Nashef A. S., Osuga D. T. & Feeney R. E., *Determination of hydrogen sulfide with 5,5 β'-dithiobis-(2-nitrobenzoic acid), N-ethylmaleimide, and parachloromercuribenzoate*. Analytical Biochem. (1977), 79, 394–405.
32. Olson K. R. , Healy M. J., Qin Z., Skovgaard N., Vulesevic B., Duff D. W., Whitfield N. L., Yang G., Wang R., Perry S. F., *Hydrogen sulfide as an oxygen sensor in trout gill chemoreceptors. Am J Physiol Regul Integr Comp Physiol*. (2008b), 295, R669-80.
33. Olson K. R., *A theoretical examination of hydrogen sulfide metabolism and its potential in autocrine/paracrine oxygen sensing*,

Indiana Respiratory Physiology & Neurobiology (2013a), 186, 173–179.

34. Olson K. R., DeLeon E. R., Gao Y., Hurley K., Sadauskas V., Batz C., Stoy G. F., *Thiosulfate: a readily accessible source of hydrogen sulfide in oxygen sensing*, (2013b), 305, R592-R603.
35. Olson K. R., Dombkowski R. A., Russell M. J., Doellman M. M., Head S. K., *Hydrogen sulfide as an oxygen sensor/transducer in vertebrate hypoxic vasoconstriction and hypoxic vasodilation*, J Exp Biol. (2006), 209, 4011-23.
36. Olson K. R., Forgan L. G., Dombkowski R. A., Forster M. E., *Oxygen dependency of hydrogen sulfide-mediated vasoconstriction in cyclostome aortas,* J Exp Biol. 211 (2008a) 2205-13.
37. Olson K. R., *Hydrogen sulfide and oxygen sensing: implications in cardiorespiratory control*, J Exp Biol. (2008c), 211, 2727-34.
38. Olson K. R., *Hydrogen sulfide as an oxygen sensor*. Antioxid Redox Signal. (2015), 10, 377-97.
39. Olson K.R. and Straub K.D., *The role of hydrogen sulfide in evolution and the evolution of hydrogen sulfide in metabolism and signalling*, Physiology (Bethesda) (2016), 31, 60–72.
40. Panza E., De Cicco P., Armogida C., Scognamiglio G., Gigantino V., Botti G., Germano D., Napolitano M., Papapetropoulos A., Bucci M., Cirino G., Ianaro A., *Role of the cystathionine γ lyase/hydrogen sulfide pathway in human melanoma progression*, Pigment Cell Melanoma Res. (2014), 28, 61-72.
41. Papapetropoulos, A., Pyriochou, A., Altaany, Z., Yang, G., Marazioti, A., Zhou, Z., Szabó, C. (2009). *Hydrogen sulfide is an endogenous stimulator of angiogenesis*, Proceedings of the National Academy of

Sciences, 106(51), 21972–21977 Free Radical Biology and Medicine (2016), 93,55–164.

42. Paul B.D. and Snyder S.H., *H_2S: a novel gasotransmitter that signals by sulfhydrat*ion, Trends Biochem. Sci. (2015), 40, 687–700.
43. Pereira S.L., Ramalho-Santos J., Branco A. F., Sardão V. A., Oliveira P. J., and Carvalho R. A, *Metabolic remodeling during H9c2 myoblast differentiation: relevance for in vitro toxicity studies*, Cardiovascular Toxicology (2011), 11, 180–190.
44. Pietri R.*,* Román-Morales E., López-*Garriga J., Hydrogen sulfide and hemeproteins: knowledge and mysteries*, *Antioxid. Redox Signal (2011)*, 15, 393–404.
45. Semenza G. L., *Hypoxia-inducible factors: mediators of cancer progression and targets for cancer therapy*, Trends in pharmacological sciences – Elsevier (2012), 33, 207-214.
46. Singh S. and Banerjee R., *PLP-dependent H_2S biogenesis*, Biochim. Biophys. Acta (2011), 1814, 1518–1527.
47. Solaini G., Baracca A., Lenaz G. Sgarbi G., *Hypoxia and mitochondrial oxidative metabolism*, Biochimica et Biophysica Acta (BBA) - Bioenergetics (2010), 67, 1171-1177.
48. Srere, P. A., *Citrate synthase,* Methods Enzymol. (1969), 13, 3–11.
49. Szabo C., Coletta C., Chao C., Modis K., Szczesny B., Papapetropoulos A., Hellmich M. R., *Tumor-derived hydrogen sulfide, produced by cystathionine- -synthase, stimulates bioenergetics, cell proliferation, and angiogenesis in colon cancer*, Proceedings of the National Academy of Sciences (2013), 305, 12474-12479.
50. Szabo C., Ransy C., Modis K. Andriamihaja M, Murghes B., Coletta C., Olah G., Yanagi K., Bouillaud F., *Regulation of mitochondrial*

bioenergetic function by hydrogen sulfide. Part I. Biochemical and physiological mechanisms, Br. J. Pharmacol. (2014), 171, 2099–2122.

51. Takano N., Peng Y.-J., Kumar G. K., Luo W., Hu H., Shimoda L. A. Suematsu M., Prabhakar N. R., and Semenza G. L*., Hypoxia-Inducible Factors Regulate Human and Rat Cystathionine β-Synthase Gene Expression*, Biochem J. (2014), 458, 203–211.
52. Teng H., Wu B., Zhao K., Yang G., Wu L., Wang R., *Oxygen-sensitive mitochondrial accumulation of cystathionine β-synthase mediated by Lon protease*, Proceedings of the National Academy of Sciences of the United States of America (2013), 110, 12679–84.
53. Wu H., Chen Q., *Hypoxia activation of mitophagy and its role in disease pathogenesis*, Antioxidants & Redox Signaling, (2015), 22, 1032-1046.
54. Wu, B., Teng, H., Zhang, L., Li, H., Li, J., Wang, L., & Li, H., I*nteraction of hydrogen sulfide with oxygen sensing under hypoxia.* Oxidative Medicine and Cellular Longevity, (2015) 2015:758678
55. Yuan G., Vasavda C, Peng Y. J, Makarenko V. V., Raghuraman G, Nanduri J, Gadalla M. M., Semenza G.L., Kumar G. K., Snyder S. H., Prabhakar N. R., *Protein kinase G-regulated production of H_2S governs oxygen sensing,* Sci Signal. (2015).
56. Zhang F., Bosch-Marce M., Shimoda L. A., Shun Y. S., Baek J. H., Wesley J. B., Gonzales F. J., Semenza G. L., *Mitochondrial autophagy is an HIF-1-dependent adaptive metabolic response to hypoxia*, J Biol Chem. (2008) 283, 10892–10903.
57. Zhang W., Braun A., Bauman Z., Olteanu H., Madzelan P., Banerjee R., *Expression profiling of homocysteine junction enzymes in the NCI60 panel of human cancer cell lines*, Cancer Res. (2005), 65, 1554–60.

58. Zhao W., Zhang J., Lu Y., Wang R., *The vasorelaxant effect of H_2S as a novel endogenous gaseous K(ATP) channel opener*. The EMBO Journal, (2011), 20, 6008–6016.

Paper 4

A Novel Ferritin-based Nanocarrier for Efficient Mitoxantrone Encapsulation and Selective Delivery to Cancer Cells

Elisabetta Falvo[1], Francesca Malagrinò[1,2,] Alessandro Arcovito[3], Francesco Fazi[4], Gianni Colotti[1], Elisa Tremante[5], Patrizio Di Micco[2], Giulio Fracasso[6], Alessandro Giuffrè[1], Pierpaolo Ceci[1]

[1]Institute of Molecular Biology and Pathology, National Research Council of Italy (CNR), Rome, Italy; [2]Department of Biochemical Sciences "A. Rossi Fanelli", Sapienza University of Rome, Rome, Italy; [3]Institute of Biochemistry and Clinical Biochemistry, Catholic University of Sacred Heart, Rome, Italy; [4]Department of Anatomical, Histological, Forensic & Orthopedic Sciences, Section of Histology & Medical Embryology, Sapienza University of Rome, Rome, Italy; [5]Regina Elena National Cancer Institute, Rome, Italy; [6]Department of Medicine, University of Verona, Verona, Italy
The first two authors contributed equally to this work.

Correspondence: Pierpaolo Ceci
[1] Institute of Molecular Biology and Pathology, National Research Council of Italy (CNR), Rome, Italy
Tel +39 (06) 49910862
Fax +39 (06) 4440062
Email pierpaolo.ceci@cnr.it

Elisabetta Falvo
[1] Institute of Molecular Biology and Pathology, National Research Council of Italy (CNR), Rome, Italy
Tel +39 (06) 49910862
Fax +39 (06) 4440062
Email elisabetta.falvo@uniroma1.it

Abstract: A genetically engineered human ferritin heavy chain (HFt)-based construct has been recently shown by our group to efficiently entrap and deliver doxorubicin to cancer cells. This construct, named HFt-MP-PAS, contained a tumor-selective sequence (MP) responsive to proteolytic cleavage by tumor proteases (MMPs), located between each HFt subunit and an outer shielding polypeptide sequence rich in proline (P), serine (S) and alanine (A) residues (PAS). HFt-MP-PAS displayed excellent therapeutic efficacy in a xenogenic pancreatic cancer model in vivo, leading to a significant increase in overall animal survival in treated mice. Here we report a new construct obtained by the genetic insertion of two glutamate residues in the PAS sequence of HFt-MP-PAS. Such new construct, named HFt-MP-PASE, efficiently encapsulate the anti-cancer drug mitoxantrone (MIT), and the resulting MIT-loaded nanoparticles proved to be more soluble and monodispersed than the HFt-MP-PAS counterparts. Importantly, in vitro MIT-loaded HFt-MP-PASE nanoparticles kill several cancer cell lines of different origin (pancreatic, colon, sarcoma and breast) at least as efficiently as the free drug.

Keywords: protein-cage nanocarrier; pasylated ferritin; mitoxantrone; drug-encapsulation; drug-delivery; cancer

Introduction

Human ferritin heavy chain (HFt)-based constructs have been shown to efficiently entrap and deliver chemotherapeutics (*e.g.*, cisplatin, doxorubicin, 5-fluorouracil and gefitinib) to cancer cells.[1–9] HFt is a multimeric protein-cage consisting of 24 identical subunits that self-assemble into a symmetric shell-like sphere, with external and internal diameters of 12 and 8 nm, respectively.[10–16] Drug molecules are usually encapsulated inside the HFt

internal cavity. An important advantage of the HFt system is the ability to effectively bind to and enter many types of tumor cells via the transferrin receptor 1 (TfR1, CD71). A wide number of tumors express up to 100 times higher levels of TfR1 than healthy cells and actively internalize the HFt:TfR1 ligand-receptor complex to accumulate the large amount of iron required for unrestrained cancer cell growth.[17,18]

Recently, to increase both the *in vivo* half-life of native HFt and the stability of HFt-drug complexes, we have developed novel HFt-based constructs, named HFt-MP-PAS, suitable for drug delivery. In these constructs the N-terminus of each HFt subunit is genetically fused to: i) a PAS polypeptide sequence, *i.e.*, a sequence rich in proline (P), alanine (A) and serine (S) residues;[5,19] and ii) a tumor-selective sequence (MP) responsive to proteolytic cleavage by tumor proteases (MMPs), inserted between each HFt subunit and the outer PAS polypeptide.[20] The PAS shield was aimed at hampering the interaction between drug-loaded HFt and TfR1 in healthy tissues and reducing internalization by normal cells, already limited by the low expression of the receptor. The MP sequence allows the PAS shield to be selectively removed by stimuli present in the tumor microenvironment (*i.e.*, MMPs specific for this sequence) so that the resulting unmasked HFt can freely interact with and be internalized by TfR1 overexpressed in cancer cells.

The HFt-MP-PAS constructs proved to i) encapsulate in the internal cavity three times more doxorubicin (DOXO) than wild-type HFt, ii) form more stable complexes (*i.e.*, drug leakage was negligible) and iii) possess higher *in vivo* circulation time. Importantly, DOXO-loaded HFt-MP-PAS (HFt-MP-PAS-DOXO) displayed excellent therapeutic efficacy in a human pancreatic cancer model *in vivo,* significantly increasing overall animal survival.[19] The nanocarriers efficacy was even superior to the novel

albumin-based DOXO delivery system (INNO-206), currently in phase III clinical trials. We ascribed to the PAS shield the increase in DOXO encapsulation, protein-drug complex stability and circulation time with respect to HFt. The higher *in vivo* efficacy of HFt-MP-PAS-DOXO with respect to other DOXO delivery systems is likely due to both effective PAS removal by tumor specific MMPs and efficient DOXO delivery into the cell nucleus, as revealed by confocal microscopy studies.[19]

The goal of the present study was to improve and widen the use of HFt as drug-delivery system and in particular to exploit these nanocarriers as delivery system for drugs with solubility problems or high nonspecific toxicity (i.e. lower therapeutic index). So far, HFt-based constructs have been demonstrated to efficiently entrap cisplatin, doxorubicin, 5-fluorouracil and gefitinib as chemotherapeutic molecules.[1–8] Here we report the first encapsulation of the anti-cancer drug mitoxantrone (MIT) in HFt-based constructs. MIT is a synthetic anthracenedione developed to improve the therapeutic profile of anthracyclines and a clinically well-established anticancer agent which targets DNA topoisomerase I and ubiquitin-specific peptidase 11 (USP11) enzyme, a component of the DNA repair complex. Despite some limitations, MIT shows high efficacy in several types of cancer.[21,22] To widen MIT applicability and improve its therapeutic index, a selective delivery system is needed. Here we found that, although the previously designed HFt-MP-PAS construct is able to bind several MIT molecules, stability and homogeneity of the complex are lower than those obtained with DOXO. To obtain higher yields and monodispersed materials, we genetically re-engineered HFt-MP-PAS by adding glutamate residues (E) in the PAS sequence and obtained a new construct, named HFt-MP-PASE. Thanks to this modification, MIT-loaded HFt-MP-PASE nanoparticles (HFt-MP-PASE-MIT) proved to be both more soluble and monodispersed than the

HFt-MP-PAS counterpart, yet displaying high *in vitro* killing efficacy against cancer cells and preferential drug delivery into the cell nucleus. The novel HFt-MP-PASE construct herein described further extends the array of drugs deliverable by HFt-based nanosystems for therapeutic purposes.

Material and methods

Protein design

MIT-loaded HFt-MP-PAS complexes (HFt-MP-PAS-MIT) were found in the present work to be less stable and homogeneous than the previously reported HFt-MP-PAS-DOXO complexes. Therefore, as an attempt to reduce protein aggregation and increase stability, we decided to introduce negatively charged residues in the outer shield-forming PAS sequence fused to each HFt subunit. Indeed, analysis of the previously obtained HFt-MP-PAS construct[20] suggested that introduction of two glutamate residues in the PAS sequence would cause sufficient electrostatic repulsion to prevent aggregation between different 24-meric assemblies, without affecting subunit assembly within the 24-mer. To distribute the negative charges on the surface of the construct as much as possible, glutamic acid residues were placed after 12 residues of the PAS sequence repeat reported previously: ASPAAPAPASPAEPAPSAPAASPAAPAPASPAEPAPSAPA.

Protein structure visualization and modelling of PAS chains were performed using the software InsightII (Accelrys Inc).

Cloning, overexpression and purification of HFt-MP-PASE constructs

The *HFt-MP-PASE* gene was obtained by genetically adding two glutamate (E) residues, at positions 21 and 42, to the previously designed 40-residue long *HFt-MP-PAS* gene.[20]

The expression vector pET-11a containing the *HFt-MP-PASE* gene was assembled by GENEART AG (Germany). Gene synthesis was performed taking into account codon-optimization for high level expression in *Escherichia coli*. The recombinant proteins HFt-MP-PAS and HFt-MP-PASE were expressed in *E. coli*, purified and quantified as previously described.[5]

Native agarose gel electrophoresis

Protein mobility was assessed by agarose gel electrophoresis under native conditions. The 1% agarose gels were run in TAE buffer (40 mM Tris-acetate and 2 mM EDTA, pH 8.0) and stained with Coomassie.

MIT encapsulation in HFt-based nanocarriers

MIT (MedKoo Biosciences, USA) was encapsulated using the HFt disassembly/reassembly procedure previously described for DOXO[5] (Scheme 1). Briefly, solutions of HFt-MP-PAS or HFt-MP-PASE in 0.1 M NaCl were incubated for 10 min at pH 2.0 (pH adjusted with HCl). Then, MIT was added to the solution at 250:1 molar ratio with respect to the protein. The pH was initially maintained at 2.5 for 5 min and then increased to 7.5 using NaOH. The resulting solution was stirred at room temperature for 30 min, filtered and dialyzed o.n. *vs* phosphapte buffer saline (PBS) at pH 7.4 to remove unbound MIT. After dialysis, solutions were centrifuged at 15.000 rpm for 30 min at 4°C. Supernatant was collected, concentrated with 30 kDa Amicon Ultra-15 centrifugal devices, sterile filtered and stored at 4°C in the dark. HFt and MIT content of the samples was determined by the Lowry method and UV-vis spectroscopy, respectively, after extracting MIT in 1 N

HCl, 95% ethanol. MIT was quantified by using the calculated molar extinction coefficient ε = 19200 $M^{-1}cm^{-1}$ at 610 nm.

Size exclusion chromatography (SEC) and dynamic light scattering (DLS) analyses

SEC experiments were performed using a Superose 6 gel-filtration column equilibrated with PBS.

DLS experiments were carried out with a Zetasizer Nano S (Malvern Instruments, Malvern, U.K.) equipped with a 4 mW He–Ne laser (633 nm). Measurements were performed at 25°C with an angle of 173° with respect to the incident beam. The average hydrodynamic diameters (*Z*-average diameter) of the scattering particles were determined by peak intensity analyses. Results are the average of at least five measurements of samples from three different syntheses. All samples were prepared at 1 mg/mL in filtered H_2O_{dd}.

Data from both SEC and DLS experiments were analysed with Origin 8.0 (Originlab Corporation, Northampton, MA).

Stability of MIT-loaded HFt-based nanocarriers (HFt-MP-PASE-MIT)

MIT release from HFt-based nanocarriers was evaluated every 7 days for 2 months in PBS at 4°C and 37 °C. Drug release was evaluated by SEC, simultaneously following the optical contributions of the protein and the drug at 280 nm and 610 nm, respectively.

Cell-binding of HFt-based nanocarriers

Fluorescence Activated Cell Sorting (FACS) experiments were carried out after incubation of SW480 and SW620 cell lines (ATCC, Manassas, VA, USA) with 0.8, 4 and 8 μM HFt-MP-PASE-MIT at 37°C for 1 h or 3 h. Cells (3.5×10^5) were grown in a 6-well plate and incubated at 37°C with 2 ml

medium (Dulbecco's Modified Eagle Medium + 10% fetal bovine serum, Invitrogen-Gibco). After washing with PBS, cells were detached by trypsin-EDTA solution and samples were assayed in a flow cytometer (CyAN ADP; Dako Italia S.p.a., Milan, Italy) using the Summit 4.3 software (Beckman Coulter, Milan, Italy) for data acquisition and analysis.

Cell-localization of HFt-based nanocarriers

In confocal microscopy experiments, cells grown on round glass slides were treated with 20 μM MIT and HFt-MP-PASE-MIT using the same protocol described for the cell-binding assays and then fixed in 4% formaldehyde in PBS. After washing with PBS, slides were incubated for 30 min with 1:100 Lamin A/C (4C11) mouse monoclonal antibody (Cell Signaling #4777) in PBS/1% BSA, stained with goat anti-mouse IgG (H+L) secondary antibody, Alexa Fluor 488, and mounted with Vectashield (Vector Labs, Burlingame, CA, USA). Cells were examined with a Leica TCS SP2 fluorescence confocal microscope (Leica Microsystems, Wetzlar, Germany) using excitation wavelengths of 488 nm (argon laser) and 633 nm (helium-neon laser). Photomicrographs were acquired with the LAS AF Software (Leica Microsystems, Wetzlar, Germany).

Antiproliferative effects of HFt-MP-PASE-MIT construct *in vitro*

Human cells from fibrosarcoma (HT1080), triple-negative breast (MDA-MB-231), prostatic (PC3) and colorectal (SW480 and SW620) cancer were grown in Dulbecco's Modified Eagle Medium; pancreatic PaCa44, Capan-1 and MiaPaCa2 cell lineswere grown in RMPI 1640 medium. All growth media were also added with 2 mM glutamine, 10% of FBS and antibiotics. Cancer cells (5×10^3) were seeded in 90 μL of complete medium in 96-well culture microplates. The day after, cells were incubated in triplicate with 10 μL of serially diluted free MIT or HFt-MP-PASE-MIT. After 72 hour-incubation at

37 °C with drugs, the medium was replaced with fresh medium w/o phenol red supplemented with XTT (2,3-Bis-(2-Methoxy-4-Nitro-5-Sulfophenyl)-2H-Tetrazolium-5-Carboxanilide) reagent (Sigma-Aldrich, St Louis, MO, USA), according to the manufacturer's instructions. Finally, after a variable time ranging from 1 to 3 hours of incubation at 37°C cell viability was measured at 450 nm by a microplate reader (VERSAmax, Molecular Devices, Sunnyvale, CA, USA). The percentage of cell viability was estimated by comparing cells treated with free MIT or HFt-MP-PASE-MIT to mock treated cells. To compare the killing efficacy, we evaluated the IC_{50}, *i.e.*, the compound concentration yielding 50% cell viability.

Results and discussion

MIT encapsulation in HFt-MP-PAS

MIT encapsulation inside HFt-MP-PAS was achieved following the disassembly/reassembly procedure reported previously.[5] The encapsulation efficiency, however, was slightly lower than reported previously for DOXO (about 90 molecules entrapped per construct) [5]: only about 55 MIT molecules were indeed found by UV-visible spectroscopy and size-exclusion chromatography (SEC) to be bound by a HFt-MP-PAS 24-mer. HFt-MP-PAS-MIT complex recovery and drug loading capacities are reported in Table 1.

Sample polydispersity was assessed by SEC and dynamic light scattering (DLS). Both techniques showed the presence of slightly higher molecular species as compared to monodispersed HFt-MP-PAS-MIT complex (Figure 1). In particular, DLS revealed the presence of larger particles (mean diameter of 20.5 nm) as compared to the monomeric form of the protein 24-mer (mean diameter of 17.0 nm). The MIT-encapsulating product is thus less

homogenous than previously reported for DOXO due to the presence of higher molecular weight species (likely dimers) in solution.[5]

Design and production of novel HFt-MP-PASE fusion protein

In order to improve the construct yield and homogeneity, we genetically re-engineered the HFt-MP-PAS fusion protein by inserting two glutamate residues (E) in the PAS sequence (HFt-MP-PASE). This modification was aimed at reducing HFt-MP-PAS aggregation following MIT incorporation, through insertion of negative charges in the outer shield of the assembly surface.

The fusion protein HFt-MP-PASE was obtained *via* recombinant protein technology and purified from the cellular soluble fraction at high yield, similar to HFt-MP-PAS (about 150 mg per liter of *E. coli* cell culture). The effect on protein mobility of the negatively charged glutamate residues (48 per protein) inserted on the protein surface was assessed by performing agarose gel electrophoresis under native conditions (supporting Figure 1). At variance with denaturant SDS-PAGE, in native electrophoresis protein mobility depends on both protein charge and molecular mass. Assuming the latter to be comparable for HFt-MP-PAS and HFt-MP-PASE, the observed difference in protein mobility has to be ascribed to the additional negative charges in the HFt-MP-PASE construct (Figure 2).

MIT encapsulation in HFt-MP-PASE

As shown in Figure 1 and Table 1, the efficiency of MIT encapsulation in HFt-MP-PASE was comparable to that one in HFt-MP-PAS. MIT-loaded HFt-MP-PASE constructs, however, were more soluble and monodispersed than the HFt-MP-PAS counterparts, displaying no higher

molecular weight species in solution (Table 1 and Figure 1). DLS experiments indicated that HFt-MP-PASE-MIT samples have approximately the same size as our previously reported HFt-MP-PAS-DOXO, with a mean diameter of 17.0 nm (Figure 1B).[5] These results indicate that insertion of the glutamate residues in HFt-MP-PASE-MIT leads to higher protein solubility and homogeneity compared to the HFt-MP-PAS counterpart, likely preventing MIT-mediated protein-protein interactions in solution. In addition, the slightly higher number of MIT molecules per 24-mer observed for HFt-MP-PAS in comparison to HFt-MP-PASE (56.0 vs 47.0) can be likely ascribed to a significant presence of MIT molecules on the surface of the former construct.

Stability of HFt-MP-PASE-MIT nanocarrier

HFt-MP-PASE-MIT complex was tested by storing the nanoparticles for 2 months in PBS at 4°C or 37°C and evaluating their MIT content by SEC analysis every 7 days. HFt-MP-PASE-MIT showed excellent stability, with less than 10% MIT being released after 2 months storage at 4°C (Figure 3) and no sign of turbidity or precipitation.

Cell internalization and localization of HFt-based nanocarriers

To determine whether MIT-containing HFt-based constructs undergo cell surface binding and/or internalization, they were incubated with colon cancer cells SW480 and SW620 at 37°C for 1 or 3 h and MIT-associated fluorescence was visualized by confocal microscopy.

Figure 4 shows HFt-MP-PASE-MIT localization in the SW480 (upper panel) and SW620 (lower panel) cell lines. After 3 hour-incubations HFt-MP-PASE-MIT massively accumulate in the nuclei of both cell lines, as shown by staining with the nuclear membrane marker Lamin A/C (in green). In particular, MIT localizes in intranuclear structures assumed to be nucleoli on

the basis of size, position and shape, as previously proposed for colon carcinoma and breast cancer cells.[23,24] A comparison between cells treated with free MIT, HFt-MP-PAS-MIT or HFt-MP-PASE-MIT is shown in Figure 5. In all cases MIT localizes inside the cell nuclei, but in the case of free MIT and HFt-MP-PAS-MIT the drug is partly present also in the cytoplasm. Overall, cells treated with HFt-MP-PASE-MIT showed the highest accumulation of MIT in the nuclei. In both cell lines tested HFt-MP-PASE-MIT accumulation was time- and dose-dependent, the accumulation being more pronounced in SW480 than in SW620 cells (Figure 6).

In vitro antiproliferative effects of HFt-MP-PASE-MIT nanocarriers

To assess the ability of MIT-loaded HFt-MP-PASE to kill cancer cells *in vitro*, we have performed XTT viability assays on a wide range of human cancer cells of different origin: fibrosarcoma HT1080; triple-negative breast MDA-MB-231; pancreatic PaCa-44, Capan-1 and MiaPaCa2; colorectal SW480 and SW620 cancer cells.

Not only MIT preserved its pharmacological activity after encapsulation in HFt-MP-PASE constructs, but the MIT-loaded nanocarrier display IC_{50} values similar to those of naked MIT in all cell lines tested, and even lower in some cases (see Table 2). This is remarkable in that naked drugs can freely diffuse into cells, whereas the HFt-MP-PASE constructs can only deliver MIT by undergoing rate-limiting receptor-mediated uptake. Moreover, the new nanosystem HFt-MP-PASE-MIT showed, on the pancreatic cell lines, a killing efficacy of about ten time higher than the currently used drug Gemcitabine (i.e. 0.43 vs 6.75 μM, 0.10 vs 2.8 μM and 0.07 vs 1.15 μM, for Paca44, Capan-1 and MiaPaCa2 cells respectively).

Conclusion

We have generated the first, to our knowledge, HFt-based protein nanocarrier able to encapsulate the MIT anti-cancer drug. To achieve this result, we have re-engineered our previously reported HFt-MP-PAS nanocarriers by inserting negatively charged aminoacid residues (glutamates) in the outer shield-forming PAS sequence. The novel system (HFt-MP-PASE) has higher solubility because of reduced drug-mediated protein-protein interactions, due to electrostatic repulsion between negative surface glutamates. Like the previously reported HFt-MP-PAS system, HFt-MP-PASE is a genetic construct that can be expressed and purified at high yield in *E. coli* as a single protein product, without requiring additional coupling and/or separation steps.

HFt-MP-PASE is able to stably encapsulate up to approximately 50 MIT molecules in the internal cavity. MIT encapsulation was shown to preserve the pharmacological activity of the drug against a panel of different cancer cells, as demonstrated by performing viability assays *in vitro*. This is noteworthy in that the construct needs to undergo receptor-mediated internalization, as opposed to free diffusion of the naked drug into the cell. This result can be ascribed, at least in part, to the considerable nuclear, likely nucleolar, accumulation of the delivered drug, as revealed by confocal microscopy experiments. We also shown that HFt-MP-PASE-MIT internalization into the cell is time- and dose-dependent, and that SW480 colorectal cancer cells incorporate slightly higher MIT amounts than SW620 cells.

All together these results strongly support the HFt-MP-PASE construct herein described as a suitable nanocarrier to be exploited for mitoxantrone-based cancer therapy *in vivo*.

Acknowledgments

We would like to thank Prof. A. Scarpa (Department of Diagnostics and Public Health University of Verona, Italy) for providing the cell line PaCa-44. The Authors thank Stefania De Grossi and Fabrizio Padula for technical support in the confocal microscopy and FACS experiments, and Veronica Morea, Alberto Boffi and Patrizio Giacomini for fruitful discussions. This research was supported by MIUR of Italy (flagship Project "Nanomax" to P.C. and PNR-CNR Aging Program 2012–2014 to A.G.) and Associazione Italiana per la Ricerca sul Cancro - AIRC (I.G. Grant 16776 to P.C.). G.F. gratefully acknowledges Fondazione Cariverona, Verona Nanomedicine Initiative and Italian Minister of Health RF-2010-2305526 for supporting this work.

Disclosure

The authors report no conflicts of interest in this work.

FIGURES AND TABLES

Figure 1

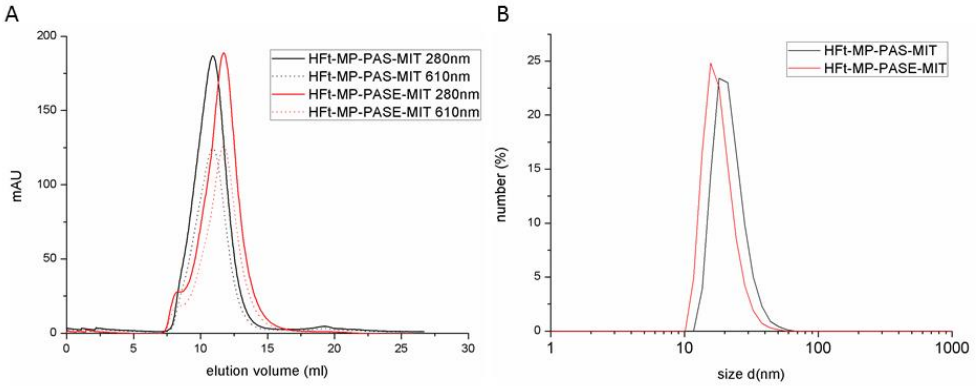

Figure 1 Gel-filtration elution profiles and particle size distribution of HFt-based constructs. (**A**) SEC analysis of MIT-loaded HFt-MP-PAS (black) and

HFt-MP-PASE (red) constructs. Elution profiles obtained following simultaneously protein and MIT contributions at 280 nm (solid) and 610 nm (dotted), respectively. (**B**) DLS profiles of the same constructs.

Figure 2

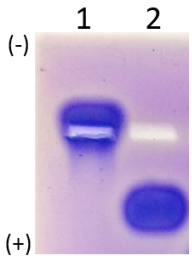

Figure 2 Native agarose gel electrophoresis band migration profiles. Lane HFt-MP-PAS (15 µg); Lane 2, HFt-MP-PASE (15 µg).

Figure 3

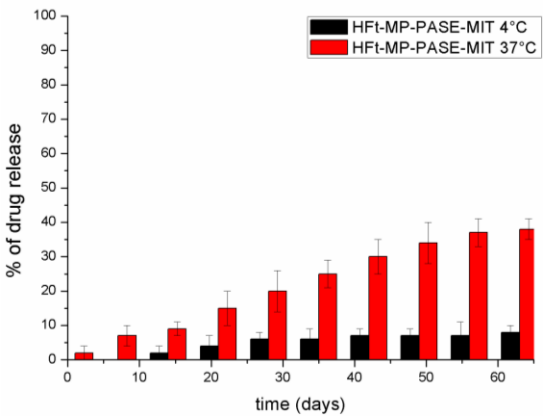

Figure 3 Drug release from HFt-MP-PASE-MIT complexes. MIT-loaded nanocarriers were stored at 4 °C and 37 °C in PBS and assayed for their MIT content by SEC at given times. The percentage of MIT leakage was assessed

by comparing the elution profiles simultaneously collected at 280 nm and 610 nm.

Figure 4

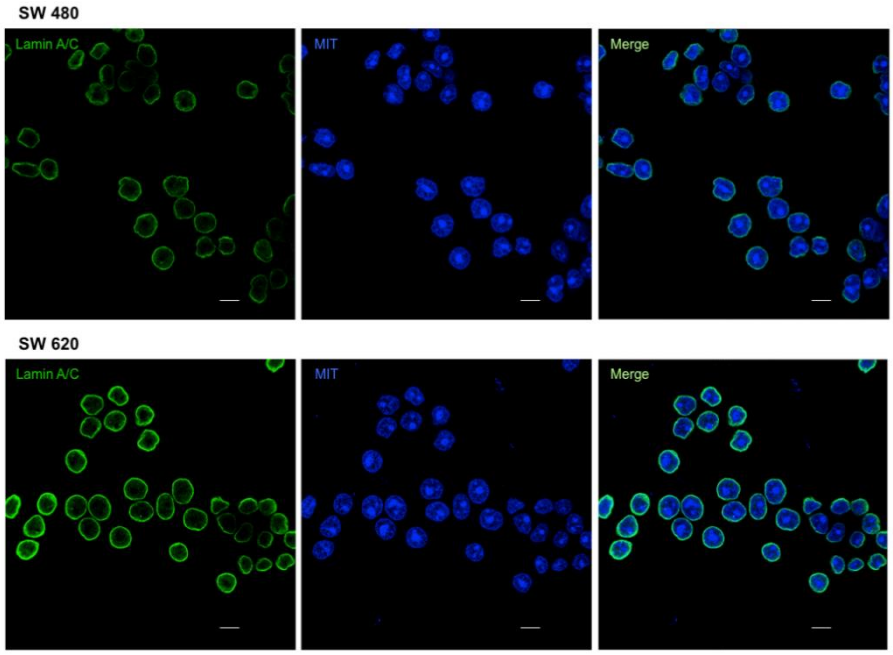

Figure 4 HFt-MP-PASE-MIT (20 μM MIT concentration) localization in SW480 (upper panel) and SW620 (lower panel) colon cancer cell lines after 3 h-incubation. Left panels: Lamin A/C staining (nuclear membrane marker, green); central panels: MIT (blue); right panels: merge. The white bar indicates a 10 μm length.

Figure 5

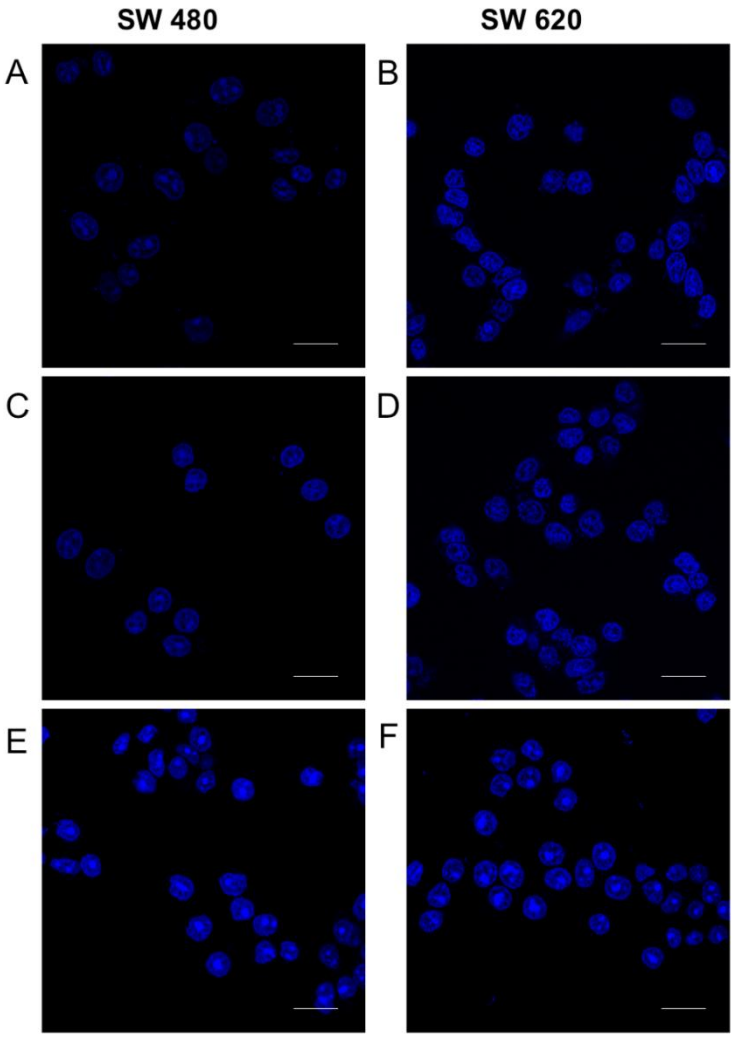

Figure 5 Localization of MIT (panels **A**, **B**), HFt-MP-PAS-MIT (panels **C**, **D**) and HFt-MP-PASE-MIT (panels **E**, **F**) in SW480 (panels **A**, **C** and **E**) and SW620 (panels **B**, **D** and **F**) colon cancer cell lines after 3 h incubation. MIT concentration is 20 μM in all experiments. The white bar indicates a 20 μm length. Representative images are shown.

Figure 6

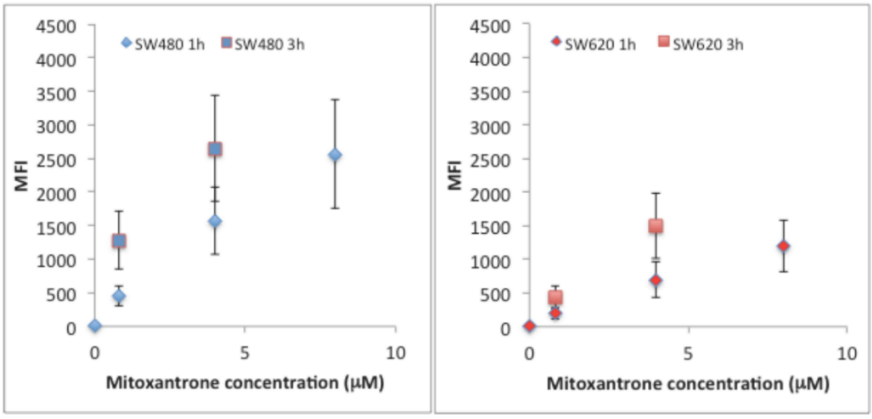

Figure 6 Cellular uptake of HFt-MP-PASE-MIT nanocarriers by FACS analysis. FACS experiments were carried out after incubation of SW480 (left panels) and SW620 lines (right panels) with 0.8, 4 and 8 µM of MIT-containing HFt-MP-PASE at 37°C for 1 or 3 h. Graphs show the mean fluorescence intensity (MFI) upon incubation with different doses of HFt-MP-PASE-MIT.

Scheme 1

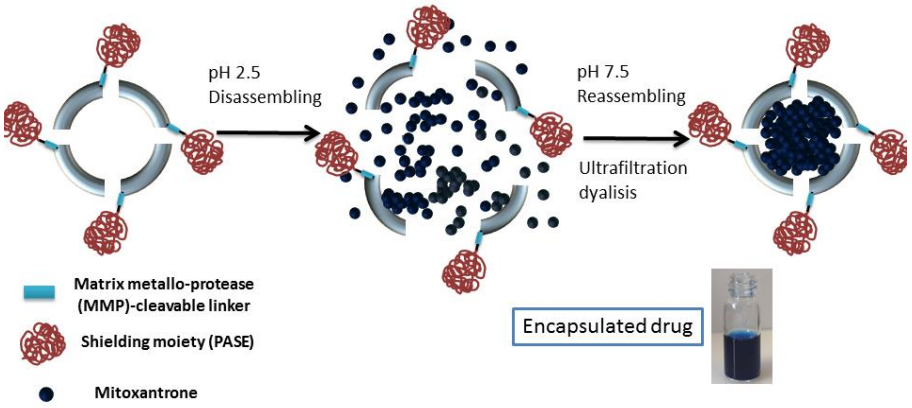

Scheme 1. Schematic representation of the synthesis of HFt-MP-PASE-MIT. For clarity purposes, only 4 out of the 24 modified HFt N-termini are shown.

Table 1

Protein	**Protein recovery (%)**	**Number of MIT molecules per 24-mer**
HFt-MP-PAS	65±4	56±4
HFt-MP-PASE	90±3	47±5

Table 1. MIT encapsulation by HFt-based nanocarriers. Mean ± standard deviation (n = 3)

Table 2

Cancer cells	**IC_{50} (μM)** ***Free MIT***	**IC_{50} (μM)** ***HFt-MP-PASE-MIT***
SW480	0.005 ± 0.001	0.004 ± 0.001
SW620	0.004 ± 0.001	0.005 ± 0.001

MDA-MB-231	0.03 ± 0.009	0.02 ± 0.007
HT1080	0.01 ± 0.008	0.009 ± 0.005
PaCa44	0.43 ± 0.12	0.43 ± 0.34
Capan-1	0.72 ± 0.23	0.10 ± 0.04
MiaPaCa2	0.11 ± 0.06	0.07 ± 0.02

Table 2. Killing efficacy of MIT and HFt-MP-PASE-MIT against human cell lines PaCa-44, Capan-1 and MiaPaCa2 (pancreatic carcinoma), HT1080 (fibrosarcoma), MDA-MB-231 (breast cancer) and SW480 and SW620 (colorectal cancer). Mean ± S.E.M. (n =3)

REFERENCES

1. Falvo, E., Tremante, E., Fraioli, R., et al. (2013) Antibody-drug conjugates: targeting melanoma with cisplatin encapsulated in protein-cage nanoparticles based on human ferritin. *Nanoscale*, **5** (24), 12278–85.
2. Yang, Z., Wang, X., Diao, H., et al. (2007) Encapsulation of platinum anticancer drugs by apoferritin. *Chem Commun*, (33), 3453–3455.
3. Liu, X.Y., Wei, W., Huang, S.J., et al. (2013) Bio-inspired protein-gold nanoconstruct with core-void-shell structure: beyond a chemo drug carrier. *J. Mater. Chem. B*, **1** (25), 3136–3143.
4. Liang, M., Fan, K., Zhou, M., et al. (2014) H-ferritin-nanocaged doxorubicin nanoparticles specifically target and kill tumors with a single-dose injection. *Proc Natl Acad Sci U S A*, **111** (41), 14900–14905.
5. Falvo, E., Tremante, E., Arcovito, A., et al. (2015) Improved Doxorubicin Encapsulation and Pharmacokinetics of Ferritin-Fusion Protein Nanocarriers Bearing Proline, Serine, and Alanine Elements. *Biomacromolecules*.
6. Kilic, M.A., Ozlu, E., and Calis, S. (2012) A Novel Protein-Based Anticancer Drug Encapsulating Nanosphere: Apoferritin-Doxorubicin Complex. *J. Biomed. Nanotechnol.*, **8** (3), 508–514.
7. Zhen, Z., Tang, W., Chen, H., et al. (2013) RGD-Modified Apoferritin Nanoparticles for Efficient Drug Delivery to Tumors. *ACS Nano*, **7** (6), 4830–4837.

8. Zhang, L.B., Li, L., Di Penta, A., et al. (2015) H-Chain Ferritin: A Natural Nuclei Targeting and Bioactive Delivery Nanovector. *Adv. Healthc. Mater.*, **4** (9), 1305–1310.
9. Blazkova, I., Nguyen, H. V, Dostalova, S., et al. (2013) Apoferritin modified magnetic particles as Doxorubicin carriers for anticancer drug delivery. *Int J Mol Sci*, **14** (7), 13391–13402.
10. Vannucci, L., Falvo, E., Fornara, M., et al. (2012) Selective targeting of melanoma by PEG-masked protein-based multifunctional nanoparticles. *Int J Nanomedicine*, **7**, 1489–1509.
11. Heger, Z., Skalickova, S., Zitka, O., et al. (2014) Apoferritin applications in nanomedicine. *Nanomedicine (Lond).*, **9** (14), 2233–45.
12. Truffi, M., Fiandra, L., Sorrentino, L., et al. (2016) Ferritin nanocages: A biological platform for drug delivery, imaging and theranostics in cancer. *Pharmacol. Res.*, **107**, 57–65.
13. Bode, S.A., Minten, I.J., Nolte, R.J., and Cornelissen, J.J. (2011) Reactions inside nanoscale protein cages. *Nanoscale*, **3** (6), 2376–2389.
14. Bellapadrona, G., Sinkar, S., Sabanay, H., et al. (2015) Supramolecular assembly and coalescence of ferritin cages driven by designed protein-protein interactions. *Biomacromolecules*, **16** (7), 2006–2011.
15. Lee, E.J., Lee, N.K., and Kim, I.S. (2016) Bioengineered protein-based nanocage for drug delivery. *Adv Drug Deliv Rev*.
16. Schoonen, L., and van Hest, J.C.M. (2014) Functionalization of protein-based nanocages for drug delivery applications. *Nanoscale*, **6** (13), 7124–7141.
17. Fan, K., Cao, C., Pan, Y., et al. (2012) Magnetoferritin nanoparticles for targeting and visualizing tumour tissues. *Nat. Nanotechnol.*, **7** (7), 459–464.
18. Li, L., Fang, C.J., Ryan, J.C., et al. (2010) Binding and uptake of H-ferritin are mediated by human transferrin receptor-1. *Proc Natl Acad Sci U S A*, **107** (8), 3505–3510.
19. Fracasso, G., Falvo, E., Colotti, G., et al. (2016) Selective delivery of doxorubicin by novel stimuli-sensitive nano-ferritins overcomes tumor refractoriness. *J. Control. Release*, **239**, 10–18.
20. Fracasso, G., Falvo, E., Colotti, G., et al. (2016) Selective delivery of doxorubicin by novel stimuli-sensitive nano-ferritins overcomes tumor refractivity. *J. Control. Release*.
21. Evison, B.J., Sleebs, B.E., Watson, K.G., et al. (2016) Mitoxantrone, More than Just Another Topoisomerase II Poison. *Med. Res. Rev.*, **36** (2), 248–299.
22. Hou, L., Feng, Q., Wang, Y., et al. (2016) Multifunctional hyaluronic

acid modified graphene oxide loaded with mitoxantrone for overcoming drug resistance in cancer. *Nanotechnology*, **27** (1), 15701.
23. Vibet, S., Mahéo, K., Goré, J., et al. (2007) Differential subcellular distribution of mitoxantrone in relation to chemosensitization in two human breast cancer cell lines. *Drug Metab. Dispos.*, **35** (5), 822–828.
24. Fox, M.E., and Smith, P.J. (1995) Subcellular localisation of the antitumour drug mitoxantrone and the induction of DNA damage in resistant and sensitive human colon carcinoma cells. *Cancer Chemother. Pharmacol.*, **35** (5), 403–410.

CONCLUSIONS

The results obtained along this thesis work allowed to gain insight into H_2S metabolism (synthesis and catabolism), particularly regarding the interplay between this key gaseous signalling molecule, CO and O_2 in homocystinuria and colon cancer. Moreover, a novel human ferritin-based drug delivery system was obtained able to carry the anticancer drug mitoxantrone and kill colon cancer cells with high efficacy. The acquired knowledge will hopefully set the basis for the discovery of new pharmacological targets and therapeutic interventions in diseases associated to altered H_2S metabolism, such as colon cancer.

Conclusion 1

Classic homocystinuria is rare metabolic disease caused by mutations in the gene of cystathionine β-synthase (CBS). To gain insight into the molecular bases of classic homocystinuria, the pathogenic p.P49L CBS protein variant was investigated. P49L mutation in CBS causes a mild form of homocystinuria with sporadic responsiveness to vitamin B6 treatment. We found that the p.P49L CBS variant, recombinantly produced in *E. coli* and purified, displays impaired H_2S-generating activity, rescued by PLP supplementation along the protein purification. Surprisingly, the investigated protein variant displayed a markedly increased affinity for CO binding to the protein ferrous heme, resulting into a much higher susceptibility of p.P49L

CBS to CO inhibition, compared to the wild-type protein. In light of the enhanced susceptibility to CO inhibition documented here, the p.P49L CBS variant could be inhibited *in vivo* by physiological CO concentrations, thereby contributing to pathological accumulation of homocysteine. We suggest that this may represent a novel, possibly more general, pathogenic mechanism in classical homocystinuria.

Conclusion 2

O_2 and H_2S are key molecules in living systems, able to control each other's availability and biologic effects with interesting consequences in human physiology and patho-physiology. Under hypoxic conditions, H_2S stability and synthesis are enhanced, and the resulting higher H_2S levels are known to protect cells against hypoxia and ischemia/reperfusion damage. We assessed the effect of hypoxia on the ability of the cells to dispose H_2S at the level of mitochondria, the main site of H_2S detoxification. The maximal mitochondrial sulfide-oxidizing activity was measured by quantitatively evaluating by high-resolution respirometry the stimulatory effect produced on cell respiration by sulfide injection. By comparing SW480 colon cancer cells grown under normoxic conditions (air O_2) or exposed to hypoxia (1% O_2), we found that, following 24 h-exposure to hypoxia, the cells retain their ability to metabolize sulfide but with reduced efficacy compared to untreated

cells. The lower mitochondrial sulfide-oxidizing activity observed in hypoxia-treated cells likely originates from the reduced mitochondrial content of these cells, independently assessed by performing citrate synthase activity assays. Whereas physiologically this may represent a regulatory mechanism to ensure higher protective H_2S levels at low O_2 tension, under pathological conditions of chronic hypoxia the observed lower sulfide-detoxifying activity could lead to higher risk of sulfide toxicity.

Conclusion 3

We reported the first human ferritin (HFt)-based protein nanocarrier able to encapsulate the anti-cancer drug mitoxantrone (MIT). A new Hft construct, named HFt-MP-PASE, was obtained by engineering a previously designed construct (HFt-MP-PAS, Falvo 2016). The new construct proved to be monodispersed and more soluble than the parental HFt-MP-PAS construct. Of relevance, HFt-MP-PASE displayed preferential drug delivery into the cell nucleus, as revealed by confocal microscopy, and high *in vitro* killing efficacy against colorectal cancer cells. We also showed that cell internalization of HFt-MP-PASE loaded with MIT (HFt-MP-PASE-MIT) is time- and dose-dependent, and that, following HFt-MP-PASE-MIT administration, the SW480 colorectal cancer cells incorporate slightly higher MIT amounts than SW620 cells. The collected evidence shows that the new

HFt-MP-PASE construct herein described is a suitable nanocarrier to be exploited for mitoxantrone-based cancer therapy *in vivo*. This new construct further extends the array of drugs deliverable by HFt-based nanosystems for therapeutic purposes.

MATERIALS AND METHODS

1. Materials

1.1.Chemical reagents

Trypan blue, sodium sulfide nonahydrate ($Na_2S \cdot 9H_2O$), 5,5'-dithiobis-(2-nitrobenzoic acid) (DTNB), acetyl coenzyme A (acetyl-CoA), oxaloacetate, CelLytic^{TM}MT Cell lysis reagent, protease inhibitor cocktail (P8340), anti-SQR antibody (HPA017079), thiazolyl blue tetrazolium bromide (MTT), 2,3-bis-(2-methoxy-4-nitro-5-sulfophenyl)-2H-tetrazolium-5-carboxanilide (XTT), Luria Bertani broth (LB), δ-aminolevulinic acid, ampicillin, superoxide dismutase, catalase, homocysteine, S-adenosyl-L-methionine (AdoMet), glucose oxidase, dithionite, pyridoxal-5'-phosphate (PLP), DNase I and bicinchoninic acid (BCA) assay kit were purchased from Sigma. The secondary antibody, the polyvinylidene difluoride membrane and the nitrocellulose membrane were from GE Healthcare Life Sciences. The Mini-PROTEAN TGX stain-free precast gels, the Clarity Western ECL Substrate, the *Laemmli* protein sample buffer, the running buffer 10X Tris/Glycine/SDS and the Bradford protein assay solution were purchased from Bio-Rad. 20X MOPS SDS running buffer, 4X NuPage LDS sample buffer, Bis-TRIS NuPage gels and Coomassie brilliant blue was from Life Technologies. Tween20 was from Chemik. Bovine serum albumin (BSA) and lysozyme were from AppliChem. Kanamycin, chloramphenicol, isopropyl-1-thio-ß-D-

galactopyranoside (IPTG) were purchased from Nzytech. The phenylmethylsulfonyl fluoride (PMSF) was from Merck, Terrific Broth (TB) was Fisher Scientific and mitoxantrone (MIT) was from MedKoo Biosciences. NucleoSpin RNA buffer set was ordered from Macherey-Nagel; Maxima First Strand cDNA synthesis kit (Thermo Scientific); SYBR Green qPCR master mix 2X Thermo Scientific. Cell media, non-essential aminoacids, glutamine and the antibiotics used for human cell culture were purchased from Sigma, Euroclone or Gibco.

1.2. Human cell lines

The human colon cancer cell lines SW480 and SW620 were purchased from the American type Culture Collection (ATCC®). The cell lines present different grades (Broders classification) and stages (Dukes classification) of cancer development (Dukes, 1932) (Broders,1925). The grading is a measure of histological differentiation of cancer and helps to understand how quickly a cancer may grow and spread, whereas the staging is a measurement of the extent of cancer in the body, i.e., the tumour size and if it has spread [reviewed in (Wu, 2007)].

Broders grades	Differentiation	Prognosis
1	well differentiated	Good
2	moderately differentiated	both good and bad
3	poorly differentiated	Bad
4	undifferentiated (anaplasia)	Bad

Dukes stages	Localization	Prognosis
A	mucosa	Good
B	extra-rectal tissues	both good and bad
C	lymph nodes metastases	Bad
D	distant metastases	Bad

The SW480 and SW620 cell lines are considered good model of colon cancer progression (Hewitt, 2000). SW620 cells are lymph node metastatic

cells derived from the same patient from which the primary adenocarcinoma cells SW480 were derived one year before (Leibovitz, 1976).

SW480 cell line

Number ATCC®: CCL-228™; organism: *Homo sapiens*, human; tissue: colon; morphology: epithelial; disease: colorectal adenocarcinoma; gender: male; age: 50; ethnicity: Caucasian; Dukes stage: B; Broders grade: 3-4. According to (Leibovitz, 1976).

SW620 cell line

Number ATCC®: CCL-227™; organism: *Homo sapiens*, human; tissue: colon; derived from metastatic site: lymph node; morphology: epithelial; disease: colorectal adenocarcinoma; gender: male; age: 51 years; ethnicity: Caucasian; Dukes stage: C; Broders grade: 4. According to (Leibovitz, 1976).

1.3. Expression vectors

pET28b-CBS

pET28b plasmid containing human CBS cDNA and restriction sites for NdeIand XhoI, yielding an *N*-terminally His-tagged protein. The plasmid

confers kanamycin and chloramphenicol resistance and encodes for the *full-length* wild-type CBS.

pET28b-CBS p.P49L

pET28b plasmid containing human CBS cDNA with 146 C>T transition in the CBS gene exon 1 and restriction sites for NdeI and XhoI, yielding an N-terminally His-tagged protein. The plasmid confers kanamycin and chloramphenicol resistance and encodes for the *full-length* CBS mutant p.P49L.

pET28b- CBS$\Delta_{409\text{-}551}$-p.P49L

pET28b plasmid containing human CBS cDNA with 146 C>T transition in the CBS gene exon 1, restriction sites for NdeI and XhoI and a premature stop codon at position 409, yielding an *N*-terminally His-tagged protein devoid of the C-terminal 143 residues corresponding to the AdoMet binding domain. The plasmid confers kanamycin and chloramphenicol resistance and encodes for the *truncated* CBS$\Delta_{409\text{-}551}$ mutant p.P49L.

pET11a- HFt-MP-PASE

pET11a plasmid containing the HFt-MP-PASE gene, with two glutamate (E) residues at positions 13 and 33 with respect to the previously designed 40-residue long HFt-MP-PAS gene (Falvo, 2016). The expression vector pET-11a containing the HFt-MP-PASE gene confers ampicillin resistance and was assembled by GENEART AG (DE).

2. Methods

2.1. Human cell cultures and treatments

In order to prevent bacteria, fungi, mycoplasma and virus contaminations, standard operating procedures and good laboratory practices were followed.

2.1.1. Human cell cultures

The human colon cancer cell lines SW480 and SW620 were grown in Dulbecco's Modified Eagle Medium (DMEM) containing 4.5 $g \cdot L^{-1}$ glucose, supplemented with 2 mM L-glutamine, 10% (v/v) heat-inactivated fetal bovine serum (FBS), 100 $U \cdot mL^{-1}$ penicillin and 100 $\mu g \cdot mL^{-1}$ streptomycin. Cells were cultured in 25 cm^2 or 75 cm^2 flasks at 20% O_2 (v/v), 37°C, 5% CO_2 (v/v) and were subcultured every two/three days at approximately 70-80% confluence.

2.1.2. Hypoxic treatment

At a confluence of 50-60%, cells were incubated in the *Galaxy 14 S* (Eppendorf) incubator at 1% O_2 (v/v), 37°C, 5% CO_2 (v/v) for 24 h. After incubation, the cells had reached approximately 70-80% confluence. After trypsinization, the cells were washed in the culture medium, counted using

the trypan blue dye exclusion test, centrifuged at 1.000 g for 5 min and resuspended in fresh medium at a final density of 8 x 10^6 cells·mL^{-1}.

2.1.3. Trypan blue dye exclusion test

Trypan blue is a commonly used assay to stain dead cells. A 1:1 (v/v) mixture of cell suspension and 0.4% trypan blue dye was placed into a 1.5 mL-eppendorf tube, mixed gently and left at room temperature for 5 min. Cells were then counted using a counting chamber (hemocytometer). Viable cells do not incorporate the dye, whereas nonviable cells can be easily identified from their distinctive blue colour. Trypan blue-positive cells were always less than 5%.

2.1.4. Mycoplasma detection test using RT-PCR

Possible contamination of cell cultures by mycoplasma was periodically tested by real time-polymerase chain reaction (RT-PCR) assays.

Primers	***Sequences***
Myc F	5’ TCCAGGWCAYGCTGACTA 3’
Myc R	5’ ATTTTWGGAACKCCWACTTG 3’

Under sterile conditions and using RNase-free materials, SW480 and SW620 cells (70-80% confluence) were harvested by trypsinization and centrifugation (1.000 g for 5 min at 20 °C). The cell pellet was then washed twice with PBS, centrifuged (1.000 g for 5 min at 20 °C) and the supernatant discarded. The pellet was used to carry out RNA extraction and purification using NucleoSpin RNA buffer set, according to the manufacturer's instructions. The purity of extracted RNA was assessed using a *Cary 60 UV-VIS* spectrophotometer (Agilent) by measuring the 260/280 nm absorbance ratio (A_{260}/A_{280}). RNA was considered pure when the A_{260}/A_{280} ratio was 1.9 - 2.1 in 10 mM Tris-HCl (pH 7.5). Absorption at 235 nm, if detected, indicated the presence of contaminants. Possible contamination by phenol or urea would result in absorption bands at 230 nm or 270 nm, respectively. Protein contamination would result in a high absorption at 280 nm and thus lower A_{260}/A_{280} ratio. The total RNA was used as a template for the cDNA synthesis. Reverse transcription was performed using 1-2 µg RNA and the Maxima First Strand cDNA synthesis kit, using a RT-PCR machine (Mx3000P, Agilent). The samples were incubated at 25°C for 10 min, and then 15 min at 50°C. The reaction was terminated by incubating the samples at 85°C for 5 min. The resulting cDNA was stored at -20°C. For quantitative RT-PCR assays, SYBR Green qPCR master mix 2X has been used. SYBR green is an intercalating-dye which is able to bind double-stranded DNA and

upon excitation emit light (excitation at 470 nm; emission at 510 nm). Thus, fluorescence increases as a PCR product accumulates. The cDNAs were amplified using initial denaturation step (95 °C for 10 min) and then 45 cycles of amplification step (95 °C for 10 sec, 60 °C for 30 sec and 72°C for 30 s).

Reaction Mixture

Reagent	**Starting conc**	**Volume**	**Final conc**
qPCR Master Mix	2X	12.5 µl	1X
F Primer	3 µM	3 µl	0.3 µM
R Primer	3 µM	3 µl	0.3 µM
cDNA	-	-	~ 500 ng
Water	-	up to 25 µl	-

2.1.5. Protein extraction

Cells were harvested by trypsinization and centrifugation (1.000 g for 5 min at 20 °C), washed with PBS and then lysed using the CelLytic^{TM}MT cell lysis reagent in the presence of the 100X protease inhibitor cocktail. After 15-min incubation at 4°C, the cells were centrifuged at 20.000 g for 10 min and the resulting supernatant was stored at -80°C. Cell lysates were then

assayed for their citrate synthase activity (see *2.6*) and by Western blotting (*2.5.3.*).

2.2. Cell proliferation assays

The thiazolyl blue tetrazolium bromide (MTT) and the 2,3-bis-(2-methoxy-4-nitro-5-sulfophenyl)-2H-tetrazolium-5-carboxanilide (XTT) assays are commonly used methods to assess cell viability and proliferation. MTT is a water-soluble yellow tetrazolium salt which is reduced by mitochondrial dehydrogenase enzymes leading to formation of a purple formazan dye. XTT is a yellow tetrazolium salt which forms, instead, an orange formazan dye. These conversions occur only in metabolically active and viable cells and can be detected spectrophotometrically. A linear relationship exists between the signal produced and the number of viable cells; therefore, both MTT and XTT are widely accepted assays to measure cell proliferation and, in this thesis work, they were performed on SW480 and SW620 cell lines. Briefly, 200 µL of cell suspension with a density of 25 cells μL^{-1} (yielding 5.000 cells) were seeded in wells of a 96-well plate. After 24 h-incubation at 37°C and 5% CO_2, the medium was replaced with fresh medium and the cells were incubated with increasing concentrations (from 0.0001 to 10 µM, logarithmic scale) of free mitoxantrone and HFt-MP-PASE-MIT. After 72 hour-incubation at 37°C and 5% CO_2, the medium was

supplemented with 20 µL MTT (0.33 ng mL^{-1} final) or was replaced with fresh medium w/o phenol red supplemented with XTT. Finally, after a variable time ranging from 1 to 3 hours of incubation at 37°C and 5% CO_2, 100 µl of DMSO were added in order to dissolve the coloured formazan crystals produced by reduction of the tetrazolium salts. The cell viability tested with the XTT assay was measured at 450 nm in a microplate reader (VERSAmax, Molecular Devices, Sunnyvale, CA, USA) or at 570 nm (after subtracting the absorbance at 690 nm) when viability was assessed by MTT using an *Appliskan* plate-reader. The percentage of cell viability was estimated by comparing cells treated with free MIT or HFt-MP-PASE-MIT to mock treated cells. To compare the killing efficacy, we evaluated the IC_{50}, *i.e.*, the compound concentration yielding 50% cell viability.

2.3. Bacterial cell cultures

In order to prevent bacteria, fungi, mycoplasma and virus contaminations, standard operating procedures and good laboratory practices were followed.

2.3.1. Generation of competent cells

Competent cells were obtained as follows. 1 mL of BL21-Gold (DE3) cells was grown overnight at 37°C in 100 mL Luria Bertani broth (LB). The cells were then incubated at 37°C under shaking for 1.5-3 h until the optical

density at 600 nm (OD_{600}) reached 0.4-0.6. Cells were then incubated for 30 min on ice and centrifuged at 4.000 g for 20 min at 4°C. The supernatant was discarded, the pellet gently resuspended in 10 mL of a cold solution of 0.1 M $CaCl_2$ and then incubated on ice for 2 hours. Finally, the cells were centrifuged at 4.000 g for 20 min at 4°C, the supernatant discarded and the pellet was resuspended in 20% glycerol and frozen at -80°C in 100 µL aliquots.

2.3.2. Transformation of competent cells

Competent cells were transformed as it follows. 1 µL of the plasmid of interest (see *1.3*) was gently added to 100 µL of competent BL21-Gold (DE3) cells and the mix was incubated on ice for 30 min before undergoing the thermic shock at 42°C for 1 min, followed by 2-min incubation on ice. Afterwards, 900 µL of sterile LB broth were added and the cells were incubated at 37°C for 1 h (200 rpm). Finally, 200-300 µL of transformed cells were plated on LB-agar plates containing the appropriate antibiotics, and incubated at 37°C overnight.

2.4. Recombinant proteins expression and purification

Recombinant human proteins *full-length* CBS wild-type, *full-length* CBS mutant p.P49L, *truncated* $CBS\Delta_{409-551}$ mutant p.P49L, modified ferritin

(HFt-MP-PASE) have been expressed in *Escherichia coli* and purified. The vectors used to transform *Escherichia coli* BL21(DE3) competent cells were reported in *1.3*.

2.4.1. Expression and purification of full-length CBS wild-type and p.P49L mutant

According to (Vicente, 2014) , transformed cells were grown at 37°C in LB broth containing 25 mg L^{-1} kanamycin and 34 mg L^{-1} chloramphenicol until A_{600nm} reached 0.4–0.5. Gene overexpression was induced by the addition of 0.5 mM isopropyl-1-thio-ß-D-galactopyranoside (IPTG), whereas heme biosynthesis was stimulated by the addition of δ-aminolevulinic acid (final concentration of 75 mg L^{-1}) to the culture medium. After incubation at 120 rpm and 22 °C for 4 h, cells were harvested by centrifugation and the pellet was resuspended in the buffer A containing 50 mM potassium phosphate buffer (KPi), 300 mM KCl, 10% glycerol pH 7.0, supplemented with 1 mg mL^{-1} lysozyme, 1 mM phenylmethylsulfonyl fluoride (PMSF), and a few grains of DNase I (10 ml per litre of culture). The resuspended cells were incubated on ice for 30 min and then disrupted by sonication. After centrifugation at 8.200 g for 5 min at 4°C, 10 mM imidazole was added to the cleared supernatant. Purification of the His-tagged protein was performed by affinity chromatography using a 1-mL HisTrap FF crude column (GE

Healthcare). Chromatography was carried out in an ÅKTA Prime fast performance liquid chromatography system (GE Healthcare). The column was washed with 15 volumes of buffer B (Buffer A containing 10 mM imidazole with or without 20 µM pyridoxal-5'-phospate [PLP]) at a rate of 1 mL min^{-1}, and the protein was then eluted in 20 volumes of a linear imidazole gradient up to a final concentration of 500 mM. The imidazole was then removed using a PD10 desalting column (GE Health- care) and the purified protein was concentrated in a Vivaspin 15R 30-kDa tube (Sartorius). Purity of the isolated proteins was assessed by SDS-PAGE and their concentration was determined by the Bradford method (see *Quantification and biochemical detection of proteins*), whereas the heme concentration in the isolated oxidized proteins was determined using ε_{428nm} = 92.700 M^{-1} cm^{-1} (Carballal, 2008).

2.4.2. Expression and purification of truncated CBS$\Delta_{409-551}$ mutant p.P49L

According to (Vicente, 2016), transformed cells were grown at 37°C in LB broth containing 25 mg L^{-1} kanamycin and 34 mg L^{-1} chloramphenicol until A_{600nm} reached 0.4–0.5. Protein overexpression was induced by the addition of 0.5 mM isopropyl-1-thio-ß-D-galactopyranoside (IPTG), whereas heme biosynthesis was stimulated by the addition of δ-aminolevulinic acid to the culture medium to a final concentration of 35 mg L^{-1}. After incubation for

16 h at 120 rpm and 22 °C, cells were harvested by centrifugation and the pellet was resuspended in buffer A which contained 50 mM potassium phosphate buffer (KPi), 300 mM KCl, 10% glycerol (pH 7.0), supplemented with 1 mg mL^{-1} lysozyme (AppliChem), 1 mM phenylmethylsulfonyl fluoride (PMFS), and a few grains of DNase I (10 ml per litre of culture). Following a 30-min incubation on ice, cells were lysed by sonication and centrifuged at 8.200 g for 10 min at 4°C. The cleared supernatant was supplemented with 10 mM imidazole and loaded at 2.5 mL min^{-1} onto a 5-ml HisTrap FF crude column (GE Healthcare) previously equilibrated with 15 volumes of buffer B (Buffer A containing 10 mM imidazole) at a rate of 5 mL min^{-1}. Protein purification was carried out in an ÅKTA Prime fast performance liquid chromatography system (GE Healthcare) and the protein was eluted in 20 volumes of a linear imidazole gradient up to a final concentration of 500 mM. The pooled fractions were concentrated with an Amicon Ultra-15 centrifugal filter unit with an Ultracel-30 membrane (Millipore), and the protein was further purified by size exclusion chromatography, using a HiLoad 26/600 Superdex S200 column (GE Healthcare) previously equilibrated with buffer A as such or supplemented with 20 µM pyridoxal-5'-phospate (PLP) (buffer C). The protein was loaded onto the column and eluted with buffer A or buffer C at a rate of 0.5 ml/min. Purity of the isolated proteins was assessed by SDS-PAGE and their

concentration was determined by the Bradford method (see *Quantification and biochemical detection of proteins*), whereas the heme concentration in the isolated oxidized proteins was determined using ε_{428nm} = 92.700 M^{-1} cm^{-1} (Carballal, 2008).

2.4.3. Expression and purification of the PASE-derivative of human ferritin (HFt-PASE)

According to (Falvo, 2016), cells harboring the designed plasmid were grown at 37°C in 1 L ampicillin-containing Terrific Broth (TB) until OD_{600} reached 0.6. Gene overexpression was induced by addition of 0.5 mM isopropyl-1-thio-ß-D-galactopyranoside (IPTG) and cells were further grown overnight at 22°C. Cells were then harvested by centrifugation (6.000 rpm for 20 min), resuspended in 50 mM Tris-HCl (pH 7.5), 0.5 mM dithiothreitol (DTT), 1 mM ethylenediamine tetra-acetic acid (EDTA), and 300 mM NaCl and then disrupted by sonication in the presence of 1 mM phenylmethylsulfonyl fluoride (PMFS). The lysate was centrifuged at 16.000 rpm for 45 min and the supernatant containing the soluble fraction was incubated at 37 °C for 40 min with 0.1 mg mL^{-1} DNase supplemented with 10 mM $MgCl_2$, heated to 55 °C for 8 min and finally centrifuged to remove denatured proteins. The recovered supernatant was heated to 72 °C for 8 min, and then centrifuged to remove denatured proteins. The recovered

supernatant was precipitated using an ammonium sulphate cut at 75% saturation (w/v). The pellet was resuspended and dialyzed overnight against phosphate saline buffer (PBS) pH 7.5 and then loaded on a strong anion exchange HiTrap Q HP column (Q Sepharose High Performance GE Healthcare, Boston, USA), previously equilibrated with the same buffer. In these conditions, HFt samples eluted from the column, whereas other *E. coli* proteins and DNA contaminants did not. The recovered HFt samples were ultracentrifuged at 35.000 rpm for 55 min at 6°C using a Beckman L8-70M ultracentrifuge (Beckman Coultier). The recovered supernatant was then precipitated using ammonium sulphate at 65% saturation (w/v). The pellet was resuspended and dialyzed overnight against PBS pH 7.5, pooled, concentrated using concentration tubes with cut-off 30 KDa Amicon Ultra-15 centrifugal filter devices (Millipore, Billerica, MA, USA), sterile filtered, and finally stored at 4 °C. Typical yields were 100 mg of pure proteins per 1 L culture. The purity of all the preparations was assessed using SDS-PAGE electrophoresis and Coomassie brilliant blue staining (see *Quantification and biochemical detection of proteins*). Protein concentration was determined spectrophotometrically at 280 nm, using a molar extinction coefficient (on a 24-mer basis) of 4.56×10^5 M^{-1} cm^{-1} (ProtParam sofware, www.expasy.org).

2.4.3.1. Encapsulation of mitoxantrone in the HFt-based nanocarriers

The chemotherapeutic agent mitoxantrone (MIT) was encapsulated using the previously reported HFt disassembly/reassembly method used for doxorubicin (DOXO) (Falvo 2016). Briefly, solutions of HFt-MP-PASE (see *2.3*) in 0.1 M NaCl were incubated for 10 min at pH 2.0 (pH adjusted with HCl). Then, MIT was added to the solution at a 250:1 molar ratio with respect to the protein. The pH was initially maintained at 2.5 for 5 min and then increased to 7.5 using NaOH. The resulting solution was stirred at room temperature for 30 min, filtered and dialyzed overnight *vs* phosphate buffer saline (PBS) at pH 7.4 to remove unbound MIT. After dialysis, solutions were centrifuged at 15.000 rpm for 30 min at 4°C. The supernatant was collected, concentrated with 30 kDa Amicon Ultra-15 centrifugal devices, sterile filtered and stored at 4°C in the dark. HFt and MIT content of the samples was determined by the Lowry method and UV-VIS absorption spectroscopy, respectively, after extracting MIT in 1 N HCl, 95% ethanol. MIT was quantified by using the calculated molar extinction coefficient ε_{610} =19.200 M^{-1} cm^{-1}.

2.5. Preparation of gasotransmitters stock solutions

2.5.1. Sulfide solution

Stock solutions of Na_2S were prepared by quickly washing with degassed Milli-Q water the surface of a Na_2S crystal, and then dissolving it in degassed Milli-Q water under a N_2 atmosphere. The concentration of Na_2S in solution was measured spectrophotometrically using 5,5'-dithiobis-(2-nitrobenzoic acid) (DTNB) according to (Nashef, 1977) in a Cary 60 UV-VIS spectrophotometer. DTNB is widely used for thiol quantitation using the extinction coefficient ε_{412}=13.600 M^{-1} cm^{-1}. The reaction between DTNB and H_2S generates two molecules of the yellow compound 5-thio-2-nitrobenzoate anion (NTB^-) and this stoichiometry was taken into account for the calculation of the H_2S concentration. Briefly, 100 µL of 5 mM DTNB solubilised in 100 mM HEPES, pH 7.1, was added to 850 µl of ultrapure water in a 1mL-quarz cuvette. After blank determination, three consecutive kinetic runs were collected, each following the addition of 3 µL of the Na_2S solution. The observed absorption change values (ΔA) were used to determine the concentration of the Na_2S solution using ε_{412} = 13.600 M^{-1} cm^{-1} and dividing the resulting value by 2 (Nashef, 1977). The Na_2S working solutions was prepared diluting a ~1 M freshly prepared stock solution with

degassed ultrapure water in a syringe and were stored on ice and protected from light before the use.

2.5.2. Carbon monoxide solution

Carbon monoxide (CO) stock solutions were prepared by thoroughly equilibrating degassed buffer (50 mM KPi, 300 mM KCl 10% glycerol, 100 µM EDTA, pH 7.0) with the pure gas at 1 atm, yielding 1mM CO at 20°C.

2.5.3. Nitric oxide solution

Nitric oxide (NO) solution was prepared by equilibrating degassed ultra-pure water with NO· gas at 1 atm and 20°C using a tonometer. In these conditions, the solubility of NO· is 2 mM. The concentration of NO· in solution was determined by titrating CcOX. The reduced enzyme indeed binds NO· according to a 1:1 stoichiometry leading to a characteristic absorption spectrum. Finally, NO· solution was kept on ice and protected from light before the use.

2.6. Protein quantification and immunodetection

2.6.1. Bicinchoninic acid (BCA) and Bradford assays

Total protein content in the extracts derived from the cultivated SW480 cells (see *2.1.4*) and the concentration of the purified recombinant proteins (see *2.3*) were obtained by bicinchoninic acid (BCA) and Bradford assays, respectively. BCA assays were carried out using the BCA Kit. A standard curve was obtained using a series of dilutions of bovine serum albumin (BSA) (0, 0.3, 0.6, 0.9, 1.2, 1.5, 1.8, 2 μg μL^{-1}). Then, 5 μL of sample and standard protein were diluted in 200 μL of BCA working solution (obtained mixing solutions A and B in a 50:1 ratio) in a 96-well plate. After incubating the plate at 37°C for 30 min, the absorbance at 562 nm was measured using a plate-reader (Appliskan Multimode). Protein concentration in the sample was calculated with reference to the BSA standard curve. To perform the Bradford method the Protein Assay Solution was used. A series of dilution of the BSA stock solution were made in order to obtain a standard curve (0, 2, 6, 8, 10 μg μL^{-1}). Then, 5 μL of sample and standard were diluted in 200 μL of the Bradford solution in a 96-well plate. After incubating the plate at 25°C for 5 min, the absorbance at 595 nm was measured using a plate-reader (Appliskan Multimode). The protein concentration of the sample was calculated with reference to the BSA standard curve.

2.6.2. SDS-electrophoresis

Purified proteins (see *2.3*) were analyzed by SDS polyacrylamide gel electrophoresis (SDS-PAGE). We used precast Bis-Tris NuPage gels at 10% or 4-12% acrylamide. The running buffer was the 20X MOPS SDS running buffer and the sample were loaded using the 4X NuPage LDS sample buffer. The electrophoretic run was performed at 100-120 V. The proteins were stained using Coomassie brilliant blue.

2.6.3. Western blot analysis

For Western blotting assays, SW480 cells were lysed as described previous (see *2.1.1*, *2.1.2* and *2.1.4*). After total protein content determination by BCA assay, proteins (20 µg) were mixed with 4X *Laemmli* protein sample buffer and separated on 10% SDS-PAGE using Mini-PROTEAN TGX stain-free precast gels and the running buffer 10X Tris/glycine/SDS. The formulation of these gels includes trihalo compounds which lead to UV fluorescence emission on reaction with proteins (Rivero-Gutiérrez, 2014; Short & Posch, 2011), allowing to estimate and normalize the total loaded protein, using a ChemiDoc MP imaging system (Bio-Rad) without resorting to any staining procedure. Proteins were then transferred onto a polyvinylidene difluoride (PVDF) or a nitrocellulose membrane. The

membranes were blocked by PBS containing 0.1% (v/v) Tween 20 and 3% of BSA for 1 h at room temperature and then incubated overnight at 4°C with rabbit polyclonal antibody against human SQR (1:150), followed by incubation with horseradish peroxidase-conjugated secondary antibody. Afterwards, membranes were washed and developed using Clarity Western ECL substrate. Finally, the intensity of the target protein band was normalized to total protein content assessed as described above.

2.7. Citrate synthase activity determination

SW480 cell lysates obtained as described in *2.1.1*, *2.1.2* and *2.1.4* were assayed for their citrate synthase activity (Srere, 1969). Citrate synthase is an enzyme of the mitochondrial matrix, commonly used as a quantitative marker of mitochondrial mass. This is an enzyme of the Krebs cycle which catalyses the reaction between acetyl coenzyme A (acetyl CoA) and oxaloacetic acid (OAA) to form citric acid. The hydrolysis of the thioester of acetyl CoA results in the formation of CoA with a thiol group (CoA-SH). The thiol reacts with the 5,5'-dithiobis-2-nitrobenzoic acid (DTNB) to form the yellow product 5-thio-2-nitrobenzoic acid (TNB). TNB formation was assessed spectrophotometrically using a *Cary 60 UV-VIS* spectophotometer and ε_{412}=13.600 M^{-1} cm^{-1}. The assay was performed at 30°C under stirring using a 1mL-cuvette and the following reaction mixture:

Reagent	Starting conc	Volume	Final conc
Buffer Tris-HCl	100 mM	910 µl	100 mM
Acetyl-CoA	30 mM	10 µl	0.3 mM
DTNB	10 mM	10 µl	0.1 mM
OAA	10 mM	50 µl	0.1 mM
Lysates		20 µl	

Finally, the activity was normalized to million cells.

2.8. H_2S consumption measurements

2.8.1. Respirometric method

O_2 consumption measurements were carried out at 37°C under stirring by high resolution respirometry using an Oxygraph-2k (OROBOROS Instruments, Innsbruck, Austria). The instrument allows to measure the O_2 concentration (µM) and the O_2 consumption rate (OCR) (nM s^{-1}) in real time through an O_2 Clark-type electrode. The probe of this electrode is a platinum wire coated with Ag/AgCl. The gas selectivity is achieved by a gas-permeable membrane isolating the probe from the other redox-active non-gaseous molecules and by setting the applied polarization voltage to 0.67 V,

specific for O_2 reduction to H_2O ($1/2\ O_2 + 2\ e^- + 2\ H^+ \rightarrow H_2O$). The oxygen electrode was calibrated by recording the signal in air-equilibrated buffer (corresponding to $[O_2]$ in the range 200-300 μM, calculated from the solubility of the gas in the experimental conditions used) and subtracting the signal measured on addition of sodium dithionite ($[O_2] = 0$). The instrument is equipped with two 1.5 mL-chambers and a titration-injection microPump (Tip-2k) used to perform controlled sulfide injections directly into the measuring chambers.

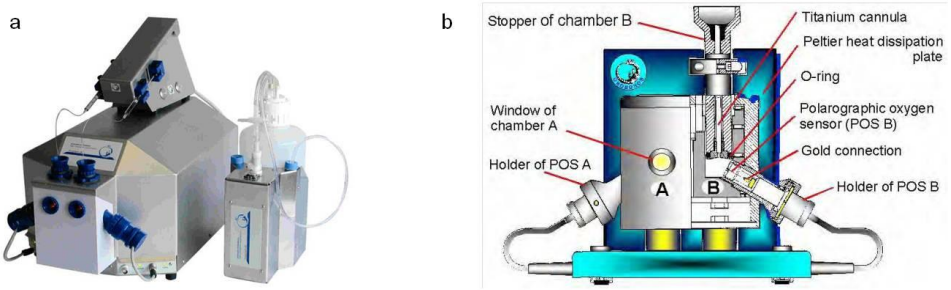

Figure 1. a) The OROBOROS Oxygraph 2k with the titration-injection microPump (Tip-2k) on top. b) Inside view of the instrument. Image from Oroboros Oxygraph 2k Instruction Manual.

To carry out respirometric assays, SW480 cells were harvested as described in *2.1* and *2.2*. After equilibration and calibration of the instrument with complete cell medium, 4×10^6 cells were added into each chamber at a final density of 2.6×10^6 cells mL^{-1}. Basal respiration was monitored for ~ 10

min and then 10 µM rotenone was added. In a set of control experiments, performed to determine the sulfide autoxidation and sulfide-induced extra-mitochondrial O_2 consumption to be subtracted, both 10 µM rotenone and 5 µM antimycin A were added to the chamber. After stabilization of O_2 consumption in the presence of rotenone (or rotenone and antimycin A), a solution of sulfide (3-5 mM) was injected at increasing rate (10 nL s^{-1}, 20 nL s^{-1}, 40 nL s^{-1}, 80 nL s^{-1} and 160 nL s^{-1}). Each sulfide injection lasted 180 s and was restarted only after restoration of the O_2 consumption rate measured in the absence of sulfide.

According to (Abou-Hamdan, 2015), the mitochondrial sulfide-oxidizing activity in a cell suspension can be evaluated from the stimulatory effect produced on cell respiration by sulfide injection. The protocol provides:

- Addition of rotenone (a specific inhibitor of complex I) to prevent complex I from working in a reverse mode, as reported for colon cancer cells;
- Addition of rotenone and antimycin A (a specific inhibitor of complex III) to block mitochondrial sulfide oxidation.
- Injections of Na_2S at increasing flow rates in order to stimulate mitochondrial respiration. The injections were repeated at increasing injection rate until inhibition of complex IV occurred.

The maximal sulfide-oxidizing activity was calculated from the maximal oxygen consumption stimulation by Na_2S (occurring at the highest injection rate non inhibitory for CcOX) taking into account the H_2S/O_2 stoichiometric coefficient (1.33) reported in (Lagoutte, 2010). Finally, data were normalized to millions of cells and citrate synthase activity.

2.9. H_2S synthesis measurements

2.9.1. Amperometric methods

In order to detect the H_2S production, the amperometric assays were performed using an ISO-H2S-2 hydrogen sulfide-selective sensor coupled to an Apollo4000 Free Radical Analyzer (World Precision Instruments).

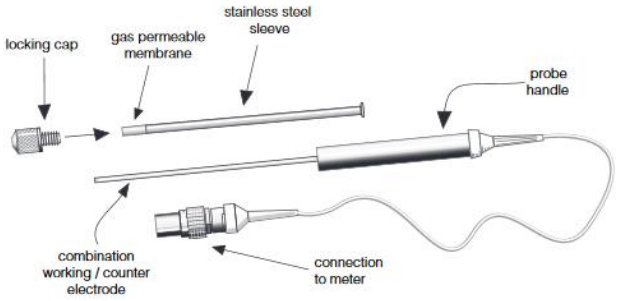

Figura 2. ISO-H2S-2 sulfide selective electrode. Image from ISO-H2S-2 Instruction Manual.

Hydrogen sulfide (H_2S) diffuses through a selective membrane covering the sensor and is oxidized, resulting in an increase in electrical current. The changes in electrical current, expressed in pA, are proportional to the concentration of hydrogen sulfide in the sample. ISO-H2S-2, therefore, has been used for measuring H_2S concentrations in samples. It is important, to keep the pH constant during the measurements and acquire calibration curves under similar conditions. Briefly, according to (Vicente, 2017), H_2S production by recombinant human CBS variants was measured at 37°C in the presence of 50 mM potassium phosphate buffer (KPi), 300 mM KCl, 10% glycerol and 100 µM EDTA (pH 7.0). Purified CBS (0.5–1 µM) was incubated for 10 minutes with 50 µM PLP, 260 U mL^{-1} catalase and 0.4–2.0 mM homocysteine in the absence or presence of 0.5 mM AdoMet, after which 10 mM cysteine was added to trigger the reaction. After monitoring H_2S production for 3 minutes, the electrode was internally calibrated by adding 4 µM NaHS (corresponding to 2µM H_2S at pH 7.0). Finally, 50 µM *o*-acetylserine and 200 nM *Entamoeba histolytica* o-acetylserine sulfhydrylase were added to the reaction mixture to remove H_2S from solution and bring the signal back to baseline

2.9.2. Lead acetate assay

H_2S activity assays by the lead acetate method were carried out in a thermostated cuvette under stirring, according to (Chiku, 2009). H_2S production by the recombinant human CBS p.P49L variant was measured at 37°C in a reaction buffer containing 50 mM potassium phosphate buffer (KPi), 300 mM KCl, 10% glycerol and 100 µM EDTA (pH 7.0). Purified CBS (0.5–1µM) was incubated for 10 minutes with 50 µM PLP, 260 U mL^{-1} catalase, and 0.4–2.0 mM homocysteine in the absence or presence of 0.5 mM AdoMet. Afterwards, 10mM cysteine was added to trigger the reaction. Lead acetate (400 µM) was added to the reaction mix prior to cysteine addition. The reaction of H_2S with lead acetate generates a brown precipitate of lead sulfide, detected as an absorption increase at 390 nm using an *Agilent Cary-60 UV-VIS* spectrophotometer. The molar extinction coefficient for lead sulfide under these conditions was determined to be 5.500 M^{-1} cm^{-1}. NaHS was used as standard.

2.10. Equilibrium titrations

UV-visible absorption spectra of oxidized and reduced p.P49L and WT CBS (see *2.3*) were recorded in a *Cary-60 UV-VIS* spectrophotometer (Agilent). Anaerobic titrations of reduced CBS p.P49L with CO were performed at 20°C in the same spectrophotometer. Gas exchange was

prevented either by filling the quartz cuvette and sealing it with a rubber-cap or by adding mineral oil on top of the aqueous medium. Anaerobic conditions were ensured by nitrogen flushing and addition of glucose oxidase (4 U mL^{-1}), catalase (13 µg mL^{-1}), superoxide dismutase (12 U mL^{-1}), and glucose (3 mM) to scavenge contaminant oxygen, hydrogen peroxide, and superoxide anion in the reaction buffer (50 mM potassium phosphate buffer (KPi), 300 mM KCl, 10% glycerol, 100 µM EDTA, pH 7.0, with or without PLP (see *2.3*). p.P49L and WT CBS (1.4–1.6 µM in heme, as determined using ε_{428nm} = 92.700 M^{-1} cm^{-1} (Carballal, 2008) were reduced with 90 µM sodium dithionite, diluted from a 45 mM stock solution (quantitated using ε_{314nm}= 8.043 $M^{-1}\cdot cm^{-1}$ (Dixon, 1971). CO stock solutions were prepared as reported in *2.4*. After each CO addition with a gas-tight Hamilton syringe, the spectral changes were visually inspected in real time and a new addition was immediately made when no more changes were observed. According to (Puranik et al., 2009), two apparent K_d ($K_{d,1}$ and$K_{d,2}$) were used to satisfactorily fit the CO affinity data. The $K_{d,1}$ and $K_{d,2}$ values were obtained by fitting the data to:

$$PL = \frac{\alpha_1\left[(P_T + L_T + K_{d1}) - \sqrt{(P_T + L_T + K_{d1})^2 - 4P_T L_T}\right] + \alpha_2\left[(P_T + L_T + K_{d2}) - \sqrt{(P_T + L_T + K_{d2})^2 - 4P_T L_T}\right]}{2}$$

Where P_L is the concentration of CO-bound CBS p.P49L, P_T and P_L are, respectively, the total CBS p.P49L and CO concentrations, and $K_{d,1}$ and $K_{d,2}$ are, respectively, the protein fractions binding CO at higher ($K_{d,1}$) and lower ($K_{d,2}$) affinity.

2.11. Stopped-flow absorption spectroscopy measurements

Time-resolved absorption spectroscopy experiments were carried out in a thermostated stopped-flow instrument (DX.17MV, Applied Photophysics), equipped with a photodiode-array (light path = 1 cm). To avoid light-induced artifacts, the intensity of the white-light incident beam was decreased and a filter cutting UV light at $\lambda < 360$ nm was employed. Absorption spectra were recorded with an acquisition time of 10 ms per spectrum according to a logarithmic time scale.

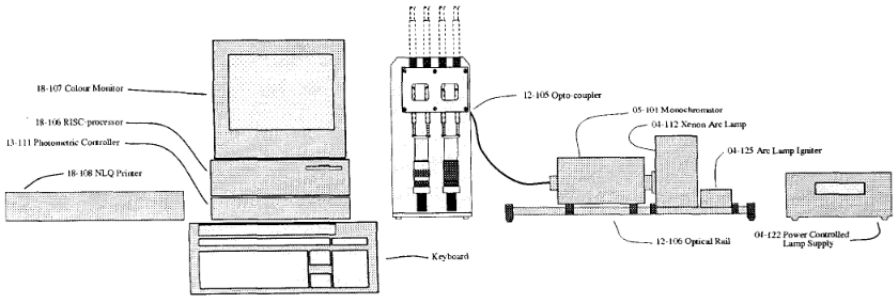

Figure 3. Schematic representation of a stopped-flow instrument. In this apparatus, two solutions (A and B) can be mixed in equal volume or, prior to data recording, A and B can

pre-mixed and, after a pre-set delay time, further mixed with an equal volume of a third solution (C). Image from DX.17MV Stopped Flow Instruction Manual.

All reactions were carried out at 25°C in the reaction buffer containing 50 mM potassium phosphate buffer (KPi), 300 mM KCl, 10% glycerol, 100 µM EDTA (pH 7.0), in the presence or absence of PLP (see *2.3*). CBS p.P49L was thoroughly flushed with nitrogen, and then glucose oxidase (4 U mL^{-1}), catalase (13 µg mL^{-1}), superoxide dismutase (12 U mL^{-1}), and glucose (3 mM) were added to scavenge oxygen, hydrogen peroxide and superoxide anion. The protein was then placed on ice, protected from light to prevent possible damaging photoreactions. When indicated, CBS p.P49L was incubated with AdoMet for ≥ 10minutes, prior to reduction with 90 µM sodium dithionite. CO association kinetics were studied by mixing in the stopped-flow apparatus reduced CBS p.P49L, in the absence or presence of AdoMet, with CO solutions and the spectra were recorded over time. CO dissociation kinetics were evaluated by mixing the Fe(II)-CO adduct of CBS p.P49L with NO· stock solutions (see *2.4*).

2.12. Data Analysis

CO affinity titrations and CO binding and dissociation kinetic data were analyzed with the software MATLAB (Mathworks). Global fit analysis

of spectral data was performed by singular value decomposition analysis combined with curve fitting. Oxygen consumption rate (OCR) was acquired using DatLab software (Oroboros Instruments). Densitometric analysis of blotted membranes and of total protein load on gel was carried out with Image Lab software (Bio-Rad). IC_{50} values were calculated using OriginLab software (OriginLab Corporation).

ABBREVIATIONS

CoA: coenzyme A

AdoMet: S-adenosyl-L-methionine

AOAA: aminooxyacetic acid

ATP: adenosine triphosphate

BCA: bicinchoninic acid

BSA: bovine serum albumin

CBS: cystathionine β-synthase

CoQ: coenzyme Q

CRC: colorectal cancer

CSE: cystathionine γ-lyase

DAO: D-amino acid oxidase

DOXO: doxorubicin

DTNB: 5,5'-dithiobis-(2-nitrobenzoic acid)

EDTA: ethylenediamine tetra-acetic acid

ETC: electron transport chain

ETHE1: persulfide dioxygenase or ethylmalonic encephalopathy 1

Ft: ferritin

GHS: glutathione

*h*CBS: human cystathionine β-synthase

HFt: heavy chains ferritin

HIF: hypoxia-inducible factor

IPTG: isopropyl-1-thio-ß-D-galactopyranoside

KPi: potassium phosphate buffer

LB: Luria Bertani broth

LFt: light chains ferritin

MIT: mitoxantrone

MMP: metalloproteinase

MST: 3-mercaptopyruvate sulfurtransferase

MTT: thiazolyl blue tetrazolium bromide

NAD: nicotinamide adenine dinucleotide

NP: nanoparticle

OAA: oxaloacetic acid

PBS: phosphate buffered saline

PLP: pyridoxal 5'-phosphate

PMSF: phenylmethylsulfonyl fluoride

SAM: S-adenosyl-*L*-methionine

SOU: sulfide oxidizing unit

SQR: sulfide:quinone oxidoreductase

TfR1: transferrin receptor 1

TNB: 5-thio-2-nitrobenzoic acid

XTT: 2,3 – bis - (2-methoxy-4-nitro-5-sulfophenyl) - 2H – tetrazolium – 5 - carboxanilide

REFERENCES

References

Abou-Hamdan A, Guedouari-Bounihi H, Lenoir V, Andriamihaja M, Blachier F, Bouillaud F, (2015). "Oxidation of H_2S in mammalian cells and mitochondria", Methods in Enzymology, *554*, 201–228.

Abou-Hamdan AR, Roger CT, Guedouari-Bounihi H, Galardon E, Bouillaud, F, (2016). "Positive feedback during sulfide oxidation fine-tunes cellular affinity for oxygen", Biochim Biophys Acta., 1857,1464-1472.

Asimakopoulou A, Panopoulos P, Chasapis CT, Coletta C, Zhou Z, Cirino G, Giannis A, Szabo C, Spyroulias GA, Papapetropoulos A, (2013). "Selectivity of commonly used pharmacological inhibitors for cystathionine β-synthase (CBS) and cystathionine β-lyase (CSE)", British Journal of Pharmacology, *169*, 922–932.

Banerjee R, Evande R, Kabil O, Ojha S, Taoka S, (2003). "Reaction mechanism and regulation of cystathionine beta-synthase", Biochim Biophys Acta., 1647:30-5.

Bateman A, (1997) The structure of a domain common to archaebacteria and the homocystinuria disease protein. Trends Biochem Sci., 22:12–13.

Beaumont M, Andriamihaja M, Lan A, Khodorova N, Audebert M, Blouin JM, Grauso M, Lancha L, Benetti PH, Benamouzig R, Tomé D, Bouillaud F, Davila AM, Blachier F, (2016). "Detrimental effects for colonocytes of an increased exposure to luminal hydrogen sulfide: the adaptive response", Free Radical Biology and Medicine, 93:155-164.

Bellini M, Mazzucchelli S, Galbiati E, Sommaruga S, Fiandra L, Truffi M, Rizzuto MA, Colombo M, Tortora P, Corsi F, Prosperi D, (2014). "Protein nanocages for self-triggered nuclear delivery of DNA-targeted chemotherapeutics in Cancer Cells", J Control Release, 196:184-96.

Binkley F & Du Vigneaud V, (1942). "The formation of cysteine from homocysteine and serine by liver tissue of rats", J Biol Chem, 144:507-511.

Blachier F, Davila AM, Mimoun S, Benetti PH, Atanasiu C, Andriamihaja M, Benamouzig R, Bouillaud F, Tomé, D, (2010). "Luminal sulfide and large intestine mucosa: Friend or foe?", Amino Acids, *39*:335–347.

Blazkova I, Nguyen HV, Dostalova S, Kopel P, Stanisavljevic M, Vaculovicova M, Stiborova M, Eckschlager T, Kizek R, Adam V, (2013). "Apoferritin modified magnetic particles as Doxorubicin carriers for anticancer drug delivery", Int J Mol Sci, 14:13391-402.

Bradley AM, Loscalzo J, (2009). "The treatment of hyperhomocysteinemia", Annu Med Rev, 60, 39–54.

Broders AC, (1925). "The Grading of Carcinoma", Minn Med, 8:726-730.

Bublil EM, Majtan T, Park I, Carrillo RS, Hůlková H, Krijt J, Kožich V, Kraus JP, (2016). "Enzyme replacement with PEGylated cystathionine β-synthase ameliorates homocystinuria in murine model", The Journal of Clinical Investigation, 126:2372–2384.

Cai W, Wang M, Ju L, Wang C, Zhu Y, (2010). "Hydrogen sulfide induces human colon cancer cell proliferation: role of Akt, ERK and p21", Cell Biology International, 34:565–572.

Carballal S, Madzelan P, Zinola CF, Graña M, Radi R, Banerjee R, Alvarez B, (2008). "Dioxygen reactivity and heme redox potential of truncated human cystathionine β-synthase", Biochemistry 47:3194–3201.

Carbonero F, Benefiel AC, Gaskins HR, (2012). "Contributions of the microbial hydrogen economy to colonic homeostasis", *Nature Reviews Gastroenterology & Hepatology*, *9*:504–518.

Ceci P, Morea V, Fornara M, Bellapadrona G, Falvo E, Ilari A, *(*2012). "*Biomimetic materials synthesis by ferritin-related, cage-shaped proteins.*, Adv. Topics in Biomineralization, Jong Seto (Ed.), ISBN: 978-953-51-0045-4, InTech.

Chao C, Bohannon FJ, Mrazek A, Coletta C, Szabo C, Hellmich MR, (2014). "Cysthionine-β-synthetase inhibition in combination with standard-chemotherapy decreases colorectal cancer metastasis to the liver", Nitric Oxide 39:S21.

Chao C, Zatarain JR, Ding Y, Coletta C, Mrazek AA, Druzhyna N, Johnson P, Chen H, Hellmich JL, Asimakopoulou A, Yanagi K, Olah G, Szoleczky P, Törö G, Bohanon FJ, Cheema M, Lewis R, Eckelbarger D, Ahmad A, Módis K, Untereiner A, Szczesny B, Papapetropoulos A,

Zhou J, Hellmich MR, Szabo C, (2016). “Cystathionine-β-synthase inhibition for colon cancer: enhancement of the efficacy of aminooxyacetic acid via the prodrug approach”, Molecular Medicine, 22:361-379.

Chen X, Jhee KH, Kruger WD, (2004). ”Production of the neuromodulator H_2S by cystathionine beta-synthase via the condensation of cysteine and homocysteine”, J. Bio.l Chem., 279, 52082-52086.

Cherney MM, Pazicni S, Frank N, Marvin KA, Kraus JP, Burstyn JN, (2007). “Ferrous human cystathionine beta-synthase loses activity during enzyme assay due to a ligand switch process”, Biochemistry, 46:13199-210.

Chiku T, Padovani D, Zhu W, Singh S, Vitvitsky V, Banerjee R, (2009). “H_2S biogenesis by human cystathionine gamma-lyase leads to the novel sulfur metabolites lanthionine and homolanthionine and is responsive to the grade of hyperhomocysteinemia”, J Biol Chem, 284:11601–11612.

Cooper CE & Brown GC, (2008). “The inhibition of mitochondrial cytochrome oxidase by the gases carbon monoxide, nitric oxide, hydrogen cyanide and hydrogen sulfide: Chemical mechanism and physiological significance”, Journal of Bioenergetics and Biomembranes, 40:533–539.

Crichton RR & Boelaert JR, (2009). “Inorganic Biochemistry of Iron Metabolism from Molecular Mechanisms to Clinical Consequences”, 3rd Ed., John Wiley and Sons, Chichester, 183–222.

Cutrin JC, Crich SG, Burghelea D, Dastrù W, Aime S, (2013). “Curcumin/Gd loaded apoferritin: a novel "theranostic" agent to prevent hepatocellular damage in toxic induced acute hepatitis”, Mol Pharm, 10:2079-85.

Daniels TR, Bernabeu E, Rodríguez JA, Patel S, Kozman M, Chiappetta DA, Holler E, Ljubimova JY, Helguera G, Penichet ML, (2012). “The transferrin receptor and the targeted delivery of therapeutic agents against cancer”, Biochim Biophys Acta, 1820:291-317.

Dixon M, (1971). “The acceptor specificity of flavins and flavoproteins. I. Techniques for anaerobic spectrophotometry” BBA— Bioenergetics, 226:241–258.

Druzhyna N, Szczesny B, Olah G, Módis K, Asimakopoulou A, Pavlidou A, Szoleczky P, Gerö D, Yanagi K, Törö G, López-García I, Myrianthopoulos V, Mikros E, Zatarain JR, Chao C, Papapetropoulos A, Hellmich MR, Szabo, C, (2016). “Screening of a composite library of clinically used drugs and well-characterized pharmacological compounds for cystathionine β-synthase inhibition identifies benserazide as a drug potentially suitable for repurposing for the

experimental therapy of colon cancer", Pharmacological Research, 113:18-37.

Dukes CE, (1932). "Classification of Cancer of Rectum", Journal of Pathology and Bacteriology, 323:332.

Ereño-Orbea J, Majtan T, Oyenarte I, Kraus JP, Martínez-Cruz LA, (2013). "Structural basis of regulation and oligomerization of human cystathionine β-synthase, the central enzyme of transsulfuration", Proceedings of the National Academy of Sciences of the United States of America, 110:E3790-9.

Ereño-Orbea J, Majtan T, Oyenarte I, Kraus JP, Martínez-Cruz LA, (2014). "Structural insight into the molecular mechanism of allosteric activation of human cystathionine β-synthase by *S*-adenosylmethionine", Proceedings of the National Academy of Sciences, 111:E3845–E3852.

Falvo E, Tremante E, Arcovito A, Papi M, Elad N, Boffi A, Morea V, Conti G, Toffoli G, Fracasso G, Giacomini P, Ceci P, (2016). "Improved Doxorubicin Encapsulation and Pharmacokinetics of Ferritin-Fusion Protein Nanocarriers Bearing Proline, Serine, and Alanine Elements", Biomacromolecules, 17:514-22.

Falvo E, Tremante E, Fraioli R, Leonetti C, Zamparelli C, Boffi A, Morea V, Ceci P, Giacomini P, (2013). "Antibody-drug conjugates: targeting

melanoma with cisplatin encapsulated in protein-cage nanoparticles based on human ferritin", Nanoscale. 5:12278-85.

Fan K, Cao C, Pan Y, Lu D, Yang D, Feng J, Song L, Liang M, Yan X, (2012). "Magnetoferritin nanoparticles for targeting and visualizing tumour tissues", Nat Nanotechnol, 7:459-64.

Fan K, Li N, Qi J, Yin P, Zhao C, Wang L, Li Z, Zha X, (2014). "Wnt/β-catenin signaling induces the transcription of cystathionine-γ-lyase, a stimulator of tumor in colon cancer". Cell Signal, 26:2801-8.

Fantechi E, Innocenti C, Zanardelli M, Fittipaldi M, Falvo E, Carbo M, Shullani V, Di Cesare Mannelli L, Ghelardini C, Ferretti AM, Ponti A, Sangregorio C, Ceci P, (2014). "A smart platform for hyperthermia application in cancer treatment: cobalt-doped ferrite nanoparticles mineralized in human ferritin cages", ACS Nano, 8:4705-19.

Fracasso G, Falvo E, Colotti G, Fazi F, Ingegnere T, Amalfitano A, Doglietto GB, Alfieri S, Boffi A, Morea V, Conti G, Tremante E, Giacomini P, Arcovito A, Ceci P, (2016). "Selective delivery of doxorubicin by novel stimuli-sensitive nano-ferritins overcomes tumor refractoriness", J Control Release, 239:10–18.

Fu M, Zhang W, Wu L, Yang G, Li H, Wang R, (2012). "Hydrogen sulfide (H_2S) metabolism in mitochondria and its regulatory role in energy production, Proc Natl Acad Sci U S A, 109:2943-8.

Garret, RH, Grisham CM, (1998). “Biochimica” 506-511. Bologna: Zanichelli Ed. (Prima Ediz).

Goubern M, Andriamihaja M, Nubel T, Blachier F, Bouillaud F, (2007). “Sulfide, the first inorganic substrate for human cells”, The FASEB Journal, 21:1699–1706.

Gumulec J, Fojtu M, Raudenska M, Sztalmachova M, Skotakova A, Vlachova J, Skalickova S, Nejdl L, Kopel P, Knopfova L, Adam V, Kizek R, Stiborova M, Babula P, Masarik M, (2014). “Modulation of induced cytotoxicity of doxorubicin by using apoferritin and liposomal cages”, Int J Mol Sci, 15:22960-77.

Hancock J T, Whiteman M, (2016). “Hydrogen sulfide signaling: Interactions with nitric oxide and reactive oxygen species”, Annals of the New York Academy of Sciences, 1365:5–14.

Harari D, Kuhn N, Abramovich R, Sasson K, Zozulya AL, Smith P, Schlapschy M, Aharoni R, Köster M, Eilam R, Skerra A, Schreiber G, (2014). “Enhanced in vivo efficacy of a type I interferon superagonist with extended plasma half-life in a mouse model of multiple sclerosis”, J Biol Chem, 289:29014-29.

Harrison PM, Arosio P, (1996). “The ferritins: molecular properties, iron storage function and cellular regulation”, Biochim Biophys Acta, 1275:161-203.

Heger Z, Skalickova S, Zitka O, Adam V, Kizek R, (2014). "Apoferritin applications in nanomedicine", Nanomedicine (Lond), 9:2233–45.

Hellmich MR, Coletta C, Chao C, Szabo C, (2015). "The Therapeutic Potential of Cystathionine β-Synthetase/Hydrogen Sulfide Inhibition in Cancer", Antioxidants & Redox Signaling, 22:424-448.

Hellmich MR, Szabo C, (2015). "Hydrogen sulfide and cancer. Handbook of Experimental Pharmacology", 230:233-241.

Hewitt RE, McMarlin A, Kleiner D, Wersto R, Martin P, Tsokos M, Stamp GW, Stetler-Stevenson WG, (2000). "Validation of a model of colon cancer progression", The Journal of Pathology, *192*:446–54.

Hildebrandt TM &Grieshaber MK, (2008). "Three enzymatic activities catalyze the oxidation of sulfide to thiosulfate in mammalian and invertebrate mitochondria", FEBS J., 275, 3352–3361.

Hill BC, Woon T, Nicholls P, Peterson IIJ, Greenwood C, Thomsont AJ, (1984). "Interactions of sulphide and other ligands with cytochrome c oxidase", 224:591–600.

Hine C, Harputlugil E, Zhang Y, Ruckenstuhl C, Cheon B, Brace L, Longchamp A, Treviño-Villarreal JH, Mejia P, Ozaki CK, Wang R, Gladyshev VN, Madeo F, Mair WB, Mitchell JR, (2016). "Endogenous Hydrogen Sulfide Production Is Essential for Dietary Restriction Benefits", Cell , 132–144.

Hnízda A, Majtan T, Liu L, Pey AL, Carpenter JF, Kodíček M, Kožich V, Kraus JP, (2012). "Conformational properties of nine purified cystathionine β-synthase mutants", Biochemistry, 12, 51(23):4755-63.

Jackson MR, Melideo SL, Jorns MS, (2012). "Human sulfide: quinone oxidoreductase catalyzes the first step in hydrogen sulfide metabolism and produces a sulfane sulfur metabolite", Biochemistry, *51*:6804–6815.

Jain RK, (1999). "Transport of molecules, particles, and cells in solid tumors", Annu Rev Biomed Eng, 1:241-63.

Johnson-Winters K, Tollin G, Enemark JH, (2010). "Elucidating the catalytic mechanism of sulfite oxidizing enzymes using structural, spectroscopic, and kinetic analyses", Biochemistry, 49:7242–725.

Kabil O, Banerjee R, (2014). "Enzymology of H_2S Biogenesis, Decay and Signaling", Antioxidants & Redox Signaling, 20:770–782.

Kabil O, Vitvitsky V, Banerjee R, (2014). "Sulfur as a signaling nutrient through hydrogen sulfide", Annual Review of Nutrition, 3*4*:171–205.

Kabil O, Weeks CL, Carballal S, Gherasim C, Alvarez B, Spiro TG, Banerjee R, (2011). "Reversible heme-dependent regulation of human cystathionine β-synthase by a flavoprotein oxidoreductase", Biochemistry, 50:8261–8263.

Kang HJ, Kang YJ, Lee YM, Shin HH, Chung SJ, Kang S, (2012). "Developing an antibody-binding protein cage as a molecular recognition drug modular nanoplatform", Biomaterials, 33:5423-30.

Kilic MA, Ozlu E, Calis S, (2012). "A novel protein-based anticancer drug encapsulating nanosphere: apoferritin-doxorubicin complex", J Biomed Nanotechnol, 8:508-14.

Kim M, Rho Y, Jin KS, Ahn B, Jung S, Kim H, Ree M, (2011). "pH-dependent structures of ferritin and apoferritin in solution: disassembly and reassembly", Biomacromolecules, 12:1629-40.

Kimura H, (2015). "Hydrogen sulfide and polysulfides as signaling molecules", Proc Jpn Acad Ser B Phys Biol Sci, 91:131-59.

Kimura H, (2017). "Hydrogen sulfide and polisulfide signaling", *Antioxidant & Redox Signaling*, *27*:619–621.

Kimura, H. (2014). The physiological role of hydrogen sulfide and beyond. *Nitric Oxide*, *41*, 4–10.

Kolluru GK, Bir SC, Yuan S, Shen X, Pardue S, Wang R, Kevil CG, (2015). "Cystathionine γ-lyase regulates arteriogenesis through NO-dependent monocyte recruitment*",* Cardiovascular Research, 4, 590–600.

Lagoutte E, Mimoun S, Andriamihaja M, Chaumontet C, Blachier F, Bouillaud F, (2010). "Oxidation of hydrogen sulfide remains a priority in mammalian cells and causes reverse electron transfer in

colonocytes", Biochimica et Biophysica Acta - Bioenergetics, 1797:1500–1511.

Lee EJ, Lee NK, Kim IS, (2016), "Bioengineered protein-based nanocage for drug delivery", Adv Drug Deliv Rev, 106:157-171.

Leibovitz A, Stinson JC, McCombs III WB, Mccoy CE, Mazur KC, Mabry ND, (1976). "Classification of human colorectal adenocarcinoma cell lines", Cancer Research, 36:4562–4569.

Leschelle X, Goubern M, Andriamihaja M, Blottière HM, Couplan E, Gonzalez-Barroso MD, Petit C, Pagniez A, Chaumontet C, Mignotte B, Bouillaud F, Blachier F, (2005). "Adaptative metabolic response of human colonic epithelial cells to the adverse effects of the luminal compound sulfide", Biochimica et Biophysica Acta (BBA) - General Subjects, 1725:201–212.

Li K, Zhang ZP, Luo M, Yu X, Han Y, Wei HP, Cui ZQ, Zhang XE, (2012). "Multifunctional ferritin cage nanostructures for fluorescence and MR imaging of tumor cells", Nanoscale 4:188-93.

Li L, Fang CJ, Ryan JC, Niemi EC, Lebrón JA, Björkman PJ, Arase H, Torti FM, Torti SV, Nakamura MC, Seaman WE, (2010). "Binding and uptake of H-ferritin are mediated by human transferrin receptor-1", Proc Natl Acad Sci U S A, 107:3505-10.

Liang M, Fan K, Zhou M, Duan D, Zheng J, Yang D, Feng J, Yan X, (2014). "H-ferritin-nanocaged doxorubicin nanoparticles specifically target and kill tumors with a single-dose injection", Proc Natl Acad Sci U S A, 111:14900-5.

Libiad M, Yadav PK, Vitvitsky V, Martinov M, Banerjee R, (2014). "Organization of the human mitochondrial hydrogen sulfide oxidation pathway. Journal of Biological Chemistry, 289:30901–30910.

Ma-Ham AH, Wu H, Wang J, Kang XH, Zhang YY, Lin YH, (2011). "Apoferritin-based nanomedicine platform for drug delivery: equilibrium binding study of daunomycin with DNA", J Mater Chem; 21:8700–8708.

Masson N, Ratcliffe PJ, (2014). "Hypoxia signaling pathways in cancer metabolism: the importance of co-selecting interconnected physiological pathways", Cancer & Metabolism, 2:3.

Matallo J, Vogt J, McCook O, Wachter U, Tillmans F, Groeger M, Szabo C, Georgieff M, Radermacher P, Calzia E (2014). "Sulfide-inhibition of mitochondrial respiration at very low oxygen concentrations", Nitric Oxide - Biology and Chemistry, 41:79-84.

Meier M, Janosik M, Kery V, Kraus JP, Burkhard P, (2001). "Structure of human cystathionine [beta]-synthase: a unique pyridoxal 5[prime]-phosphate-dependent heme protein". Embo J, 20:3910–3916.

Mendes MI, Colaço HG, Smith DE, Ramos RJ, Pop A, van Dooren SJ, Tavares de Almeida I, Kluijtmans LA, Janssen MC, Rivera I, Salomons GS, Leandro P, Blom HJ, (2014). "Reduced response of Cystathionine Beta-Synthase (CBS) to S-Adenosylmethionine (SAM): identification and functional analysis of CBS gene mutations in Homocystinuria patients", Journal of Inherited Metabolic Disease, 37:245– 254.

Mimoun S, Andriamihaja M, Chaumontet C, Atanasiu C, Benamouzig R, Blouin JM, Tomé D, Bouillaud F, Blachier F, (2012). "Detoxification of H_2S by differentiated colonic epithelial cells: implication of the sulfide oxidizing unit and of the cell respiratory capacity". Antioxidant & Red, 17:1-10.

Módis K, Asimakopoulou A, Coletta C, Papapetropoulos A, Szabo C, (2013). "Oxidative stress suppresses the cellular bioenergetic effect of the 3-mercaptopyruvate sulfurtransferase / hydrogen sulfide pathway". Biochemical and Biophysical Research Com Munications, 433:401–407.

Módis K, Bos EM, Calzia E, Van Goor H, Coletta C, Papapetropoulos A, Hellmich MR, Radermacher P, Bouillaud F, Szabo C, (2014). "Regulation of mitochondrial bioenergetic function by hydrogen sulfide. Part II Pathophysiological and therapeutic aspects". British Journal of Pharmacology, 171:2123–2146.

Módis K, Coletta C, Erdélyi K, Papapetropoulos A, Szabo C, (2013). "Intramitochondrial hydrogen sulfide production by 3-mercaptopyruvate sulfurtransferase maintains mitochondrial electron flow and supports cellular bioenergetics", FASEB Journal, 27:601–611.

Morikawa T, Kajimura M, Nakamura T, Hishiki T, Nakanishi T, Yukutake Y, Nagahata Y, Ishikawa M, Hattori K, Takenouchi T, Takahashi T, Ishii I, Matsubara K, Kabe Y, Uchiyama S, Nagata E, Gadalla MM, Snyder SH, Suematsu M, (2012). "Hypoxic regulation of the cerebral microcirculation is mediated by a carbon monoxide-sensitive hydrogen sulfide pathway", Proceedings of the National Academy of Sciences, 109:1293–1298.

Mudd SH, Kovby FS, Levy HL, (1985). "The natural history of homocystinuria due to cystathionine beta-synthase deficiency", The American Journal of Human Genetics, 37:1–31.

Mustafa AK, Gadalla MM, Sen N, Kim, S, Mu W, Gazi SK, Barrow RK, Yang G, Wang R, Snyder, SH, (2010). "H_2S Signals Through Protein S-Sulfhydration". Sci Signal, 2:ra72.

Muz B, De La P, Feda P, Abdel A, Azab K, Azab AK, (2015). "The role of hypoxia in cancer progression, angiogenesis, metastasis, and resistance to therapy", Hypoxia, 83—92.

Nagy P, (2013). “Kinetics and mechanisms of thiol-disulfide exchange covering direct substitution and thiol oxidation-mediated pathways”, Antioxid Redox Signal. 18:1623-41.

Nagy P, Pálinkás Z, Nagy A, Budai B, Tóth I, Vasas A, (2014). “Chemical aspects of hydrogen sulfide measurements in physiological samples”, Biochimica et Biophysica Acta - General Subjects, 1840:876–891.

Nashef AS, Osuga DT, Feeney RE, (1977). “Determination of hydrogen-sulfide with 5,5′-Dithiobis-(2-nitrobenzoic acid), N-ethylmaleimide, and parachloromercuri-benzoate, Anal Biochem, 79:394–405.

Nicholls DG & Ferguson SJ, (2013). Bioenergetics. IV ed, Respiratory Chains, 91–157.

Nicholls P & Kim JK, (1982). “Sulphide as an inhibitor and electron donor for the cytochrome c oxidase system” Can J Biochem, 60:613–623.

Nicholls P, Marshall DC, Cooper CE, Wilson MT, (2013). “Sulfide inhibition of andmetab- olismby cytochrome c oxidase”, Biochem. Soc. Trans. 41:1312–1316.

Oliveriusová J, Kery V, Maclean KN, Kraus JP, (2002). “Deletion mutagenesis of human cystathionine beta-synthase. Impact on activity, oligomeric status, and S-adenosylmethionine regulation”, J Biol Chem, 277:48386–48394.

Olson KR, (2015). “Hydrogen Sulfide as an Oxygen Sensor”, Antioxidants & Redox Signaling, 22:377–397.

Ono K, Akaike T, Sawa T, Kumagai Y, Wink DA, Tantillo DJ, Hobbs AJ, Nagy P, Xian M, Lin J, Fukuto JM, (2014). “Redox Chemistry and Chemical Biology of H_2S, Hydropersulfides and Derived Species: Implications to Their Possible Biological Activity and Utility”, Free Radic Biol Med, 77:82-94.

Papapetropoulos A, Pyriochou A, Altaany Z, Yang G, Marazioti A, Zhou Z, Jeschke MG, Branski LK, Herndon DN, Wang R, Szabó C, (2009). “Hydrogen sulfide is an endogenous stimulator of angiogenesis”. Proceedings of the National Academy of Sciences of the United States of America, 106:21972–21977.

Petersen LC, (1977). “The effect of inhibitors on the oxygen kinetics of cytochrome c oxidase”, Biochim Biophys Acta, 460:299–307.

Powell MA, Somero GN, (1986). “Hydrogen sulfide oxidation is coupled to oxidative phos- phorylation inmitochondria of Solemya reidi”, Science, 233:563–566.

Puranik M, Weeks CL, Lahaye D, Kabil O, Taoka S, Nielsen SB, Groves JT, Banerjee R, Spiro, TG, (2009). “Dynamics of Carbon Monoxide Binding to Cystathionine β-Synthase”, *Journal of Biological Chemistry*, *281*:13433–13438.

Ramasamy S, Singh S, Taniere P, Langman MJS, Eggo MC, (2006). "Sulfide-detoxifying enzymes in the human colon are decreased in cancer and upregulated in differentiation", American Journal of Physiology. Gastrointestinal and Liver Physiology, 291:G288-96.

Rich PR, Meunier B, Mitchell R, Moody J, (1996). "Coupling of charge and proton movement in cytochrome c oxidase", Biochim Biophys Acta, 1275:91–95.

Rivero-Gutiérrez B, Anzola A, Martínez-Augustin O, De Medina FS, (2014). "Stain-free detection as loading control alternative to Ponceau and housekeeping protein immunodetection in Western blotting". *Analytical Biochemistry*, *467*:1–3.

Rundhaug JE, (2003). "Matrix metalloproteinases, angiogenesis, and cancer: commentary re: A. C. Lockhart et al., Reduction of wound angiogenesis in patients treated with BMS-275291, a broad spectrum matrix metalloproteinase inhibitor. Clin. Cancer Res., 9: 00-00, 2003", Clin Cancer Res, 9:551-4.

Schiff M & Blom HJ, (2012). "Treatment of inherited homocystinurias" Neuropediatrics. 43, 295–304.

Schlapschy M, Binder U, Börger C, Theobald I, Wachinger K, Kisling S, Haller D, Skerra A, (2013). "PASylation: a biological alternative to

PEGylation for extending the plasma half-life of pharmaceutically active proteins", Protein Eng Des Sel. 26, 489-501.

Schoonen L & van Hest JCM, (2014). "Functionalization of protein-based nanocages for drug delivery applications", Nanoscale, 6, 7124–7141.

Semenza GL, (2013). "Hypoxia-inducible factors: mediators of cancer progression and targets for cancer therapy", Trends Pharmacol Sci., 33, 207–214.

Shibuya N & Kimura H, (2013). "Production of hydrogen sulfide from D-cysteine and its therapeutic potential", Front Endocrinol (Lausanne), 4, 1–5.

Shibuya N, Koike S, Tanaka M, Ishigami-Yuasa M, Kimura Y, Ogasawara Y, Fukui K, Nagahara N, Kimura H, (2013). "A novel pathway for the production of hydrogen sulfide from D-cysteine in mammalian cells", Nat Commun., 4.

Short R, Posch A, (2011). "Stain-Free Approach for Western Blotting", GEN, *31*:5–7.

Simsek E, Kilic MA, (2005). "Magic ferritin: a novel chemotherapeutic encapsulation bullet", J Magn Magn Mater., 293, 509–513.

Singh S & Banerjee R, (2012). "PLP-dependent H_2S biogenesis" 1814, 1518–1527.

Singh S, Madzelan P, Stasser J, Weeks CL, Becker D, Spiro G, Penner-Hahn J, Banerjee R, (2010). “Modulation of the heme electronic structure and cystathionine β-synthase cctivity by second coordination sphere ligands: the role of heme ligand switching in redox regulation, 103, 689–697.

Singh S, Padovani D, Leslie RA, Chiku T, Banerjee R, (2009). “Relative contributions of cystathionine beta-synthase and gamma-cystathionase to H_2S biogenesis via alternative trans-sulfuration reactions”, Journal of Biological Chemistry, *284*(33), 22457–22466.

Solaini G, Baracca A, Lenaz G, Sgarbi G, (2010). “Hypoxia and mitochondrial oxidative metabolism”, Biochimica et Biophysica Acta (BBA) - Bioenergetics, 1797, 1171–1177.

Srere PA, (1969). “Citrate synthase”, Methods in Enzymology, 13, 3-11.

Szabo C & Hellmich, MR, (2013). “Endogenously produced hydrogen sulfide supports tumor cell growth and proliferation”, Cell Cycle, *12*, 2915–2916.

Szabo C, (2015). “Gasotransmitters in cancer: from pathophysiology to experimental therapy” Nature Reviews Drug Discovery, 15, 185-203.

Szabo C, Coletta C, Chao C, Modis K, Szczesny B, Papapetropoulos A, Hellmich MR, (2013). “Tumor-derived hydrogen sulfide, produced by cystathionine-β-synthase, stimulates bioenergetics, cell proliferation,

and angiogenesis in colon cancer", Proceedings of the National Academy of Sciences, 110, 12474–12479.

Szabo C, Ransy C, Módis K, Andriamihaja M, Murghes B, Coletta C, Olah G, Yanagi K, Bouillaud F, (2014). "Regulation of mitochondrial bioenergetic function by hydrogen sulfide. Part I. Biochemical and physiological mechanisms", British Journal of Pharmacology, 171, 2099–2122.

Takano N, Peng YJ, Kumar GK, Luo W, Hu H, Shimoda, LA, Suematsu M, Prabhakar NR, Semenza GL, (2014). "Hypoxia-inducible factors regulate human and rat cystathionine β-synthase gene expression", HHS Public Access. Biochem., 1, 203–211.

Taoka S & Banerjee R, (2001). "Characterization of NO binding to human cystathionine β-synthase: possible implications of the effects of CO and NO binding to the human enzyme", Journal of Inorganic Biochemistry, 87, 245–251.

Taoka S, West M, Banerjee R, (1999)."Characterization of the heme and pyridoxal phosphate cofactors of human cystathionine beta-synthase reveals nonequivalent active sites", Biochemistry 38, 38, 2738–2744.

Teng H, Wu B, Zhao K, Yang G, Wu L, Wang R, (2013). "Oxygen-sensitive mitochondrial accumulation of cystathionine β-synthase mediated by

Lon protease", Proceedings of the National Academy of Sciences, 110, 12679–12684.

Tiranti V, Viscomi C, Hildebrandt T, Di Meo I, Mineri R, Tiveron C, Levitt MD, Prelle A, Fagiolari G, Rimoldi M, Zeviani M, (2009). "Loss of ETHE1, amitochondrial dioxygenase, causes fatal sulfide toxicity in ethylmalonic encephalopathy" Nat. Med., 15, 200–5

Toney MD, (2012). "Controlling reaction specificity in pyridoxal phosphate enzymes", Biochim Biophys Acta., 1814, 1407–1418.

Truffi M, Fiandra L, Sorrentino L, Monieri M, Corsi F, Mazzucchelli S,(2016) "Ferritin nanocages: A biological platform for drug delivery, imaging and theranostics in cancer", Pharmacol. Res., 107, 57–65.

Uchida M, Flenniken ML, Allen M, Willits DA, Crowley BE, Brumfield S, Willis AF, Jackiw L, Jutila M, Young MJ, Douglas T, (2006). "Targeting of cancer cells with ferrimagnetic ferritin cage nanoparticles", J Am Chem Soc., 128, 16626-33.

Vannucci L, Falvo E, Ceci P, (2014). "Multifunctional Protein-Based Nanoparticles for Cancer Theranosis", 2014, 231-253.

Vannucci L, Falvo E, Fornara M, Di Micco P, Benada O, Krizan J, Svoboda J, Hulikova-Capkova K, Morea V, Boffi A, Ceci P, (2012). "Selective targeting of melanoma by PEG-masked protein-based multifunctional nanoparticles", Int J Nanomedicine., 1489-509.

Vicente JB, Colaço, HG, Mendes MIS, Sarti P, Leandro, P, Giuffrè A, (2014). "NO• binds human cystathionine β-synthase quickly and tightly", Journal of Biological Chemistry, 289, 8579–8587.

Vicente JB. Colaço HG, Sarti P, Leandro P, Giuffrè A, (2016). "S-adenosyl-L-methionine modulates CO and NO· binding to the human H_2S-generating enzyme cystathionine β-synthase", Journal of Biological Chemistry, 291, 572–581.

Wallace JL & Wang R, (2015). "Hydrogen sulfide-based therapeutics: exploiting a unique but ubiquitous gasotransmitter", Nature Reviews Drug Discovery, *14*, 329–345.

Wang R, (2002). "Two's company, three's a crowd: can H_2S be the third endogenous gaseous transmitter?", FASEB J., 16, 1792-8.

Wang, R (2012). "Physiological implications of hydrogen sulfide : a whiff exploration that blossomed", Physiol Rev., 92, 791–896.

Weeks CL, Singh S, Madzelan, P, Banerjee R, Spiro TG, (2009). "Heme regulation of cystathionine β-synthase activity: insight from fluorescence and Raman spectroscopy", Journal of Th, *131*, 12809–12816.

Weisiger RA, Pinkus, LM, Jakoby WB, (1980). "Thiol S- methyltransferase: suggested role in detoxication of intestinal hydrogen sulfide", Biochemical Pharmacology, 29, 2885–2887.

Worwood M, Cragg SJ, Williams AM, Wagstaff M, Jacobs A, (1982). "The clearance of 131I-human plasma ferritin in man", Blood., 60, 827-33.

Wu B, Teng H, Zhang L, Li H, Li J, Wang L, Li H., (2015). "Interaction of hydrogen sulfide with oxygen sensing under hypoxia", Oxidative Medicine and Cellular Longevity, 758678.

Wu H & Chen Q, (2015). "Hypoxia activation of mitophagy and its role in disease pathogenesis" Antioxidants & redox signaling, 22, 1032-46.

Wu JS, (2007). "Rectal Cancer Staging", Clinics, *1*, 148–157.

Xing R, Wang X, Zhang C, Zhang Y, Wang Q, Yang Z, Guo Z, (2009). "Characterization and cellular uptake of platinum anticancer drugs encapsulated in apoferritin", J Inorg Biochem. 103, 1039-44.

Yan F, Zhang Y, Kim KS, Yuan HK, Vo-Dinh T, (2010). "Cellular uptake and photodynamic activity of protein nanocages containing methylene blue photosensitizing drug", Photochem Photobiol, 86, 662-6.

Yong R & Searcy DG, (2001). "Sulfide oxidation coupled to ATP synthesis in chicken liver mitochondria ", Comp Biochem Physiol B Biochem Mol Biol., 129, 129-37.

Yuan G, Vasavda C, Peng YJ, Makarenko VV, Raghuraman G, Nanduri J, Gadalla MM, Semenza GL, Kumar GK, Snyder SH, Prabhakar NR, (2015). "Protein kinase G-regulated production of H_2S governs oxygen sensing", Sci Signal., 8.

Zhang F, Bosch-Marce M, Shimoda LA, Shun YS, Baek JH, Wesley JB, Gonzales F. J., Semenza G. L., (2008). “Mitochondrial autophagy is an HIF-1-dependent adaptive metabolic response to hypoxia”, J Biol Chem., 283, 10892–10903.

Zhang L, Li L, Di Penta A, Carmona U, Yang F, Schöps R, Brandsch M, Zugaza JL, Knez M., (2015). “H-Chain Ferritin: A Natural Nuclei Targeting and Bioactive Delivery Nanovector”, Adv Healthc Mater., 4, 1305-10.

Zhao W, Zhang, J Lu, Y, Wang R, (2001). “The vasorelaxant effect of H_2S as a novel endogenous gaseous KATP channel opener”, EMBO Journal, *20*, 6008–6016.

Zhen Z, Tang W, Chen H, Lin X, Todd T, Wang G, Cowger T, Chen X, Xie J, (2013). “RGD-modified apoferritin nanoparticles for efficient drug delivery to tumors”, ACS Nano., 7, 4830-7.